Underground UHF-EM Transillumination:

A Feasibility Study

by

Paul Thomas Lafleche, B.Sc., M.Sc.

A thesis submitted to the faculty of Graduate Studies and Research in partial fulfillment of the requirements for the Degree of Doctor of Philosophy.

Department of Geological Sciences
McGill University
Montreal, Canada
April, 1985

Abstract

A feasibility study into the use of UHF-EM transillumination measurements in geophysics is presented. The electrical properties and absorption rates of common crustal materials are examined with the goal of identifying specific conditions under which sufficient material penetration at UHF frequencies is available.

A prototype 445 MHz continuous-wave transillumination instrument designed for underground use is described. Test surveys, with this instrument, were conducted at the Big Nickel Mine in Sudbury, Ontario, to obtain a number of through-rock absorption rates. Estimated effective resistivities of between 500 and 1500 ohm-metres are determined from the survey data.

Effective conductivities and permittivities from AC and DC electrical property measurements on geological samples from the mine site corroborate these transillumination survey results.

The results of the field surveys indicate that the UHF-EM transillumination technique is a feasible and useful geophysical method.

Résumé

On présente une étude de faisabilité concernant l'utilisation des mesures de transillumination EM - UHF en géophysique.

Les propriétés électriques et les taux d'absorbtion des matériaux les plus répandus de la croute sont étudiés dans le but d'identifier les conditions particulières sous les quelles on obtient une pénétration suffisante aux fréquences UHF.

On décrit un prototype d'instrument de transillumination à onde continue opérant à 445 MHz et conçu pour usage sousterrain. On a procédé à des relevés d'essais avec cet instrument à la mine Big Nickel à Sudbury en Ontario pour obtenir un certain nombre de taux d'absorbtion à travers le roc. A partir des données des relevés, les résistivités efficaces sont évaluées et se situent dans l'intervalle de 500 à 1500 ohm-mètres.

Les valeurs de conductibilité efficace et de permitivité, trouvées à partir de mesures de propriétés electriques en excitation continue et alternative sur des échantillons géologiques provenant de la mine, corroborent les résultats de ces relevés de transillumination.

Les résultats des relevés de terrain indiquent que la technique de transillumination EM - UHF est réalisable et qu'il s'agit d'une méthode géophysique utile.

Table of Contents

Acknowledgements

This thesis describes the work undertaken as part of a research project into the applications of VHF/UHF electromagnetic waves in geophysics. The project was funded under research grants 138/04/81, 90/04/82 and 54/04/83 granted to Dr. O.G. Jensen and Mr. P.T LaFleche of McGill University. The author is indebted to Dr. L.S. Collett for his assistance in securing funding for the project and his support throughout the duration of the research. The author was funded by a National Science and Engineering Research Council Postgraduate Scholarship and a Noranda Bradfield Fellowship. The author wishes to express his gratitude to Mr. R. Pemberton of Noranda Exploration in obtaining the latter funding.

The author gratefully acknowledges the support and assistance of his thesis supervisor Dr. O.G. Jensen and for their assistance in obtaining a suitable survey location, Mr. R. Pemberton of Noranda Exploration and Mr. J. Dowsett of Inco Ltd.

The field work was conducted in the first year with the aid of Mr. A. Lachapelle. Messrs J.P. Todoeschuck and P. Golde participated in the second field season. The extraordinary efforts of Messrs. Todoeschuck and Golde in performing under several adverse conditions for long durations is especially appreciated.

Technical matters were discussed with Drs. O.G. Jensen, Jean Roy, Robert Bazinet and Paul Lorrain whose ideas were instrumental in the successful development of the equipment. The geology of the Sudbury area and the Big Nickel Mine was discussed with Dr. J. Stevenson. The author acknowledges the assistance of John Todoeschuck in proofreading this manuscript and for engaging in many illuminating discussions about this work. The assistance of Mr. D. Leischman in the machining and construction of the equipment is especially appreciated.

The author wishes to acknowledge the support of his contemporaries: Mssrs J. Todoeschuck, M. Pilkington, E. Nichols, A. Rigoti, C. Tsingas, P. Keating, A. Vafidis, K. Williams, R. Del Valle and F. Boadu; Drs. P. Tyraskis, W.C. Yang and J. Roy, Misses C. Parker, C. Samson and E. Baranyi. The author also acknowledges the support of the geophysics staff members of McGill University: Dr. V. Saull, Dr. W.M. Telford and Dr. D.J. Crossley.

The author gratefully acknowledges the assistance of the supervisors of the Big Nickel Mine during the periods of his field work, Messers Tom Jewiss and Jeff Sewell. The help of the mining engineer, Mr. M. Assadi, in providing unrestricted freedom of access to the various areas of the mine and in providing technical assistance is also sincerely appreciated. The staff of the Big Nickel Mine went out of their way to assist the author and his associates in any way

they could and provided moral support with their interest in the project.

The author acknowledges the encouragement and support provided by Dr. I. Johnson and Mr. Z. Doborzynski throughout the project.

The support of the author's fiancee, Miss Lisanne Losier, in enduring his four long years of effort is sincerely appreciated.

List of Figures

List of Tables

List of Appendices

Chapter 1

Introduction

1.1 Scope of the project

The very high frequency (VHF) and ultra high frequency (UHF) radio bands have not been much exploited for geophysical exploration in North America. Research and development of geophysical systems which employ these frequencies has been based upon pulsed radar systems as opposed to the continuous-wave transillumination technique which is the subject of this thesis. The limited penetration of electromagnetic waves at VHF/UHF frequencies is cited as the reason for their infrequent use. Given the average value of surface resistivity of 100-200 ohm-metres (Keller, 1966) over the North American continent, as measured at radio frequencies, the ground penetration to one skin depth (ie. 37% of surface field amplitude) would be limited to a few metres or less. Due to this fact, surface radar has been found to be most useful in engineering geophysical applications such as the determination of overburden thickness, permafrost depth, water table depth and ice thickness or for locating buried cables, pipes, fractures, voids, gravels and tunnels. The high spatial resolution made available through the use of VHF/UHF frequencies can, however, justify their use in certain

geophysical environments. Where the electrical resistivity is extremely high and the dielectric losses are minimal, the useful penetration can be on the order of hundreds of metres. Pulsed radar has, for example, been found to be extremely useful in underground mapping of the salt and coal mines of the United States and Europe (Stewart, 1976, Unterberger, 1978, Coon, 1981). Penetration distances of over 1 kilometre in salt have been recorded.

The research project reported in this thesis, funded by the Department of Energy Mines and Resources Canada, developed out of previous work conducted at McGill University on VLF/LF-electromagnetic (EM) methods (see Collett and Jensen, 1981). It is recognized that in the high resistivity/low permittivity ground material which covers large areas of Canada, the substantial penetration of higher frequency electromagnetic waves would allow for more detailed subsurface mapping than is available from conventional geophysical technology. The high degree of resolution available at VHF and UHF frequencies could help in the solution of many complex problems posed in contemporary mining and in new fields such as radioactive waste disposal.

The main object of the research upon which this thesis is based is to demonstrate the feasibility of using UHF continuous-wave EM transillumination instrumentation in a typical Canadian mining environment. Although pulsed radar,

at similiar frequencies, has already enjoyed some success in specific environments, it has not been widely used in Canada. We, here, shall argue that UHF continuous-wave EM can be usefully applied in Canadian geological environments. To this end, we developed a prototype, portable UHF transmitter-receiver system and made surveys using this instrument at the Big Nickel Mine in Sudbury, Ontario to demonstrate the feasibility and advantages of the technique. We shall address in this thesis the important questions concerning transmitter power, antenna design, receiver specifications and electro-mechanical assembly. We shall consider the feasibility of producing a second-generation borehole system and discuss the problems concerning the operating frequency and effective radiated power.

1.2 Historical background

1.2.1 Absorption of radio frequency waves in earth materials

An estimate of the expected absorption rate of EM waves at a particular operating frequency is a prerequisite in judging whether the use of a radio frequency (RF) technique is justified in an exploration or mining problem. Early work on geophysical RF-EM techniques involved investigations to determine to what depth signals from a remote transmitter could penetrate the surface of the earth. Experiments by Eve and Steel (1929) at McGill University revealed that radio frequency EM waves could indeed penetrate sufficiently far to be of use in mapping small

scale structures. They conducted their experiments on radio frequency reception in the Mount Royal Tunnel, Montreal, Canada, during the late 1920's. Although signals were received through up to 90 metres of overburden and limestone, results proved inconclusive because the presence of rails, pipes and cables, which might have acted as EM waveguides, cast doubt upon the signal origin. Lee (Eve, Keys and Lee, 1929) received standard radio broadcast signals through 90 metres of overburden at Mammoth Cave, Kentucky. Silverman and Sheffet (1942) conducted similiar experiments in a coal mine near Tulsa, Oklahoma and attempted to determine the earth resistivity. Signals were successfully received through 23 metres of material.

Significant advances in electronics and measuring technology considerably boosted the amount of research into radio frequency absorption rates in natural earth materials in the early 1960's. While the majority of the studies involved the laboratory measurement of the absorption rate directly or the electrical parameters (permittivity, permeability and conductivity) from which the absorption rate can be indirectly derived, later work included more geophysically interesting in-situ measurements. An historical summary of some of the most important research into VHF/UHF-EM geophysical properties of rocks and other natural earth materials follows.

Smith-Rose (1934) conducted laboratory measurements of

the permittivities and conductivities of common soils and granite rock samples. His results show that the conductivity of the granite samples increased by several orders of magnitude, while the permittivity decreased very slightly, with frequency between 1 kHz and 10 MHz.

Von Hippel (1954) produced several tables of loss tangents and relative permittivities of a variety of materials at frequencies ranging from 100 Hz to 10 GHz. These tables, based upon laboratory measurements, were originally compiled and published as a report by the Laboratory for Insulation Research of the Massachusetts Institute of Technology in 1953. Although the vast majority of these tables list results for organic and inorganic chemical compounds, there is a small but important section concerning natural soils of varying moisture content. The measurements show that the electrical properties of the soils are strongly dependent upon their water content and can vary considerably as a function of frequency.

deBettencourt and Frazier (1962) conducted in-situ borehole measurements at 155 kHz in a fractured granite rock. The technique involved lowering a transmitter and receiver down a borehole and recording the change in signal strength as a function of transmitter-receiver separation. The attenuation factor of the medium was determined from the signal strength versus distance plot and an estimated conductivity (1.11×10^{-3} S) was calculated based upon an assumed relative permittivity value (9).

Tsao and deBettencourt (1968) measured the in-situ attenuation and phase factors of the complex propagation constant between boreholes at VLF and LF frequencies. Estimates of the bulk effective conductivities and permittivities of the medium between the two boreholes were calculated. Bulk conductivities varied between 2.5 x 10^{-3} S and 10^{-3} S at 50 kHz.

Campbell and Ulrichs (1969) measured the relative permittivities and loss tangents of dry terrestrial rock samples as a function of temperature at 450 MHz and 35 GHz. The relative permittivity did hot change significantly with measuring frequency, however, the loss tangents were generally observed to be significantly higher at 35 GHz.

Saint-Amant and Strangway (1970) measured the dielectric permittivities and loss tangents of dry rock samples as a function of temperature between 100 Hz and 1 MHz. The permittivity remained relatively constant over the frequency range, while the loss tangent was observed to decrease rapidly with increasing frequency between 100 Hz and 100 kHz.

Cook (1970) measured the electrical properties of bituminous coal samples, between 5 and 100 MHz using a capacitance test cell and an RF impedance bridge. He observed a decrease in both the resistivity and permittivity of coal as a function of frequency. Cook later (1975) conducted a series of laboratory measurements on a variety

of rock types commonly encountered in mining. He listed absorption coefficients (attenuation factor/frequency) for granite , gneiss, schist, gypsum, limestone, serpentine, monzonite, quartzite and coal over a range of frequencies from 1 to 25 MHz. Radar probing distances for these rock types were calculated. He showed that the radar probing distances for the coal samples decreased rapidly with increasing frequency after 10 MHz. The granite , limestone and schist samples exhibited a much less pronounced decrease in probing distance as a function of frequency.

Grubb and Wait (1971) measured the in-situ complex propagation constant of granite, between 1 MHz and 10 MHz, with a dual borehole receiver system. The effective conductivity and permittivity of the granite were calculated from the attenuation and phase factors. The conductivity was found to increase from 0.93×10^{-3} S/m to 1.75×10^{-3} S/m while the relative permittivity decreased from 16.2 to 8.4 over the frequency range.

Hoekstra and Delaney (1974) measured the complex dielectric permittivity as a function of frequency and water content for various common soils. Results were similiar to those reported by Von Hippel (1954), the permittivity and loss tangent decreased as the measuring frequency increased. A minimum in the loss tangent was observed at 100 MHz, after which it increased slightly and then levelled off.

Lytle et al. (1976) measured relative dielectric permittivities and plane-wave skin depths between probes

down adjacent boreholes. The tests, carried out within hard rock in a permafrost environment, were conducted over a range of frequencies between 5 and 50 MHz. Relative permittivities varied between 5 to 30 and skin depths varied between 10 and 140 metres. Lytle and Lager (1976) measured the in situ conductivity, using a continuous-wave system, and the dielectric permittivity, using a swept frequency technique, in tunnel rock between 3 and 50 MHz. Bulk conductivities of 2×10^{-3} S/m to 5×10^{-3} S/m and relative permittivities of 5 to 7 were recorded.

Grubb et al. (1976) measured the in-situ complex propagation constant, in a granite medium, over the frequency range 300 kHz to 25 MHz using both a dual receiver downhole system and a single hole mutual impedance system. The calculated effective conductivities and permittivities were similar in both cases and agreed well with the results from laboratory measurement of hand samples. The measured relative permittivities varied from 9.5 to 7.5 over the frequency range.

Annan and Davis (1976) determined the in-situ dielectric permittivity of frozen clay and silt soils and ice using a pulsed radar (150 MHz center frequency) in a wide angle reflection and refraction (WARR) sounding. Measured relative permittivities varied between 2 and 4.

1.2.2 Pulsed radar techniques

The development of radar during the Second World War regenerated interest in using radio frequency waves for geophysical applications. Haycock, Madsen and Hurst (1949) and Prichett (1952), among others, considered the possibility of adapting radar techniques to the search for oil. Prichett measured the radio wave absorbtion rate in shale by lowering a transmitter and receiver down parallel boreholes. He calculated an attenuation rate of approximately .61 dB/m at 1.652 MHz. Given the performance specifications of his apparatus this corresponds to a maximum penetration distance of only 18.3 metres, considerably short of the several hundred metres required for petroleum exploration.

The development of compact lightweight and improved radar components in the early 1960's stimulated renewed attempts to apply the impulse radar technique to geophysical problems. Harrison (1970), Weber and Andrieux (1970), Watts and England (1976) and Narod and Clarke (1980) developed airborne radar systems for measuring ice thickness and for determining subglacial relief in polar, glacial and northern coastal regions. Operating frequencies typically range between 10 MHz and 1 Ghz depending on the desired penetration depth and the electrical properties of the ice. Reflections through 2 kilometres of ice have been obtained with the lower frequency systems (Waite, 1966). The higher frequency systems cannot easily penetrate more than 100

metres of warm or dirty ice (Narod and Clarke, 1980).

Pulsed radar has become an important geophysical tool in the salt mining industry. The loss tangent of salt exhibits a minimum between 1 MHz and 100 MHz while its permittivity is relatively constant between 1 kHz and 1 GHz. Its low absorption loss at VHF/UHF frequencies and the high degree of homogeneity which salt usually exhibits allows sufficient radar penetration to detect discontinuities, anhydrite zones, salt-cap rock boundaries and brine cavities in advance of mining. Varying the frequency of operation allows the option of changing the resolution and probing distance to suit local conditions. Unterberger (1978) reports detection distances underground of up to 1400 metres using a portable 230 MHz system with a 20 kW peak power output. Stewart and Unterberger (1976), Unterberger (1978), Tarantolo and Unterberger (1978) and Nickel et al. (1983) have all developed and extensively used radar systems underground in salt domes. Tarantolo and Unterberger (1978) worked on a procedure for detecting flooded boreholes in advance of underground mining. Unterberger (1974) considered the possibility of developing a laser radar (1-8 micrometre wavelength) for use in probing within salt. Nickel et al. (1980) developed a borehole reflection sonde for logging within salt domes. Radar has also been successfully used underground in potash mines to map sylvite/anhydrite or sylvite/clay boundaries (Kyle et al.,

1983).

The relative homogeneity and moderate RF losses of coal allow for useful radar measurements in coal mines. Cook (1970) measured the RF properties of freshly collected bituminous coal samples and determined that penetration distances of the order of 50 metres at 100 MHz were feasible. Coon et al. (1981) detected reflections from targets buried within 15 metres of coal at frequencies ranging from 20 MHz to 500 MHz. They were also able to locate a 15 centimetre diameter borehole 6 metres within a coal pillar.

Fowler (1981) successfully mapped clay veins within coal pillars and small water-filled fractures adjacent to coal drifts using a radar system operating with a 350 MHz center-frequency pulse. Reflections were obtained through 10 metres of coal. Fowler and Hale (1980) conceived a prototype synthetic pulsed radar system which instead of transmitting a broadband pulse, transmits the frequency spectrum of such a pulse. The technique promised to combine the advantages of pulse and continuous-wave EM methods while exhibiting none of the limiting features of the respective systems. A transmission test showed that the prototype unit could receive a signal through 60 metres of coal.

Radar systems are currently being used in several engineering applications where great penetration distances are not necessary. GSSI (1981) manufactures a surface radar system used for mapping shallow overburden features.

Oyo Corporation (1984) manufactures a similiar system. Both systems have a center frequency of 120 MHz. Xadar (1981) manufactures the synthetic-pulse radar system, described above, which can be adapted to surface or underground use. A-Cubed (Davis et al., 1984a) manufactures a portable, ground pulsed radar system.

Rossiter et al. (1975) used the radio interferometry technique developed by Annan (1973) to estimate depths and permittivities of dielectric layers in an ice field. Owen and Suhler (1980, 1981) developed a dual borehole pulse propagation system to detect soil sinkholes and solution cavities in karst terrain.

Surface radar has been used to map ground water flow (Davis et al., 1984b) and soil stratigraphy (Davis et al., 1984a). Borehole radar has been used in hydrological studies to detect voids and fractures (Davis et al., 1984b). Moffatt and Puskar (1976) developed an underground radar to detect voids and faults in soft-rock environments.

Wright et al. (1984) developed a borehole radar which is used in testing for structural features and inhomogeneities in rock masses proposed as nuclear waste disposal sites.

Jezek (1985) used the Scott Polar research Institute (S.P.R.I.) Mark II radar to map the descent of boreholes in glaciers. A passive radar target was lowered down the borehole and tracked from three surface radar stations. The

results from the radar measurements were found to be in good agreement with the borehole geometry as determined from a conventional inclinometer survey.

Pulsed radar has been employed as a mapping tool in archeological studies. Dolphin et al. (1974) developed a portable system for locating underground chambers. Dolphin et al. (1978) used an improved version of their original radar system to probe an abandoned and partially caved-in mine working from the surface.

The relatively low absorption rate of electromagnetic energy in permafrost makes it a suitable candidate for radio frequency EM work. Impulse radar has been used in permafrost mapping (Annan and Davis, 1976; Judge, 1985).

Annan and Davis (1977) have compiled a list of radar ranges and performance specifications for the radars described in the literature up to that time.

1.2.3 Continuous wave electromagnetics

Continuous-wave VHF/UHF electromagnetics has been used considerably less in geophysics than pulsed radar. There are currently no commercial manufacturers of VHF/UHF continuous-wave EM geophysical equipment in North America. All systems discussed thus far in the literature have been developed by the authors for a specific task. The Russian radio-wave absorption technique (Buselli, 1980) has been used in the Far East and Eastern Block countries. The method consists of measuring the decay of the field from a

dipole antenna and comparing it to the theoretically calculated field decay in free space. Kaspar and Pecen (1975) developed a three frequency (2, 5, 8 MHz) system to detect caves in a karst environment. Rao and Rao (1983) used a 1 MHz underground radio-wave absorption system in a copper mine.

Many of the continuous-wave EM surveys described in the literature were conducted to measure the electrical properties of specific materials. Examples outlined in section 1.2.1 above include Lytle et al. (1976), Grubb et al. (1976) and Lytle and Lager (1976). The latter researchers investigated the possible modes of propagation between an underground transmitter and receiver, operating between 3 and 50 MHz, in a system of interconnecting vehicular tunnels. Tsao and deBettencourt (1968) measured the relative received signal strengths, at VLF and LF frequencies, due to the through-rock and up-over-down propagation paths between a transmitter and receiver lowered down two widely separated boreholes.

Renewed interest in continuous-wave EM systems has been encouraged by the need to solve the problems of radioactive waste disposal. Several groups in North America are currently involved in studies into RF geophysical techniques for use in determining the structural integrity of a rock mass. Likewise the use of RF techniques in advance of mining is generating considerable interest.

1.3 Outline of the thesis

Following in chapter 2 we shall develop and discuss the necessary theory of VHF/UHF electromagnetics. The electrical properties of natural earth materials are examined and the theoretical rates of absorption of electromagnetic energy for several common materials are calculated. The effect of the conductivity, permittivity, permeability and operating frequency on the absorption rate of a material is examined. The problems of impedance matching and reflection, refraction and diffraction at the air-wall rock interface is discussed. Methods for the processing of continuous-wave transillumination data are examined.

In chapter 3, we discuss the continuous-wave instrumentation developed by previous researchers and describe the instrumentation which has been conceived and designed for the purpose of this research. The performance characteristics of the instrumentation are discussed.

In chapter 4, we discuss the desired characteristics of a test survey area and the layout and geology of the test area chosen, the Big Nickel Mine in Sudbury, Ontario. The results of the two field seasons are presented and discussed. Approximate effective conductivities are calculated from the measured absorption rate data.

In chapter 5, we deal with electrical property measurements of rocks. The techniques for taking DC and AC

resistivity measurements are examined. The instrumentation for conducting DC resistivity and AC effective resistivity and permittivity measurements on core samples is presented. The limitations and potential problems associated with the techniques are examined. The results of measurements on several core samples collected in and around the transillumination field-survey site are presented. The results are compared with the calculated resistivities from the transillumination survey and the results of previous researchers.

In chapter 6, we present the conclusions derived from this research work, offer recommendations for further research on the subject and make the necessary claim for originality.

Chapter 2

Theory

2.1 Plane wave analysis

The theory of electromagnetic wave propagation is based upon Maxwell's four equations:

$$\nabla \cdot \mathbf{D} = \rho \qquad \text{(Coulomb's Law)} \qquad (2.1.1)$$

$$\nabla \cdot \mathbf{B} = 0 \qquad \text{(Gauss' Law)} \qquad (2.1.2)$$

$$\nabla \times \mathbf{E} = -\partial \mathbf{B}/\partial t \qquad \text{(Faraday's Law)} \qquad (2.1.3)$$

$$\nabla \times \mathbf{H} = \mathbf{J} + \partial \mathbf{D}/\partial t \qquad \text{(Ampere's Law)} \qquad (2.1.4)$$

The expressions for an electromagnetic wave propagating in linear, isotropic, homogeneous and stationary media derive directly from these equations. Above and following, the notation used in developing the basic theory is:

$\mathbf{D}$ = electric displacement	(coulomb/metre^2)
$\mathbf{E}$ = electric field intensity	(volt/metre)
$\mathbf{B}$ = magnetic induction	(tesla)
$\mathbf{H}$ = magnetic field intensity	(ampere/metre)
$\mathbf{J}$ = electric current density	(ampere/metre^2)
$\mathbf{J}_f$ = free electric current density	(ampere/metre^2)
σ_f = free charge density	(coulomb/metre^3)
ε = electric permittivity	(farad/metre)
ε_0 = permittivity of free space	(farad/metre)

κ_ε = relative permittivity

μ = magnetic permeability (henry/metre)

μ_0 = permeability of free space (henry/metre)

κ_μ = relative permeability

σ = conductivity (Siemens/metre)

ρ = resistivity (ohm-metre)

ω = angular frequency (radian/second)

j = square root of negative unity

The material properties of the medium determine relationships between various of these vector fields in Maxwell's equations; in linear, homogeneous and isotropic media

$$D = \varepsilon E \qquad H = B/\mu \qquad J = \sigma E$$

where ε, σ and μ are scalar constants.

Invoking the above conditions equations 2.1.3 and 2.1.4 can be rewritten as:

$$\nabla \times E = -\mu \partial H/\partial t \tag{2.1.5}$$

$$\nabla \times H = \sigma E + \varepsilon \partial E/\partial t \tag{2.1.6}$$

Taking the curl of (2.1.6) and substituting the result in (2.1.5), the wave equations for E and H are derived:

$$\nabla^2 E - \mu\sigma \partial E/\partial t - \mu\varepsilon \partial^2 E/\partial t^2 = \emptyset \tag{2.1.7}$$

$$\nabla^2 H - \mu\sigma \partial H/\partial t - \mu\varepsilon \partial^2 H/\partial t^2 = \emptyset. \tag{2.1.8}$$

For sinusoidal fields these equations obtain

$$\nabla^2 E - j\omega\mu\sigma E + \omega^2\mu\varepsilon E = \emptyset \tag{2.1.9}$$

$$\nabla^2\mathbf{H} - j\omega\mu\sigma\ \mathbf{H} + \omega^2\mu\varepsilon H = \emptyset. \qquad (2.1.1\emptyset)$$

The second and third terms represent the electrical conduction and displacement terms respectively. The free charge density in a linear and isotropic medium can usually be assumed to be zero, under the conditions likely to be met in any conceivable geologic medium, as any imposed charge density must decay fairly rapidly (Lorrain and Corson, 197Ø). A plane wave is defined as one in which the direction of propagation is everywhere the same and the amplitude is constant along any wavefront. The vectors E and H are transverse to the propagation direction and are orthogonal to one another. In the case of a linearly polarized wave propagating in the positive z direction, with E directed along the x-axis, the solutions to equations 2.1.9 and 2.1.1Ø are

$$\mathbf{E} = E_{\emptyset}\exp(j\omega t - \gamma z)\ \hat{i} \qquad (2.1.11)$$

$$\mathbf{H} = H_{\emptyset}\exp(j\omega t - \gamma z)\ \hat{j} \qquad (2.1.12)$$

where γ is defined as the complex constant of propagation.

$$\gamma^2 = j\omega\sigma\mu + j^2\omega^2\mu\varepsilon$$

$$\gamma = j\omega\sqrt{\mu(\varepsilon - j\sigma/\omega)} \qquad (2.1.13)$$

Figure 2.1.1 illustrates the case of a plane wave travelling through a conductive medium. In free space the E and the H fields are in phase.

γ is generally a complex function of the

electromagnetic material parameters σ, ε and μ and the frequency, ω, of form:

$$\gamma = \alpha + j\beta \qquad (2.1.14)$$

Equations 2.1.11 and 2.1.12 can then be rewritten

$$\mathbf{E} = E \exp\{j(\omega t - \beta z) - \alpha z\}\, \hat{i} \qquad (2.1.15)$$

$$\mathbf{H} = H \exp\{j(\omega t - \beta z) - \alpha z\}\, \hat{j} \qquad (2.1.16)$$

The amplitudes and phases of the fields are controlled by the exponents αz and βz respectively. α is the attenuation factor expressed in nepers per metre and β is the phase factor expressed in radians per metre. Examination of equations 2.1.15 and 2.1.16 indicates that, locally the amplitude of a plane electromagnetic wave is dependent upon α and the phase is dependent upon β.

The vector cross product $\S = \mathbf{E} \times \mathbf{H}$ points in the direction of propagation. The total outward flow of energy per unit time through a surface is

$$P = \iint \S \cdot \mathbf{ds} \qquad (2.1.17)$$

$\S$ is commonly called the Poynting vector, $\mathbf{ds} = s \cdot n$ where n is the unit normal to the surface. The real average power flow through a surface is

$$P_{av} = (1/2)\mathrm{Re} \iint \S \cdot \mathbf{ds} \qquad (2.1.18)$$

2.2 Absorption of electromagnetic radiation

The major factor limiting the widespread use of radio-frequency (RF) waves in geophysics is the high rate of absorbtion of their energy in most natural earth materials. This limits their effective penetration and thus their useful geophysical "probing distance". The attenuation and phase factors of sinusoidal plane electromagnetic waves travelling through linear, isotropic, homogeneous and stationary media are described by the real and imaginary components of the complex propagation constant . The absorption rate of electromagnetic waves shall be defined as equivalent to the attenuation factor. Taking into account the complex nature of the conductivity, permittivity and permeability the propagation constant can be expressed as:

$$\gamma = j\omega \sqrt{\mu^* (\varepsilon^* - j\sigma^*/\omega)} = \alpha + j\beta \qquad (2.2.1)$$

where:

$\mu^* = \mu^*(\omega) = \mu' + j\mu''$, $\varepsilon^* = \varepsilon^*(\omega) = \varepsilon' + j\varepsilon''$ and $\sigma^* = \sigma^*(\omega) = \sigma' + j\sigma''$.

The resistivity is defined as,

$$\rho^*(\omega) = 1/\sigma^*(\omega) = \rho' - j\rho''$$

Separating γ into real and imaginary components:

$$\alpha = \omega \sqrt{\frac{ab}{2}\{(1 + \tan^2\phi)^{1/2} - 1\}} \qquad (2.2.2)$$

$$\beta = \omega \sqrt{\frac{ab}{2}\{(1 + \tan^2\phi)^{1/2} + 1\}} \qquad (2.2.3)$$

where the loss tangent of the medium is defined as

$$\tan\phi = c/b \qquad (2.2.4)$$

and

$$a = 1 \qquad (2.2.5)$$

$$b = \mu'' (\sigma'/\omega + \varepsilon'') + \mu' (\varepsilon' + \sigma''/\omega) \qquad (2.2.6)$$

$$c = -\mu'' (\varepsilon'' - \sigma'/\omega) + \mu'(\varepsilon' - \sigma''/\omega) \qquad (2.2.7)$$

In the simplest case, setting the imaginary components of the electromagnetic material parameters equal to zero, equations 2.2.2 to 2.2.4 reduce to:

$$\alpha = \omega \sqrt{\frac{\mu'\varepsilon'}{2} \{ (1 + \tan^2\phi)^{1/2} - 1)} \qquad (2.2.8)$$

$$\beta = \omega \sqrt{\frac{\mu'\varepsilon'}{2} \{ (1 + \tan^2\phi)^{1/2} + 1)} \qquad (2.2.9)$$

$$\tan\phi = \sigma' / \omega\varepsilon' \qquad (2.2.10)$$

Equation 2.2.10 is the standard definition of the loss tangent as found in the geophysical literature (Wait, 1971). The skin depth is defined as that distance at which the field amplitudes are reduced to 1/e or 36.8% of their original values. Equations 2.1.15 and 2.1.16 indicate this occurs at the depth $z = \delta$ so that:

$$\alpha \cdot \delta = 1$$

or

$$\delta = 1/ \alpha \qquad (2.2.11)$$

where δ is the skin depth in metres and α is measured in nepers per metre. At one skin depth the attenuation is equivalent to -8.686 decibels (dB), that is, one neper is

equal to 8.686 dB. The absorption loss, in decibels, is defined as

$$\mathcal{A}_{abs}\ (dB) = 8.686\alpha_{abs}\, r \qquad (2.2.12)$$

where r is the distance, in metres, traversed in a medium of attenuation factor α.

A plane sinusoidal waveform can be described by

$$x(t) = x_0 \exp j(\omega t - kz)$$
$$= x_0 \exp\{j(\omega t - k'z) - k''z\} \qquad (2.2.13)$$

where $k = k' - jk''$ is the circular wave number. The phase velocity is, then

$$v = \omega / k' \qquad (2.2.14)$$

and the wavelength in the medium,

$$\lambda = 2\pi/k' \qquad (2.2.15)$$

In comparing (2.2.13) to either (2.1.11) or (2.1.12) we find that

$$\gamma = jk \qquad (2.2.16)$$

and that

$$v = \omega/\beta \qquad (2.2.17)$$

and

$$\lambda = 2\pi/\beta \qquad (2.2.18)$$

In free space equations 2.2.17 and 2.2.18 reduce:

$$v = 1/\sqrt{\varepsilon_0\mu_0} = c \qquad (2.2.19)$$

and

$$\lambda = 2\pi/\omega\sqrt{\varepsilon_0\mu_0} \qquad (2.2.20)$$

where c is the speed of light. The index of refraction n = c/v. In a linear homogenous, isotropic and stationary medium,

$$n = c\,\beta/\omega = c\sqrt{\frac{ab}{2}\{(1 + \tan^2\phi)^{1/2} + 1\}} \quad . \qquad (2.2.21)$$

Equation 2.2.2 shows that the rate of decrease in the field amplitudes is strongly dependent upon the loss tangent of the medium. In the simple case, shown by equations 2.2.8 to 2.2.10, the loss tangent is a function of ε, σ and μ. A more general solution for α and β can be derived by making the simplifying assumption that $\mu'' = 0$, which will be the case in most instances (Olhoeft and Strangway, 1974). Equations 2.2.2 to 2.2.4 then reduce to:

$$\alpha = \omega\sqrt{\mu'(\varepsilon' + \sigma''/\omega)\{(1 + \tan^2\phi)^{1/2} + 1\}} \qquad (2.2.22)$$

$$\beta = \omega\sqrt{\mu'(\varepsilon' + \sigma''/\omega)\{(1 + \tan^2\phi)^{1/2} - 1\}} \qquad (2.2.23)$$

$$\tan\phi = \frac{\sigma' - \omega\varepsilon''}{\omega(\varepsilon' + \sigma''/\omega)} \qquad (2.2.24)$$

The following analogy can then be taken in comparing equations 2.2.24 and 2.2.10:

$$\sigma_{ef} = \sigma' - \omega\,\varepsilon'' \qquad (2.2.25)$$

$$\varepsilon_{ef} = \varepsilon' + \sigma''/\omega \qquad (2.2.26)$$

or $$\rho_{ef} = |\rho''|^2/\rho' - \varepsilon''|\rho''|^2\omega \qquad (2.2.27)$$

Equations 2.2.25 and 2.2.26 define respectively the effective conductivity and effective permittivity. The dielectric conductivity and the conductive permittivity are respectively defined as

$$\sigma_\varepsilon = -\omega\varepsilon'' \qquad (2.2.28)$$

and

$$\varepsilon_\sigma = \sigma''/\omega \qquad (2.2.29)$$

At any one frequency the imaginary components of the permittivity and conductivity masquerade as a real conductivity and permittivity respectively. The measured values for conductivity and permittivity found in the literature are usually, in fact, the effective conductivity and effective permittivity respectively. In addition the effective permittivity measurement is generally only valid if the permeability of the material is equivalent to that of free space. Current geophysical theory describes the conductivity, permittivity and permeability as frequency-dependent, complex-valued parameters of a geological material. That is:

$\sigma^* = \sigma^*(\omega)$, $\varepsilon^* = \varepsilon^*(\omega)$ and $\mu^* = \mu^*(\omega)$

The separation of measured permittivity and conductivity values into their complex frequency dependent components is extremely difficult and can only be achieved by assuming a (geo)physical model for their behavior and solving the resulting inverse problem (Baranyi, 1984).

Equations 2.2.22 to 2.2.24 can be rewritten as:

$$\alpha = \omega \sqrt{\mu \varepsilon_{ef} \; \{(1 + \tan^2\phi)^{1/2} - 1\}} \qquad (2.2.30)$$

$$\beta = \omega \sqrt{\mu \varepsilon_{ef} \; \{(1 + \tan^2\phi)^{1/2} - 1\}} \qquad (2.2.31)$$

$$\tan \phi = \sigma_{ef} / \varepsilon_{ef} \omega \qquad (2.2.32)$$

2.3 Absorption of electromagnetic waves in common earth materials

The rate of absorption of electromagnetic waves in real materials can be determined either through direct measurement or by calculation of the attenuation factor, α. The direct method involves measuring the reduction in signal level of an electromagnetic wave as it traverses a known distance of material. This is, in fact, the most accurate method of measuring the absorption rate and is the approach taken in the author's field work. An in-situ field measurement is best as bulk samples measured in the laboratory can suffer alteration in the process of transportation. Furthermore, the measure of a small sample cannot easily be extended to larger volumes of material.

The calculation technique requires that the electrical parameters of the material be known. The rate of absorption of electromagnetic waves depends upon the electrical properties of the medium in which they are propagating. Examination of equation 2.2.8, above, indicates that the attenuation factor (and thus the absorption rate) at any frequency is a function of the permeability, permittivity

Material	Conductivity σ (S/m) range	average	Permittivity K_ϵ range	average	refer.
Permafrost	10^{-5}-10^{-2}	$.5\times10^{-3}$	4-8	6	1
Fresh water	10^{-4}-3×10^{-2}	4.85×10^{-3}		81	1
Clay, water saturated	.1-1	.45	8-12	10	1
Silt, water saturated	10^{-3}-10^{-2}	.045		10	1
Granite (dry)		10^{-8}		5	1
Limestone		10^{-9}		7	1
Sea water		4		81	1
Air		0		1	2
Ice		4.8×10^{-4}		3.2	3
Snow		2.4×10^{-5}		1.2	3
Sandy soil, dry		4.27×10^{-4}		2.55	3
Sandy soil, 2-18% water		1.09×10^{-3}		2.5	3
Clay soil, dry		7.98×10^{-4}		2.38	3
Clay soil, 20% water		1.74×10^{-1}		20.0	3
Loamy soil, dry		2.69×10^{-4}		2.47	3
loamy soil, 13% water		5.36×10^{-2}		20.0	3

Reference:
1 Morey (1974)
2 Lorrain and Corson (1970)
3 Von Hippel (1954)

Table 2.3.1 Approximate electrical conductivities and relative permittivities of various common materials at VHF/UHF frequencies.

ROCK TYPE	σ (S/m)	κ_ϵ	TAN δ	ABSORPTION (dB/m)
ANDESITE	.510E-03	5.1	.400E-02	.370E+00
ANORTHOSITE	.136E-02	6.8	.800E-02	.855E+00
BASALT	.401E-02	8.9	.180E-01	.220E+01
BASALT	.601E-02	8.0	.300E-01	.348E+01
BASALT, AMYGDALOIDAL	.252E-02	7.2	.140E-01	.154E+01
BASALT, HORNBLENDE	.218E-02	6.7	.130E-01	.138E+01
BASALT, LEUCITE-NEPHELINE	.144E-02	5.6	.103E-01	.999E+00
BASALT, OLIVINE	.345E-02	8.1	.170E-01	.198E+01
BASALT PORPHYRY, OLIVINE	.328E-02	8.2	.160E-01	.188E+01
BASALT, THEOLEIITIC	.216E-01	9.6	.900E-01	.114E+02
BASALT, VESICULAR	.298E-02	7.0	.170E-01	.184E+01
GABBRO, BYTOWNITE	.350E-02	7.0	.200E-01	.217E+01
GRANITE, ALKALI	.442E-02	5.2	.340E-01	.318E+01
GRANITE, APLITE	.247E-02	5.2	.190E-01	.178E+01
GRANITE, BIOTITE	.946E-03	5.4	.700E-02	.666E+00
GRANITE, GRAPHIC	.500E-03	5.0	.400E-02	.366E+00
GRANITE, HORNEBLENDE	.150E-02	6.0	.100E-01	.100E+01
GRANITE, PORPHORITIC BIOT	.151E-02	5.5	.110E-01	.106E+01
OBSIDIAN	.221E-01	6.8	.130E+00	.139E+02
OBSIDIAN	.184E-02	5.5	.134E-01	.129E+01
PERIDOTITE, MICA	.510E-02	6.0	.340E-01	.341E+01
PERIDOTITE, OLIVINE	.155E-02	6.2	.100E-01	.102E+01
PERIDOTITE/SERPENTINE	.150E-01	7.5	.800E-01	.897E+01
PHONOLITE	.488E-02	6.5	.300E-01	.313E+01
PUMICE	.438E-03	2.5	.700E-02	.453E+00
RHYOLITE	.127E-02	3.4	.150E-01	.113E+01
SERPENTINE	.333E-02	7.0	.190E-01	.206E+01
SERPENTINE	.176E-02	6.4	.110E-01	.114E+01
SYENITE, AUGITE	.100E-01	8.0	.500E-01	.579E+01
TRACHYTE	.325E-02	5.0	.260E-01	.238E+01
TUFF, GREY	.916E-02	6.1	.600E-01	.607E+01
TUFF, RHYOLITIC	.540E-03	3.6	.600E-02	.466E+00
TUFF, SEMI-WELDED	.716E-03	2.6	.110E-01	.727E+00
VOLCANIC ASH	.596E-02	3.4	.700E-01	.528E+01
VOLCANIC ASH SHALE	.203E-02	2.7	.300E-01	.202E+01

Table 2.3.2 : Approximate electrical conductivities and relative permittivities of various common rock types at 450 MHz (after Campbell and Ulrichs, 1969).

	FREQUENCY (MHz)			
1.000	10.000	100.000	300.000	1000.000
permafrost				
.2823D+00	.3331D+00	.3340D+00	.3341D+00	.3341D+00
fresh water				
.8806D-01	.8819D-01	.8819D-01	.8819D-01	.8819D-01
fresh water saturated clay				
.1157D+02	.3639D+02	.1089D+03	.1673D+03	.2178D+03
fresh water saturated silt				
.3639D+01	.1089D+02	.2178D+02	.2308D+02	.2327D+02
granite				
.7319D-05	.7319D-05	.7319D-05	.7319D-05	.7319D-05
limestone				
.6186D-06	.6186D-06	.6186D-06	.6186D-06	.6186D-06
sea water				
.3660D+02	.1152D+03	.3483D+03	.5470D+03	.7449D+03
air				
.0000D+00	.0000D+00	.0000D+00	.0000D+00	.0000D+00
ice				
.3155D+00	.4353D+00	.4391D+00	.4391D+00	.4391D+00
snow				
.3531D-01	.3585D-01	.3585D-01	.3585D-01	.3585D-01
sandy soil dry				
.3030D+00	.4328D+00	.4376D+00	.4376D+00	.4376D+00
sandy soil 2-18% water				
.5341D+00	.1051D+01	.1116D+01	.1117D+01	.1117D+01
clay soil 20% water				
.7178D+01	.2205D+02	.5328D+02	.6173D+02	.6348D+02
clay soil dry				
.4490D+00	.8131D+00	.8461D+00	.8465D+00	.8465D+00
loamy soil dry				
.2215D+00	.2788D+00	.2801D+00	.2801D+00	.2801D+00
loamy soil 13% water				
.3955D+01	.1140D+02	.1910D+02	.1955D+02	.1961D+02

Table 2.3.3 : Absorption rates (dB/m) for the materials listed in Table 2.3.1, at various VHF/UHF frequencies.

LIMESTONE	1.00031	SANDSTONE	1.00038
SHALE	1.00063	QUARTZITE	1.0044
GRANITE	1.0025	GABBRO	1.075
BASALT	1.075	ANDESITE	1.167
COAL	1.00003	ROCK SALT	0.99999
GRAPHITE	0.99989	PYRRHOTITE	2.57
MAGNETITE	7.28		

TABLE 2.3.4 : RELATIVE PERMEABILITIES OF VARIOUS ROCKS AND MINERALS.

FREQUENCY	.100E+03	.100E+04	.100E+05	.100E+06	.100E+07	.100E+08	.300E+09	.300E+10	.100E+11
SANDY SOIL DRY									
CONDUCTIVITY (S/m)	.373E-08	.129E-07	.520E-07	.295E-06	.245E-05	.227E-04	.425E-03	.264E-02	.506E-02
PERMITTIVITY	3.420	2.910	2.750	2.650	2.590	2.550	2.550	2.550	2.530
LOSS TANGENT	.196E+00	.800E-01	.340E-01	.200E-01	.170E-01	.160E-01	.100E-01	.620E-02	.360E-02
ABSORPTION (dB/m)	.328E-05	.124E-04	.513E-04	.296E-03	.249E-02	.233E-01	.436E+00	.270E+01	.521E+01
SANDY SOIL 2-18% WATER									
CONDUCTIVITY (S/m)	.115E-07	.197E-07	.778E-07	.417E-06	.348E-05	.348E-04	.108E-02	.125E-01	.904E-01
PERMITTIVITY	3.230	2.720	2.500	2.500	2.500	2.500	2.500	2.500	2.500
LOSS TANGENT	.640E+00	.130E+00	.560E-01	.300E-01	.250E-01	.250E-01	.260E-01	.300E-01	.650E-01
ABSORPTION (dB/m)	.190E-04	.195E-04	.806E-04	.432E-03	.360E-02	.360E-01	.112E+01	.130E+02	.935E+02
LOAMY SOIL DRY									
CONDUCTIVITY (S/m)	.119E-08	.787E-08	.524E-07	.434E-06	.253E-05	.193E-04	.268E-03	.448E-03	.190E-02
PERMITTIVITY	3.060	2.830	2.690	2.600	2.530	2.480	2.470	2.440	2.440
LOSS TANGENT	.700E-01	.500E-01	.350E-01	.300E-01	.180E-01	.140E-01	.650E-02	.110E-02	.140E-02
ABSORPTION (dB/m)	.111E-05	.766E-05	.523E-04	.440E-03	.261E-02	.201E-01	.279E+00	.469E+00	.199E+01
CLAY SOIL DRY									
CONDUCTIVITY (S/m)	.316E-08	.263E-07	.218E-06	.155E-05	.929E-05	.543E-04	.794E-03	.568E-02	.156E-01
PERMITTIVITY	4.730	3.940	3.270	2.790	2.570	2.440	2.380	2.270	2.160
LOSS TANGENT	.120E+00	.120E+00	.120E+00	.100E+00	.650E-01	.400E-01	.200E-01	.150E-01	.130E-01
ABSORPTION (dB/m)	.237E-05	.216E-04	.197E-03	.152E-02	.948E-02	.569E-01	.843E+00	.617E+01	.174E+02

FREQUENCY	.100E+06	.100E+07	.100E+08	.100E+09	.300E+09	.300E+10	.100E+11	.250E+11
WATER 1.5 C								
CONDUCTIVITY (S/m)	.919E+00	.919E+00	.968E+00	.339E+02	.462E+03	.416E+05	.218E+06	.886E+05
PERMITTIVITY	87.000	87.000	87.000	87.000	86.500	80.500	38.000	15.000
LOSS TANGENT	.190E+04	.190E+03	.200E+02	.700E+02	.320E+03	.310E+04	.103E+05	.425E+04
ABSORPTION (dB/m)	.523E+01	.165E+02	.524E+02	.998E+03	.642E+04	.193E+06	.805E+06	.813E+06
WATER 25 C								
CONDUCTIVITY (S/m)	.174E+01	.174E+01	.200E+01	.217E+02	.207E+03	.201E+05	.165E+06	.125E+06
PERMITTIVITY	78.200	78.200	78.200	78.000	77.500	76.700	55.000	34.000
LOSS TANGENT	.400E+04	.400E+03	.460E+02	.500E+02	.160E+03	.157E+04	.540E+04	.265E+04
ABSORPTION (dB/m)	.720E+01	.227E+02	.764E+02	.796E+03	.429E+04	.134E+06	.702E+06	.966E+06

TABLE 2.3.5 ABSORPTION RATES FOR COMMON SOILS AND WATER AS CALCULATED FROM THEIR ELECTRICAL PROPERTIES.

Frequency (kHz)	1	100	1,200	10,000
Granite S.1				
conductivity	.0009	.007	.028	.11
relative permittivity			12	8.5
Granite S.2				
conductivity	.0007	.005	.019	.095
relative permittivity			10	7.5
Granite S.3				
conductivity	.0039	.021	.011	.050
relative permittivity			9.5	7.5
Granite S.4				
conductivity	.000015	.0009	.0024	.015
relative permittivity			7.0	6.5
Granite S.6				
conductivity	.00003	.00026	.0016	.0070
relative permittivity			6.0	6.0

Table 2.3.6 Laboratory measured conductivities and permittivities of granite rock samples as a function of frequency (after Smith-Rose, 1934).

and electrical conductivity of the medium of propagation. Given measured values of the above three electrical parameters, for any material, one can calculate the absorption rate of electromagnetic waves in that material medium as a function of frequency. Tables 2.3.1 and 2.3.2 are a compilation, from several sources, of measured electrical conductivities and permittivities of common earth materials at radio frequencies. The electrical parameters listed in Table 2.3.2 were measured at 450 MHz. The measuring frequencies for the data listed in Table 2.3.1 are unavailable for the data from Morey (1974). The absorption rates for these materials, at several frequencies across the band of interest, are calculated from equation 2.2.8 and listed in Table 2.3.3. Several assumptions have been made in this calculation.

First, the permeability in each case is assumed to be equal to that of free space, μ_0. This is generally a valid assumption for most common geologic materials. Table 2.3.4 lists the value of the relative permeability, κ_μ, for several such materials. Note that for most materials listed, the relative permeability does not differ significantly from that of free space. No attempt has been made to decompose the permeabilities into their complex valued components.

Second, the measured electrical conductivities and permittivities listed in Tables 2.3.1 and 2.3.2 are assumed to be real valued. Given a real valued permeability, the

imaginary component of the conductivity or permittivity will be reflected in the real component of the other as discussed in section 2.2 (equations 2.2.25 to 2.2.29).

Third, the electrical parameters listed in Table 2.3.1 are assumed independent of frequency within the VHF/UHF band. This is not necessarily the case however. Saint-Amant and Strangway measured the electrical parameters as a function of frequency and temperature for dry, powered and solid rock samples. Figures 2.3.1 and 2.3.2 show curves of relative permittivity and loss tangent versus frequency for solid basalt and granite samples respectively. The permittivity is relatively independant of frequency between 100 Hz and 1 MHz for samples measured at surface temperature (27-32 C). The conductivity, as calculated from the loss tangent, decreases with increasing frequency. Von Hippel (1954) has compiled data on the measured permittivities and loss tangents, for various organic and inorganic materials, in the frequency range 100 Hz to 10 GHz. Table 2.3.5 summarizes Von Hippels data for those materials which are geophysically interesting. The conductivities are calulated from equation 2.2.10 using Von Hippel's values for loss tangent and permittivity. In the case of water, the conductivity increases and the permittivity then decreases with frequency between 100 kHz and 10 GHz. Because of this, the absorption rate for water increases with frequency in this frequency range. In fact, water exhibits an extremely

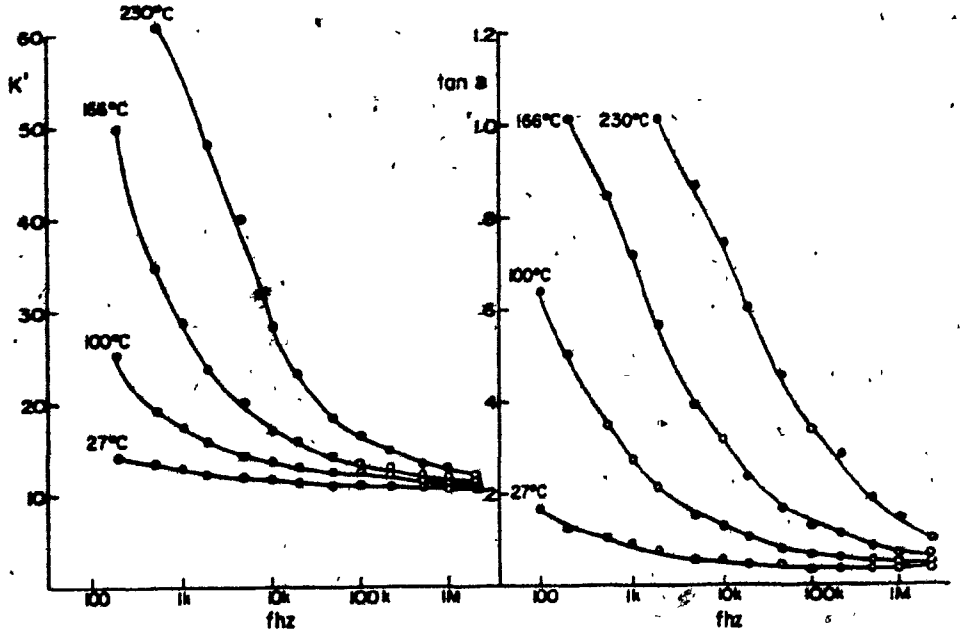

Figure 2.3.1 Relative dielectric permittivity and loss tangent of solid basalt as a function of frequency and temperature (after Saint-Amant and Strangway, 1970).

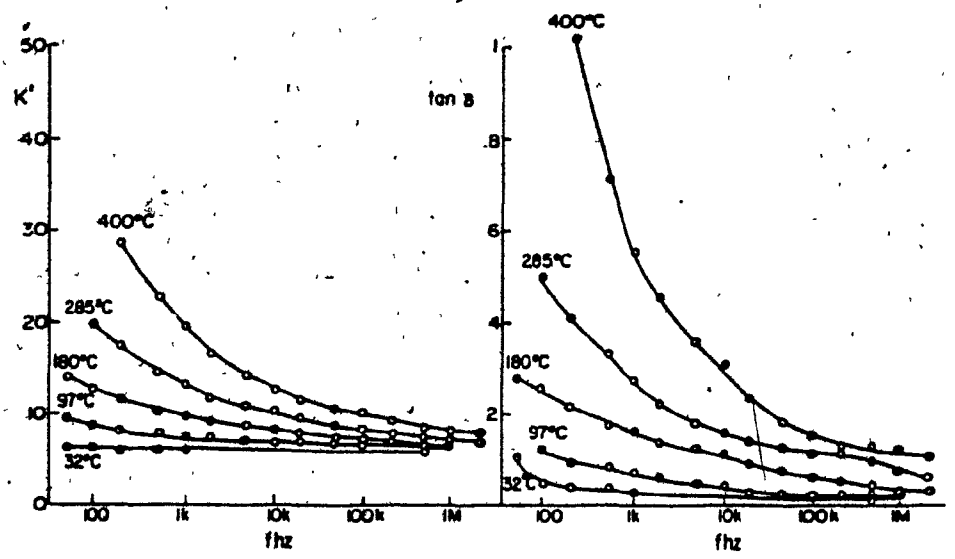

Figure 2.3.2 Relative dielectric permittivity and loss tangent of solid granite as function of frequency and temperature (after Saint-Amant and Strangway, 1970).

sharp natural (rotational) absorption resonance at 2.450 GHz. This arises from a very sharp increase in the imaginary component of the permittivity ( ) at this frequency. Since water is relatively nonmagnetic, an imaginary permittivity component will be reflected in the effective conductivity (equation 2.2.25). As discussed in section 2.2, above, the measured conductivity is, in fact, the effective conductivity. The imaginary permittivity is 180 out of phase with the real component of the conductivity and thus adds to the latter to increase the effective conductivity. This result is apparent in Von Hippel's data for water (Table 2.3.5). The measured conductivity for water is maximum at the 1 GHz measuring frequency. At 2.5 GHz it drops off slightly, suggesting a maximum value for the effective conductivity between 1 and 2.5 GHz. Smith-Rose measured the effective conductivity and permittivity of several granite samples over the frequency range 1 kHz to 10 MHz. The results, presented in Table 2.3.6 indicate an increase in measured conductivity and a decrease in measured permittivity with increasing frequency. Note that the rate of increase in the conductivity decreases with increasing frequency.

Water is taken as an important example because of the high probability that it is present in some concentration in a geologic medium. The absorption losses for wet and dry sandy soils (Table 2.3.5) illustrate the effect of water

content on the absorption rate. The wet sandy soil exhibits a higher absorption rate than the dry sandy soil throughout the frequency range. The dry soils listed in Table 2.3.5 (sandy, loamy, clayey) exhibit a relatively low absorption rate (5 dB/m or less) at even the highest measured frequency (10 GHz). Water at 300 MHz possesses a calculated absorption rate of 3740 dB/m. Given state of the art field instrumentation, even a 5 cm thick sheet of water could sufficiently attenuate a transmitted electromagnetic wave to such an extent that it could not be detected on the opposite side of the sheet, at such frequencies. Water-filled cracks, crevices, joint planes or fractures within a relatively nonabsorbing rock mass could block the transmission of an electromagnetic wave through the otherwise transparent medium.

The final assumption made about the measured electrical parameters listed in both Tables 2.3.1 and 2.3.2 is that they represent in-situ values. In other words, the laboratory measured values for electrical conductivity and permittivity are assumed identical to those values which would be obtained if the measurements had been made in place in the field. It is the in-situ measurement which is of greatest interest in determining the effective probing distance of VHF/UHF electromagnetic equipment. Laboratory samples are usually too dry and homogeneous to accurately reflect the electrical properties of the material in place.

Given the effect the presence of a small percentage of water within the material has on the absorption rate, one can deduce that a change in water content due to the drying out of a sample can alter the results significantly. Even taking the precaution of maintaining the natural fluid content of a sample does not mean that the measurements will be valid for similiar material at another location. The electrical parameters, and thus the absorption rate, will always depend strongly on the local underground conditions.

Figures 2.3.3 and 2.3.4 show the absorption versus frequency for the materials listed in Table 2.3.5. Figures 2.3.5 and 2.3.6 show similiar curves for several materials listed in Table 2.3.1. In the latter case, the electrical parameters are assumed independent of frequency, since no information on frequency dependance is supplied in the data. The absorption rates in Figures 2.3.3 and 2.3.4 increase roughly linearly with frequency on a log-log scale. A levelling-off is observed, at the highest available frequency in the case of water (Figure 2.3.4). The absorption rates, in Figures 2.3.5 and 2.3.6, are seen to increase linearly with frequency, on a log-log scale, until a certain "roll-off frequency" is reached after which the curves flatten out (ie., the absorption rate does not increase further as the frequency is increased). The roll-off frequency is related to the absorption of the material. The curves tend to flatten out at a lower frequency for the more poorly absorbing materials.

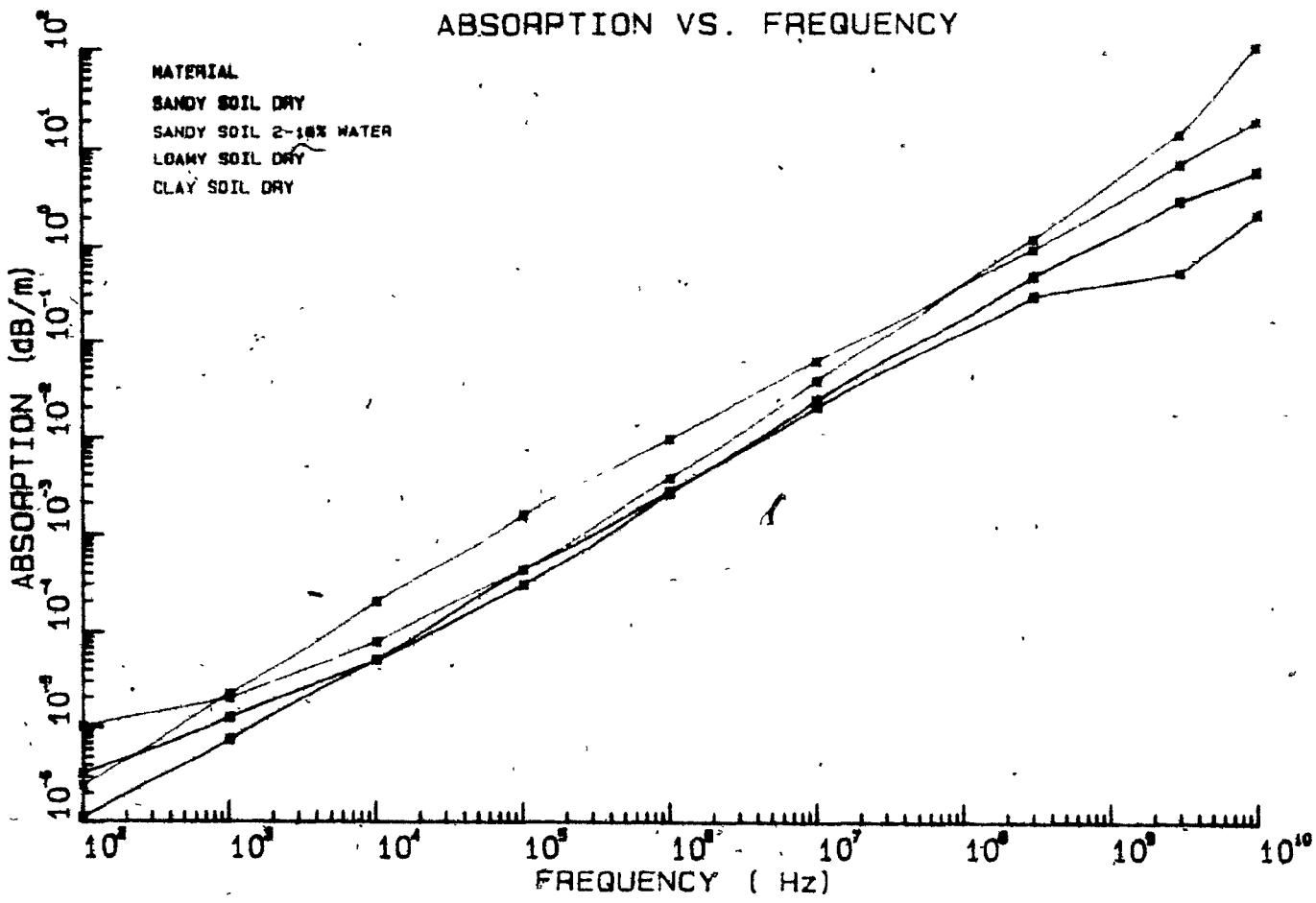

Figure 2.3.3 Absorption versus frequency plot for the soils whose electrical properties are listed in Table 2.3.5.

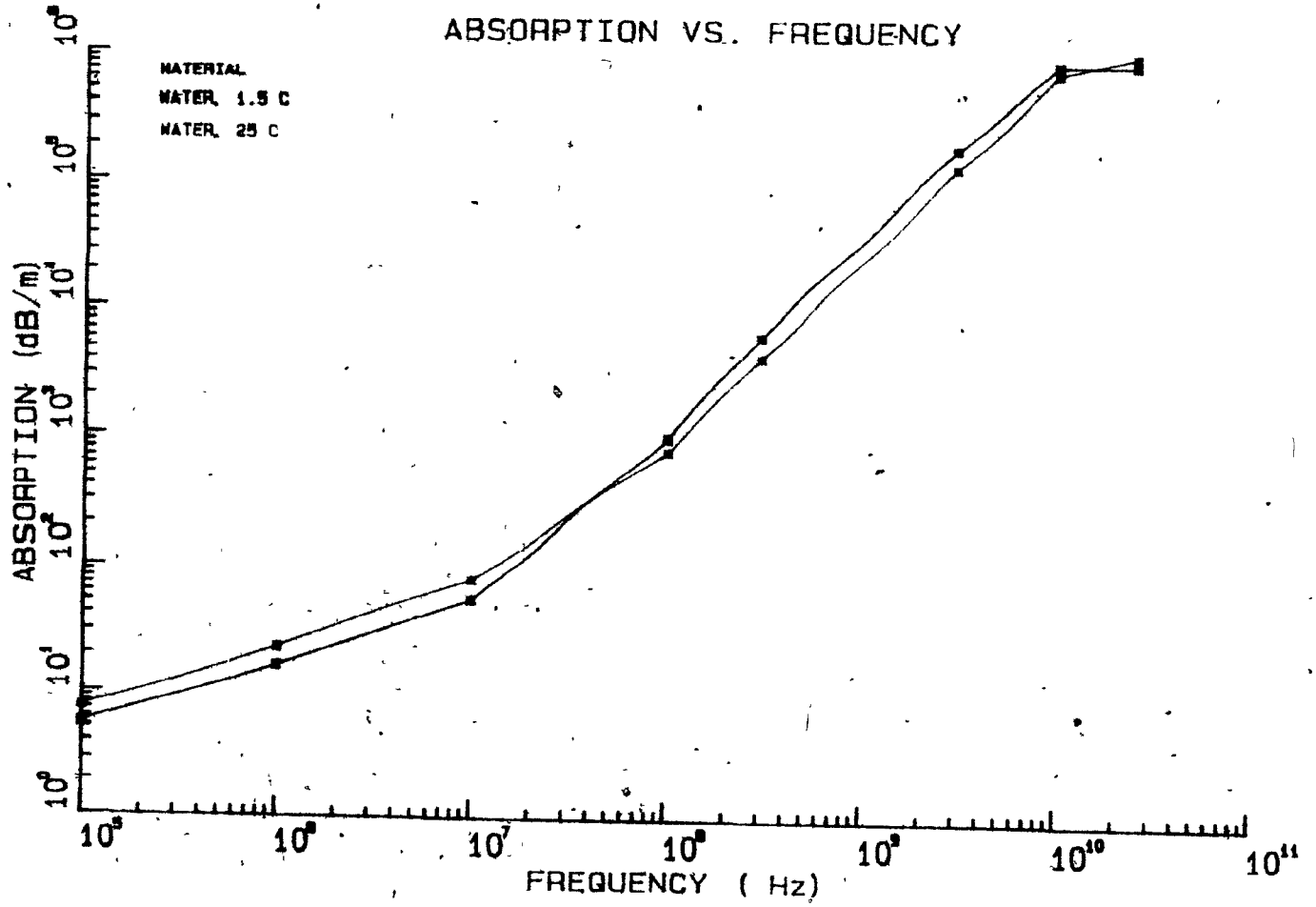

Figure 2.3.4 Absorption versus frequency plot for the water samples whose electrical properties are listed in Table 2.3.5.

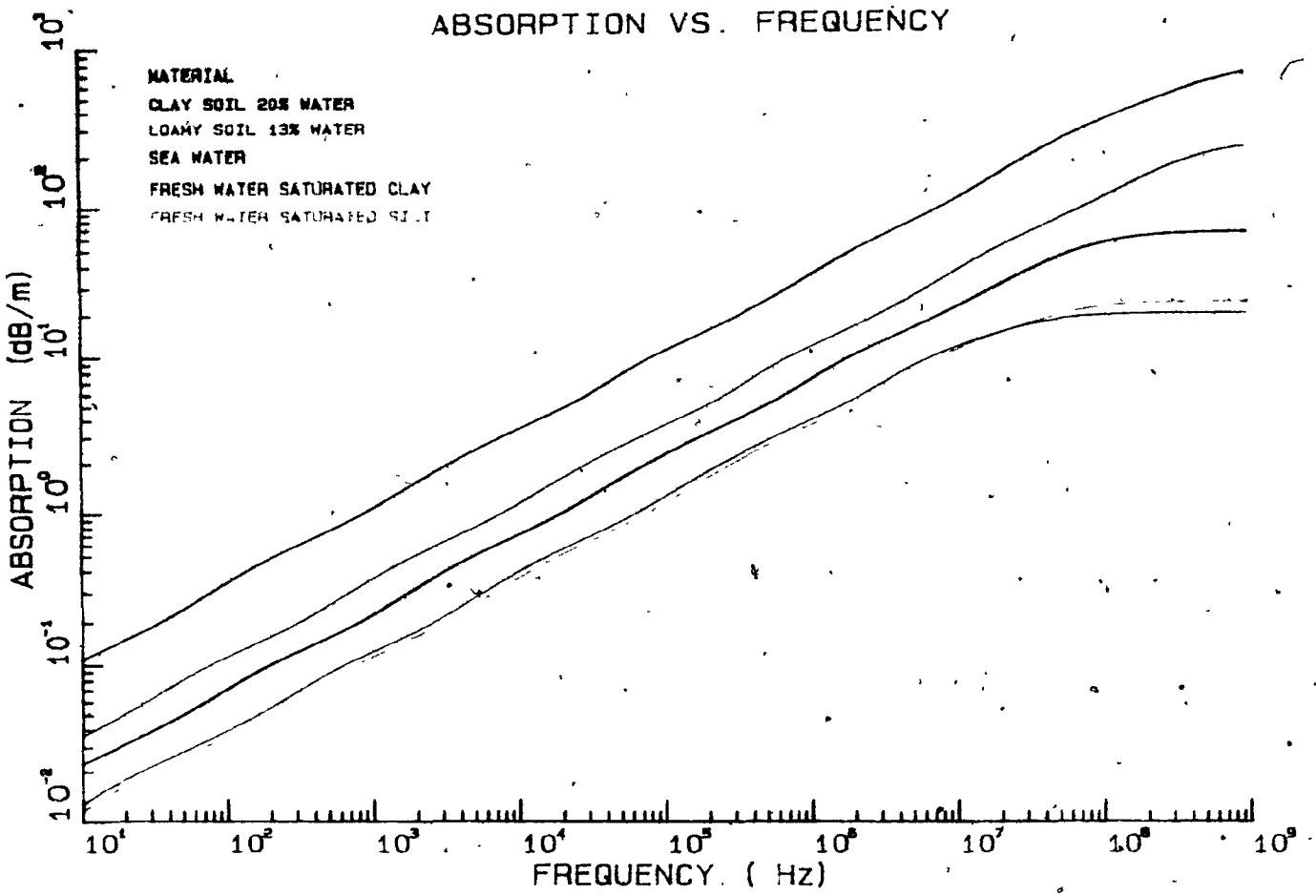

Figure 2.3.5 Absorption versus frequency plot for several of the materials whose electrical properties are listed in Table 2.3.1.

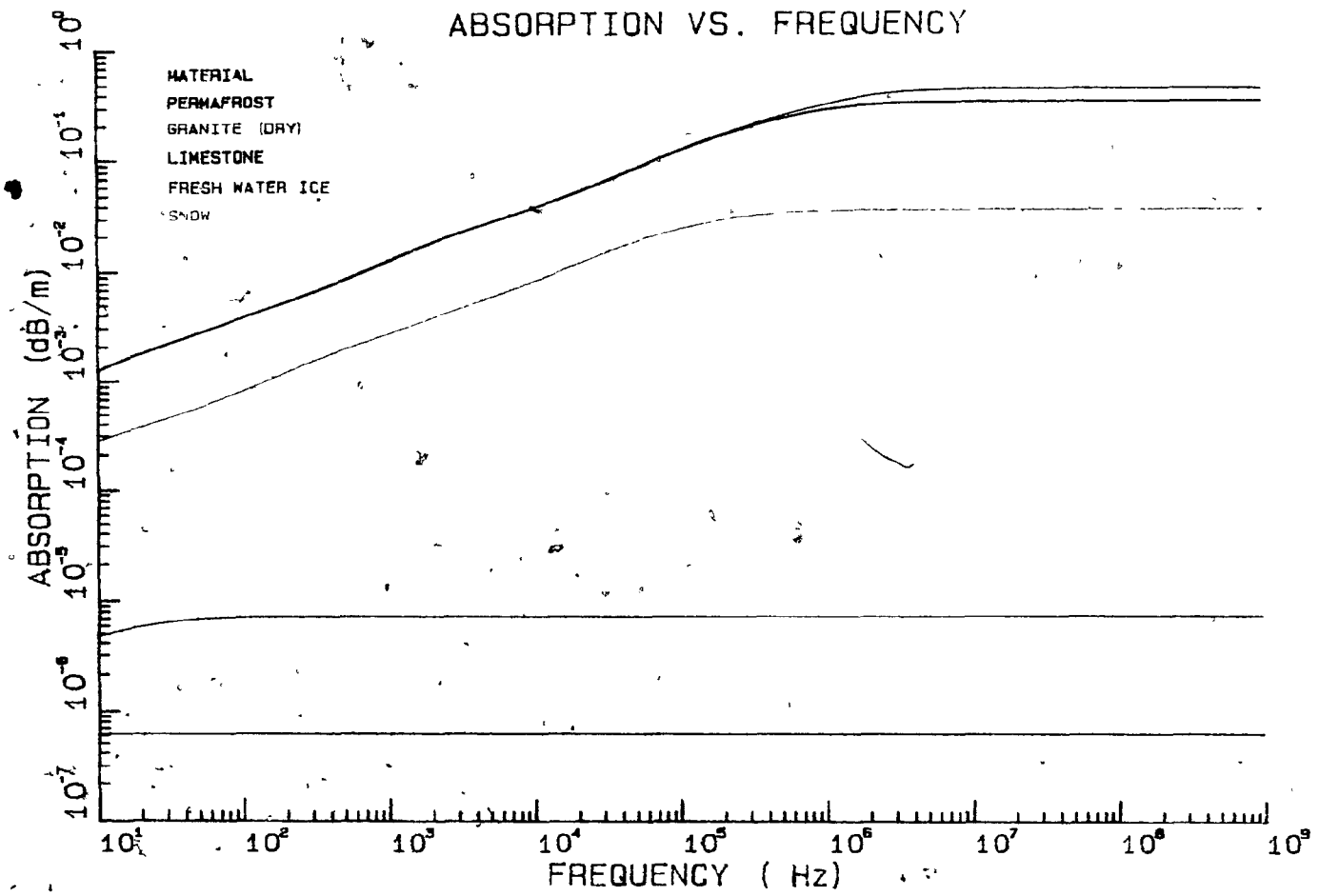

Figure 2.3.6 Absorption versus frequency plot for several of the materials whose electrical properties are listed in Table 2.3.1.

The behaviour of the absorption rate as a function of the frequency and the electrical parameters can be investigated through equation 2.2.30. The figures which are discussed in the rest of this section have been constructed from this equation which assumes that the permeability is real valued, the electrical parameters are independent of frequency over the range considered and that the imaginary components of the permittivity and electrical conductivity masquerade as real components of electrical conductivity and permittivity respectively. Figures 2.3.7 to 2.3.12 are log-log plots of the absorption rate versus frequency for materials possessing various conductivity values. The permittivity and permeability are fixed for each figure. The curves all possess a similiar shape. As discussed in the case of Figures 2.3.5 and 2.3.6, above, they increase linearly with frequency until a "roll-off frequency" is encountered, at which point they level off. The roll-off frequency is dependent upon the the values of the electrical parameters and varies in each case. The absorption rate is observed to increase with increasing conductivity in all the plots.

Figures 2.3.7 to 2.3.9 show the effect of changing the relative permittivity from the free space value (1.0) to the approximate value of water (81.0). The relative permeability is fixed at its free space value (1.0). The effect of increasing the relative permittivity from 1.0 to 81.0 (Figures 2.3.7 to 2.3.9) is to decrease the absorption

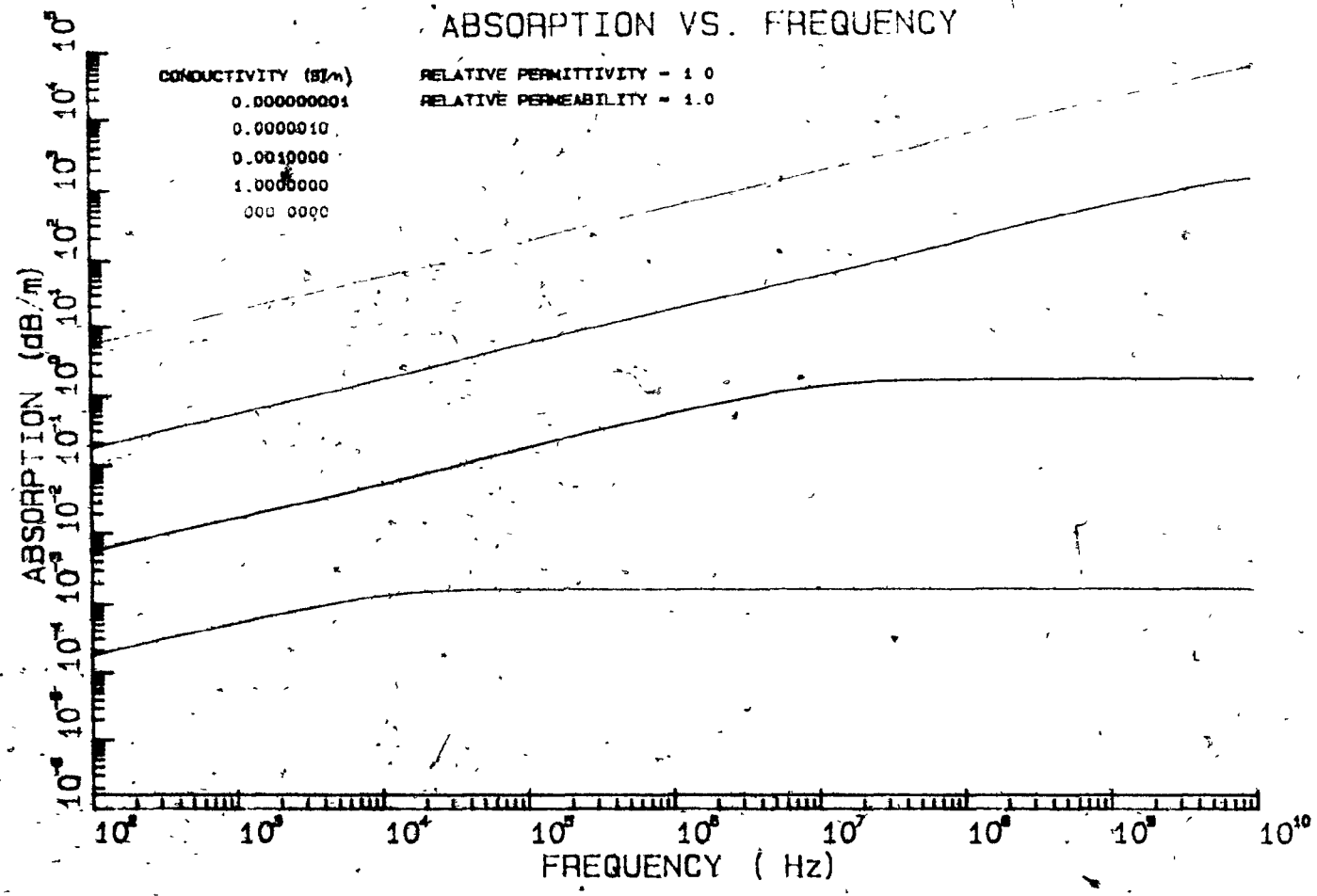

Figure 2.3.7 Absorption versus frequency plot for several conductivity values. The relative permittivity and permeability are fixed at 1.0.

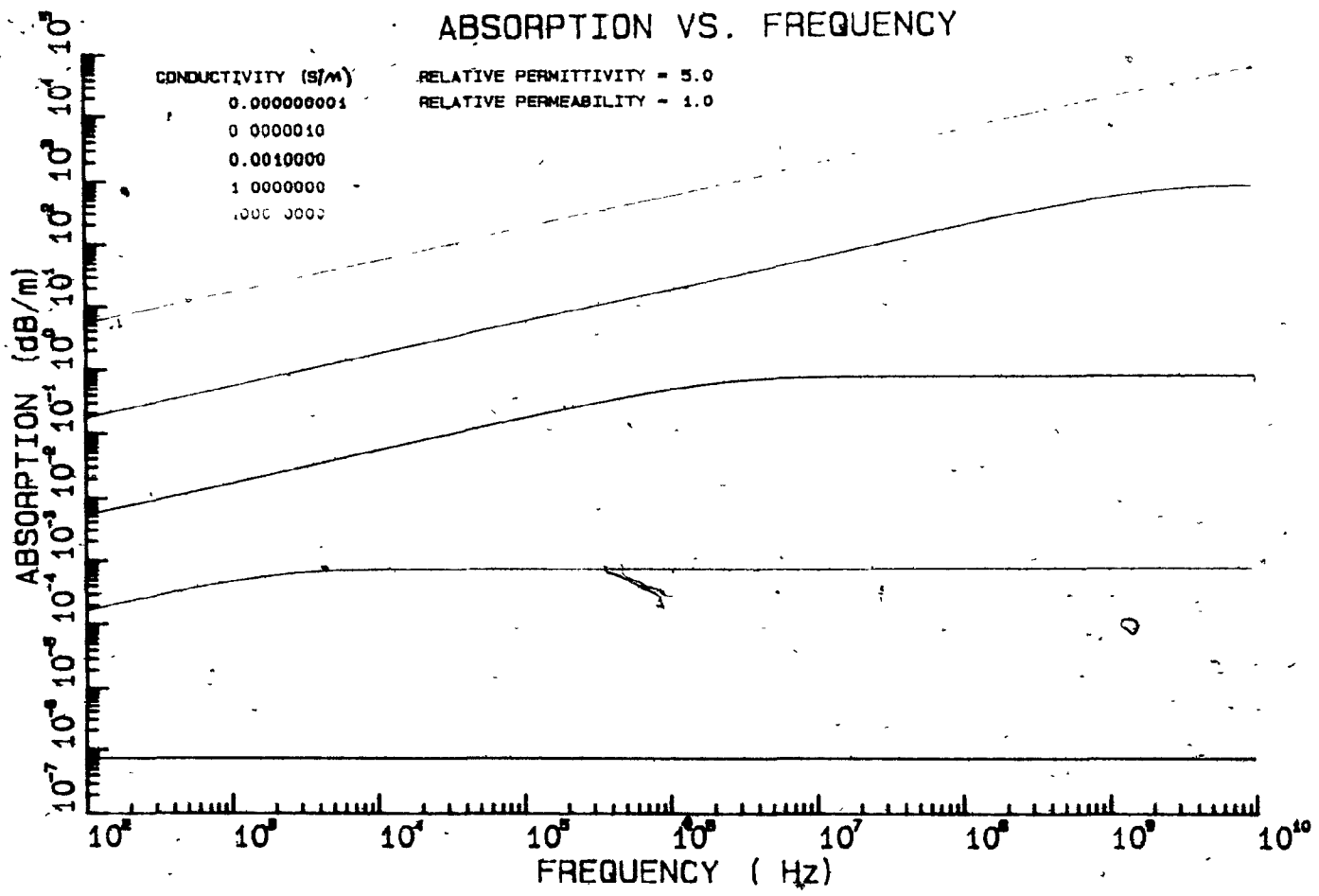

Figure 2.3.8 Absorption versus frequency plot for several conductivity values. The relative permittivity is fixed at 5.0. The relative permeability is fixed at 1.0.'

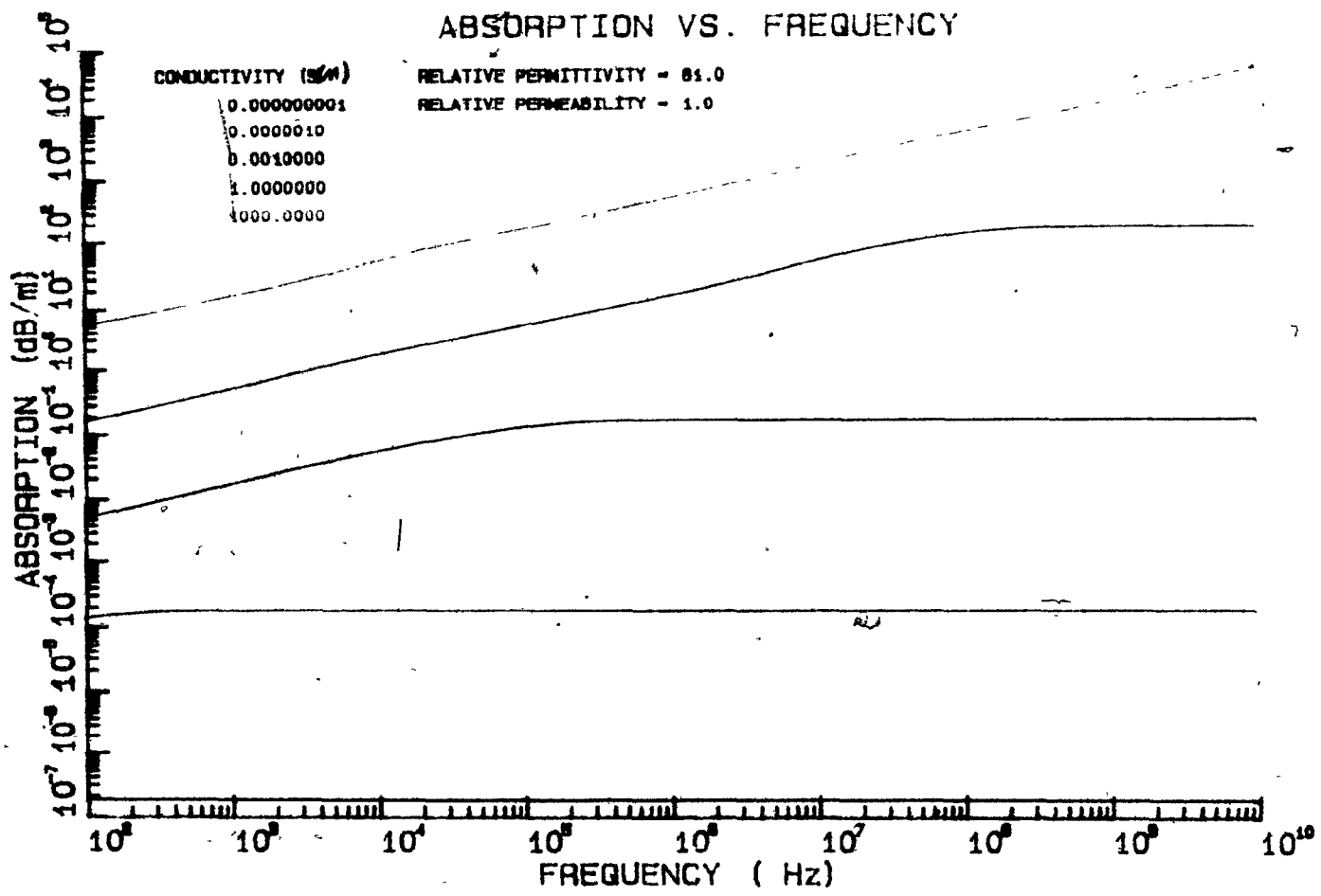

Figure 2.3.9 Absorption versus frequency plot for several conductivity values. The relative permittivity is fixed at 81.0. The relative permeability is fixed at 1.0.

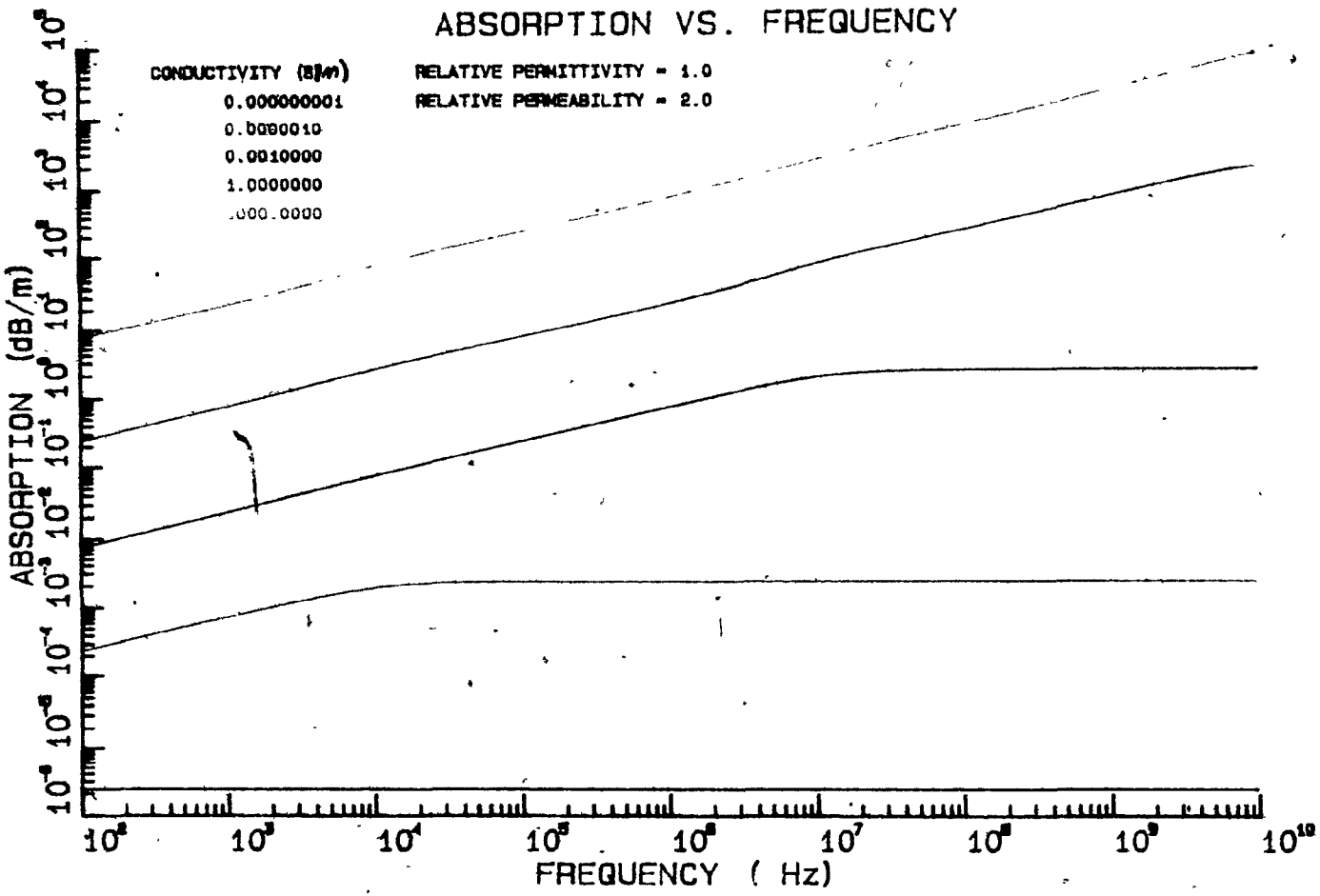

Figure 2.3.1Ø Absorption versus frequency plot for several conductivity values. The relative permittivity is fixed at 1.Ø. The relative permeability is fixed at 2.Ø.

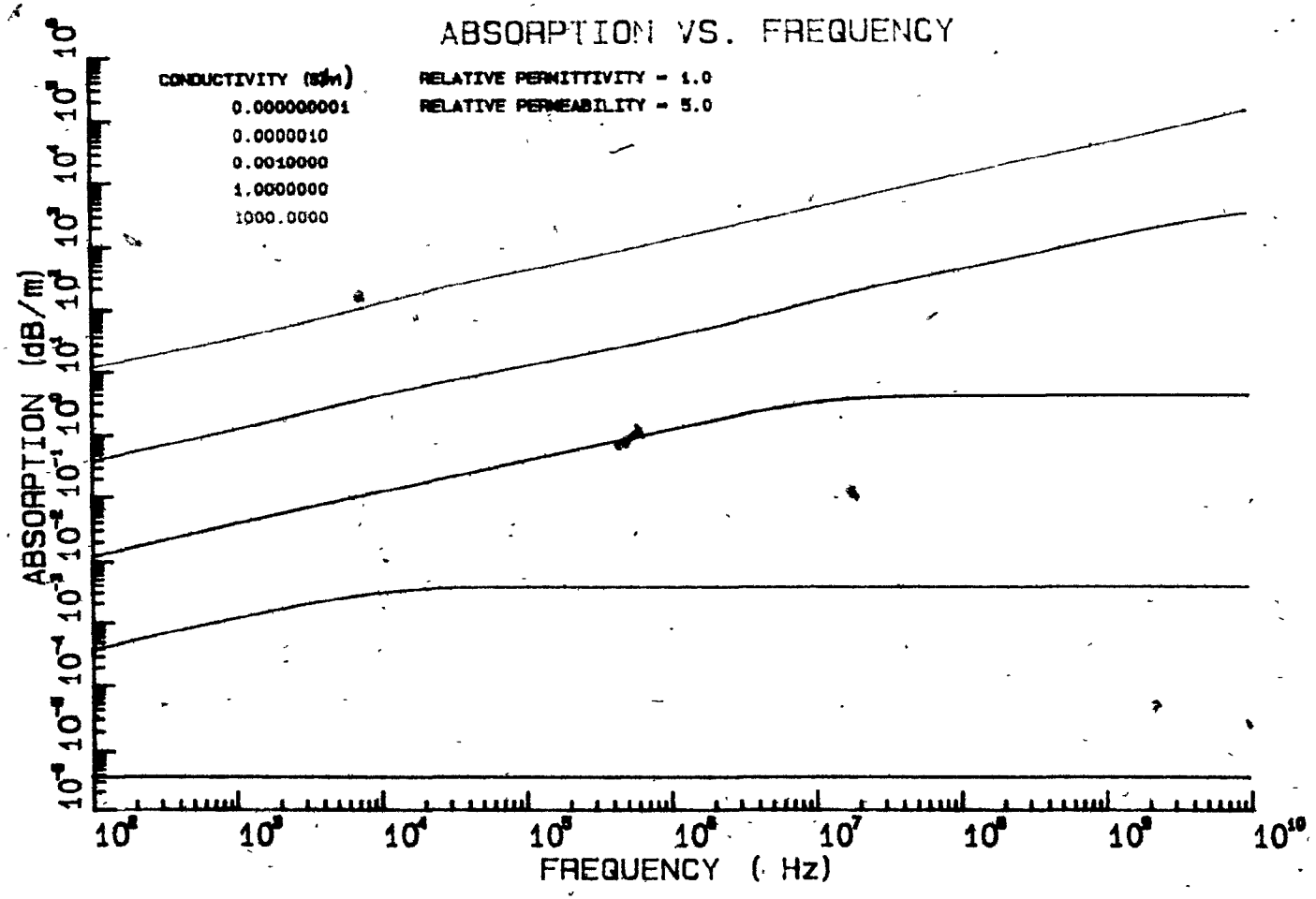

Figure 2.3.11 Absorption versus frequency plot for several conductivity values. The relative permittivity is fixed at 1.0. The relative permeability is fixed at 5.0.

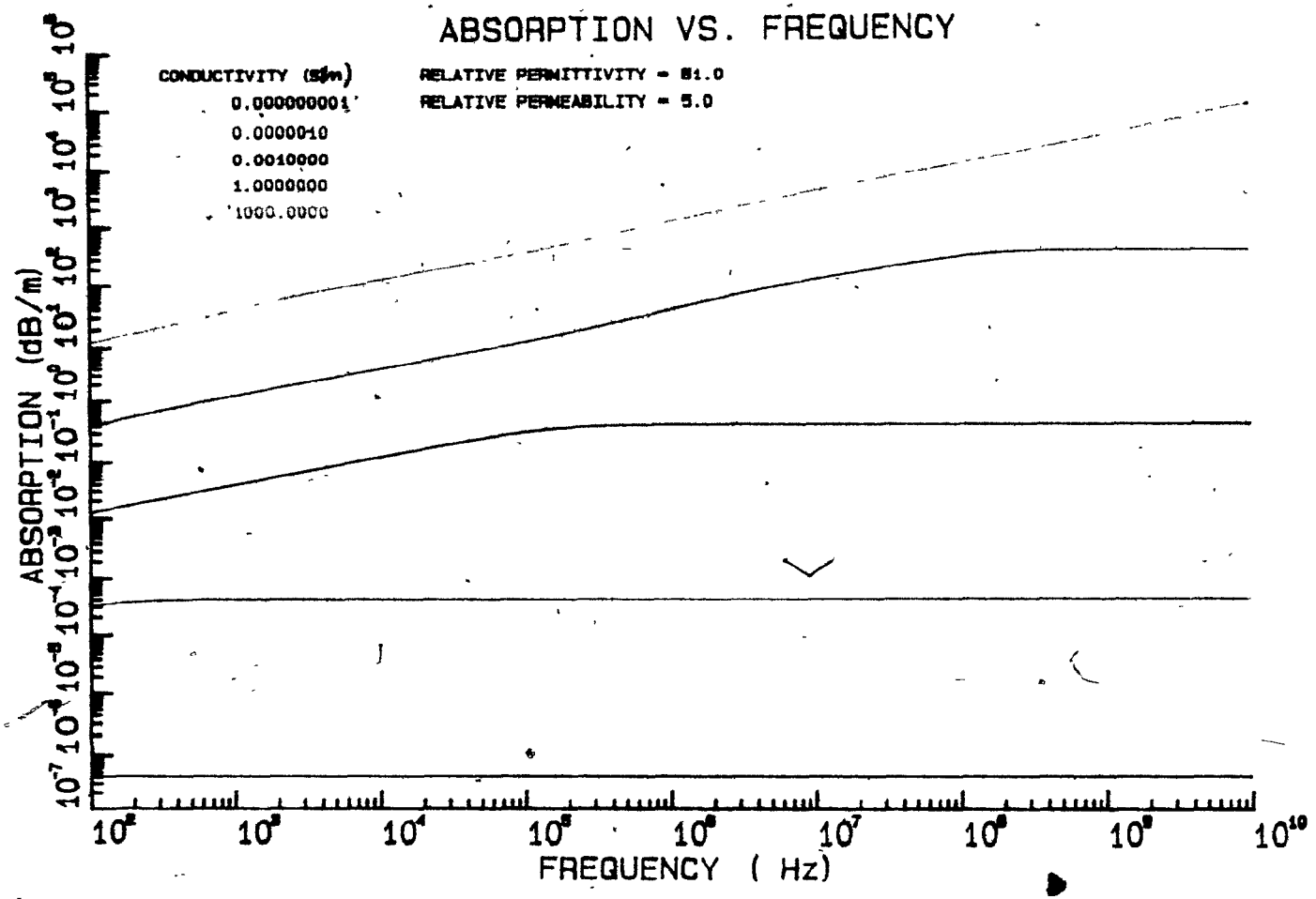

Figure 2.3.12 Absorption versus frequency plot for several conductivity values. The relative permittivity is fixed at 81.0. The relative permeability is fixed at 5.0.

rate roll-off frequency. The respective curves in the three figures are all identical at frequencies lower than their roll-off frequencies. Figures 2.3.7, 2.3.10 and 2.3.11 illustrate the effect of allowing the relative permeability to vary between 1.0 and 5.0, while the permittivity is fixed at 1.0. The absorption rate increases uniformily across the frequency spectrum as the permeability is increased. This is intuitively obvious from equation 2.2.30 which shows that the absorption rate is directly proportional to the square root of the permeability. Figure 2.3.12 is plotted for a material which possesses both high relative permittivity (81.0) and permeability (5.0).

Figures 2.3.13 to 2.3.15 are log-log plots of absorption versus conductivity for various relative permittivity values. The frequency and permeability are fixed for each figure. Three representative frequencies have been chosen (1.0, 50.0, 445.0 Mhz). The highest frequency is, in fact, the operational frequency of the author's prototype transillumination system. At the lower conductivities the respective permittivity curves are parallel and the absorption rate is higher for lower values of permittivity. At a "critical conductivity", the five permittivity curves merge together to become identical at higher conductivities. Again this is intuitively obvious because equation 2.2.30 reduces to:

$$\alpha = \omega \sqrt{\mu \varepsilon_{ef} \tan \phi} = \sqrt{\sigma_{ef} \mu' \omega} \qquad (2.3.1)$$

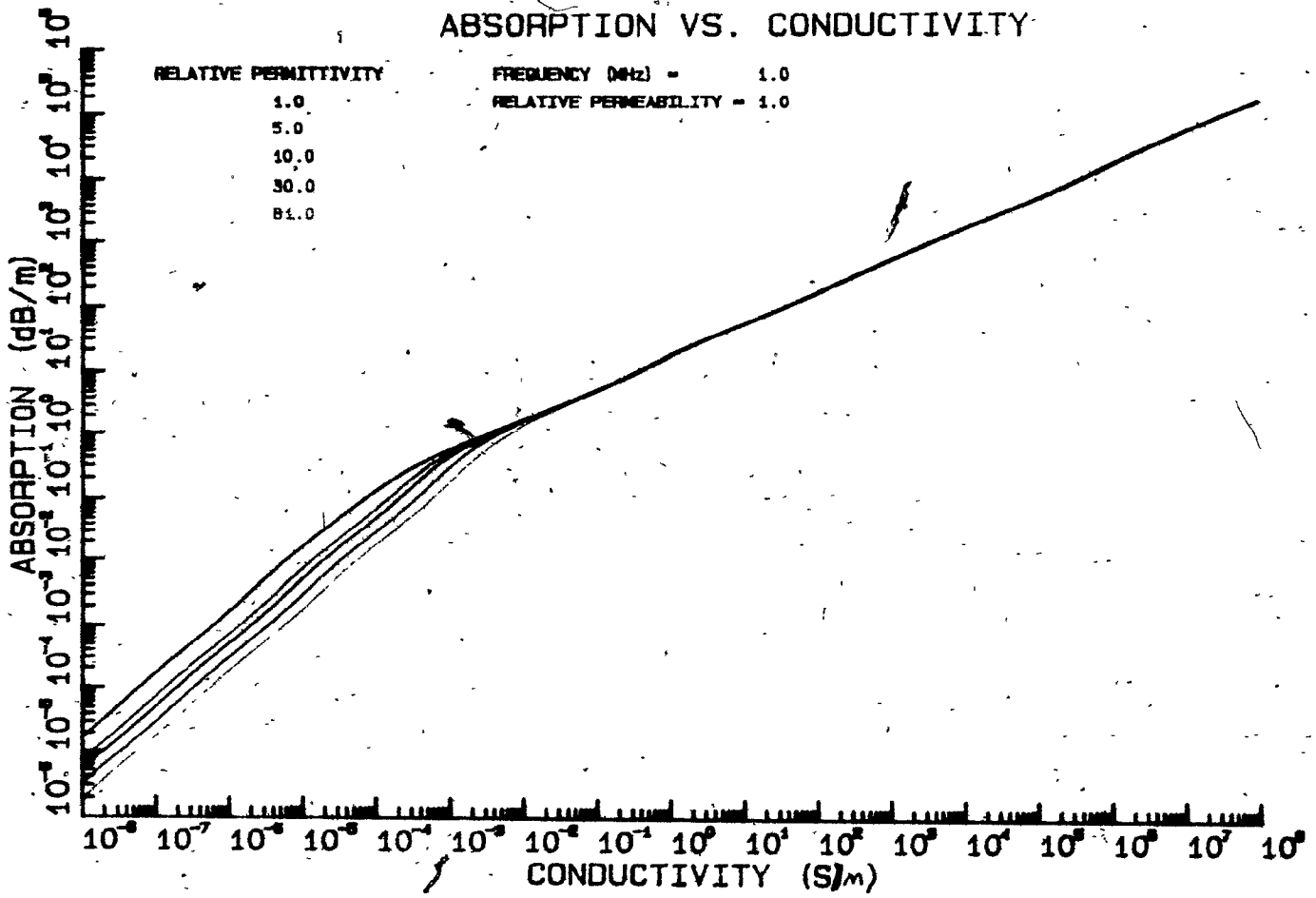

Figure 2.3.13 Absorption versus conductivity plot for several relative permittivity values. The frequency is fixed at 1 MHz. The relative permeability is fixed at 1.0.

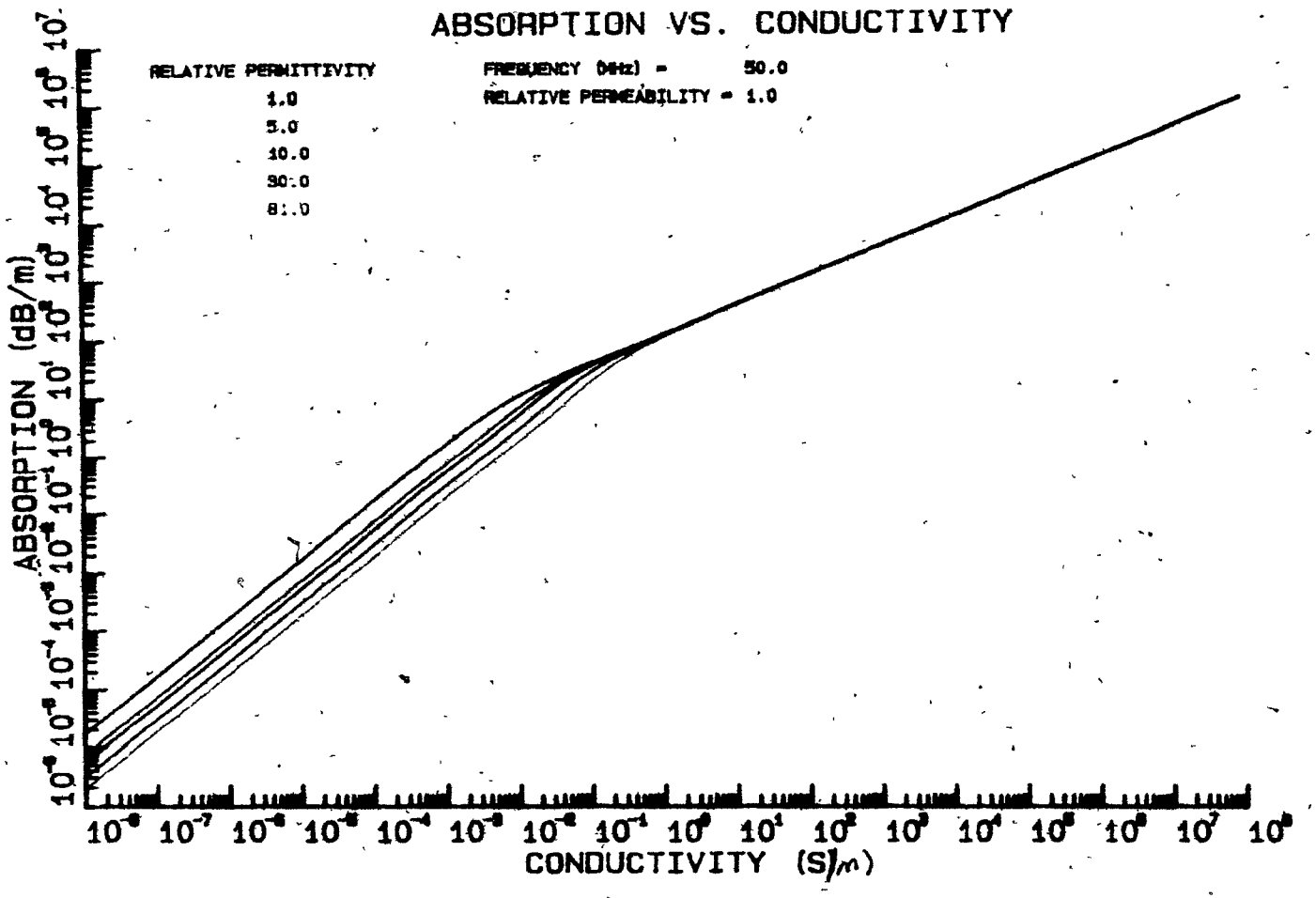

Figure 2.3.14 Absorption versus conductivity plot for several relative permittivity values. The frequency is fixed at 50 Mhz. The relative permeability is fixed at 1.0.

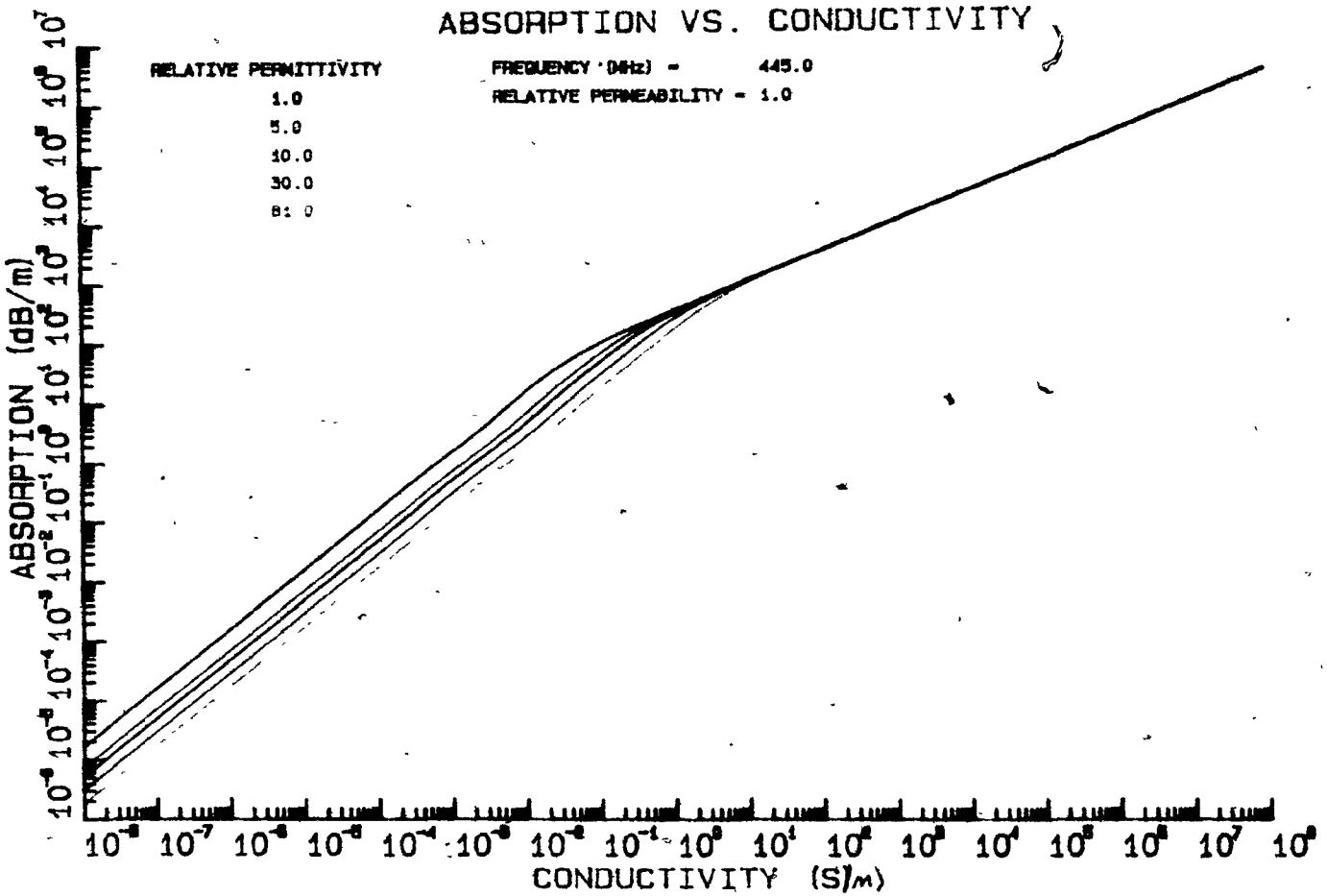

Figure 2.3.15 Absorption versus conductivity plot for several relative permittivity values. The frequency is fixed at 445 MHz. The relative permeability is fixed at 1.0.

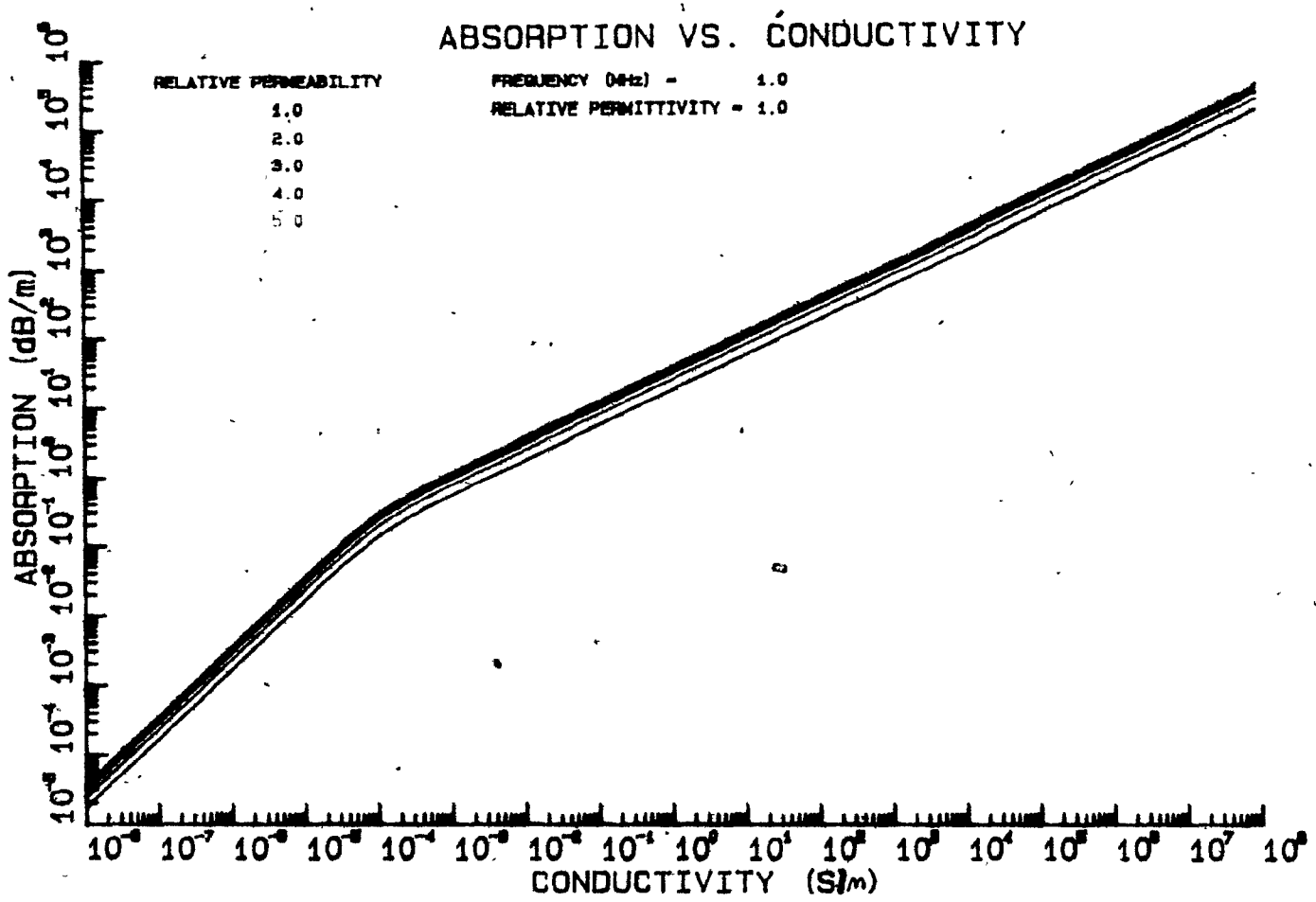

Figure 2.3.16 Absorption versus conductivity plots for several relative permeability values. The frequency is fixed at 1 MHz. The relative permittivity is fixed at 1.0.

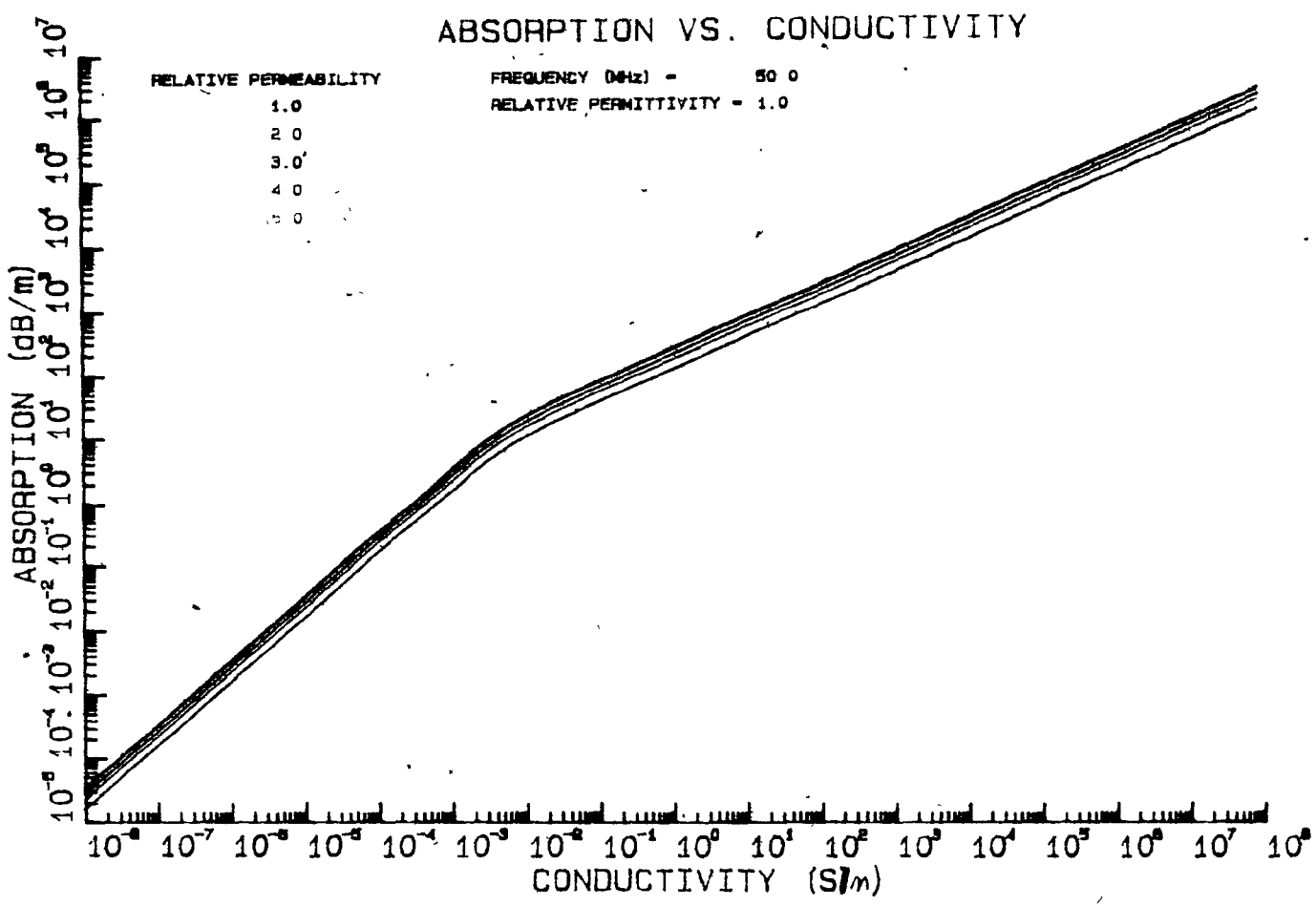

Figure 2.3.17 Absorption versus conductivity plots for several relative permeability values. The frequency is fixed at 50 Mhz. The relative permittivity is fixed at 1.0.

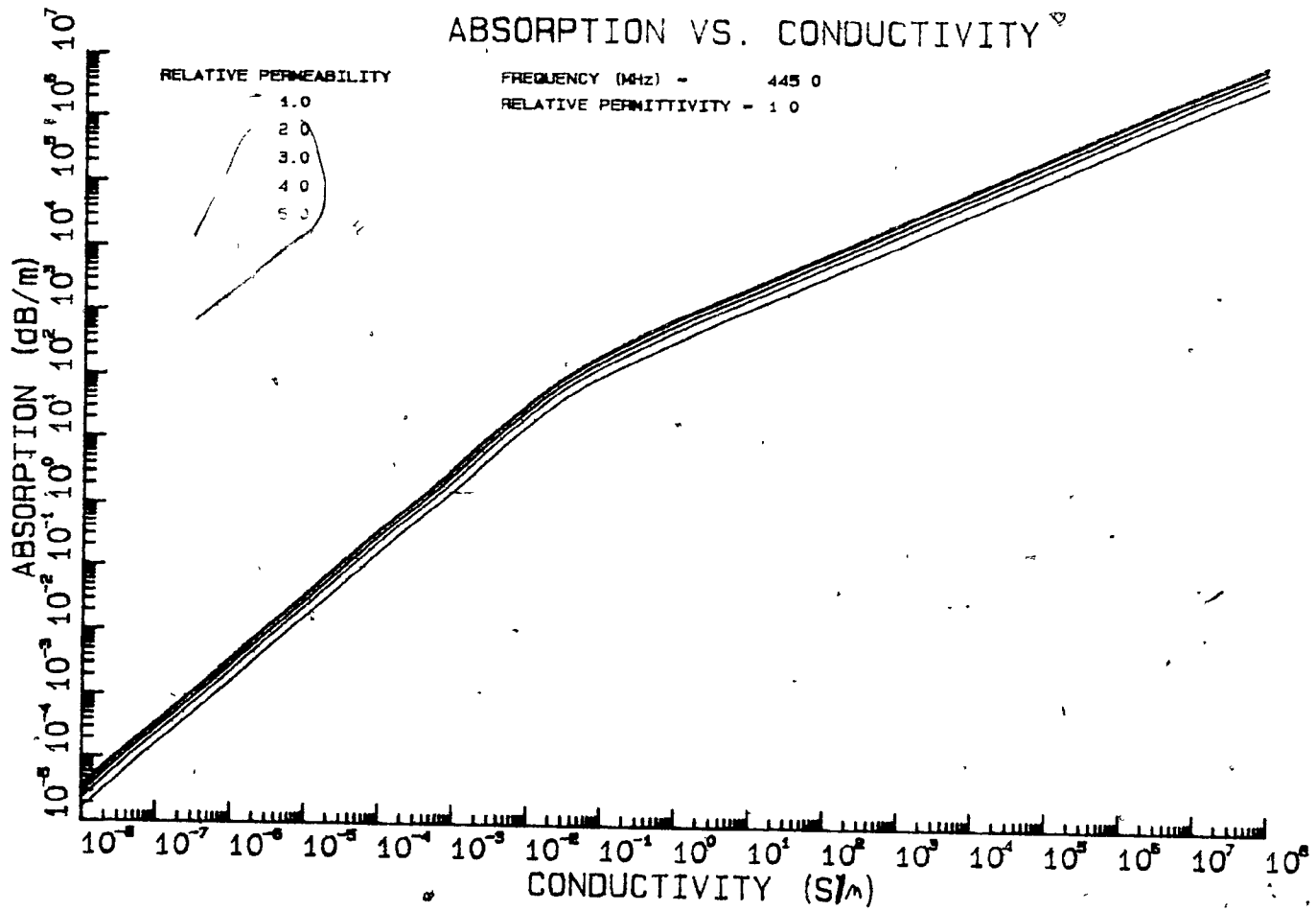

Figure 2.3.18 Absorption versus conductivity plots for several relative permeability values. The frequency is fixed at 445 Mhz. The relative permittivity is fixed at 1.0.

when the loss tangent is very much greater than unity.

Figures 2.3.16 to 2.3.18 are plots similiar to those above with the exception that the permittivity is fixed at 1.0 and curves for five different permeability conditions are shown. The respective permeability curves are parallel to each other in each figure. The absorption rate is observed to increase with increasing permeability. The curves are linear until a "critical conductivity" is reached, whereupon they bend and subsequently increase linearly with a reduced slope. The inflection points in all the above figures occur when the loss tangent is equal to unity. Many researchers have used the loss tangent as an approximate indicator of the absorption rate (ie. a low loss tangent means a low absorption rate) (Stewart and Unterberger, 1976).

2.4 Antenna theory

The overall performance of any electromagnetically radiating system depends greatly upon the characteristics of the transmitter and receiver antennas. The antenna serves to efficiently radiate or capture the propagating electromagnetic energy. The important parameters in specifying an antenna's characteristics are its radiation pattern and its gain. The field radiation pattern of an ideal dipole is shown in figure 2.4.1. The field pattern of an antenna is constructed in two orthogonal planes by plotting lines of equal field intensity as measured by a

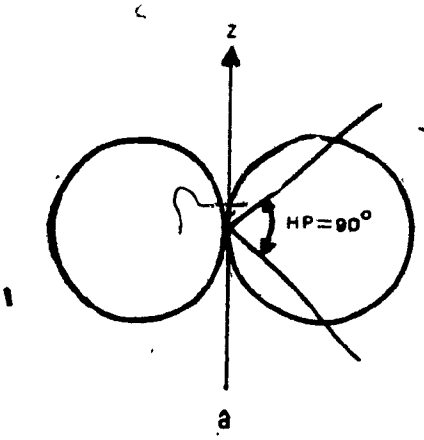

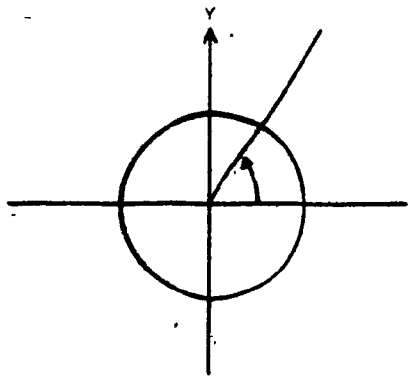

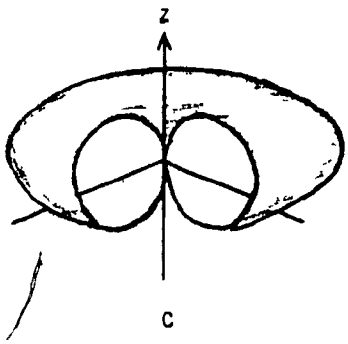

Figure 2.4.1 Field radiation pattern of an ideal dipole. (a) E-plane radiation pattern. (b) H-plane radiation pattern. (c) Three dimensional plot of the radiation pattern. (after Stutzman and Thiele, 1981)

small probe at a distance considered large with respect to the radiated wavelength. The half-power beamwidth is defined as the angle between two lines drawn from the origin to the half power points on a power plot. These correspond to the points of amplitude $1/\sqrt{2}$ on the field pattern. The normalized field pattern, in spherical coordinates, can be described as (Stutzman and Thiele, 1981)

$$F(r,\theta,\phi) = \frac{E(r,\theta,\phi)}{Emax} = \frac{H(r,\theta,\phi)}{Hmax} \qquad (2.4.1)$$

where Emax and Hmax are the maximum values of the field intensities over a sphere of radius r. The radiated field of the antenna is considered to be observed far from the antenna, ie. the "far-field". The far field of an antenna is defined as existing at a distance r, such that

$$r_f > \frac{2D^2}{\lambda} \qquad (2.4.2a)$$

$$r_f >> D \qquad (2.4.2b)$$

$$r_f >> \lambda \qquad (2.4.2c)$$

where D is the length of the radiating element of the antenna and λ is the wavelength of the radiated energy. At this distance r_f, the so-called "far-field" approximation can be used. At distances less than r_f the field pattern can differ significantly from its far field approximation. The power pattern is the square of the field pattern:

$$P(r,\theta,\phi) = |F(r,\theta,\phi)|^2 \qquad (2.4.3)$$

The radiation intensity, defined as the power radiated in a given direction per unit solid angle, is

$$U(r,\theta,\phi) = Umax\,|F(r,\theta,\phi)|^2 \qquad (2.4.4)$$

whereUmax is the maximum radiation intensity over a sphere of radius r. The total power radiated is

$$Pr = \iint U(r,\theta,\phi)\, d\Omega$$

$$= Umax \iint |F(r,\theta,\phi)|^2 d\Omega \qquad (2.4.5)$$

An isotropic radiator, having uniform radiation in all directions, has a total radiated power,

$$Pri = \iint Uav\, d\Omega = 4\pi\, Uav$$

where $$Uavi = 4\pi/Pr \qquad (2.4.6)$$

Equation 2.4.6 expresses the radiated power, Pr, in terms of the radiation intensity, Uavi, of an isotropic radiator. The directive gain of an antenna is defined as the ratio of radiation intensity in a particular direction to the average radiation intensity:

$$D(r,\theta,\phi) = \frac{U(r,\theta,\phi)}{Uavi} \qquad (2.4.7)$$

As no antenna can transform input power to radiated power with a 100% efficiency the term antenna gain is introduced:

$$G(r,\theta,\phi) = \frac{4\pi\, U(r,\theta,\phi)}{Pin} \qquad (2.4.8)$$

where Pin is the input power to the antenna terminals. The efficiency of an antenna is then:

$$e = D/G \qquad (2.4.9)$$

In considering a transmission system between two lossless antennas in free space the ratio of received-to-transmitted power is given by the Friis transmission formula (Stutzman and Thiele, 1981):

$$Pr = \frac{Pt\ Aemt\ Aemr}{r^2\ \lambda^2} \qquad (2.4.10)$$

whereAemt and Aemr are defined as the maximum effective apertures of the transmitter and receiver antennas respectively. It can be shown (Stutzman and Thiele, 1981) that, for any antenna,

$$Aem = \lambda^2\ D/4\pi \qquad (2.4.11)$$

It is assumed that the antennas are similiarly polarized and aligned for maximum coupling. The Friis transmission formula can be extended to lossless media by using equations 2.4.9 and 2.4.11:

$$Pr = \frac{Pt\ Gt\ Gr\ \lambda^2}{(4\pi r)^2} \qquad (2.4.12)$$

Expressed in decibels (2.4.12) transforms:

$$Pr(db) = Pt(dB) + Gt(db) + Gr(dB) - 60\log r(m) - 120\log f(Hz) - 32.44 \qquad (2.4.13)$$

The power lost in transmission due to the geometry of the system is then

$$As(dB) = Gt(dB) + Gr(dB) - 60\log r(m)$$

$$- 120\log f(\text{Hz}) - 32.44 \qquad (2.4.14)$$

where A_s is the spreading loss. It is dependent upon the transmitter and receiver separation, r, the transmitter and receiver antenna gains, Gt and Gr , and the operating frequency, f. The result is valid only when operating in the far-field of the antenna, as per equations 2.4.2a-c.

Figures 2.4.2 to 2.4.4 are plots of spreading loss (equation 2.4.14) versus distance (transmitter-receiver antenna separation) for several frequencies and antenna gain values. The receiver and transmitter antenna gains are assumed equal in each case. The spreading-loss-versus-distance curves are linear on a log-linear scale. The effect of increasing operational frequency is to shift the curves vertically upward along the ordinate axis. The effect of increasing the gain of the antennas is to shift the lines vertically downward. While spreading loss can be considerable, relative to the absorption loss, at small transmitter-receiver separations, its logarithmic dependance on separation means that it increases much more slowly with increasing separation than the absorption loss. The spreading loss at 100 meters for a 445 MHz transmitted wave is approximately 46 dB. Note that the spreading loss is independent of the medium traversed. It should also be noted that this loss is calculated based upon the fact that the transmitter and receiver antennas are maximum coupled and are within each others' far-field. A polarization mismatch occurs under any other coupling condition. The

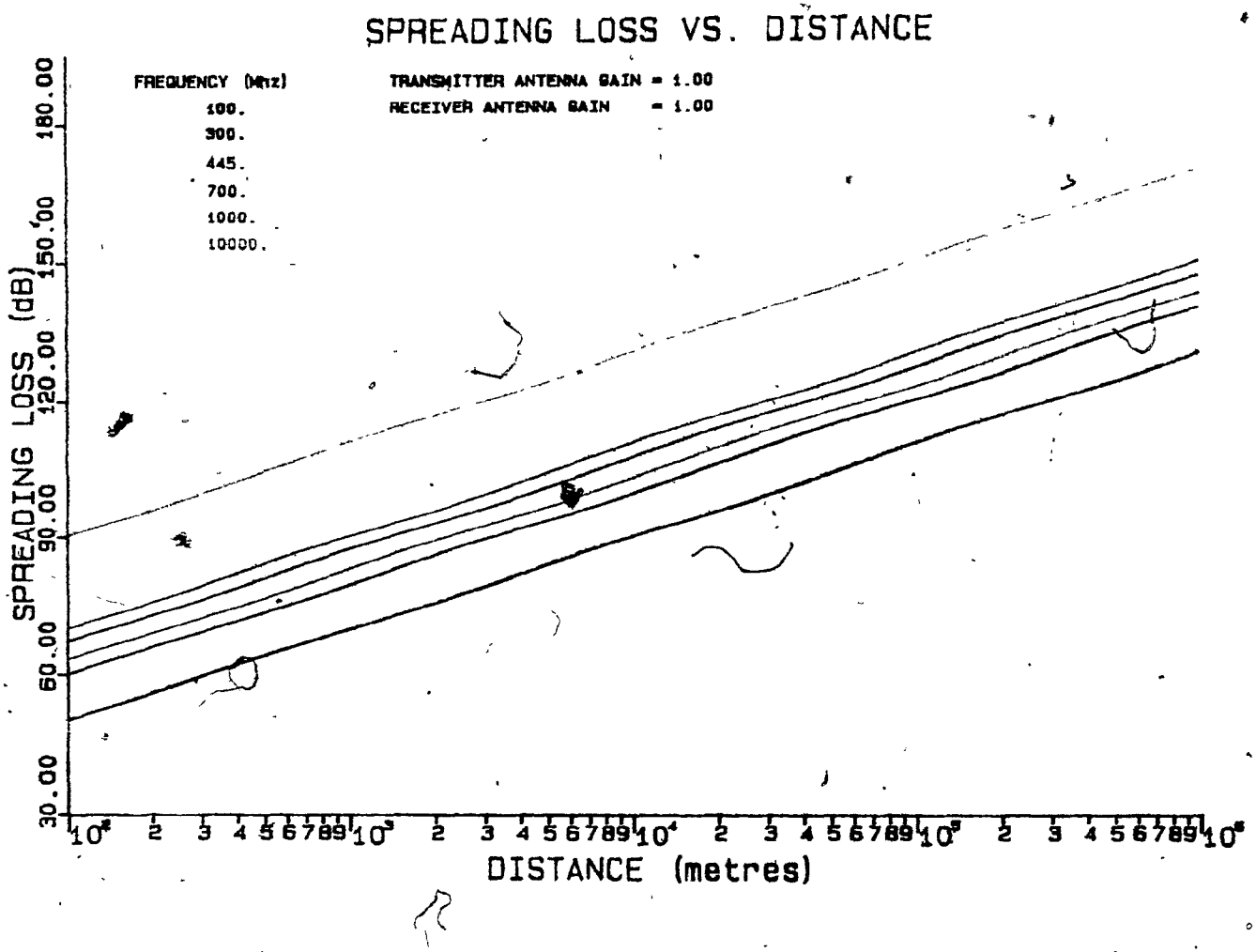

Figure 2.4.2 Spreading loss versus distance plots for several frequency values. The transmitter and receiver gains are fixed at 1.0

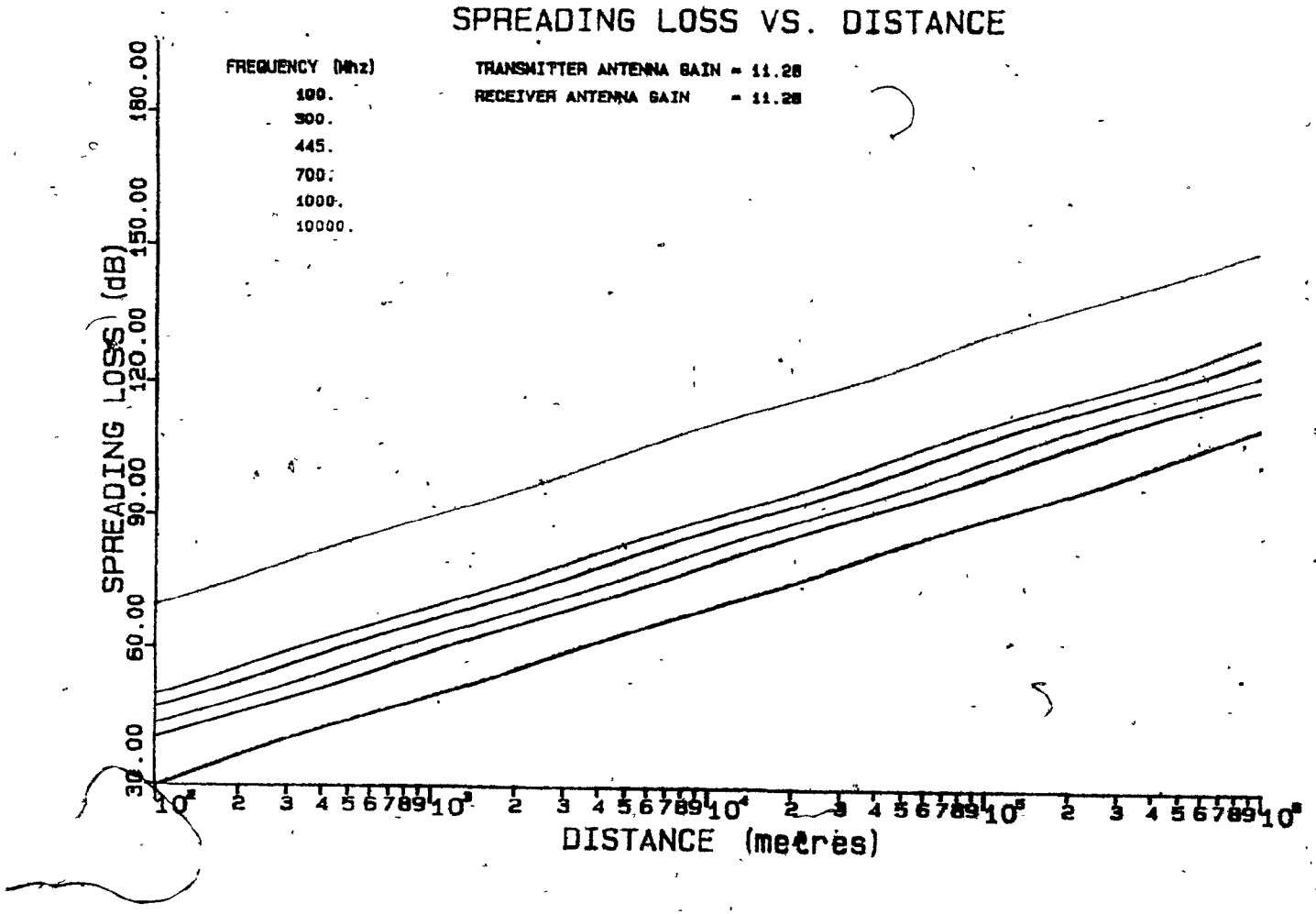

Figure 2.4.3 Spreading loss versus distance plots for several frequency values. The transmitter and receiver gains are fixed at 11.28.

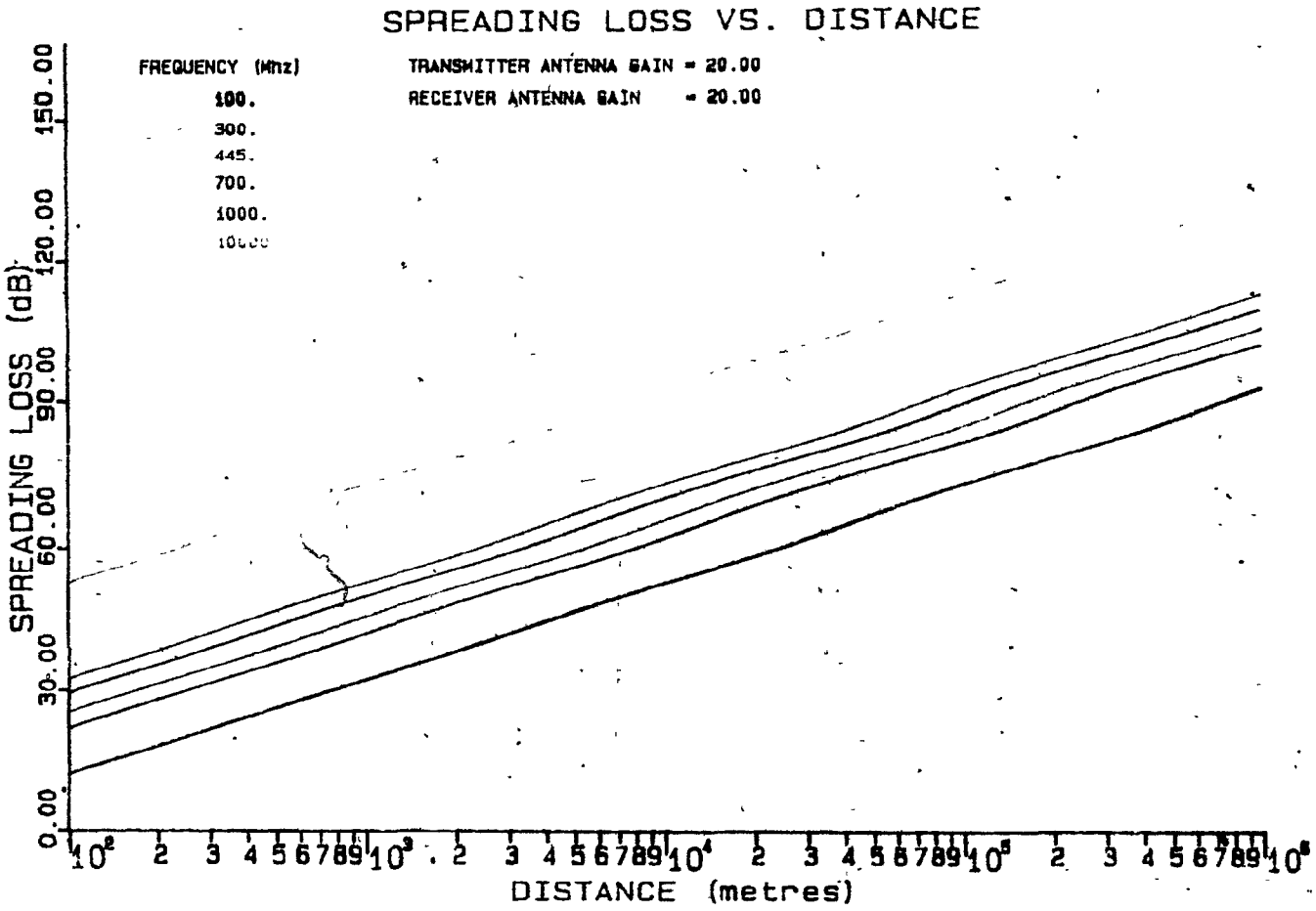

Figure 2.4.4 Spreading loss versus distance plots for several frequency values. The transmitter and receiver gains are fixed at 20.0.

real spreading loss then varies between the maximum coupled value and the minimum coupled value. In the extreme case the minimum coupled received power will be zero. The degree of polarization mismatch can be calculated for a specific antenna pair in free space. In traversing lossy media a plane polarized wave will undergo changes in orientation due to diffraction and refraction at interfaces. The maximum coupled position will then vary from place to place.

The Reciprocity Theorem (Lorrain and Corson, 1970) states that, so long as the frequency and impedances remain unchanged, the current induced in antenna "A" by a radiating antenna "B" will be identical to the current induced in antenna "B" by a radiating antenna "A". A fundamental extension of this is that the transmitter and receiver radiation patterns of a particular antenna are identical. An antenna's impedance is also independent of its operational mode.

The effective isotropically radiated power (EIRP) of a transmitter system, which considers the power output of the transmitter and the antenna gain, is calculated in decibels below one watt (dBw) from,

$$EIRP\ (dBw) = Pt(dBw) - lineloss\ (dBw) + Gt(db) \quad (2.4.15)$$

where the lineloss takes into account all ohmic losses in the transmission line.

2.5 Impedance matching

The impedance that an antenna presents to a transmitter output stage or to the input stage of a receiver is important when considering the operational efficiency of the instrument. Should an impedance mismatch exist at any junction the overall performance specifications of the system can be significantly reduced. Maximum power transfer is achieved when the impedances are matched. A mismatch will give rise to ohmic losses and cause reflections to occur at the end of a transmission line, setting up a standing wave. The impedance mismatch can best be expressed by the voltage standing wave ratio (VSWR):

$$VSWR = \frac{1 + \sqrt{PR/PF}}{1 - \sqrt{PR/PF}} \qquad (2.5.1)$$

where PR and PF are respectively the reverse and forward power travelling in the transmission line. The VSWR can also be expressed in terms of the load and antenna impedances, Zl and Zant respectively:

$$VSWR = 1 + Zant \left\{ \frac{Zl}{Zant} - 1 \right\} \qquad (2.5.2)$$

The fraction of reflected power in a transmission line is

$$\frac{PR}{PF} = \left| \frac{VSWR - 1}{VSWR + 1} \right|^2 \qquad (2.5.3)$$

A perfect impedance match exists when the VSWR equals unity. A VSWR of 1Ø corresponds to the case when two thirds of the power in the transmission line is travelling in the reverse direction. The presence of a standing wave, due to a substantial reflected current, leads to impedance changes

along the line. Damage to a transmitter output stage can occur if high levels of signal power are reflected back down the line. Impedance matching must also be considered when inserting cables or monitors into a line.

2.6 Attenuation measurement

The rate of absorption of electromagnetic energy through a section of earth material can be measured indirectly with separate transmitters and receivers placed in the transillumination mode. Figure 2.6.1 illustrates this mode. The transmitter and receiver are located on opposite sides of a rock mass. The signal level for a known transmitter output is then measured at the receiver location. The received signal amplitude will indirectly reflect the material properties of the intervening geology. The total losses in transmission can be calculated from equations 2.2.12 and 2.4.14:

$$\mathcal{A}t = 8.686\,\alpha_{abs} \cdot r + \mathcal{A}s \qquad (2.6.1)$$

The total attenuation, typically expressed in decibels (dB), is

$$\mathcal{A}t = 8.686\, r\omega \sqrt{\frac{ab}{2}\{(1 + \tan^2\phi)^{1/2} - 1\}}$$

$$+ \{ Gt + Gr - 60 \log r - 120 \log f - 32.44\} \qquad (2.6.2)$$

where all parameters are in SI units. 1 dB equals 0.1151 nepers. Figure 2.6.2 shows curves of the total attenuation (equation 2.6.2) versus distance for several absorption rates (equation 2.2.2). The frequency used in Figure 2.6.2

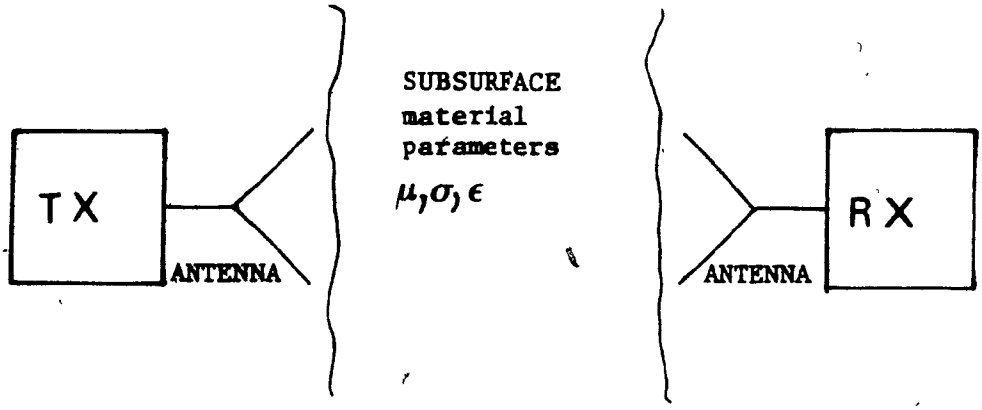

Figure 2.6.1 The transillumination survey mode. The transmitter and receiver positions are denoted by Tx and Rx respectively.

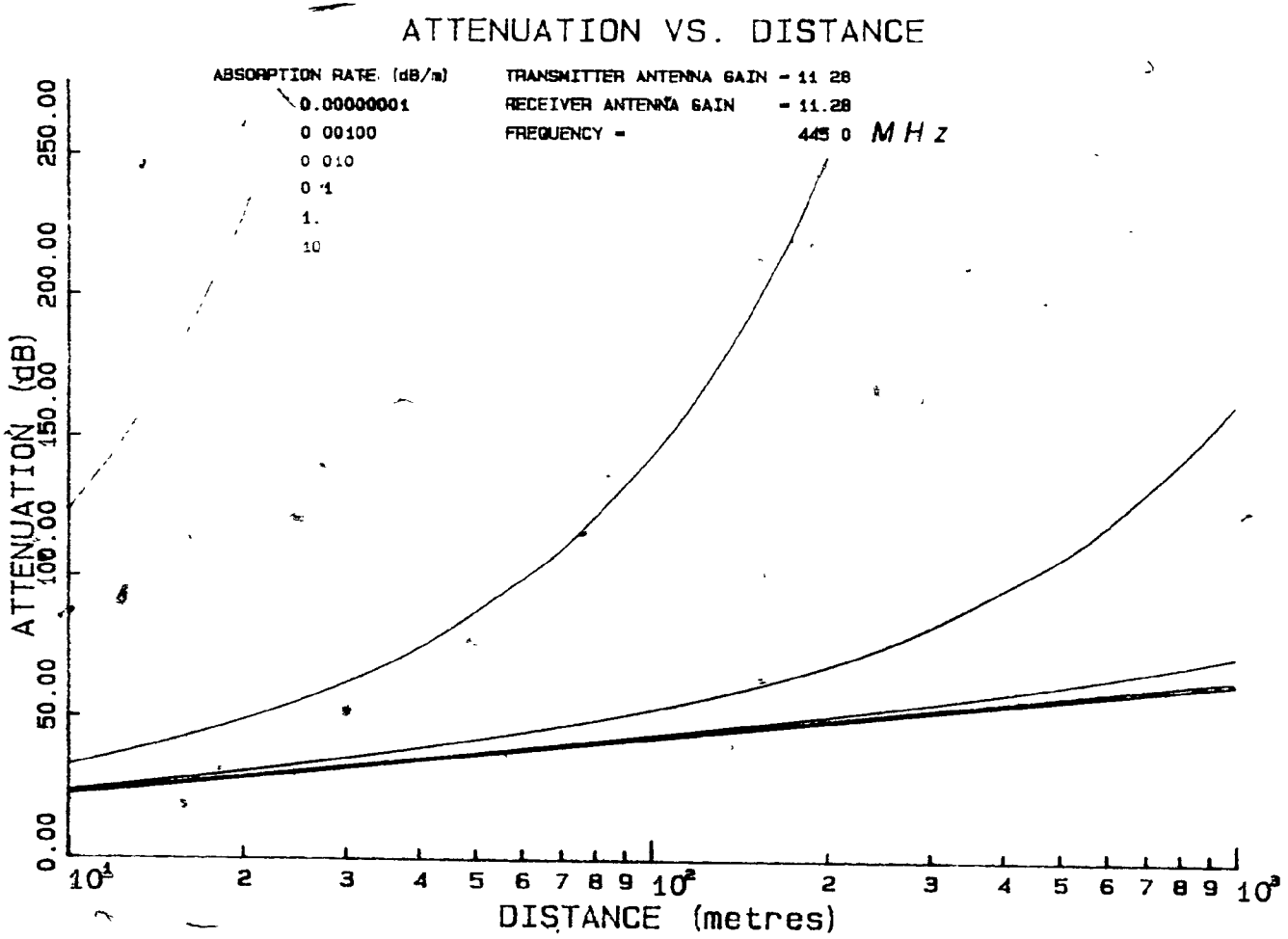

Figure 2.6.2 Attenuation versus distance plots for several absorption rate values. The transmitter and receiver gains are fixed at 11.28. The frequency is fixed at 445 MHz.

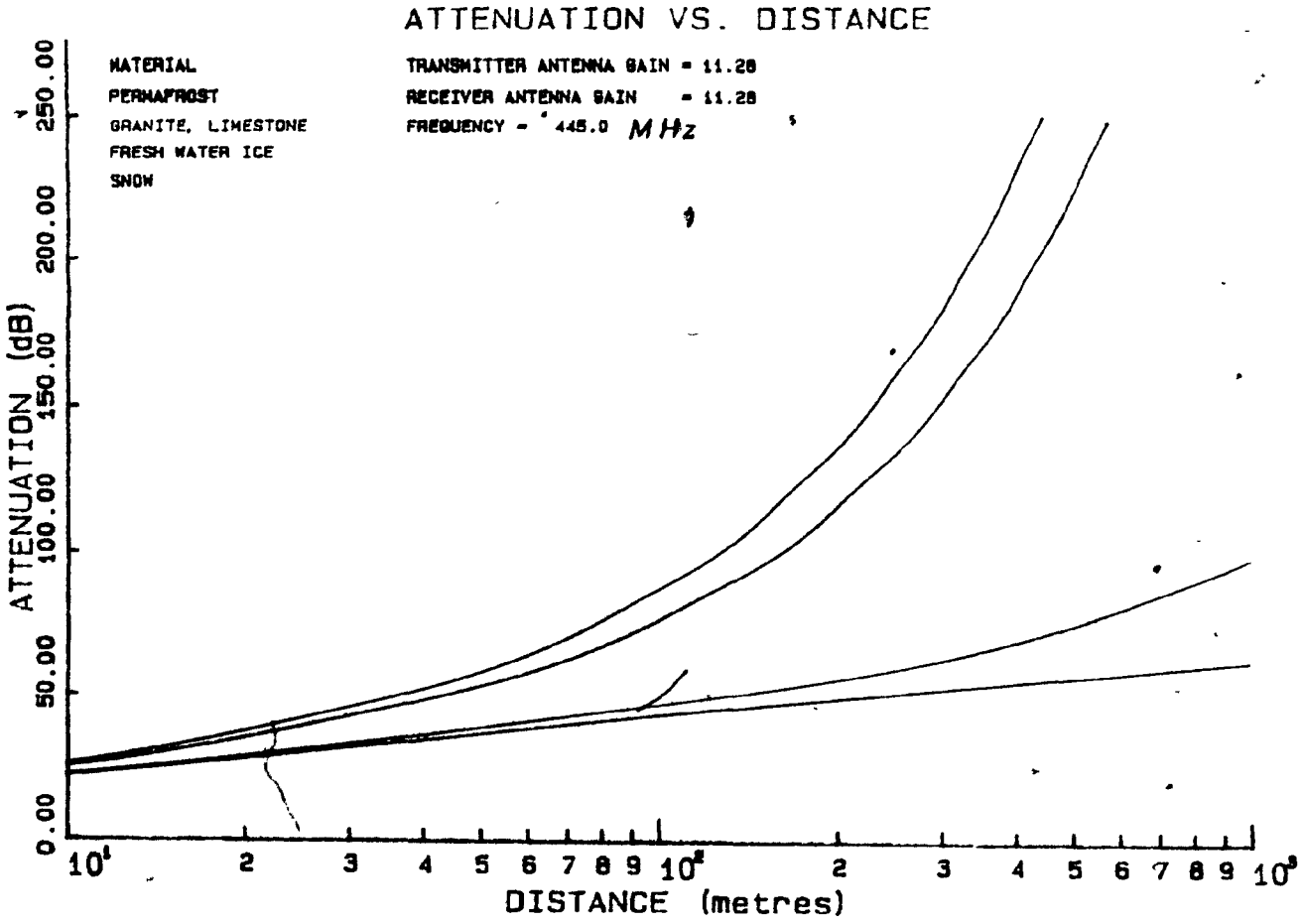

Figure 2.6.3 Attenuation versus distance plots for several of the materials whose electrical properties are listed in Table 2.3.1.

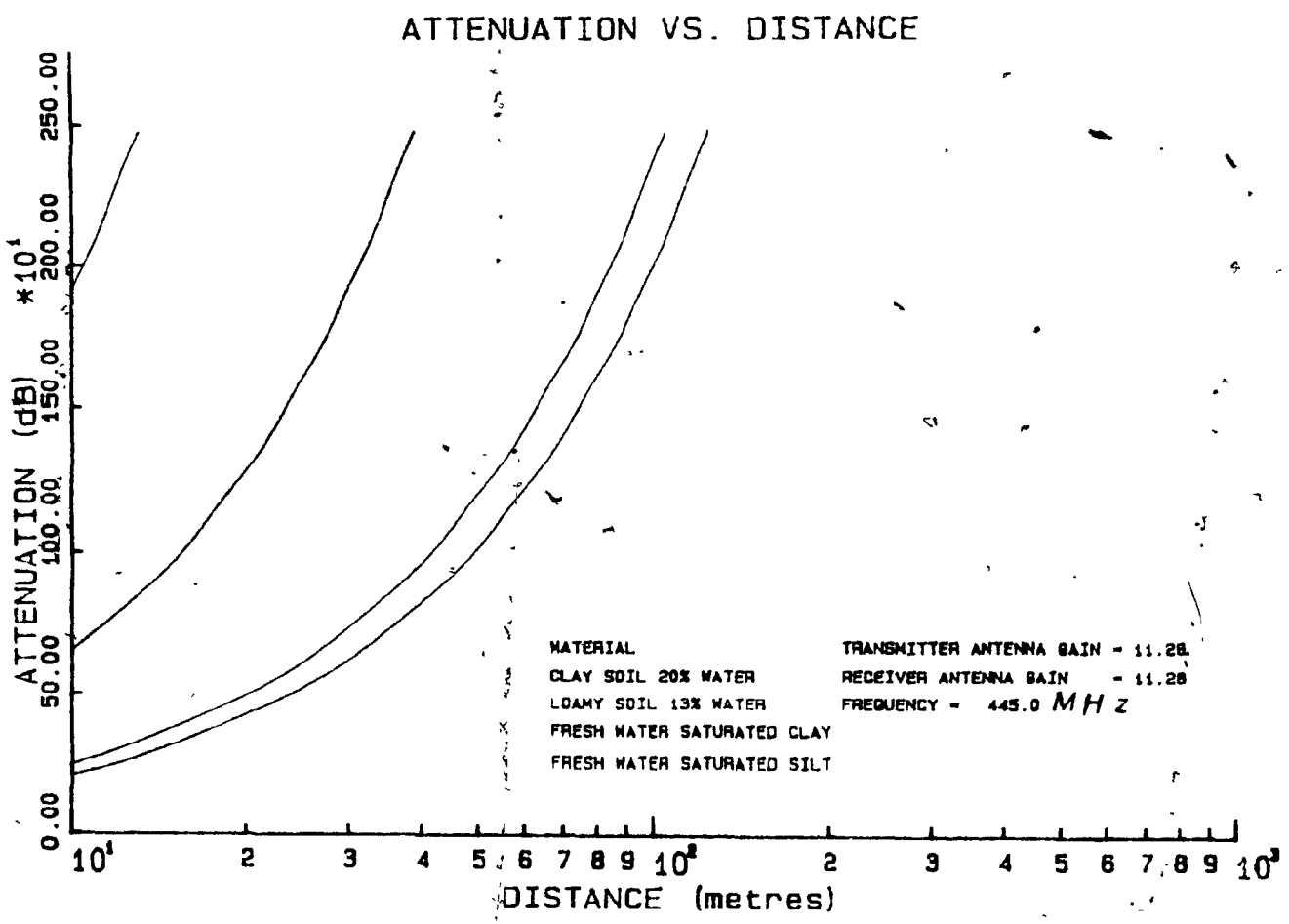

Figure 2.6.4 Attenuation versus distance plots for the common soils whose electrical properties are listed in Table 2.3.5.

(445 MHz) is the frequency used in the author's field instrumentation. Figures 2.6.3 and 2.6.4 show similiar plots for some of the materials used in creating Figures 2.3.3 and 2.3.4 above. Figure 2.6.5 shows similiar plots for selected rock samples listed in Table 2.3.2. The total attenuation experienced by a 445 MHz plane wave travelling through 10 metres of the most absorbing material presented, fresh water saturated clay (Figure 2.6.4), is 190 dB. Less than 10 metres of such clay would effectively negate the possibility of transmitting through the material to a receiver located on the opposite side. In the case of the materials plotted in Figure 2.6.3, a 445 MHz plane wave would be attenuated by less than 100 dB after traversing 100 metres of the material. The main effect to note is the dominance of the linear spreading loss component of the attenuation at short distances for the materials shown in Figure 2.6.3.

The absorption rate of any material, given the measured total attenuation, $\mathcal{A}t$, and the transmitter receiver antenna separation, can be calculated

$$\alpha_{abs} = (\mathcal{A}t - \mathcal{A}s)/8.686\ r. \qquad (2.6.3)$$

$\mathcal{A}t$ ismeasured in situ and $\mathcal{A}s$ is calculated theoretically knowing the frequency, transmitter-receiver separation and antenna gains. α_{abs} will identically represent the absorption rate of the material if all of the emitted wave energy is directed through a material which is homogenous

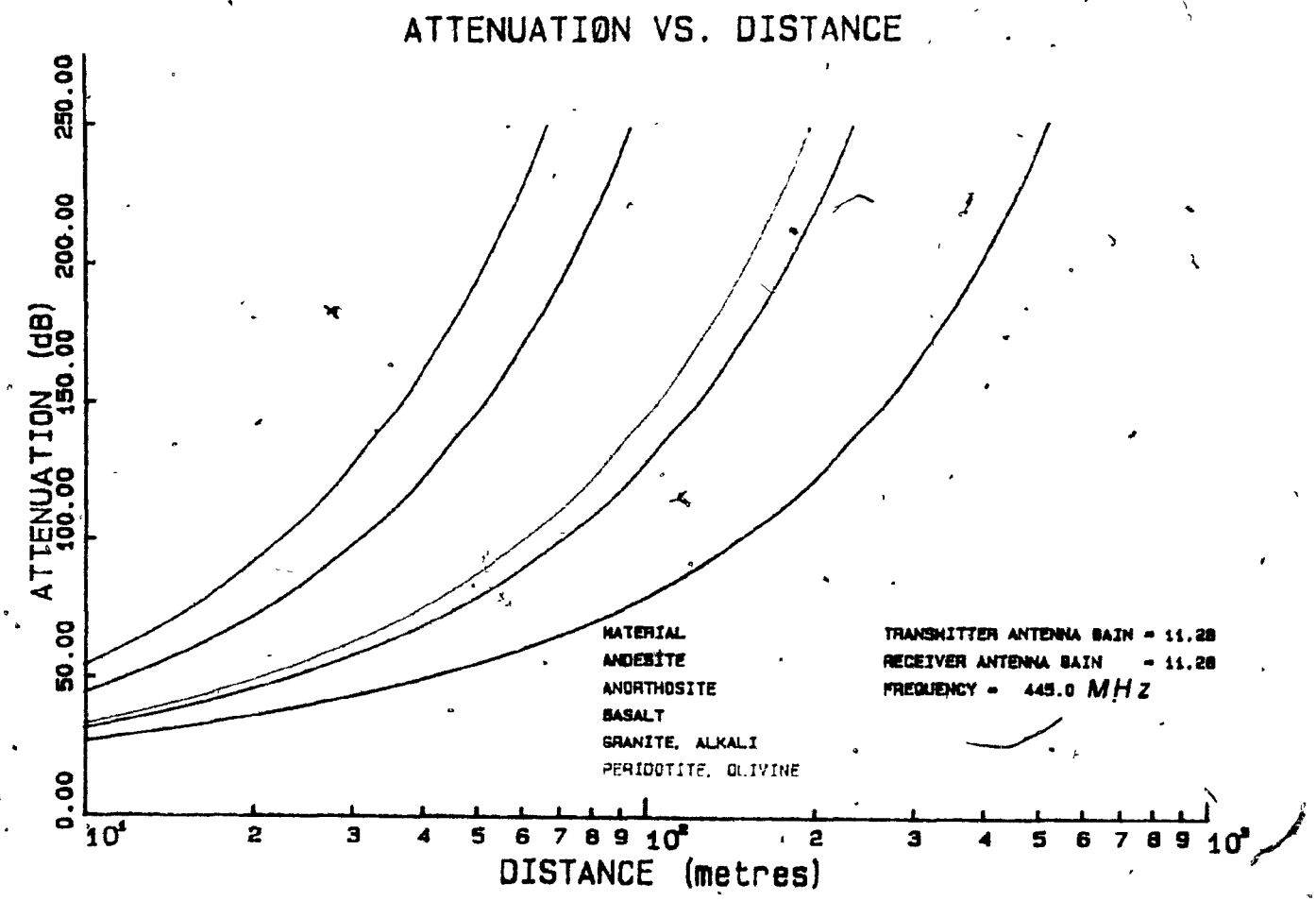

Figure 2.6.5 Attenuation versus distance plots for several of the common rock types whose electrical properties are listed in Table 2.3.2.

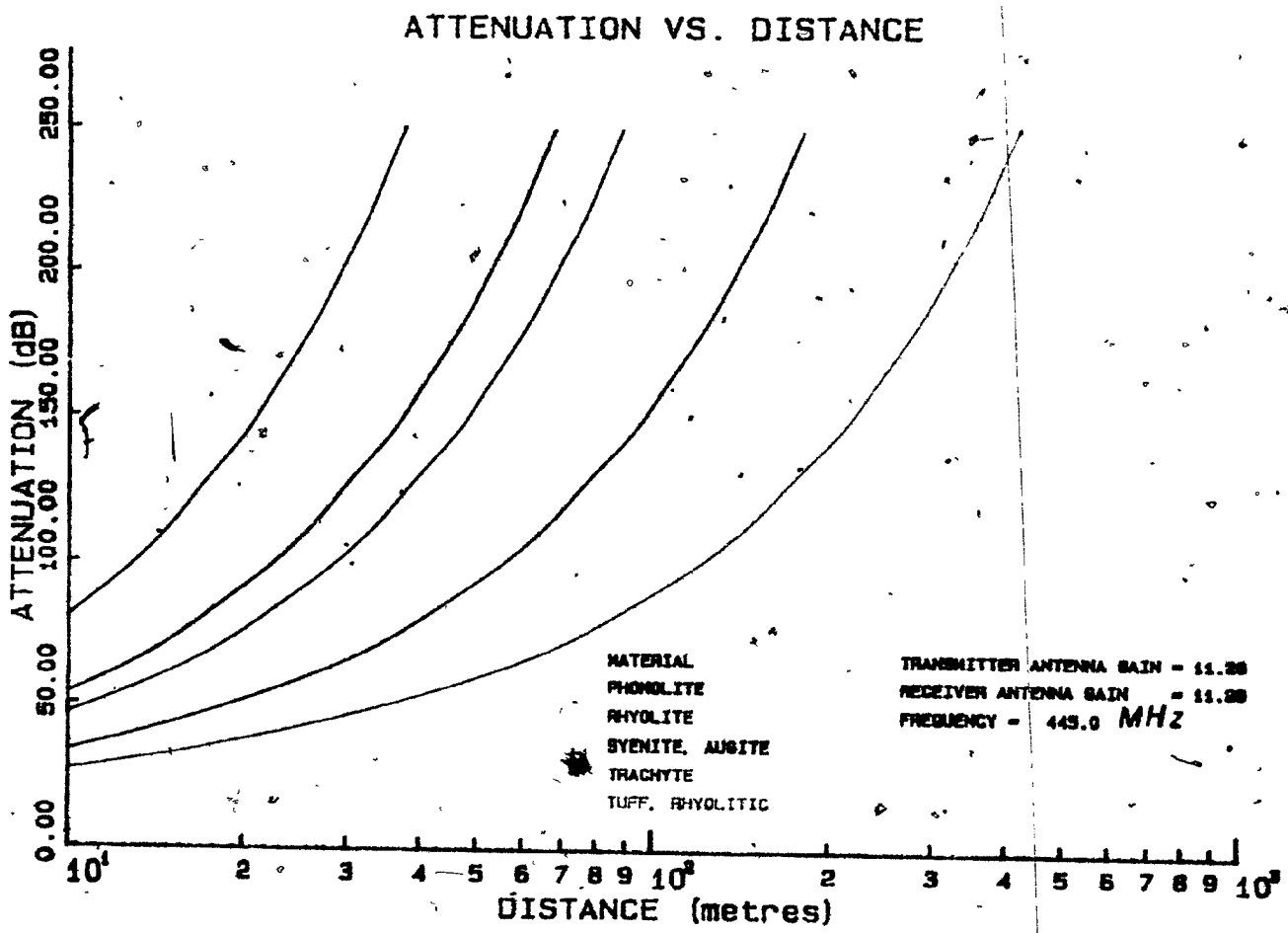

Figure 2.6.6 Attenuation versus distance plots for several of the common rock types whose electrical properties are listed in Table 2.3.2.

and isotropic. All energy lost will then be dissipated within the material. Should the medium consist of two or more materials the attenuation measurement will include the effects due to energy lost in all material traversed, plus the energy losses due to reflection, refraction and diffraction at material interfaces. Since the antennas are placed in the air directly in front of a rock face, an air-rock interface will always exist. It is generally expected that the antennas can be coupled well enough to the rock wall that the above mentioned effects are minimal in these cases.

2.7 Reflection, refraction and diffraction at an interface

The effects of reflection, refraction and diffraction at the junction between materials of differing geophysical properties can be considerable, especially when one of the media is highly permittive or conductive. The reflection and refraction of an electromagnetic wave at a boundary (Figure 2.7.1) is governed by Snell's Law of Refraction:

$$n_1 \sin\theta_i = n_2 \sin\theta_r \qquad (2.7.1)$$

where n_1 and n_2 are the indices of refraction of the two adjoining media and θ_i and θ_r are the angles of incidence and refraction respectively. The angle of reflection is equal to the angle of incidence (Jackson, 1975). Using this law and the fact that tangential components of both E and H are continuous across a boundary (Corson and Lorrain, 1970), one

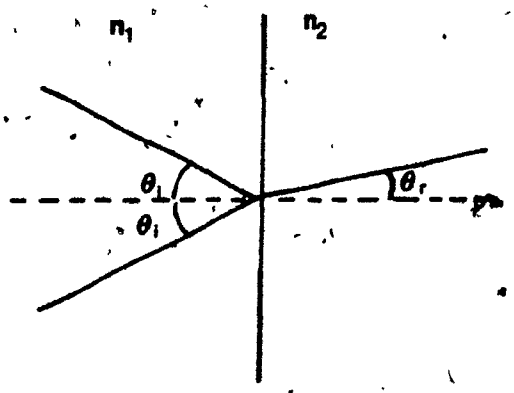

Figure 2.7.1 Reflection and refraction of a wave at a plane interface separating two media of contrasting indices of refraction. The angle of incidence, θ_i, is equal to the angle of reflection. The angle of refraction, θ_r, is related to the angle of incidence and the indices of refraction of the two media through Snell's Law.

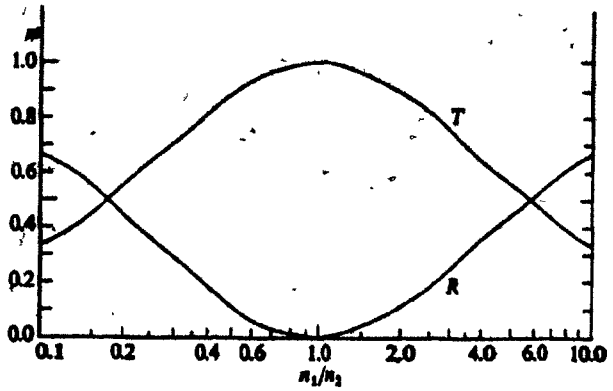

Figure 2.7.2 The coefficient of transmission, T, and the coefficient of reflection, R, at normal incidence as functions of the ratio n_1/n_2 (after Lorrain and Corson, 1970).

can calculate Fresnel's four equations which express the transmitted and reflected amplitudes for an electromagnetic wave incident on an interface. The coefficients of reflection (R) and transmission (T) at an interface between two different materials can subsequently be calculated. These coefficients are expressed in terms of the angle of incidence of the wave and the indices of refraction of the two adjoining media. The index of refraction of a linear, homogeneous, stationary and isotropic medium is give by equation 2.2.21. Figure 2.7.2 illustrates the changes in the reflection and transmission coefficients, for a wave incident normally on an interface, as a function of the ratio of the indices of refraction of the two non-magnetic media. In the case of non-normal incidence total reflection can occur when:

$$\sin \theta_c = n_2/n_1 \qquad (2.7.2)$$

where θ_c is the critical angle. If $n_1 = n_2$, $\theta_c \approx \pi/2$ (ie. total reflection occurs at glancing incidence). Tables 2.7.1 and 2.7.2 list the indices of refraction for the materials whose electrical properties are listed in Tables 2.3.1 and 2.3.2 respectively. The index of refraction can deviate significantly from unity even for relatively non-absorbing materials. In the case of a non-conductor, $\sigma = 0$, equation 2.2.21 reduces to:

$$n = c\sqrt{\varepsilon\mu} \qquad (2.7.3)$$

If the permittivity and permeability are assumed to be real

n/λ (m)	FREQUENCY (MHz) 1.	10.	100.	300.	1000.
Permafrost					
	2.90	2.46	2.45	2.45	2.45
	103.42	12.20	1.22	.41	.12
Fresh water					
	9.02	9.01	9.01	9.01	9.01
	33.26	3.33	.33	.11	.03
Fresh water saturated clay					
	63.68	20.25	6.77	4.41	3.38
	4.71	1.48	.44	.23	.09
Fresh water saturated silt					
	20.25	6.77	3.38	3.19	3.17
	14.82	4.43	.89	.31	.09
Granite					
	2.24	2.24	2.24	2.24	2.24
	134.07	13.41	1.34	.45	.13
Limestone					
	2.65	2.65	2.65	2.65	2.65
	113.31	11.33	1.13	.38	.11
Sea water					
	201.35	63.96	21.16	13.47	9.89
	1.49	.47	.14	.08	.03
Air					
	1.00	1.00	1.00	1.00	1.00
	299.79	29.98	3.00	1.00	.30
Ice					
	2.49	1.81	1.79	1.79	1.79
	120.39	16.61	1.68	.56	.17
Snow					
	1.11	1.10	1.10	1.10	1.10
	269.48	27.36	2.74	.91	.27
Sandy soil dry					
	2.31	1.62	1.60	1.60	1.60
	129.99	18.57	1.88	.63	.19
Sandy soil 2-18% water					
	3.34	1.70	1.60	1.60	1.60
	89.76	17.66	1.88	.63	.19
Clay soil 20% water					
	39.70	12.92	5.35	4.62	4.49
	7.56	2.32	.56	.22	.07
Clay soil dry					
	2.91	1.61	1.54	1.54	1.54
	103.07	18.67	1.94	.65	.19
Loamy soil dry					
	1.99	1.58	1.57	1.57	1.57
	150.85	18.99	1.91	.64	.19
Loamy soil 13% water					
	22.19	7.70	4.60	4.49	4.48
	13.52	3.90	.65	.22	.07

Table 2.7.1 : Indices of refraction and wavelengths, at various VHF/UHF frequencies, for the materials whose electrical properties are listed in Table 2.3.1.

MATERIAL	Index of Refraction	Wavelength (m)
ANDESITE	2.26	.30
ANORTHOSITE	2.61	.26
BASALT	2.99	.22
BASALT	2.83	.24
BASALT, AMYGDALOIDAL	2.69	.25
BASALT, HORNBLENDE	2.59	.26
BASALT, LEUCITE-NEPHELINE	2.37	.28
BASALT, OLIVINE	2.85	.23
BASALT PORPHYRY, OLIVINE	2.87	.23
BASALT, THEOLEIITIC	3.10	.21
BASALT, VESICULAR	2.65	.25
GABBRO, BYTOWNITE	2.65	.25
GRANITE, ALKALI	2.28	.29
GRANITE, APLITE	2.28	.29
GRANITE, BIOTITE	2.33	.29
GRANITE, GRAPHIC	2.24	.30
GRANITE, HORNEBLENDE	2.45	.27
GRANITE, PORPHORITIC BIOTITE	2.35	.28
OBSIDIAN	2.61	.25
OBSIDIAN	2.35	.28
PERIDOTITE, MICA	2.45	.27
PERIDOTITE, OLIVINE	2.49	.27
PERIDOTITE/SERPENTINE	2.74	.24
PHONOLITE	2.55	.26
PUMICE	1.58	.42
RHYOLITE	1.84	.36
SERPENTINE	2.65	.25
SERPENTINE	2.53	.26
SYENITE, AUGITE	2.83	.24
TRACHYTE	2.24	.30
TUFF, GREY	2.47	.27
TUFF, RHYOLITIC	1.90	.35
TUFF, SEMI-WELDED	1.61	.41
VOLCANIC ASH	1.85	.36
VOLCANIC ASH SHALE	1.64	.41

Table 2.7.2 : Indices of refraction and wavelengths, at 450 MHz, for the materials whose electrical properties are listed in Table 2.3.2.

valued only, the index of refraction is then directly proportional to the square roots of their values. Generally severe reflection and refraction effects can be avoided if the changes in the electrical parameters within the medium of propagation are gradual. In order to reduce the chance of an initial refraction due to the air-wall rock interface, the transmitter and receiver antennas should be set up so that their horizontal axes are normal to the wall rock surface.

Diffraction can occur if a wave interacts with any sharp boundary interface, between media of contrasting electrical properties, whose dimension could be considered large with respect to a wavelength. Tables 2.7.1 and 2.7.2 list the wavelengths, for waves of several frequencies, for the materials listed in Tables 2.3.1 and 2.3.2. The usual method of dealing with a diffracting structure is to treat it as a secondary source. The Fraunhofer diffraction region, which exists at a distance from the diffracting object which is large as compared to the wavelength of the propagating wave, is of the greatest interest in geophysics. The field strength of a transmitted plane wave, as measured along a receiving plane perpendicular to the direction of propagation, will vary greatly if a diffracting object is present. The location of simple objects can be reconstructed from a knowledge of their diffraction pattern. Fractures, cavities and sharp material boundaries in a geologic medium can diffract a wave.

2.8 System performance level

The system performance level indirectly determines the maximum distance through rock at which a signal can be detected. It is determined as follows. The minimum detectable signal at the receiver input stage is defined by the voltage and power Vrmin and Prmin respectively. The maximum signal output by the transmitter to the antenna terminalsis defined by power Ptmax or voltage Vtmax. The voltage and power are related:

$$V = \sqrt{P_1 Z} \qquad (2.8.1)$$

where Z is the impedance of the loads.

The system performance level is then defined as the highest level of signal attenuation that can be sustained while still allowing for the transmitted signal to remain detectable at the receiver. The system performance level is calculated as

$$SPL\,max(dB) = 20\log \frac{Vtmax}{Vrmin} \qquad (2.8.2)$$

in terms of signal voltages or as

$$SPL\,max(dB) = 10\log \frac{Ptmax}{Prmin} \qquad (2.8.3)$$

in terms of the signal powers. This calculation is based upon ideal conditions. That is, there are no losses in the transmission lines and the antennas are maximum coupled. Provided these conditions are met, the only losses in signal strength will be associated with the spreading, scattering

and absorption of the electromagnetic radiation by a medium. The higher the system performance level the greater the distance of rock which is penetratable.

Cook (1975) defined a performance figure for ground radars which is analagous to the system performance level. Cook's performance figure in decibels is

$$P.F. = \frac{\text{radiated peak power}}{\text{minimum detectable received signal power}} \quad (2.8.4)$$

The ratio is measured directly by aiming the transmitter antenna at the receiver antenna in a known geometric arrangement. Cook's definition incorporates the antenna gains into the performance factor by measuring the numerator and denominator of equation 2.8.4 at the antenna aperatures. Cook's performance figure is not directly equivalent to the system performance level used here. Typical ground radars possess P.F. values of between 100 and 110 dB. Cook considers P.F. values of 150 dB realizable with state of the art instrumentation.

2.9 Data reduction

An analogy can be drawn between a transillumination electromagnetic survey and the technique used in medical X-ray tomography. Both techniques measure the attenuation of energy by an object placed directly between the transmitter and receiver. The X-ray source possesses a far higher directionality than can ever be obtained at VHF/UHF frequencies and the geometry of the system is greatly scaled

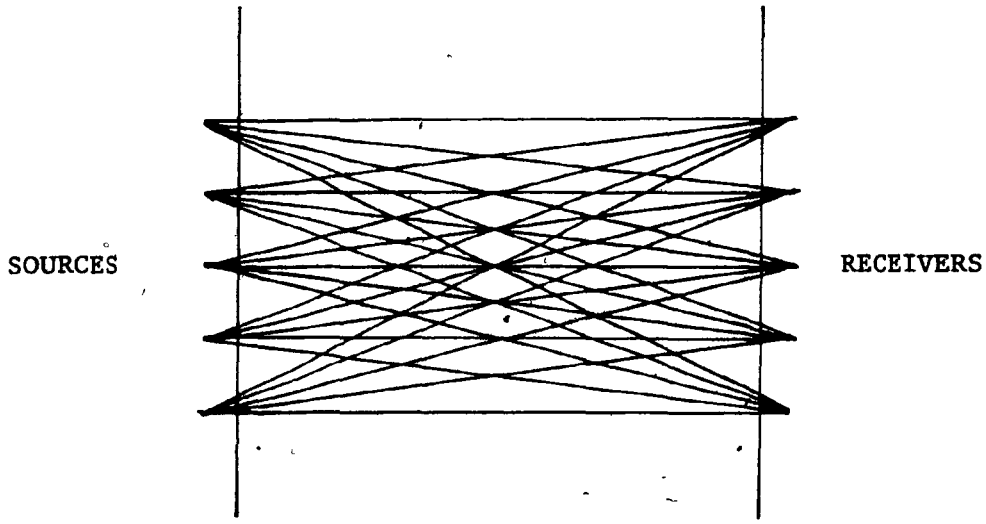

Figure 2.9.1 The construction of fan-like arrays in transillumination work.

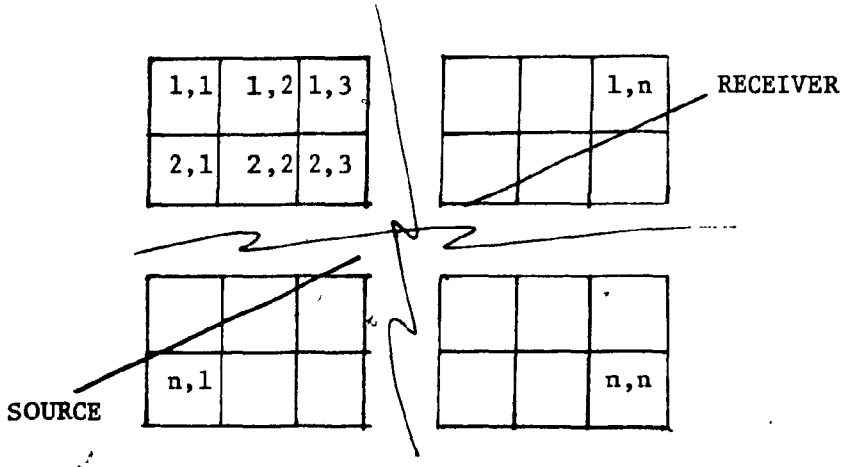

Figure 2.9.2 Division of the survey area up into a discrete grid network consisteing of several small cells.

down from the geologic case.

A considerable body of technique has been developed for the analysis of x-ray tomographs. The principle analytical technology is directly applicable to the treatment of transillumination electromagnetic survey measurements.

In the simplest tomographic reconstructions the x-ray is presumed to propagate in a straight line raypath between the transmitter and receiver. Ray bending due to reflection, refraction and diffraction are ignored. The area to be imaged is extensively surveyed by constructing fan-like receiver arrays around each transmitter location (Figure 2.9.1). The surveyed area is then divided up into a discrete grid consisting of anywhere from hundreds to tens of thousands of small cells (Figure 2.9.2). Each cell is considered to possess a representative attenuation or velocity value. This value can be solved for numerically, given the geometry of the system and the straight line raypath measurements. Measurements obtained via this system can be expressed mathematically as

$$M=G \cdot A \qquad (2.9.1)$$

or

$$M = \sum_{\lambda}^{I} \sum_{j}^{J} G \cdot A \qquad k=1,2...K \qquad (2.9.2)$$

where:

$M=\{M_k(\theta)\}$	vector of measured raypath attenuations
$G=\{G_{ij}\}$	weighting matrix incorporating the geometry
$A=\{A_{ij}\}$	cell absorption rate to be solved for
k	number of raypaths

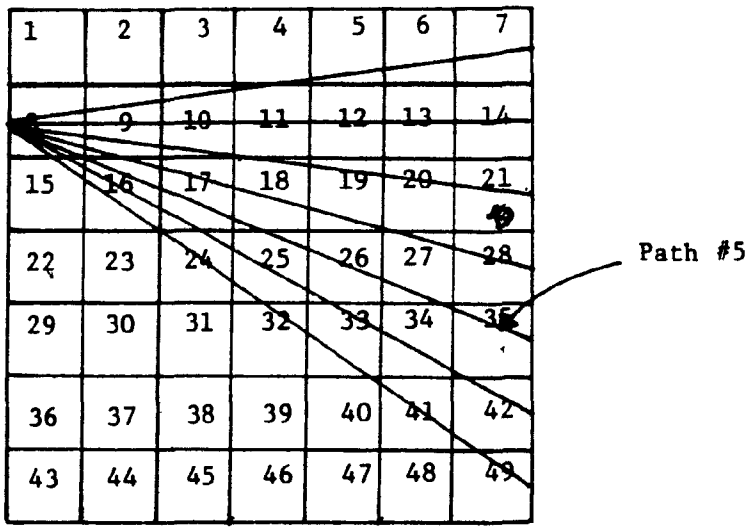

Figure 2.9.3 A 7 x 7 grid divided into 49 zones for the purpose of performing a tomographic reconstruction using the back projection technique.

ixj number of cells

If G^{-1} can easily be computed the solution is:

$$A=G^{-1}M \qquad (2.9.3)$$

Typically G^{-1} cannot be computed. Approximations in the model and various noise sources render equation 2.9.2 inconsistent (Dines and Lytle, 1979). Computational efficiency can also require that other solution techniques be used. The most common method is the iterative reconstruction technique (ART) (Lager and Lytle, 1977) of which several variations exist. These generally consist of minimising a function in order to determine the additive corrections to be made to the initial cell 'guestimates'. A solution for the attenuation matrix, A_{ij}, is then iteratively approached. A second common algorithm for solving the attenuation matrix is the simultaneous reconstruction technique (SIRT) (Lager and Lytle, 1977). The major difference between ART and SIRT is that the latter operates on all the paths passing through a given zone at the same time while the former operates on only one path at a time. Computationally the simplest solution technique is back projection (Lager and Lytle, 1977). Back projection consists of averaging the values of all paths through a given zone. The grid area is divided up as in figure (2.9.3). Then, assuming the k^{th} path is homogeneous along its length,

$$A_{ki} = M_k / L_k \qquad (2.9.4)$$

where L_k is the length of raypath k. The weighted average is taken to determine matrix coefficient A

$$A_i = \sum_k A_{ki} D_{ki} / \sum_k D_{ki} \qquad (2.9.5)$$

where D_{ki} is the distance travelled along the k^{th} raypath through the i^{th} zone.

Lager and Lytle (1977) used the ART algorithm to reconstruct an image on simulated 50 MHz data based upon an oil reservoir engineering problem. Dines and Lager (1979) used a similiar reconstruction technique to image a future subway station site at 50 MHz. Somerstein et al.(1984) used an ART algorithm modified to take into account the finite antenna beamwidth available at their operational frequency of 1.5 MHz when imaging an oil shale retort. The beamwidth was discretized into a number of infinitesmally narrow beams.

The validity of using the tomographic reconstruction technique in a given geophysical situation rests upon the satisfaction of several criteria. Straight line ray-optic propagation of the transmitted wave must be assumed. Reflection, refraction and diffraction of the waves within the medium must be negligible. Radcliff and Balanis (1981) developed a modified ART algorithm which incorporated the wave scattering effects due to refraction and first order reflection. The physical dimensions of the antennas must be small with respect to the cell size and the distance between the transmitter and receiver should be large as compared to both of the above. The geometry of the system must be well

known. The antenna positions and the relative position of the intervening wall rock should be accurately surveyed. The simple back projection reconstruction technique, equations 2.9.4 and 2.9.5 above, requires that the raypath positions be well determined in order to reconstruct the matrix D_{kl}. Furthermore the antennas must be well coupled to the wall rock surface in order to avoid initial scattering effects due to reflection and refraction at this surface. The quality of the tomographic image will be dependent upon the number of individual cells the area to be imaged is divided up into. Dines and Lytle have simulated a region between two boreholes with a 100x100 cell model and 100 equally spaced transmitter and receiver locations. Due to the geometrical considerations and the large number of survey locations typically required, the tomographic reconstruction technique is best suited for treating attenuation data collected in a borehole survey.

The data collected in this study was too sparse and insufficient geometrical control was available to attempt a meaningful tomographic inversion. Absorption losses are calculated using equation 2.6.3; an attempt to determine an average UHF conductivity for the surveyed material is also made.

Chapter 3

Instrumentation

3.1 General

Continuous-wave radio frequency instrumentation typically consists of separate transmitter and receiver systems, each possessing: a basic console containing the required electronics, a power supply, an antenna and the required interconnecting cables. Figure 3.1.1 illustrates the typical system. A short summary of such continuous-wave RF equipment follows.

Prichett's (1952) equipment for measuring the RF attenuation rate in shales consisted of a compact transmitter and receiver lowered down adjacent boreholes. The transmitter was completely self-contained and was suspended by a non-metallic rope. The receiver was suspended by a coaxial cable which carried an audio frequency signal to a filter and voltmeter located on the surface. His system operated at 1.652 MHz. The antennas were half-wave dipoles.

de Bettencourt and Frazier (1963) similiarly developed equipment for the measurement of RF-wave attenuation between boreholes. It consisted of an encapsulated transmitter and electrically short-circuited insulated dipole lowered down the hole by a distance calibrated nylon rope. A short-circuited insulated monopole connected via shielded coaxial

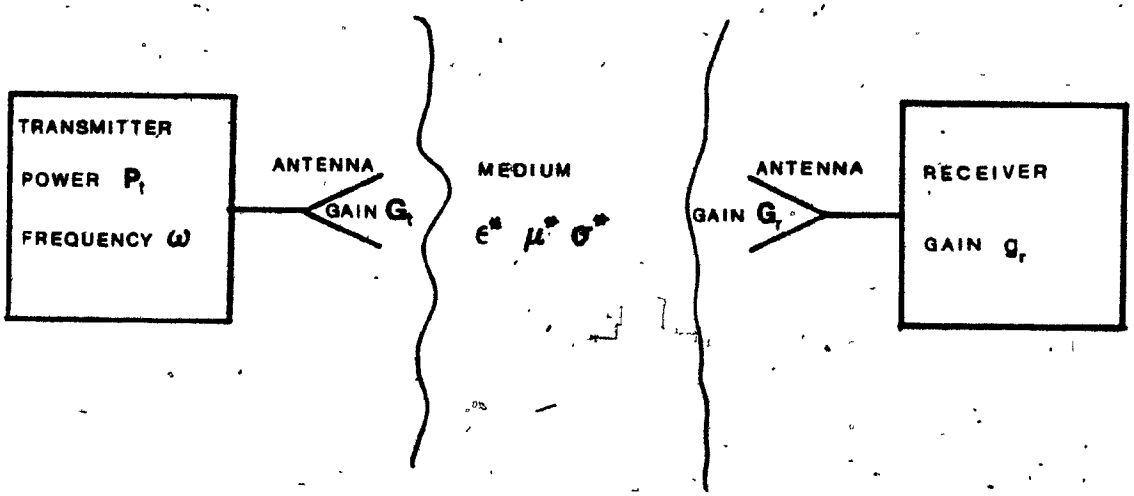

Figure 3.1.1 Typical survey setup for a continuous-wave transillumination survey.

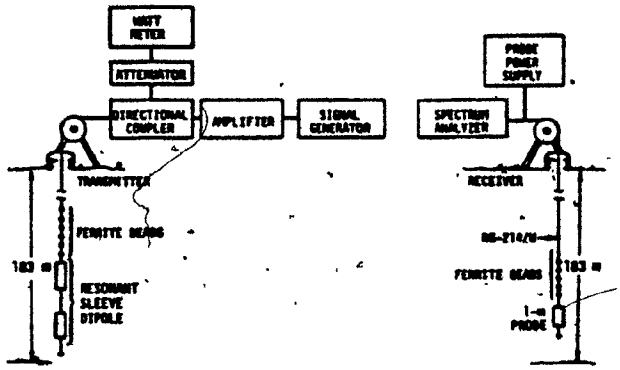

Figure 3.1.2 Transmitter-receiver setup for the CW-hole-hole experiments (after Lytle et al., 1976).

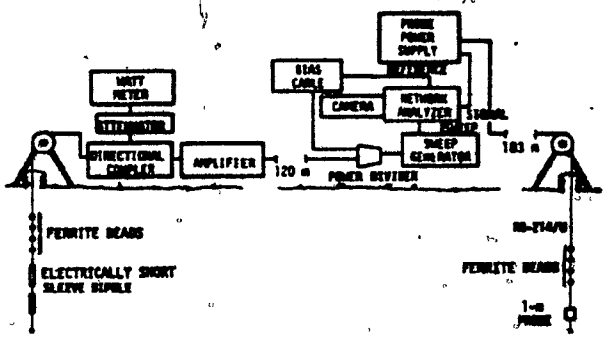

Figure 3.1.3 Transmitter-receiver setup for the swept-frequency hole-to-hole phase shift experiments (after Lytle et al., 1976).

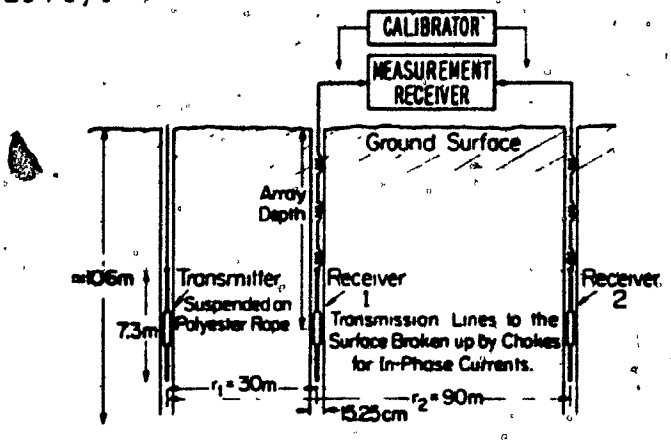

Figure 3.1.4 General arrangement of the three-hole propagation measurement system (after Grubb et al., 1976).

cable to a field intensity meter on the surface formed the receiving instrumentation. This system operated at 155 kHz.

Lytle et al. (1975) developed equipment for measuring the attenuation and phase shift of electromagnetic fields transmitted between two holes in a permafrost environment. The attenuation and phase measuring equipment are depicted in Figures 3.1.2 and 3.1.3 respectively. Measurements were made over a frequency range of from 5 to 50 MHz.

Grubb et al. (1976) developed a dual receiver system for measuring the complex propagation constant (ie. , equation 2.1.13) of the material between two boreholes. Differential signal strength and phase measurements were made between the two downhole receivers over a frequency range of from 300 kHz to 25 MHz. The transmitter-receiver arrangement is depicted in Figure 3.1.4.

Unterberger (1978) adapted a continuous-wave, frequency-modulated (CW-FM) radar altimeter for use in underground salt mines. The system operated at 4.3 GHz and used horn antennas having 18 dB of gain for both the transmitter and receiver. The transmitter output was 1 W.

Rao and Rao (1983) used a system based upon the Russian radio-wave absorption technique (Buselli, 1980). The transmitter consisted of a three-watt, crystal-controlled 1 MHz oscillator connected to a 5 metre horizontal dipole antenna. The superheterodyne receiver employed a parallel-tuned magnetic antenna.

The system developed by the author, here, for

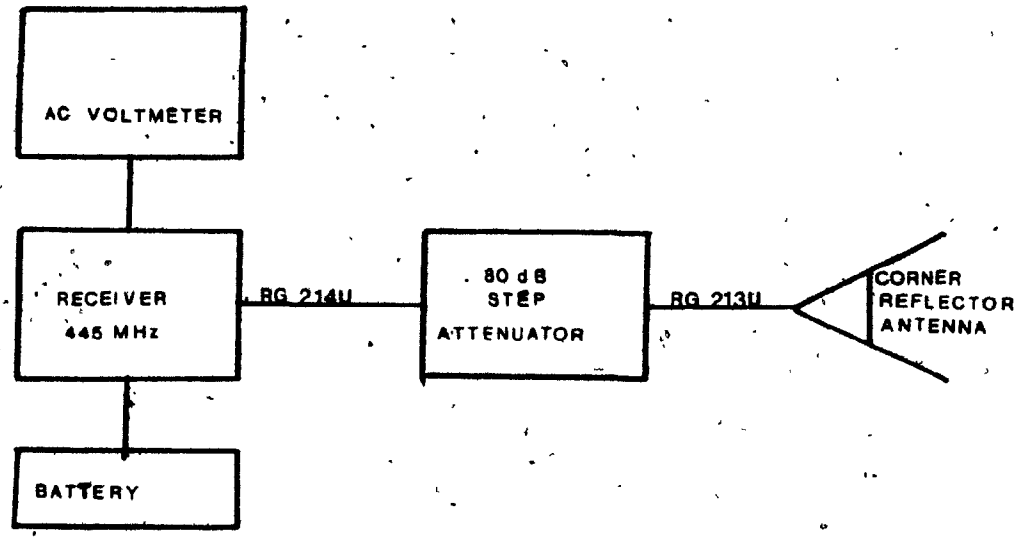

Figure 3.1.5a Block diagram of the McGill UHF receiver.

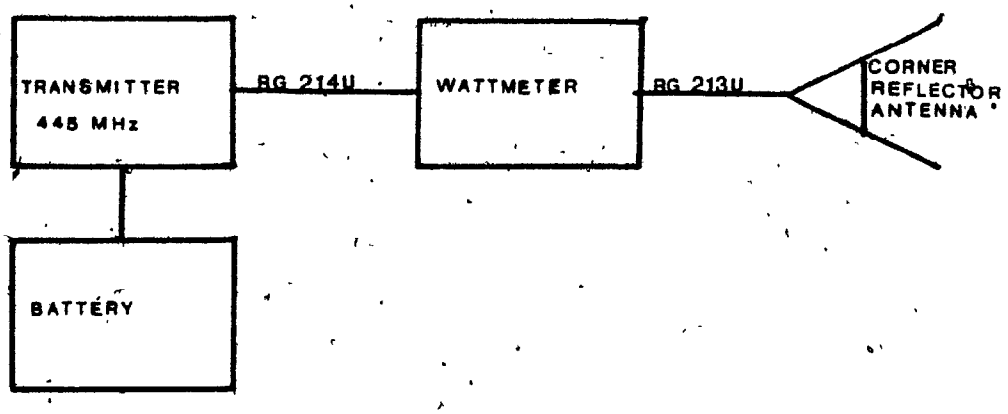

Figure 3.1.5b Block diagram of the McGill UHF transmitter.

measurement of radio-frequency absorption is shown in Figure 3.1.5a and 3.1.5b. The separate transmitter and receiver units consist of identical transceivers, antennas, batteries and interconnecting cables. A step attenuator is employed to control the received signal level which is measured by an AC voltmeter. A RF wattmeter monitors the transmitted signal power. The transmitter, receiver, antennas and associated electronics accessories are described in detail in the sections that follow.

3.2 The Radio Frequency Bands

Certain constraints were imposed upon the design of the instrumentation by the desire to operate under Federal licence. The radio frequency band is divided into the 8 component sub-bands shown in Figure 3.2.1. Individual frequency allotments within each band are governed by international agreements administered by the International Telecommunications Union (ITU). The world has been divided into three regions for this purpose (Figure 3.2.2). The frequency allocations for Region 2, which comprises the western hemisphere, are listed in Table A.1, Appendix A.

In designing the equipment, several objectives were to be satisfied. Firstly, the wavelength in air must be short as compared to the distance between the transmitter and receiver stations. This would ensure that the transmitted wavefront would be effectively planar at the receiver station and that the resolution of the system would be high

enough to locate features of interest within the intervening rock mass. Considering that the distances between transmitter and receiver would be on the order of 40 to 50 metres the wavelength should be less than 2.5 metres. Secondly, the performance characteristics of the instrument should be high enough to allow sufficient penetration (ie. 40 to 50 metres) of a geological material so that a geophysically useful survey could be performed. The losses incurred in the transillumination mode are:

$$\mathcal{A}t = 8.686\ \alpha_{abs} \cdot r + \mathcal{A}s \qquad (2.6.1)$$

$$\mathcal{A}t = 8.686\ r\ \omega \sqrt{\frac{ab}{2}\{(1 + \tan^2\phi\ )^{1/2} - 1\}}$$

$$+ \{ Gt + Gr - 60\log r - 120\log f - 32.44\} \qquad (2.6.2)$$

The spreading loss, $\mathcal{A}s$, can be reduced by increasing the gain of the antennas used. Typically this gain is limited by the need to have a compact and portable antenna. The absorption loss, $\alpha_{abs} \cdot r$, can be controlled by varying the operational frequency. As discussed in section 2.3 above, the absorption-versus-frequency curves level off after a critical frequency. This critical frequency is dependent upon the electrical properties of the medium. The curves, typically, tend to flatten out between 10 MHz and 1 GHz for many of the common materials examined in Figures (2.3.3) to (2.3.6). For the extremely resistive limestone and granite, these absorption-losses level off at much lower frequency. At wavelengths of 2.5 metres (120 MHz) or less

THE RADIO FREQUENCY BAND

Frequency								
3 kHz	30 kHz	300 kHz	3 MHz	30 MHz	300 MHz	3 GHz	30 GHz	300 GHz
VLF	LF	MF	HF	VHF	UHF			
100 km	10 km	1 km	100 m	10 m	1 m	100 cm	10 cm	1 cm
Wavelength								

Figure 3.2.1 The radio frequency bands (after Westman, 1968).

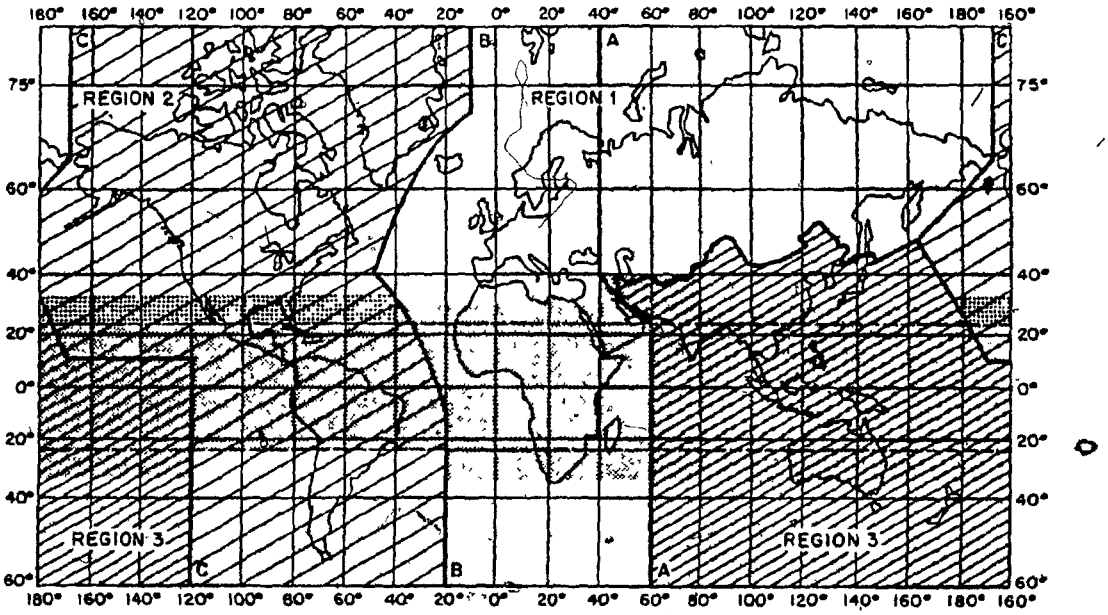

Figure 3.2.2 Division of the globe into three regions for the purpose of worldwide frequency allotment (after Westman, 1968).

the absorption rates vary between 0.5 and 100 dB/m. For the more highly absorbing materials the absorption rate continues to increase with frequency beyond 120 Mhz. Therefore, under such conditions, the frequency of operation should be kept as low as possible so that adequate penetration distances will be realizable. It is not unreasonable to expect the presence of conductive fluids infilling fractures in even the most resistiverock mass.

In view of the constraints outlined immediately above, an operating frequency of between 100 Mhz and 500 Mhz would provide a high enough degree of resolution and suitably low absorption losses so as to obtain geophysically useful results. Table A.1, Appendix A, shows that the frequencies within this suitable range are all specifically allocated. Discussions were entered into with the Federal Department of Communications (DOC) following which a frequency of 445 MHz was allocated on an experimental basis. Since there was no easily identifiable category for such geophysical equipment, an experimental licence in the amateur band (420.0-450.0 MHz) was issued. The high effective isotropic radiated power (equation 2.4.15) of the proposed transmitter system (greater than 200 Watts) exceeded the limits of the band so the transmitter was licensed for underground use only. The receiver could operate anywhere since it does not radiate. The current licence number and call sign for the McGill UHF system are 5582159234 and VE9ILU respectively.

3.3 Instrument Specifications

In designing the instrumentation, there was a desire to use modular components. These would serve to keep the instrumentation multifunctional, portable and packageable. Modifications could then be made to each component individually as required. Components could be inserted or removed according to survey conditions. The receiver should be capable of stable operation at 445 MHz and possess a gain that remains constant over a broad range of received signal amplitudes. That is, the receiver must be linear. Its antenna should be able to receive the transmitted signal and send it to the input stage of the receiver with a minimal line loss. The transmitter should provide a constant output-power signal into the transmitter line and the transmitter antenna should be capable of radiating this signal with as small a loss as possible. The system should possess a large enough gain-bandwidth product so that operation under a wide range of material absorption rates and transmitter-receiver separation distances is possible. The system performance level (equation 2.8.2) is limited to a finite maximum value which constrains the upper limit of the range of measurable attenuations (equation 2.6.1). The input saturation signal voltage, V_{rsat}, determines the minimum measurable attenuation. In the case of extremely nonabsorbing media and short transmitter-receiver separations a method for lowering the system performance

level is required so that the receiver will not saturate. This can be achieved by lowering the transmitted power, the antenna gain or the input saturation signal voltage. In practice, one would not want to change the antenna gain as this would alter the radiated and received field patterns resulting in a change in the volume of material being sampled.

3.4 The transmitter and receiver

The choice of the transmitter and receiver electronics is limited by the specifications (section 3.3). The proximity of the licensed test frequency (445.0 MHz) to the 450.0 - 470.0 MHz commercial communication band and the 470.0 - 890.0 Mhz broadcasting band, which includes for example the UHF television channels, (see table A.1, Appendix A) means that commercial radio electronic components are readily available. UHF television receivers could be modified to realize the required receiver. Power oscillators or crystal oscillators with subsequent power amplification could serve as the transmitter. Despite the fact that the option of building the system electronics from small scale components would provide a greater degree of design flexibility, the use of larger modular components allowed for less development time. The use of basic commercial equipment components facilitated the DOC licence application. The DOC was, understandably, reluctant to provide a test frequency without detailed equipment

YAESU MUSEN TRANSCEIVER FTC-4625

Transmitter:

Output power: 25 Watts

Frequency stability: > ± 5 ppm

Antenna impedance: 50Ω

Crystal multiplication: x12

Power consumption: 6.0 Amperes

Receiver:

Sensitivity: > 0.5 μV for 20 dB noise quieting
> 0.3 μV for 12 dB SINAD

Input signal saturation voltage, V_{RSAT} : approximately 1 mV

Receiver gain: 25 dB to point A
55 dB to point B
128 dB to the discriminator

Common:

Input/output jack: UHF female

Power requirements: 13.8 V DC, negative ground

Weight: 1.6 kg

Table 3.4.1 : Specifications for the FTC-4625 Transceiver (Yaesu Musen, 1980).

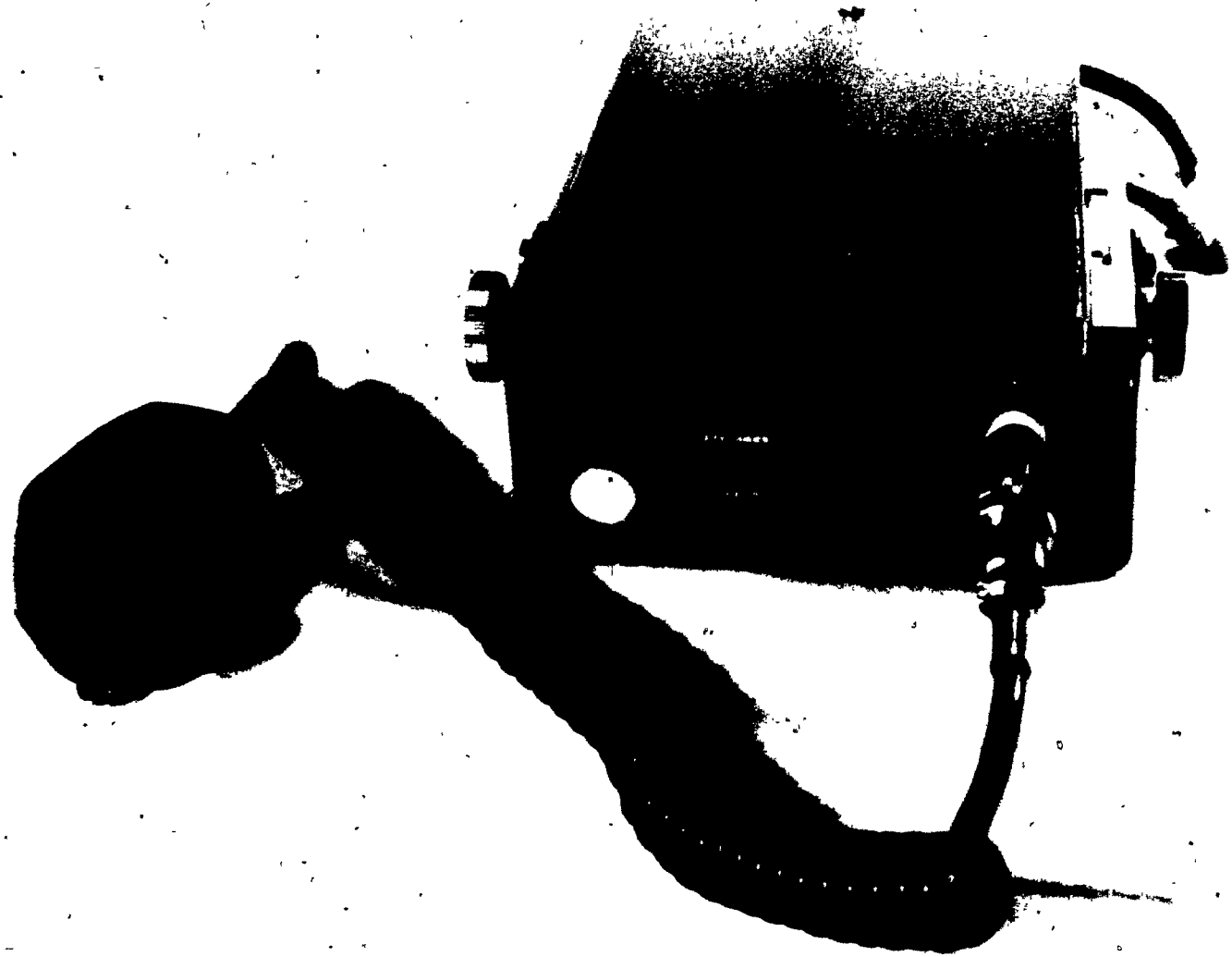

Figure 3.4.1 The Yaesu Musen FTC-4625 transceiver.

specifications. Given the difficulty of designing the instrumentation without a prior licensed frequency, it was clear that the modification of standard communication equipment was the best approach to follow. Since the transmitter and receiver must both operate at the licensed frequency, it seems reasonable to purchase them as a matched pair. Several manufacturers of radio communication equipment were approached with the problem of providing transceivers for the 445.Ø MHz frequency. Their equipment is designed to operate in the 450.Ø - 470.Ø MHz band with a radiated power of from 1 to 3Ø Watts. The only manufacturer contacted who would agree to the necessary modifications was the Yaesu Musen Co. of Japan. Two Yaesu Musen FTC-4625 transceivers were purchased with the intent of using one as the transmitter and the front end stages of the other as the receiver. Since these transceivers possess both a transmit and receive capability their functions could be interchanged to speed field operations or the spare transmit and receive channels could serve as backups. The DOC licence does not include any allowance for a modulated signal so the use of the tranceivers' audio communication capability would not be permitted.

The YAESU FTC-4625 transceiver is pictured in Figure 3.4.1. The transmit and receive channel specifications are listed in Table 3.4.1. Block diagrams of the transmit and receive channels are shown in Figures 3.4.2 and 3.4.3 respectively. The transceiver used as a transmitter will

hereafter be referred to as the transmitter and the transceiver used as a receiver will hereafter be referred to as the receiver.

The transceiver electronics, shown in Figures 3.4.2 and 3.4.3, has been left essentially unmodified from its original form. The only changes made by Yaesu Musen were in component values. These changes, over one hundred in total, were made at the factory in Japan at the request of the author. The microphones were removed (by the author) in order to comply with the special DOC licensing regulations. A single-pole, single-throw switch has been added to facilitate the switching on and off of the 445.Ø MHz carrier frequency. The transceivers normally possess the ability to operate on any one of seven preselected channels in the frequency range from 45Ø.Ø to 512.Ø MHz. Only one channel is in fact used and the range of possible additional frequencies has been severely limited by the component modifications.

The transmitter channel (Figure 3.4.2) consists of a 37.1 MHz fundamental crystal oscillator which generates the carrier. The carrier is subsequently phase modulated by the audio signal from the microphone and multiplied in frequency by 12. The resulting signal is amplified and fed out through a female UHF antenna jack. The output impedance is 5Ø ohms. The FTC-4625 possesses an add-on power booster unit which increases the output power from the standard 1ØW

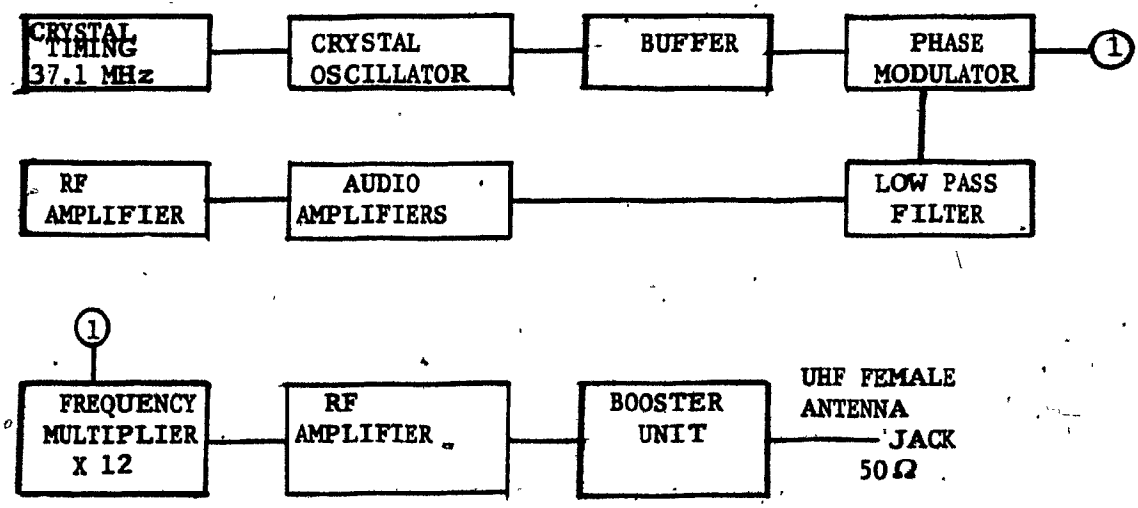

Figure 3.4.2 Block diagram of the transmitter section of the FTC-4625 transceiver circuit.

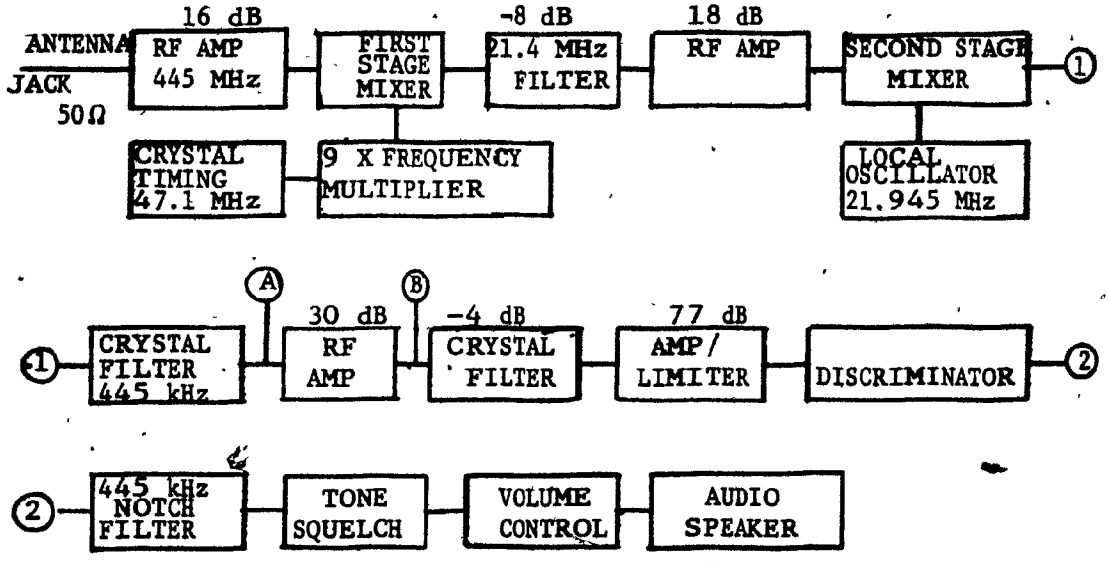

Figure 3.4.3 Block diagram of the receiver section of the FTC-4625 tranceiver circuit.

to 25W. The output power is fixed at 25 W. The transmitter is used as is with no further modifications.

The receiver channel (Figure 3.4.3) consists of a signal input through the same female UHF antenna jack. The frequency modulated input signal is filtered and amplified. It is first-stage mixed with a nine times multiplied 47.1 MHz signal produced by a crystal controlled oscillator. The resultant 21.4 MHz first intermediate frequency (IF) is subsequently amplified and filtered prior to second-stage mixing with a 21.945 MHz signal from a local oscillator. The resultant 445 kHz second IF is amplified and crystal filtered before being driven to saturation by an amplifier/limiter. The audio signal is extracted from the phase modulated clipped signal by a discriminator. A 445 kHz notch filter removes the carrier. The audio signal is amplified, volume-controlled and sent to a speaker. A tone-squelch circuit disables the audio amplifier in the absence of a carrier of preselected signal strength.

The received signal strength must be measured at some point within the receiver channel. The receiver input signal must be linearly related to the signal at the point of measurement. That is, the total gain between the input and the point of measurement must be a known finite constant. The point of measurement must follow a significant amplification of the input signal, but precede the signal driven to saturation by the amplifier/limiter. Ideally, it should be measured at a point where the signal

level itself will not be affected by its measurement. Points A and B, Figure 3.4.3, satisfy these measurement criteria. Total signal gains to points A and B are 25 dB and 55 dB respectively. All AC voltages referred to hereafter will be rms voltages. The minimum signal detectable at the input, Vrmin, is amplified to 8.9 μV and .28 mV at points A and B respectively. An input signal of amplitude Vrsat is amplified to 17.8 mV and .56 V at points A and B respectively. The signals are extracted by connecting RG-174 coaxial cables directly onto the printed circuit board at points A and B. The cables are connected to female BNC panel connectors which are mounted to the exterior casing of the transceiver. These then serve as signal output ports for the 445 kHz IF. In fact only the point B output connection was eventually used in the field. The RMS value of the signal must subsequently be measured in order to determine the received signal level. Three measuring techniques were developed although only one was eventually used in the final field surveys.

The first technique involves the use of an RF probe. An RF probe can usually be attached to any DC voltmeter of a specified input impedance. The RF probe rectifies an AC input signal and converts it to the corresponding DC RMS value. The specifications of the Fluke 85RF high frequency probe, which was used for these measurements are listed in Table 3.4.2.The Fluke 85RF requires a DC voltmeter of 10 MΩ

input resistance. The minimum voltage measurable by the probe is .25.V. Given that the saturation voltage at point B is .56 V, there must be some manner of controlling the input signal level or only a very limited attenuation range would be measurable. In fact the range of possible attenuation measurements would be only 7 dB. The lowest attenuation value measurable can be calculated as follows. Given the transmitter output voltage, Vt , and the input signal saturation voltage, Vrsat, the lowest attenuation measurable is:

$$A\,\text{min} = 20 \log \frac{Vt}{Vrsat} = 91 \text{ dB} \quad . \quad (3.4.1)$$

The system performance level calculated from equation 2.7.2, is 157 dB. The directly measurable attenuation range using the RF probe is from 150 dB to 157 dB, scarcely adequate for the survey conditions which could be encountered and far short of the receiver's range. A simple change in the spreading loss due to a change in transmitter-receiver separation could easily result in a 7 dB variation in the signal level.

An alternative measuring device is an AC voltmeter. The specifications for the Hewlett-Packard 403B AC voltmeter are listed in Table 3.4.3. Its measurement range (1 mV to 300V) is far superior to that of the RF probe. Although the low end measuring limit (high attenuation rates) is adequate, the problem of taking an attenuation measurement when the attenuation is extremely low still exists. The AC voltmeter

FLUKE 85RF HIGH FREQUENCY PROBE

AC to DC ratio: 1:1

Ratio accuracy: ±0.5 dB above 0.5V (at 1 MHz with 10 MΩ load)
±1.0 dB below 0.5V

Frequency response: +0.5 dB 100 kHz to 100 MHz
+1.0 dB 100 MHz to 200 MHz
+3.0 dB 300 MHz to 500 MHz
(relative to 1.0 MHz)

Voltage range: 0.25 to 30 V rms

Maximum input voltage: 30 V rms, 200 V dc

Input capacitance: approximately 3 pF

Response: responds to peak value of input; calibrated to read rms value of a sinewave

Table 3.4.2 : Specifications for the Model 85RF High Frequency Probe (Fluke, 1983).

HEWLETT-PACKARD 403B AC VOLTMETER

Range: 1 mV to 300 V rms full scale, 12 ranges

Accuracy: +0.2 dB 10Hz to 1 MHz, +0.4 dB 5 to 10 Hz and 1 to 2 MHz (0-50° C)

Frequency range: 5 Hz to 2 MHz

Response: responds to the rms voltage of a sine wave input

Input Impedance: 2MΩ shunted by <60 pF 1 mV to 30 mV ranges, shunted by <30 pF 100 mV to 300 V ranges

Power: 4 rechargeable batteries

Table 3.4.3 : Specifications for the Model 403B AC voltmeter (Hewlett-Packard, 1981).

is capable of directly measuring total attenuations of between 91 dB, the lowest attenuation measurable, and 157 dB. This still limits, to some extent, the flexibility of the system to measure in a low absorption environment and/or at close separations. The spreading loss with a 50 m transmitter-receiver separation is 50.4 dB. This means that for an attenuation to be measurable at this separation the absorption rate must be on the order of 1 dB/m or greater at 445 MHz. Given the measured electrical parameters and the calculated absorption rates in common materials (see Table 2.3.2), it is obvious that many common rock or soil types do not fulfil this measurability criterion. Furthermore, the situation worsens as the separation is decreased or antenna gain is added. Clearly, there exists a need to reduce the transmitted power or to raise the receiver input saturation voltage. Both options have, in fact, been implemented in this research.

The third signal measuring technique, an indirect method, is discussed in section 3.6 below.

3.5 The power and signal attenuators

The transmitter's output power is fixed at 25 W. Modification of the internal electronics to reduce the output power was considered. The removal of the add-on power booster unit would reduce the output power from 25 to 10 W or by about 4 dB. This would require the modification of approximately 10 internal connections each time a power

reduction would be needed. Also, 4 dB is not a sufficient signal reduction to justify the effort required to make this modification. Another option would be to tap off the output signal at an earlier stage. There is, however, no real location to tap off the signal prior to the radio frequency amplifier (Figure 3.4.2). Care would have to be taken that the line impedance was matched to 50 Ω. Again a considerable effort would be required for only 4 dB of signal reduction. The most logical alternative in reducing the transmitted power is to stay with the modular design concept and insert a commercial power attenuator into the transmission line. These are available for a variety of frequency ranges and power dissipation values. The specifications for the Weinschel Engineering Model 33-10-34 10 dB coaxial fixed attenuator, which was used here, are listed in Table 3.5.1. The attenuator is effectively a non-radiating resistive element which can be inserted into the transmission line between the transmitter and the antenna. It has a nominal impedance of 50 Ω over the frequency range DC to 8.0 GHz. Maximum input power is 25 W. The power attenuator has the flexibility that it can easily be inserted into the transmission line to provide 10 dB of attenuation when needed. The signal power at the transmitter antenna input terminals is then reduced to 2.5 W. The minimum measurable attenuation is consequently reduced to 81 dB. Clearly it would be more power efficient

WEINSCHEL 33-10-34 POWER ATTENUATOR

Frequency range: DC – 8.0 GHz

Nominal impedance: 50 ohms

Attenuation (dB): 10 + 0.3

Maximum VSWR: 1.1 DC to 1.5 GHz
1.2 1.5 to 4.0 GHz
1.3 4.0 to 8.0 GHz

Power rating: 25 Watts average, 5 kilowatts peak at 25° C

Temperature range: -55° to 125° C

Weight: 0.17 kg

Table 3.5.1: Specifications for the Model 33-10-34 Power Attenuator (Weinschel, 1982).

WAVETEK 5080 SIGNAL ATTENUATOR

Frequency range: DC – 2.0 GHz

Nominal impedance: 50 ohms

Attenuation: 0 to 80 dB in 1 dB steps

Maximum VSWR: 1.2 DC to 1.0 GHz
1.5 1.0 to 2.0 GHz

Power rating: 0.5 Watts maximum

Table 3.5.2: Specifications for the Model 5080 Signal Attenuator (Wavetek, 1982).

to reduce the transmitted power by reducing the power amplification in the transmitter, however for the purposes of this feasibility study little importance was placed upon designing an ideal production survey instrument. The goal was always to produce an operational prototype system which fulfills the desired specifications in the shortest time possible.

The second option in lowering the minimum attenuation measurable is to raise the receiver input saturation voltage. This can be achieved either directly or indirectly. The direct method requires a time-consuming, extensive modification of the receiver circuitry. The indirect method requires the insertion of a modular component, a calibrated signal attenuator, into the receiver transmission line. The specifications for the Wavetek 5080 signal attenuator used, here, are listed in Table 3.5.2. The attenuator can be inserted into the transmission line between the receiver antenna and the receiver input stage. It provides for a total reduction in input signal level of 80 dB in 1 dB steps over the frequency range DC to 1 GHz. The line impedance of the attenuator is 50 Ω. The signal attenuator reduces the signal level passed through to the input stage of the receiver providing a corresponding effective reduction in the receiver input saturation voltage. The minimum attenuation measurable using the transmitter's 10 dB power attenuator and the full 80 dB attenuation provided by the receiver's signal attenuator is

theoretically reduced to 1 dB. Attenuation measurements can then be taken over the range of from 1 to 157 dB allowing for a broad variety of material absorption rates and transmitter-receiver separations. In practice, the minimum attenuation measurable will be much higher than 1 dB for the reasons discussed in the following section.

3.6 Electromagnetic shielding

An accurate attenuation measurement can only be made if the signal measured at the voltmeter comes down the transmission line uniquely from the receiver antenna. Any signal which enters the transmission line or receiver electronics directly, bypassing the receiver antenna, will alter the true wave attenuation measurement. Furthermore phase differences between signals from different sources will result in the creation of a series of maxima and minima as the antenna is rotated through space. The maximum-coupled position will no longer necessarily yield the highest received signal and the direction of the true source will be obscured. Normally this situation would rarely arise. The signal collected by the antenna should be far greater in amplitude than any other signal entering the transmission line. The interconnecting cables are shielded and all in-line components possess shielded exteriors. Only a finite amount of shielding is however obtainable. Problems can arise when using a high attenuation setting on

the in-line signal attenuator. Figure 3.6.1 illustrates the case. The signal power in free space at the receiver is P. The signal attenuator reduces the the signal by a value G resulting in a signal power of P - G at the receiver input stage. The same signal in air, P, can enter the transmission line subsequent to the signal attenuator. The shielding factor at the point of entry is S. This signal then possesses the value P - S at the receiver input stage. The two signals will also differ in phase by some amount ϕ. Provided $P - G >> P - S$ the attenuation measurement will be valid. Should the case $P - G \approx P - S$ exist, the measured attenuation will vary widely with antenna direction due to the phase difference between the two contributing sources. If $P - G << P - S$, the direction in which the antenna points will have no effect on the measured attenuation; the signal from the antenna will be effectively attenuated away. The second and third conditions, described above, will only arise when large levels of signal attenuation are required in order to avoid the receiver saturation condition. This will occur when the total signal attenuation is small. The lowest attenuation measurable, when using the 10 dB power attenuator in the transmitter transmission line, is 81 dB. Should the real total attenuation fall below 81 dB, saturation will occur unless the receiver's signal attenuator is also used. The spreading loss at 25 metres separation is 34.4 dB. Clearly, cases will arise in which the absorption of the medium is low enough that saturation

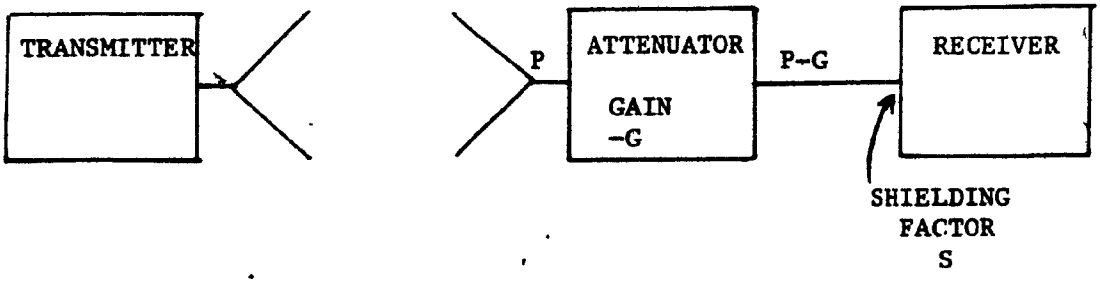

Figure 3.6.1 Illustration of the potential problems which can arise due to inadequate shielding of the receiver. P is the received signal power. G is the signal attenuator attenuation value. S is the receiver shielding factor.

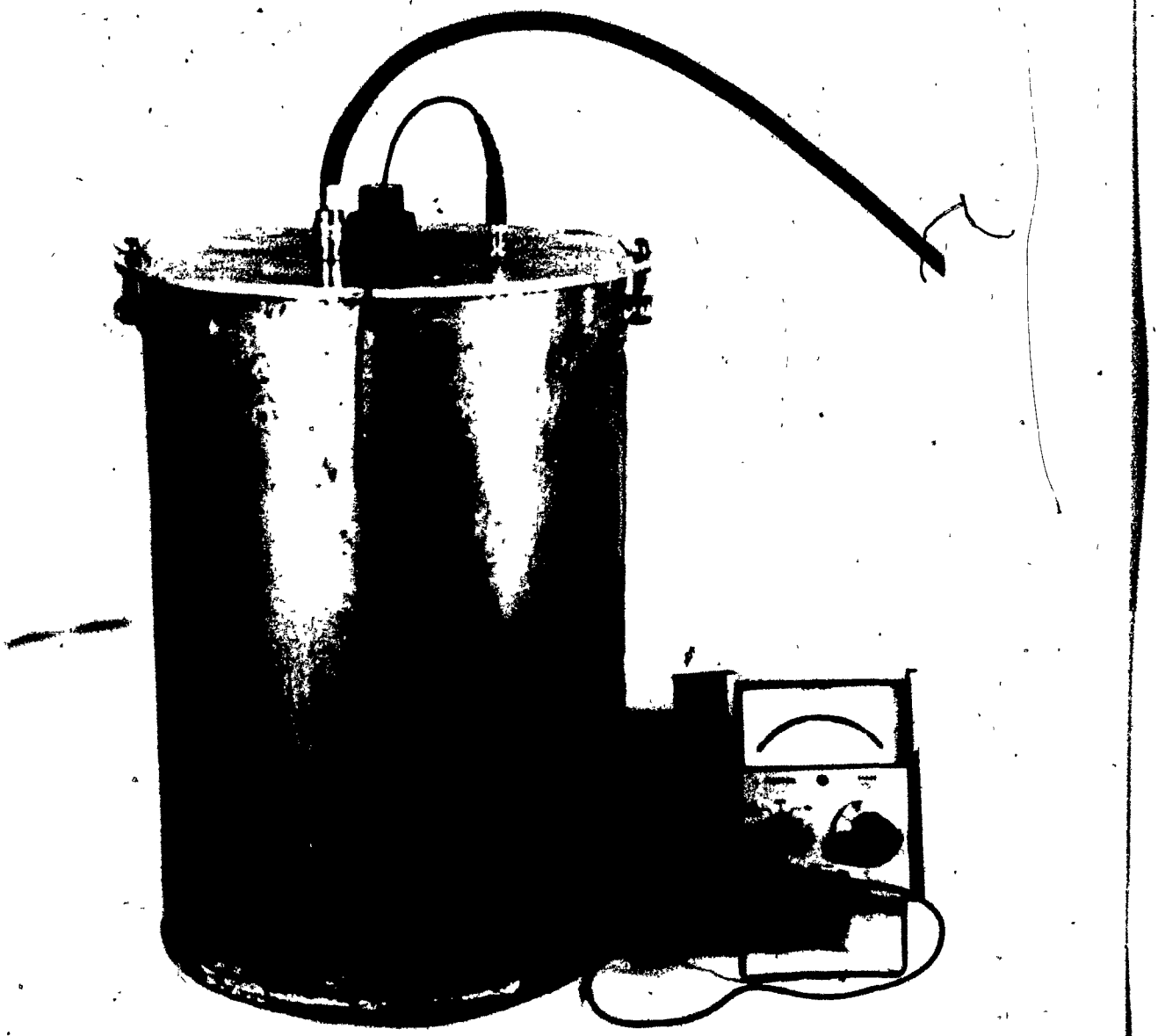

Figure 3.6.2 The aluminum canister containing the receive and the model 4038 AC voltmeter.

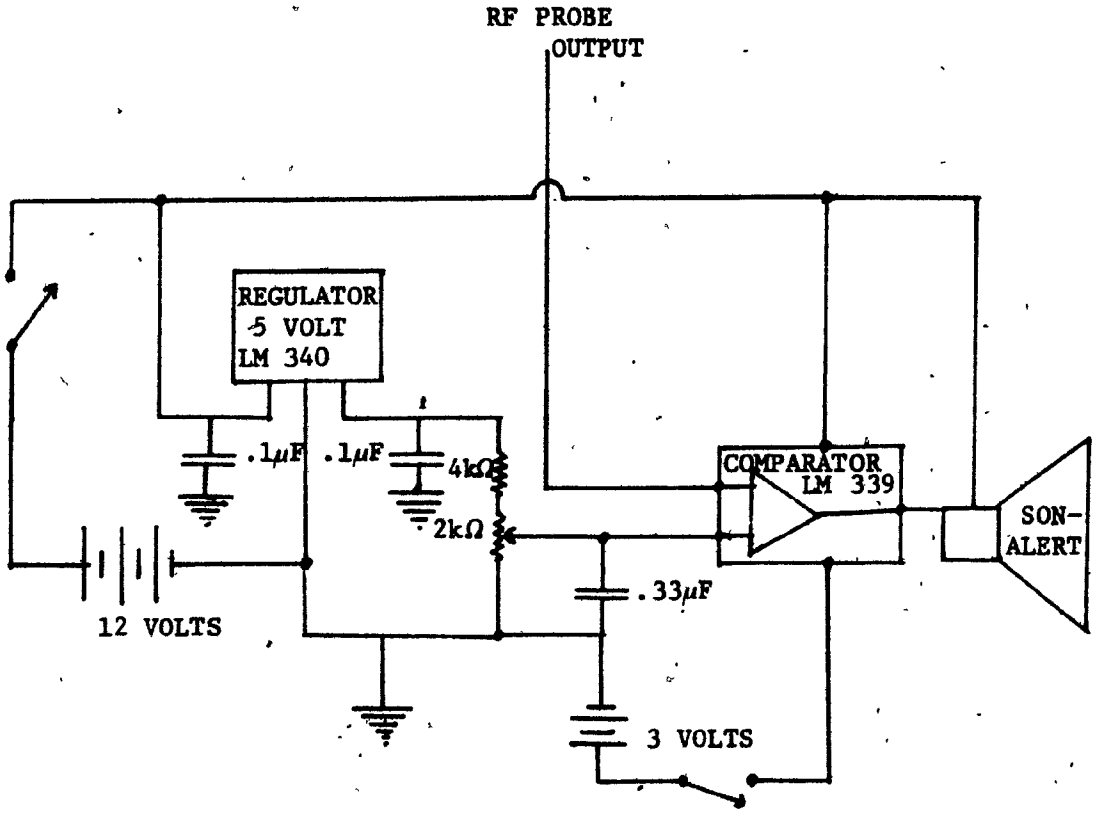

Figure 3.6.3 The comparator circuit.

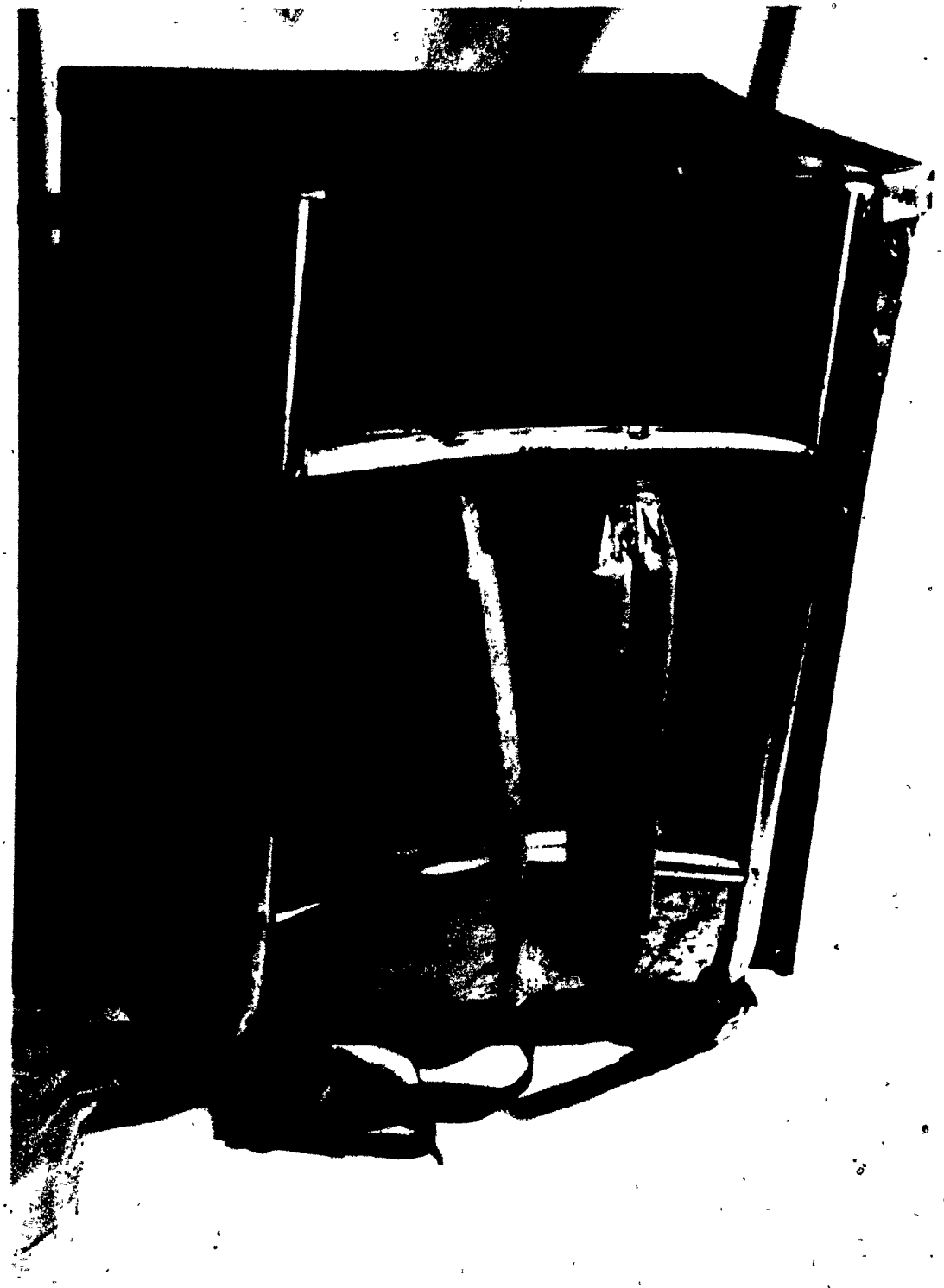

Figure 3.6.4 The copper casing housing the transmitter.

will occur. Calculated attenuation rates (Table 2.3.2) for several materials are lower than 1 dB/m.

A second path for an unwanted 445 MHz signal to enter the receiver electronics indirectly is by induction into the battery that supplies power to the receiver. Both transmitter and receiver were originally equipped with Yuasa B68-12 28 Ampere-hour lead-acid batteries. This was to provide for interchangeability of functions as discussed in section 3.4 above. The Yuasa battery should provide about 4.5 hours of continuous transmitter operation in the field. It was recognized that due to its rather large size and large number of parallel plates, this battery could act as an antenna and bring an unwanted 445 MHz signal into the receiver through the power supply lines. At short transmitter-receiver separations, the amount of signal picked up by the battery could be considerable. The receiver battery was replaced with a smaller Eveready dry-cell lantern battery for this reason. The smaller battery is adequate for the receiver's limited power consumption (0.3 Amps maximum).

Several precautions were taken with the view that a measurement requiring 60 dB of receiver signal attenuation could be needed. The receiver, its battery, the signal attenuator and the interconnecting cables have been placed in an aluminum canister (Figure 3.6.2). The canister is constructed from a 3/8 inch aluminum sheet rolled into a cylinder. The joint is welded together and a circular

bottom is welded on. A lid of similiar material is bolted on. A 3/8 inch thickness of aluminum provides for 28500 dB of attenuation at 445 MHz. All connections to the inside of the canister are made through the lid. The shaft of the attenuator protrudes through the lid providing external access to the rotary dial. The signal attenuator is rigidly flush-mounted with a copper gasket to the underside of the lid. Two bulkhead connectors are mounted on the lid. An N-type connector brings the signal from the receiver antenna into the canister and a BNC connector allows access to the 445 kHz IF from the receiver. An Emerson and Cuming Eccoshield SV RF gasket is glued to the top of the canister. The manufacturer's specifications for this gasket promise a 100 dB attenuation of an incident plane wave. The gasket is composed of a .51 mm thick conductive silicon rubber compound. Provided the lid is flush-mounted to the canister tightly enough to compress the gasket, the seal should be excellent. The sum total of all the above precautions provides about 50 dB of shielding as tested by the author. That is, the signal from the antenna can be reduced by 50 dB before it approaches the magnitude of any leakage signal reaching the receiver. This was measured in the laboratory as follows.

The transmitter and receiver were placed at a short separation so that the receiver saturated. The received signal level was monitored with the Hewlett Packard AC

voltmeter as the attenuation setting on the receiver's signal attenuator was gradually increased in 10 dB steps. Once the signal was lowered below the input signal saturation level it decreased in 10 db steps in harmony with the attenuator setting until 50 db of attenuation was reached. Increasing the attenuation from 50 to 60 dB resulted in a decrease in the monitored signal level of less than 10 dB. Increasing the attenuation from 60 to 70 dB resulted in no appreciable change in the monitored signal level. The background received signal (at point B) is on the order of 5 mV. The final measured signal with the signal attenuator set to 70 dB must be above this level for the results to be valid for we cannot expect a further decrease in signal with attenuation once this point is reached.

There will always be some finite leakage into the canister through the two bulkhead connectors, the attenuator shaft and the lid seal. The attenuator shaft seal seems quite sensitive to movement. Care has been taken to rigidly mount the attenuator.

There is some concern that the 445 kHz output port on the cylinder lid could bring a significant leakage signal into the canister or the receiver electronics. The third measuring technique, alluded to in section 3.4 above, was developed so that no output port would be necessary. Figure 3.6.3 illustrates a schematic of the measuring circuit. The 445 kHz output signal from the receiver is first rectified

by the RF probe. The resulting DC output is compared to a fixed reference supplied by the LM340 regulator. The LM339 voltage comparator compares the RF probe output and the reference signal. The output of the comparator is connected to the negative terminal of a Sonalert buzzer. The positive terminal of the Sonalert is connected to a 12 volt battery. Should the reference voltage be less than the RF probe output, the output of the comparator will be shorted to its negative supply voltage (-3 Volts in this case) and the buzzer will sound. The buzzer will only turn off when the RF probe output falls below the reference voltage. To take a measurement the attenuator is adjusted in one decibel steps until the buzzer shuts off. The attenuation setting when the buzzer just shuts off is then read off the dial. Typically the attenuation can be determined to about one decibel of precision using this technique. The RF probe and the comparator circuit are both sealed within the receiver canister. Although originally intended for field use the comparator circuit was eventually only used in tracking down sources of signal leakage in the lab.

In the event of a small transmitter-receiver separation, there is some concern about radiation from the transceiver casing. The transmitter has been placed within a copper casing to avoid this possibility (Figure 3.6.4). A bulkhead N-type connector on the side wall provides an output for the signal. An on-off switch is mounted on the

opposite side wall of the casing. The copper lid is fastened on by eight wing nuts. Although these precautions did not prove necessary in the field they were necessary in performing many close-separation tests in the lab. The result of these modifications is that the transmitter and receiver are not easily interchangeable in the field.

The actual minimum attenuation measurable is 31 dB. Thus a range of total attenuation between 31 and 157 dB is measurable.

3.7 Antennas

The characteristics of an antenna (gain, impedance, size, weight) will greatly effect the performance of the system. A higher antenna gain (equation 2.3.12) will reduce the spreading loss and increase the directivity (equation 2.3.6) of the antenna. The impedance of the antenna must be matched to the transmission line for maximum radiation of electromagnetic energy. This can be expressed in terms of the VSWR ratio (equation 2.5.2). Ideally, in the transillumination mode, the antenna should possess a pencil-beam field pattern so that the wave attenuation in a specific direction can be measured. In a tomographic reconstruction, all the wave energy is assumed to be lost along the wavepath joining the transmitter and receiver. Compact UHF antennas with the directivity of an X-ray medical tomography source are not feasible. Size and weight considerations limit the antenna gain to a finite value.

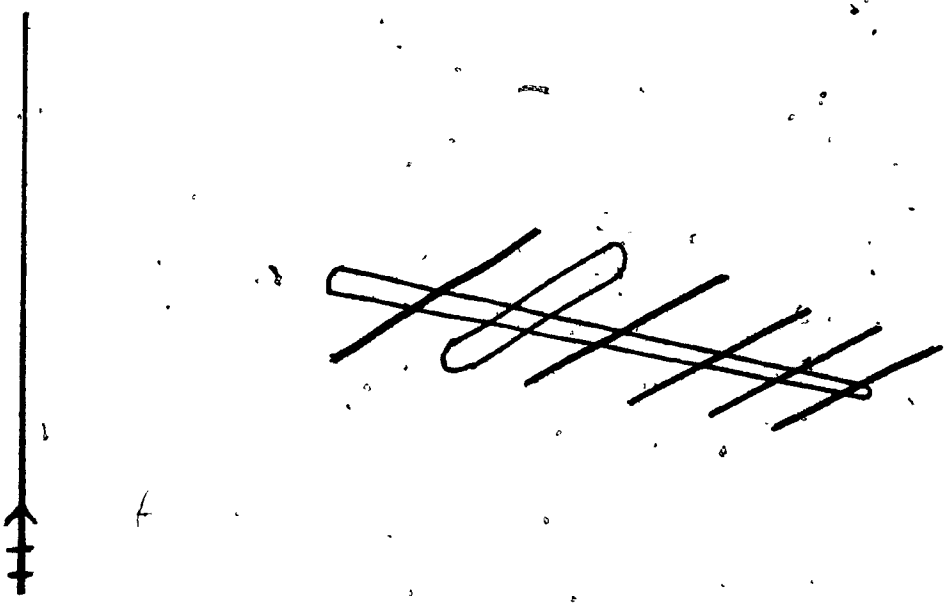

DIPOLE YAGI-UDA

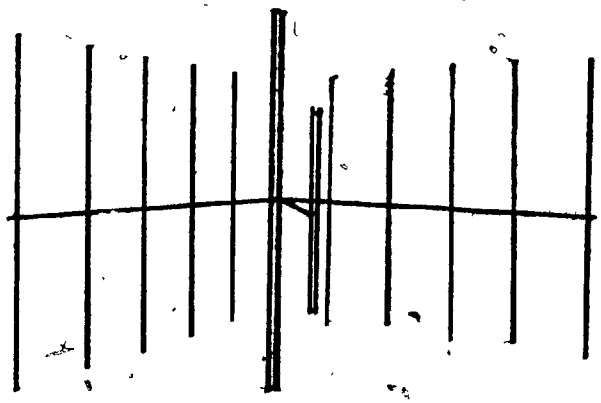

CORNER REFLECTOR

Figure 3.7.1 Standard UHF antennas.

Most UHF antennas in the 420-470 MHz frequency range possess gains of between 1 and 10 dB. The stacking of individual antennas into an array can result in gains of up to 30 dB at the cost of increased size and weight. A single UHF antenna will typically have dimensions on the order of the free space wavelength of its design center-frequency. At 445 MHz this would be about .67 metres. Several standard antenna designs are available in the UHF range. Examples of these are shown in Figure 3.7.1. The antenna typically consists of a single dipolar or folded dipolar driven element and several passive reflectors which serve to focus the field. In addition, individual antennas can be stacked into an array for increased gain. Unterberger (1978), for his "Charlie" underground pulse radar system, uses a four bay array Yagi-Uda antenna which provides 17 dB of gain at 440 MHz.

In choosing an antenna the radiation pattern is extremely important. The presence of pronounced back- or side-lobes can create secondary interference in an enclosed area. In addition, any power not radiated in the direction of the receiver can be regarded as lost. A large back-lobe could result in reflections off the instrument operator or transmitter console and add to the forward radiated field resulting in an altered field pattern. This reflected component will also vary with the position of conductive background material. The Sinclair Radio Laboratories model 403A corner reflector (Figure 3.7.1c) was chosen for its

SINCLAIR 302A CORNER REFLECTOR

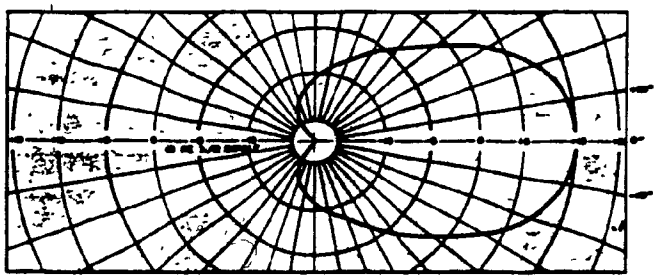

Figure 3.7.2: The horizontal radiation pattern of the SRL-302A corner reflector antenna for a vertical electric polarization (after Sinclair Radio Laboratories, 1981).

SINCLAIR 302A CORNER REFLECTOR

Frequency range: 406 -470 MHz

Nominal impedance: 50 ohms

Nominal gain: 9.5 dB

Maximum VSWR: 1.5

Power rating: 100 Watts

Polarization: vertical or horizontal

Weight: 7.7 kg

Dimensions (m): .762H x 1.270W

Table 3.7.1: Specifications for the Model 302A Corner Reflector (Sinclair Radio Laboratories, 1981).

BIRD 8085 TERMALINE LOAD RESISTER

Frequency range: DC to 3.5 GHz

Nominal impedance: 50 ohms

Maximum VSWR: 1.1 DC to 1 GHz
1.25 1 GHz to 3.5 GHz

Power rating: 25 Watts continuous duty

Temperature range: -40° to 40° C

Weight: 0.4 kg

Table 3.7.2: Specifications for the Model 8085 Termaline RF Coaxial Load Resistor (Bird, 1982).

BIRD MODEL 43 THRULINE WATTMETER

Frequency range: 2.0 MHz to 1.0 GHz

Nominal impedance: 50 ohms

Maximum VSWR: 1.05

Power rating: 1 Watt to 5 kilowatts full scale

Weight: 1.8 kg

Table 3.8.1: Specifications for the Model 43 Thruline Wattmeter (Bird, 1982).

relatively high gain and uniform field radiation pattern. The horizontal radiation pattern for a vertical electric polarization is shown in Figure 3.7.2. The antenna specifications are listed in Table 3.7.1. The antenna has a nominal gain of 11.28 dB and a half-power beamwidth of $59.^{0}$. The radiation pattern contains no large back- or side-lobes. The corner reflector consists of a central folded dipole and 19 parallel passive reflectors. The antenna can be rotated about its horizontal axis to switch from vertical electric to horizontal electric polarization. Both transmitter and receiver antenna are mounted on standard survey tripods that provide 360° of rotation about a vertical axis.

It should be mentioned, here, that in order to comply with DOC licencing requirements, all above ground and laboratory tests with the transmitter were carried out with the antenna replaced by a non-radiating dummy load. The specifications for the Bird Termaline Coaxial Resistor used, here, for this purpose are listed in Table 3.7.2.

3.8 Coupling elements

The impedance match at different junctions along the transmission line is extremely important in a UHF system. As discussed in section 2.4 above, an impedance mismatch can result in large ohmic losses along the length of the transmission line and reflections from the end of the line. Line reflections of a significant magnitude could result in transmitter failure. Large reflections can also stimulate

"frequency pulling", resulting in a variation in the operational frequency. The VSWR ratio (equations 2.5.1 and 2.5.2) is the standard measure of the impedance mismatch. All the signal carrying components in Figure 3.1.5 possess 50 ohm line impedances. Despite this nominal matching, there will always exist some finite mismatch at each junction in the transmission line. Generally each component is specified to have a maximum VSWR insertion ratio. The VSWR ratios of the individual components used are listed in their respective specification Tables (3.5.1, 3.5.2, 3.8.1). The Yaesu transceiver requires a VSWR of 1.5 or less in order to achieve its listed performance specifications. A VSWR of 1.5 is equivalent to about 4% reflected power. Given the transmitter's 25 W output, this translates into a reflected power of 1 W.

An important factor to consider is that any conductive material near the antenna can, in fact, act as a component of the transmission line and affect the radiated field. The VSWR can, in consequence, be greatly changed. A copper plate placed directly in front of the antenna will reflect much of the radiation back into the antenna and transmitter. The VSWR ratio can, therefore, indirectly indicate the "electromagnetic reflectivity" of the medium directly in front of the antenna. Should the reflection back into the antenna raise the VSWR to a substantial level (greater than 1.5) the antenna must be moved back until the VSWR falls

within specifications. In one test performed by the author, the presence of a person 1.5 meters from the antenna changed the VSWR from 1.25 to 1.5 (1.6 % to 4% reflected power).

The standard commercial instrument for measuring the VSWR ratio along a transmission line is the directional wattmeter. The wattmeter is inserted directly into the transmission line and measures the forward and reflected power. These powers are then converted to a VSWR using equation 2.5.1. The specifications for the Bird Model 43 Thruline Wattmeter used, here, are listed in Table 3.8.1. The Thruline Model 43 consists of a central cavity in which standard elements are inserted. The circuit is balanced so that it is sensitive to the conductive currents travelling in only one direction. This direction is reversed by rotating the coupling element through 180°. The insertion VSWR produced by the meter itself is less than 1.05 or .06% reflected power. The full scale meter reading and frequency range can be changed by insertion of different standard elements into the central cavity.

Originally all interconnecting cables were of the 50 ohm RG-213U type. The cables within the instrument casing were subsequently replaced by superior shielded RG-214U cables for the final field surveys.

3.9 Overall system characteristics

The overall characteristics of the McGill UHF-EM system are summarized in Table 3.9.1. Figures 3.9.1 to 3.9.4 show

the instrumentation in its final form. The transmitter and receiver each require one operator. Each unit can be transported by one man although the large dimensions of the antenna make it difficult to manouvre in close quarters. The antenna can be disassembled for easier transport. The maximum ERP of the transmitter, calculated from equation 2.4.15 above, is 223 W.

The system has an accuracy of approximately ±1.Ø dB when measuring an attenuation under a known geometry, but one must expect a higher degree of inaccuracy in actual field use. Any deviation of the antennas from their maximum-coupled position will result in a decrease in the accuracy of the measurement. Referring to Figure 3.7.2 it is evident that an orientation error of $\pm 1Ø^{0}$ of either of the antennas results in a decrease of Ø.5 dB in the received signal level. Reflection of incident energy from a rock wall will also result in a reduced level of accuracy in the measurement. Ideally, the antenna should be tuned at each position so that all the energy is radiated into the rock medium. The wattmeter can monitor, to some extent, any backreflection encountered.

McGILL UHF-EM SYSTEM

Transmitter:

Output power: 2.5 or 25 Watts
Frequency stability: > +5 ppm
Power consumption: 6.0 Amperes maximum
EIRP: 22 or 223 Watts
Console dimensions (mm): 635h x 457w x 330d, backpack mounted
Console weight: 19 Kg

Receiver:

Minimum detectable signal: 0.5 μV nominal
Input signal saturation: 1 mV nominal
Gain: 5 to 55 dB in 1 dB steps
Power consumption: 0.3 Amperes maximum
Console dimensions (mm): 508h x 356 diameter
Console weight: 19Kg

Common:

Operating frequency: 445 MHz
Antenna gain: 9.5 dB
Antenna dimensions: 762h x 1270w x 838d, tripod mounted
Line impedance: 50 Ohms
Power supply: 12 Volt, negative ground

Table 3.9.1: Specifications for the McGill UHF-EM system.

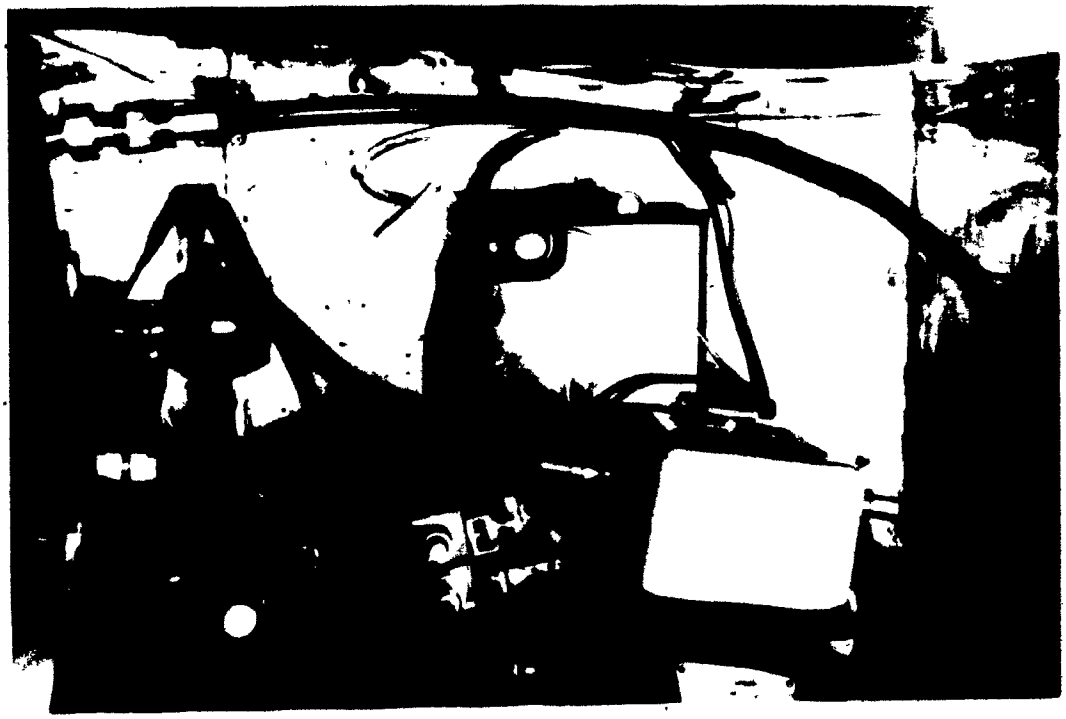

Figure 3.9.1 The McGill UHF transmitter.

Figure 3.9.2 The McGill UHF transmitter and antenna.

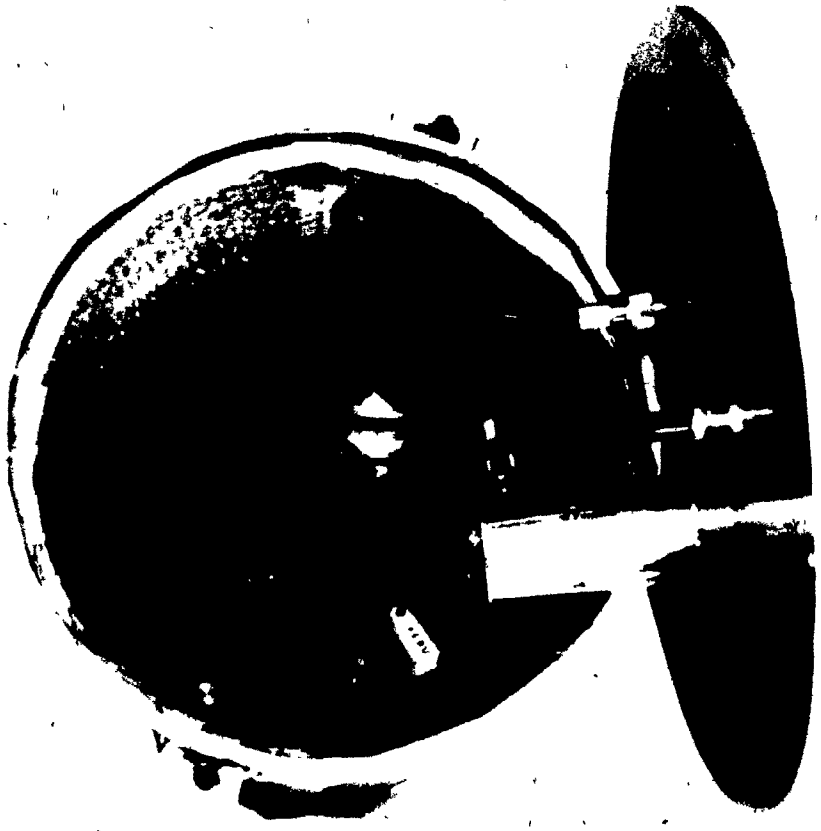

Figure 3.9.3 The McGill UHF receiver.

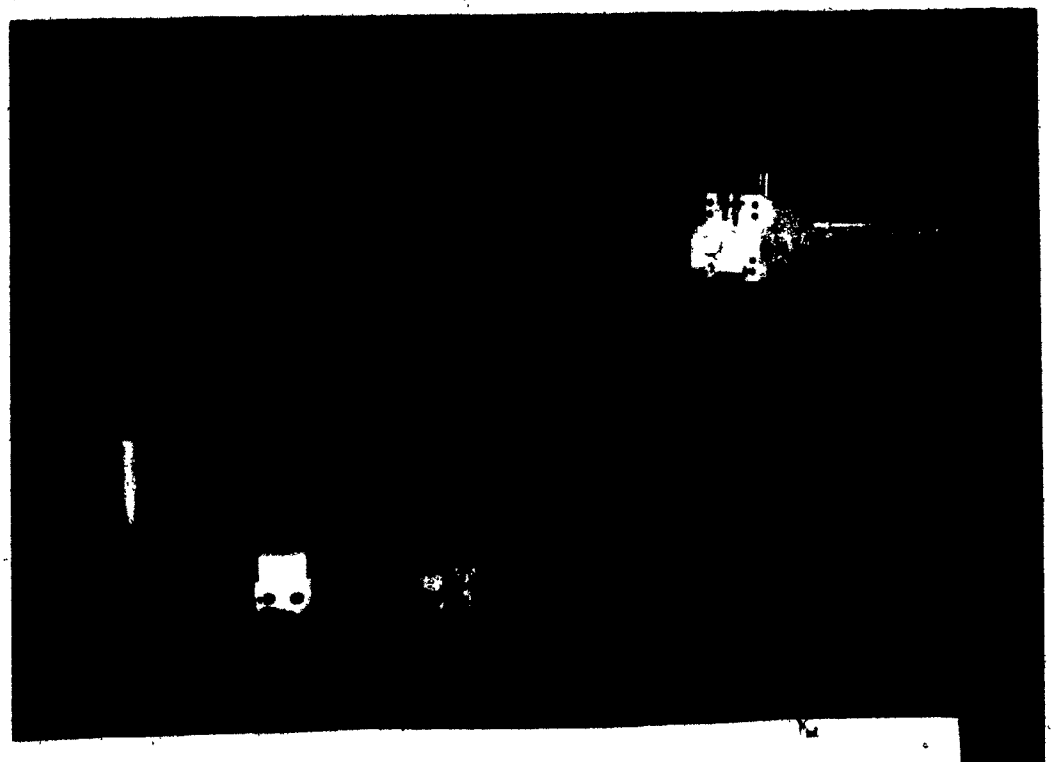

Figure 3.9.4 The McGill UHF receiver and antenna.

Chapter 4

Field Surveys

4.1 General

The geology of the test sites is extremely important in demonstrating the feasibility of the UHF transillumination system. The general scope of the project has been to investigate the feasibility of using continuous UHF waves in a typical Canadian shield environment. Given that goal it is only reasonable to carry out the test surveys in this environment. Several criteria are required of any test site. It should be within an area which is locally geologically interesting. Given the nature of the equipment and the DOC licencing requirements, the site must be underground. Site access should be free and unrestricted as the time required to transport and align the equipment at each location can be significant. Since the transmitter and receiver must be synchronised to operate simultaneously and they may be located in separate passageways, freedom of movement around the site for communications purposes is essential. Possible cultural noise sources should be minimal. For example, the continuous motion of equipment or workers within the survey area could seriously affect attenuation measurements. The underground openings and passageways must be of sufficient dimension and must be laid out so that useful through-material measurements can be

made. Several measurements through different distances of geologic material are necessary in order to verify a calculated absorption rate. The ability to use fan-like arrays in order to detect inhomogenieties in the rock mass would be desirable. The site should be safe. Lighting and electrical power are not needed on site and since they could create unwanted noise sources, if present, it is preferable that none exist. An accurate mine survey should be available or obtainable.

An operating mine could properly provide these site requirements. The major drawback in surveying an operating mine is that the survey would interfere with on-going mining operations such as blasting and vehicle movement. The survey would have to be carried out in a quiet area of the mine to avoid such interference. The proximity of loaded explosive charges is also an important consideration. At least one mining company contacted indicated that radio frequency radiation could ignite their blasting caps. The requirement for ease of access is also difficult to fulfill in an active mine. The survey would have to be timed so as to accommodate lift schedules, for example. Given the fact that this prototype transillumination equipment was largely untested, communication between the transmitter and receiver location would be necessary. Considerable time could be wasted due to logistical problems of these kinds.

In consideration of the site requirements, the Big

Nickel Mine in Sudbury, Ontario was selected as the feasibility test site. Figure 4.1.1 shows the location of this mine. The Big Nickel is operated 6 months per year as a mining-research and tourist facility by Science North. It offers a site in an ideal geologic setting where access and movement would be unimpeded. The absence of any real mining activity reduced the possible level of cultural noise and potential safety problems. The geometry of the mine permitted a variety of different transmitter and receiver locations and configurations. The mine is essentially barren of any economic mineralisation. This is a distinct advantage as the absence of pockets of extremely absorbing material ensures that the transmitted wave will sufficiently penetrate the rock mass such that some geophysically interesting attenuation measurements could be obtained.

The mine, shown in plan view in Figure 4.1.2 is partially rail-tracked and contains extensive overhead protective fencing in the areas visited by tourists. These could provide for a channelling of the transmitted signal down the drifts and cause uninterpretable measurements. The main areas of the mine are marked in Figure 4.1.2. The floors of the north and central stope are partially covered by small pools of water. Drifts are of the common 8 feet by 8 feet design.

4.2 Geology of the Big Nickel Mine and surrounding area

The Big Nickel Mine is located just south of the

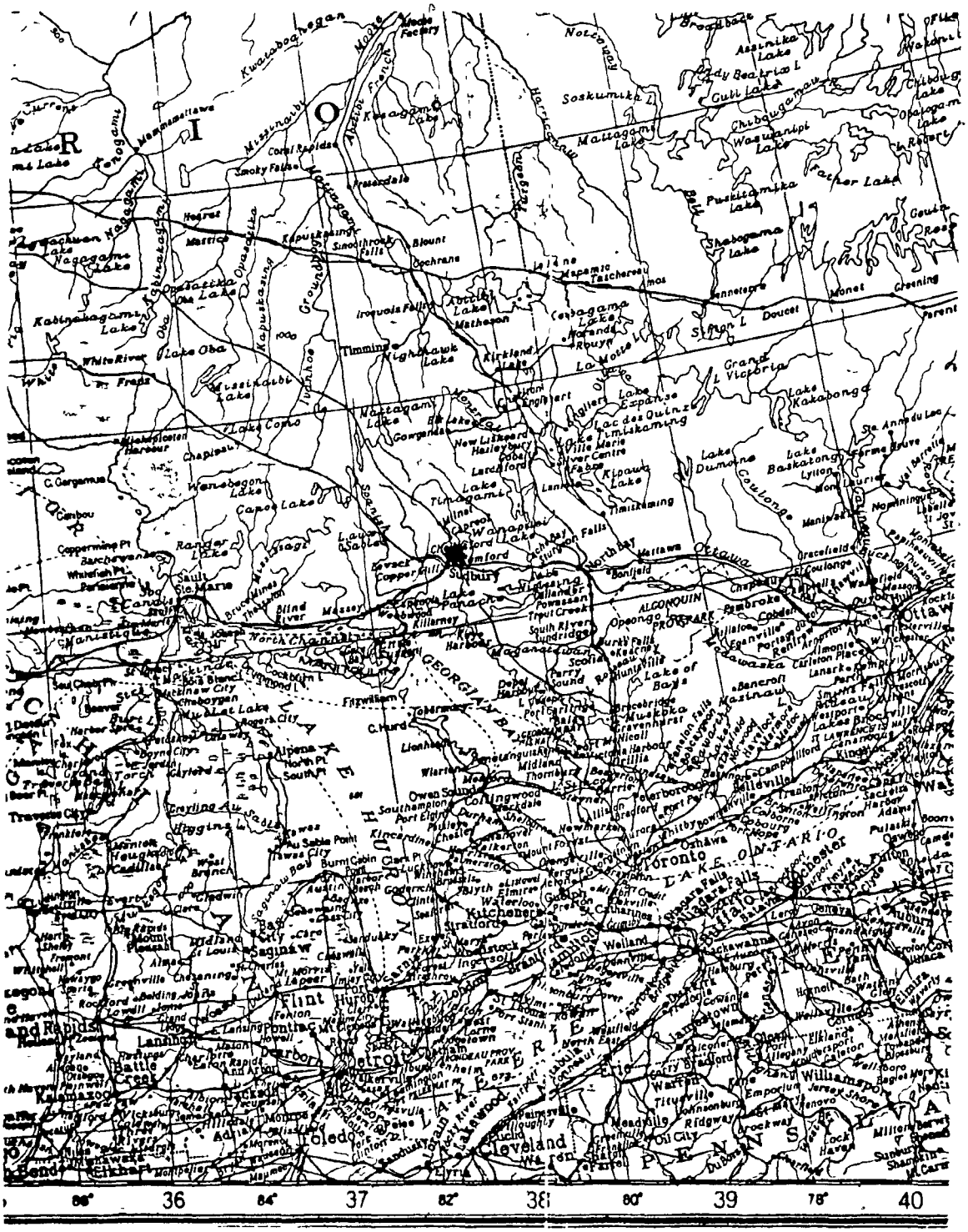

Figure 4.1.1 Location map for the Big Nickel-Mine.
Scale: 1:5892480

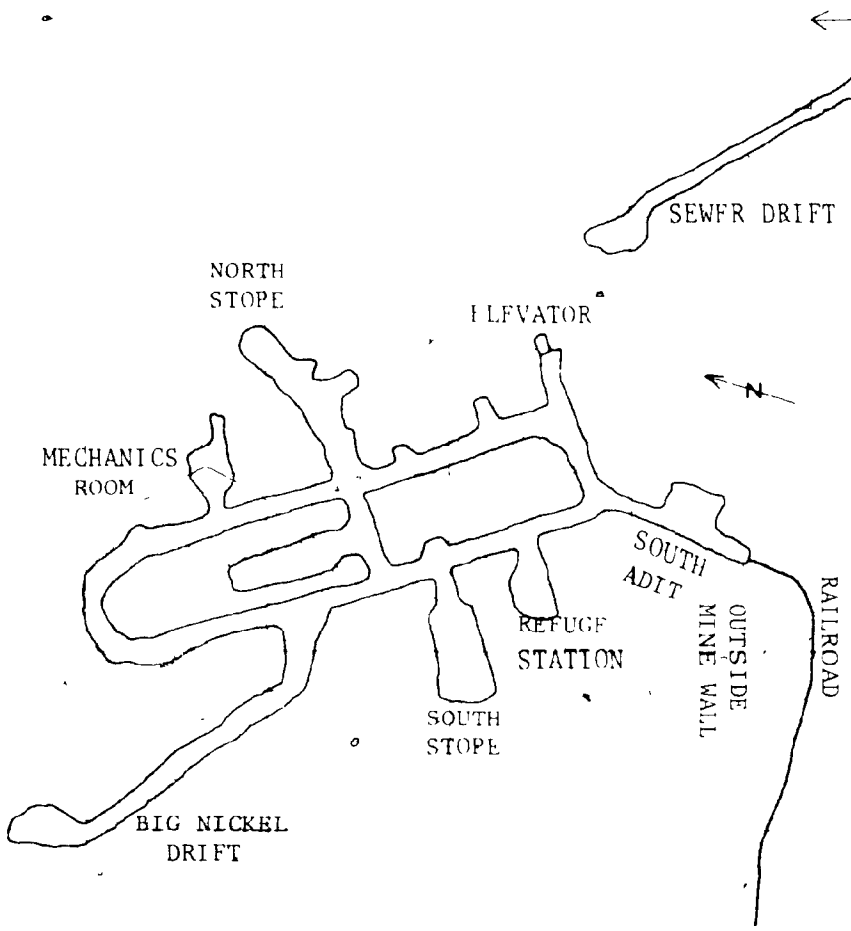

Figure 4.1.2 Layout of the Big Nickel Mine in 1985.

Figure 4.2.1 Geological map of the Sudbury area.

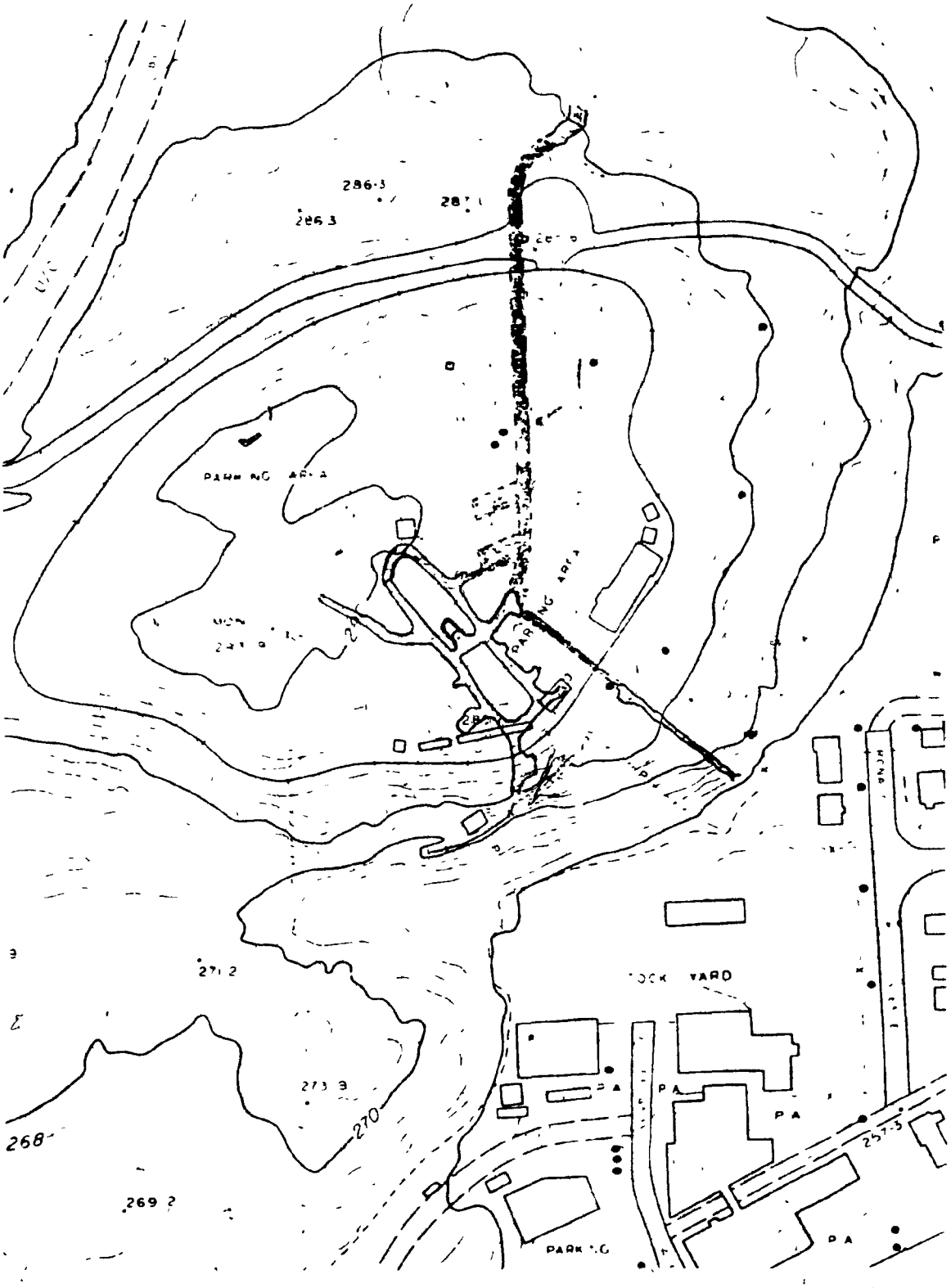

Figure 4.2.2 The Big Nickel Mine and surrounding area.
Scale: 1:200

Sudbury Basin in the Southern Province of the Canadian Shield. Figure 4.2.1 shows the local geology of the area. The rocks surrounding the mine site belong to the Elliot Lake Group of the Huronian Supergroup. These consist of sediments laid down approximately 2150 to 2500 million years ago. The Big Nickel Mine lies within the McKim Formation which consists of metamorphosed pelites and poorly sorted sandstones. The McKim Formation is distinguished by three main facies: a greywacke, a laminated argillite-siltstone and a quartz-feldspar sandstone. Bedding is observed to dip 60° + to the southwest in the mine area. The mine itself is located in a small hill rising roughly 34 metres above the surrounding area (Figure 4.2.2). The surface above the mine is completely exposed except where gravel infill has been placed to create a parking lot. The thin sections made from samples collected by the author in and above the mine show the mine to consist of rocks of the argillite-siltstone facies or more accurately to be quartz-sericite greywackes. The hand specimen examination of the samples and cores show the lithology to be uniform over the mine area. An analysis of a sample of this rock type by Knight (1965) showed a mineralogical content of 50% quartz, 27.5% muscovite and 17.5% chlorite. Figure 4.2.3 shows a sample of the rock. A thin section description of three of the samples follows.

The thin sections show the samples to consist of angular quartz grains matrixed by abundant sericite mica. Bedding is observed as a variation in the grain size.

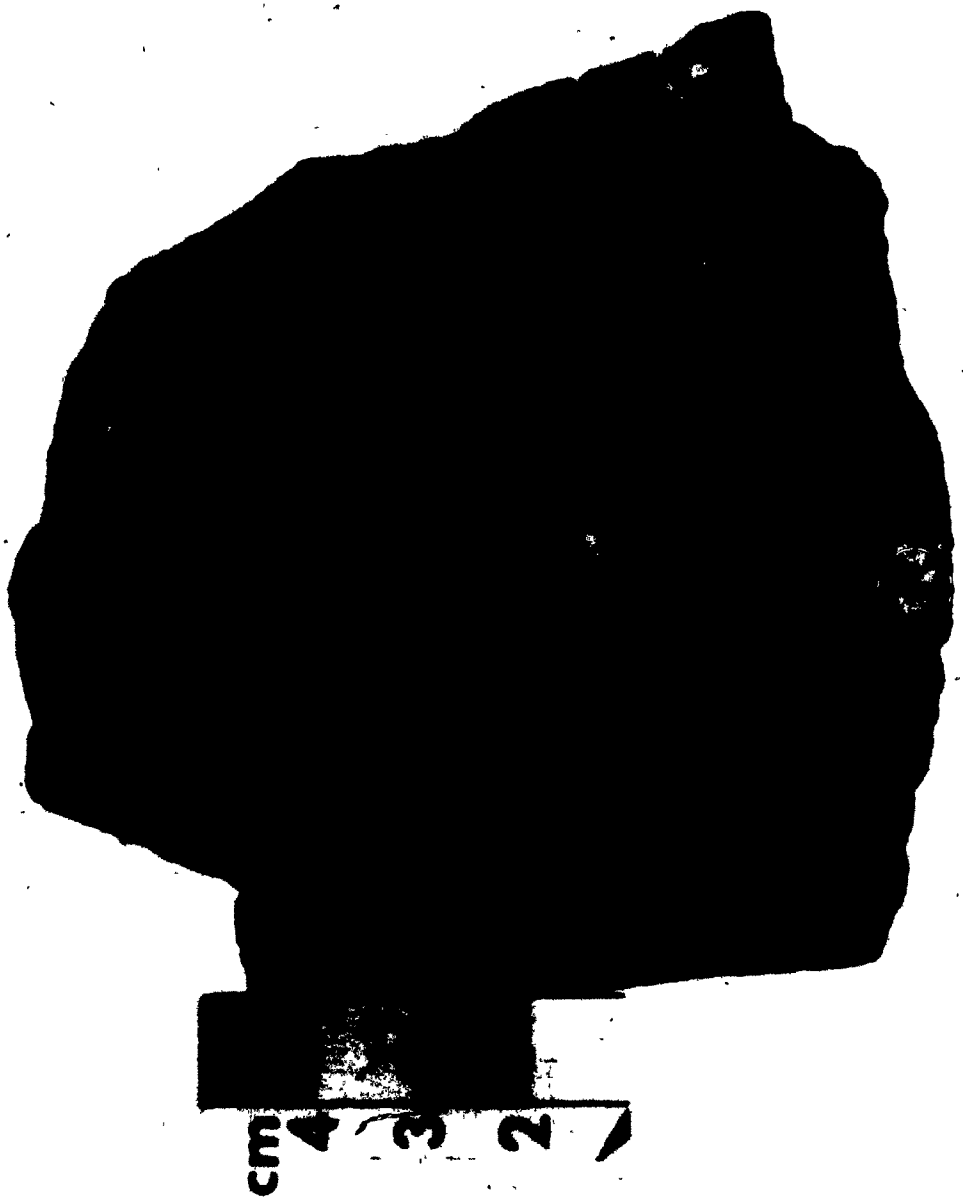

Figure 4.2.3 A typical rock sample taken underground at the Big Nickel Mine.

Figure 4.2.4 Thin section, taken under plane light, of a rock sample from the Big Nickel Mine. Magnification 16x

Figure 4.2.5 Thin section, taken under polarized light, of a rock sample from the Big Nickel Mine. Magnification 16x

Large subrectangular altered porphyroblasts of sericite mica and quartz, originally derived from staurolite or andalusite, are common. A small quantity (less than 0.5%) of small pyrite grains is found to be evenly distributed throughout the matrix. The pyrite content remains fairly constant in directions both parallel to and across the bedding. Quartz content varies across the bedding planes. Figures 4.2.4 and 4.2.5 show representative thin sections of the rock.

Jointing is observed underground on the walls of all the drifts. No regular pattern to the jointing is evident. A minor amount of ground water seepage exists along some joint planes.

4.3 Test survey #1, Big Nickel Mine, 1983

The initial test survey with the prototype equipment was carried out in the summer of 1983 at the Big Nickel Mine site. The equipment used was essentialy the same as described in Chapter 3, above, with the important exception that none of the described shielding precautions were incorporated. The transmitter and receiver instrumentation were mounted on open backpack frames, the interconnecting cables which carried the 445 MHz signal were of the RG-213U type and the receiver was powered by the large Yuasa battery. The 10 dB Weinschel power attenuater was not available at the time, so no provision had been made for reducing the transmitted power.

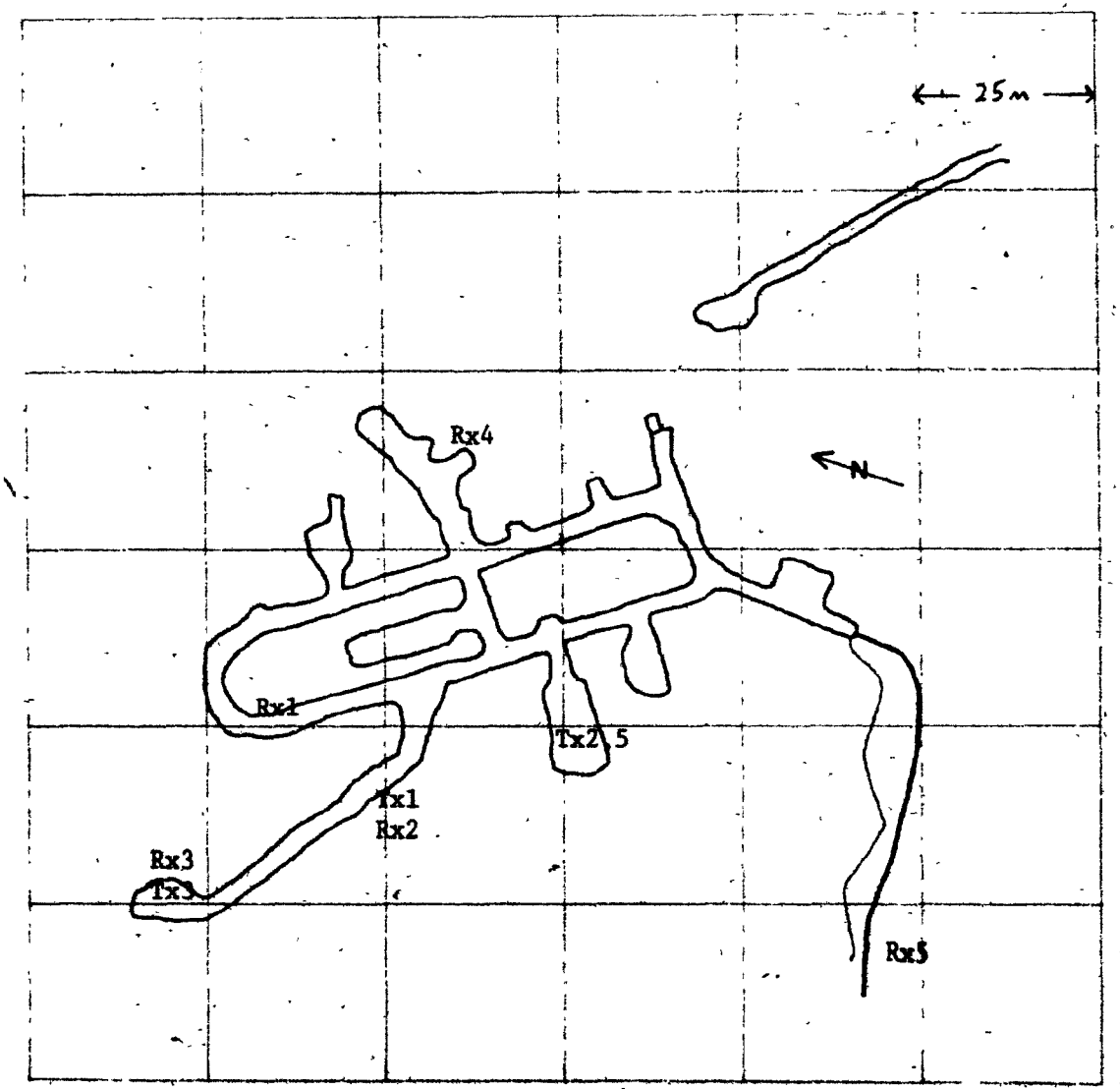

Figure 4.3.1 Survey sites, at the Big Nickel Mine, for test survey #1, 1983. Transmitter and receiver locations are denoted by Tx and Rx respectively.

Measurements were taken at several locations with both the transmitter and receiver underground and the transmitter underground and the receiver on the surface above the mine. Figure 4.3.1 shows a layout of the Big Nickel Mine with the first year's transmitter and receiver survey locations marked as Tx and Rx respectively. Initially both the transmitter and receiver were placed underground in separate drifts and a measurement of the wall rock attenuation for the material between the two drifts was attempted. Tx1 and Rx1 indicate the first survey site. The received signal at this location was such that the receiver saturated. The changing of attenuation settings on the 80 dB signal attenuator had no detectable effect on the observed signal. The direction in which the antenna pointed also had no detectable effect on the received signal level. Furthermore, replacing the antenna with the resistive dummy load did not alter the results. The amount of signal bypassing the antenna input and entering the receiver electronics directly by an alternative route, such as the power supply lines, was enough to cause saturation. Similiar results were obtained at survey location Tx2-Rx2. Obviously two problems were encountered. First, the shielding of the receiver was inadequate. Second, either the rock attenuation was considerably less than originally considered when designing the instrument or the signal was propagating, with very little attenuation throughout the interconnecting drifts. It was not originally envisaged,

quite erroneously as it turns out, that receiver saturation due to inadequate signal attenuation would present problems. A temporary correction for the receiver shielding problem was attempted using aluminum foil. This however proved to be ineffective. The only immediate on-site solution was to find a transmitter-receiver geometry where the signal attenuation was sufficient to allow for a non-saturated signal to be measured. This would require that either the spreading loss (equation 2.4.14) or absorption loss (equation 2.2.12) be increased substantially. It would be necessary to ensure that the interconnecting drifts would not act as conductive waveguides which carry the signal from the transmitter to the receiver. If the wall rock were sufficiently nonabsorbing this should not be a problem. An indirect measurement of the wall rock conductivity can be made by measuring the reflected power in the transmission line (Section 3.8). The average VSWR (equation 2.5.1), measured at several locations within the mine with the Bird wattmeter was only 1.20, indicating a reflected power of only 0.8% or 0.2 W. Assuming that all the energy reflected from the wall rock is recollected by the transmitter antenna and can be measured as a reverse power in the transmission line, a reflection coefficient can be approximated. A transmission reflection coefficient of 0.8%, at normal incidence, corresponds to a refractive index ratio of less than 1.05 (Figure 2.7.2) between the air and immediate

wall rock. This indicates (equation 2.2.21) that β is approximately equal to $\omega\sqrt{\varepsilon_0\mu_0}$ or $\sigma \approx 0$, $\mu \approx \mu_0$ and $\varepsilon \approx \varepsilon_0$. It can therfore be assumed that very little waveguide channelling of the transmitted wave could occur due to the wall rock itself. Other possible waveguides could, however, arise due to the metal rails, overhead protective fencing or water and mud on the mine floor found in many locations throughout the mine. In order to investigate this possibility the receiver was placed on the surface at location Rx3 and the transmitter was placed at the end of the Big Nickel drift at Tx3. The transmitter antenna was beamed directly upward while the receiver antenna was elevated slightly off the ground and directed downward. The antennas were oriented for maximum coupling. At this point in time there existed approximately 7 metres of rock between the roof of the mine and the surface. Since the transmitter antenna was placed on the floor of the mine the actual transmitter-receiver separation was 10 metres. There was no possible alternative wavepath between the transmitter and receiver. In this instance the receiver did not immediately saturate when 30 dB of attenuation was used on the signal attenuator. When the antenna, however, was pointed directly upward the receiver saturated. This corresponds to the case $P - G \approx P - S$ described in Section 3.6. The measured attenuation varies with antenna direction due to a signal of different phase bypassing the antenna and entering the receiver circuitry directly. Given that one should expect

the antenna to be the preferential route for the signal to enter the receiver, increasing the total attenuation until the 80-dB signal attenuator is not required to obtain a non-saturated reading, should allow one to take a proper measurement. The receiver was subsequently removed to position Rx4 and again oriented for maximum coupling. A received signal level of 0.4 V with the attenuator set to 11 dB was measured. Orienting the antenna away from the maximum-coupled position substantially reduced the received signal level. Unfortunately locating exactly the position of the receiver with respect to the transmitter was difficult in this instance. The equipment was removed to position Tx5-Rx5. The distance between the transmitter and receiver was 49.5 metres of which 45 metres was rock. There were no interconnecting tunnels between the two measurement stations and the two sets of metallic doors on the south adit exit were closed. The rail line which exits the south adit does not enter the South Stope. The roof of the south stope was not covered in protective metal fencing. The received signal varied with antenna direction and the maximum-coupled antenna position yielded the maximum received signal, indicating that the signal travelled from the transmitter to the receiver through the wall rock. Rotation of the receiver antenna about its horizontal axis indicated that the maximum received signal occured when the antenna was vertically polarized. There were no prominant

Relative Permittivity	1.	5.	10.	30.	81.
Conductivity (S)	.718E-03	.161E-02	.227E-02	.393E-02	.646E-02
Resistivity (ohm-m)	1392.00	622.57	440.23	254.17	154.68
Index of Refraction	1.00	2.24	3.16	5.48	9.01

Table 4.3.1 Resistivities, conductivities and indices of refraction, as a function of the relative permittivity, for test survey #1, site Tx5-Rx5. The relative permeability is assumed to be equal to unity.

secondary maxima of the received field detected. The received signal was -3.8 dBV. Correcting for the transmitter output power, spreading loss and receiver gain, one obtains an absorption of 52.9 dB over 44.5 metres or an absorption rate of 1.18 dB/m. Table 4.3.1 lists resistivity values and indices of refraction, calculated from equation 2.2.8, for several estimated permittivities. The permeability was assumed to be equal to that of free space. Figures 4.3.2 and 4.3.3 show the transmitter and receiver in operation at locations Tx5 and Rx5 respectively.

Given the results of the initial field trials, it was recognized that the shielding of the receiver must be substantially improved before continuing with any further surveys. Figure 4.3.1 shows the mine plan as it existed the first year. The sewer drift, from which several successful measurements were completed in the second year (1984), was in the process of being widened and extended. Indeed several areas of the mine site were under extensive expansion by drilling and blasting. The area between the south stope and the south adit was the only area where meaningful measurements could be taken given the initial nature of the equipment.

4.4 Test survey #2, Big Nickel Mine, 1984

The second field survey was conducted at the Big Nickel Mine-site in the summer of 1984. It was not possible to return earlier since the mine was closed for the winter.

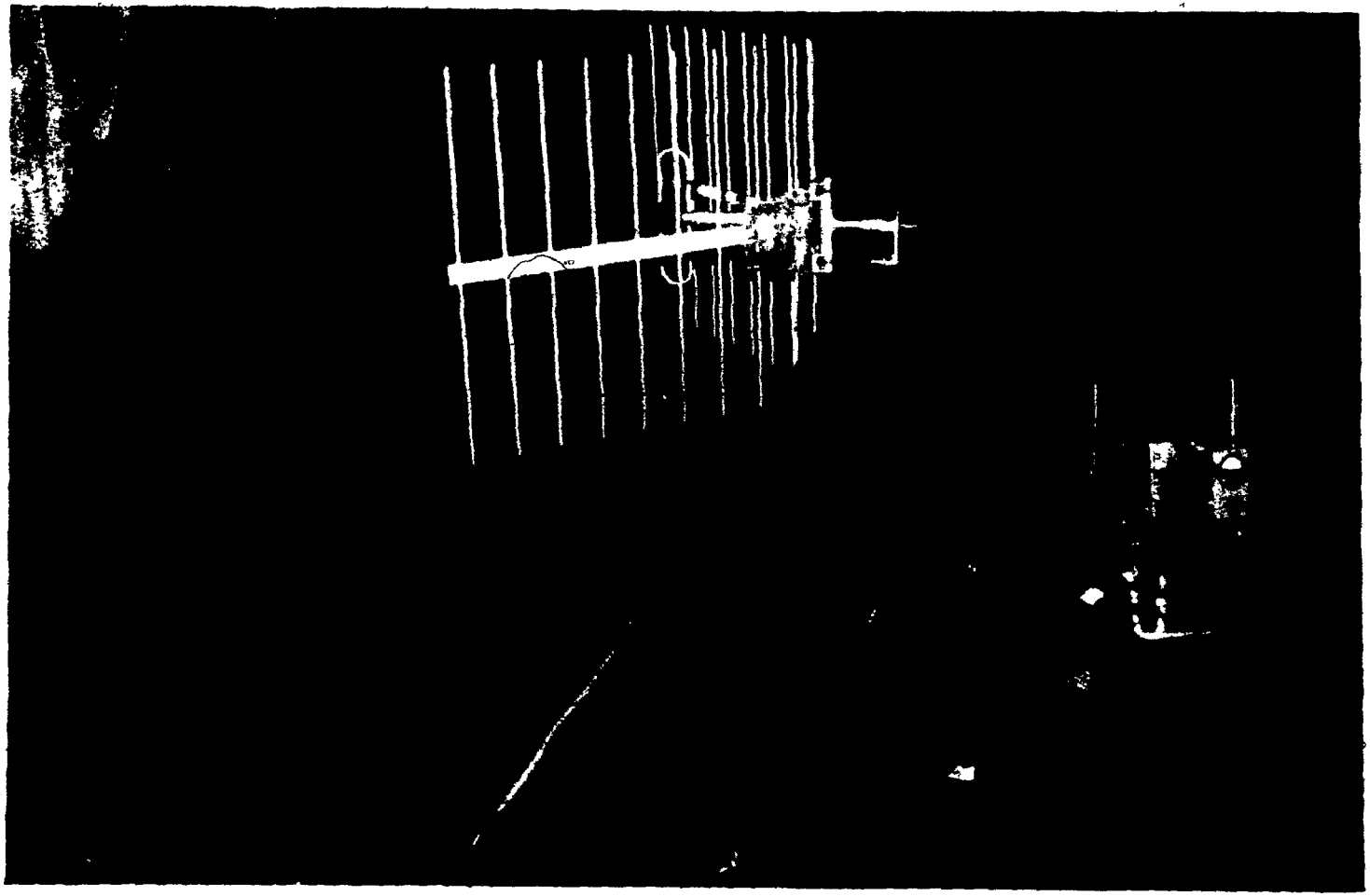

Figure 4.3.2 The McGill UHF transmitter underground at location Tx5.

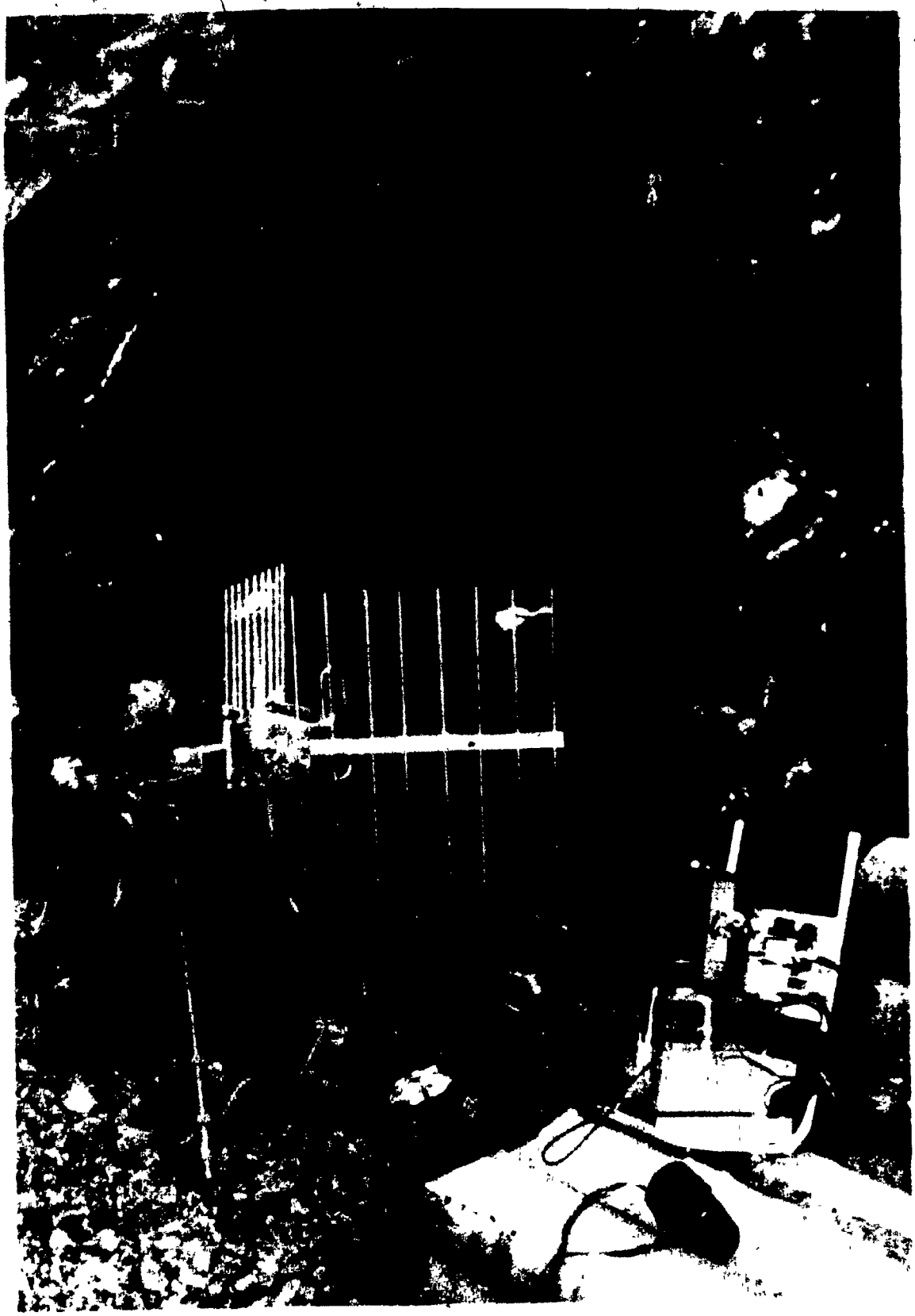

Figure 4.3.3 The McGill UHF receiver at location Rx5.

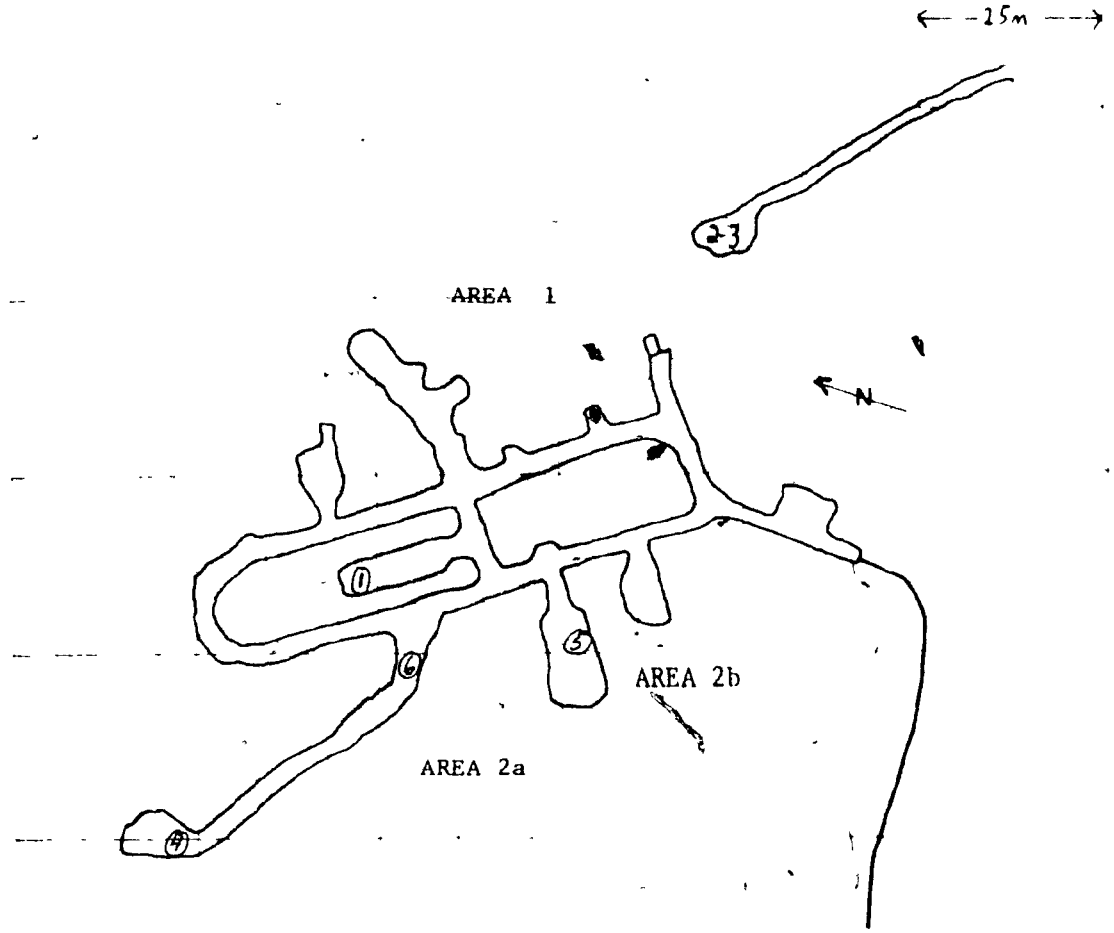

Figure 4.4.I Survey areas at the Big Nickel Mine for test survey #2, 1984.

Extensive changes had been implemented and the newly expanded area accessible for surveying is shown in Figure 4.4.1. The major improvements, so far as available survey sites are considered, is the addition of the sewer drift which is located to the southeast of the mine. Presently there exists no direct connection between the sewer drift and the mine itself, although a future connection is planned. The entrance to the drift is located approximately 13 metres below the elevation of the south adit. Another addition was the commencement of an east adit which will eventually connect with the north stope. This provides another underground location which does not directly connect to the mine site. The central stope, which had been inaccessible during the previous year, was now enlarged and extended.

Six survey sites are shown on Figure 4.4.1. Two areas of interest for subsequent examination are also indicated as mine areas #1 and #2. The individual transmitter (Tx) and receiver (Rx) locations for each site are shown on Figures 4.4.2 to 4.4.7. Tables 4.4.1 to 4.4.6 list the transmitter-receiver separations, through-rock distances, reduced attenuation measurements and calculated absorption rates obtained for each survey. The calculated absorption rates have been determined by correcting the measured attenuation at each location for the spreading loss and dividing the resultant absorption by the through-rock distance. A discussion of each survey site follows.

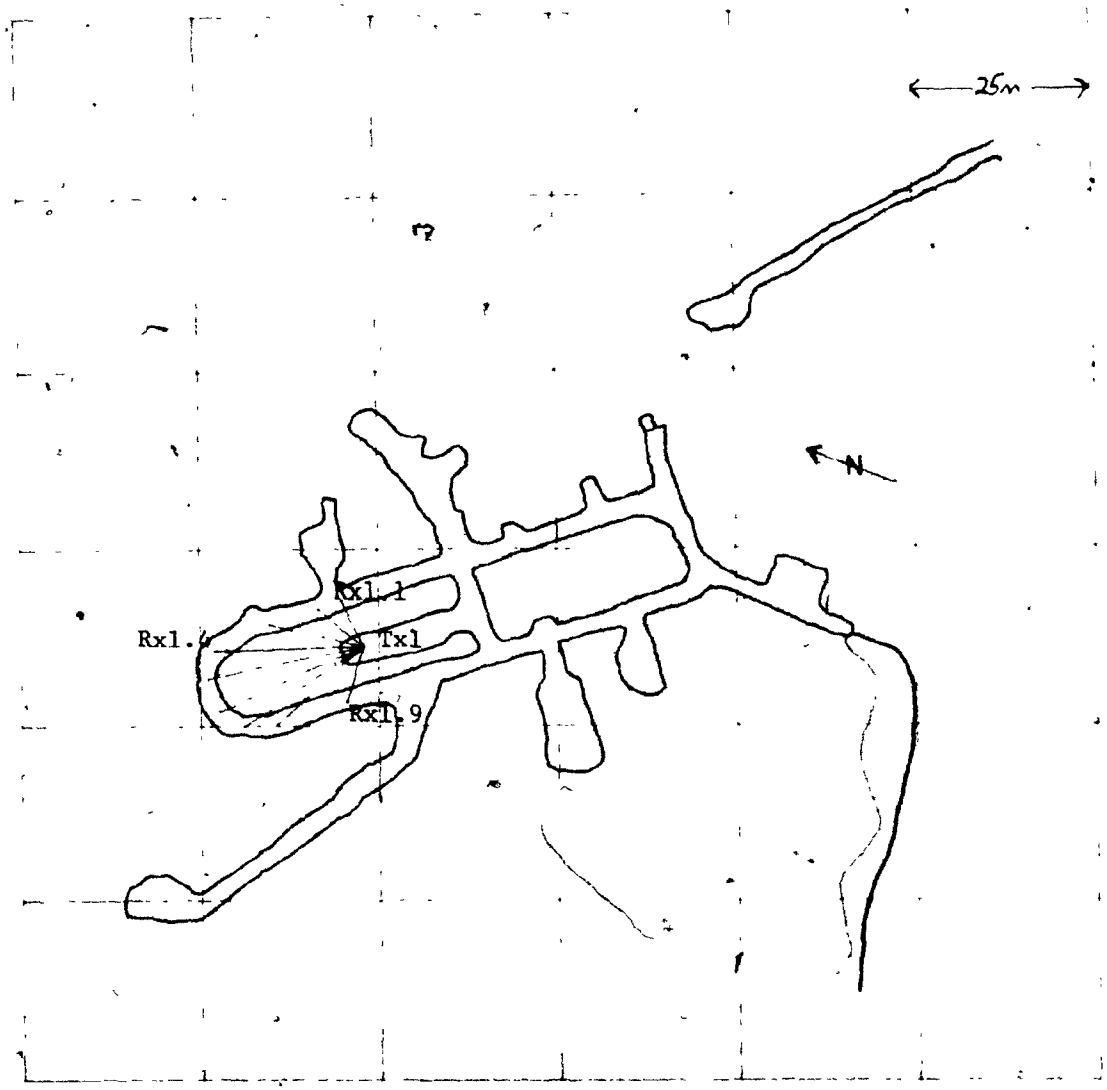

Figure 4.4.2 Transmitter (Tx) and receiver (Rx) locations for survey #1.

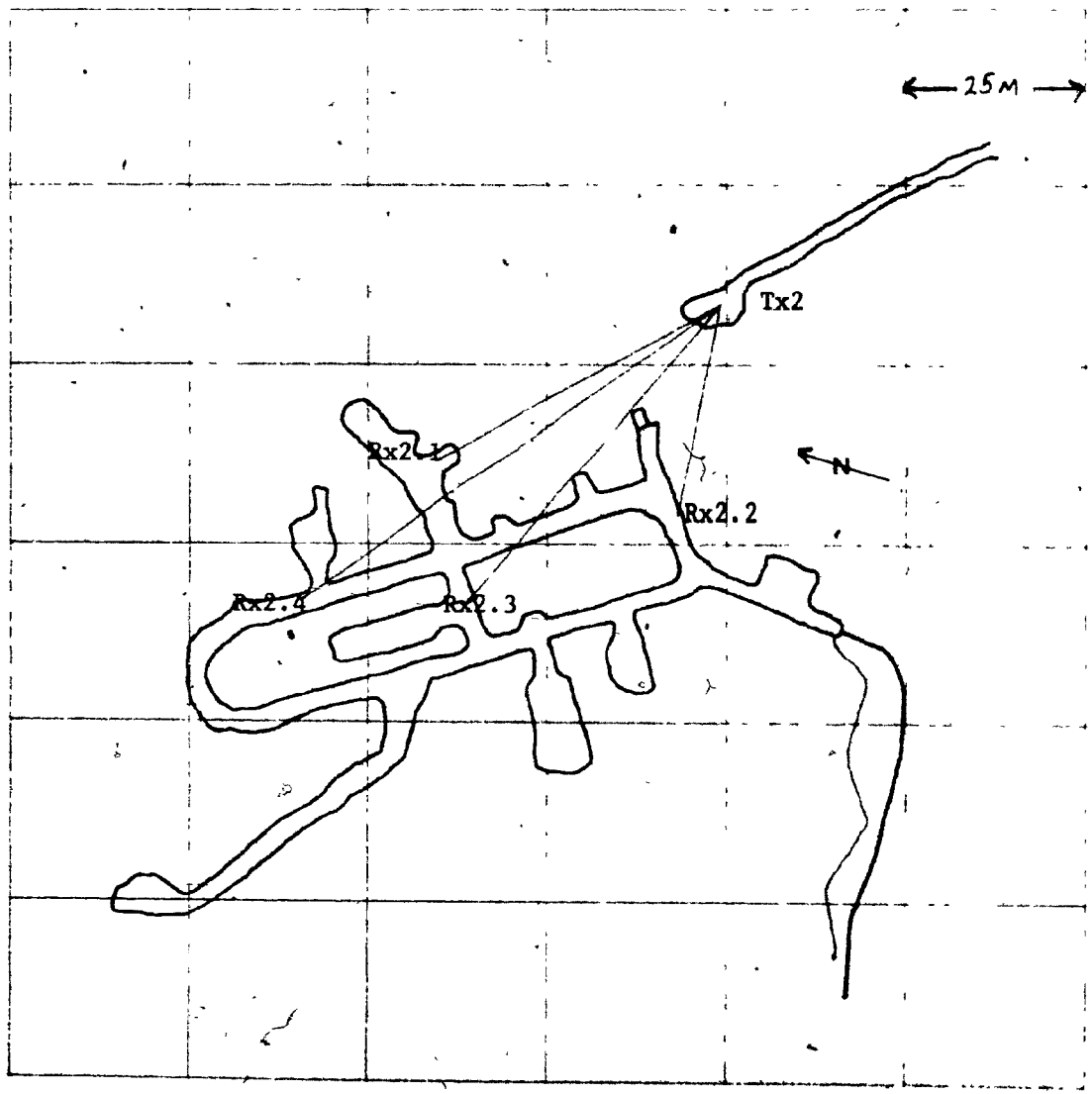

Figure 4.4.3 Transmitter (Tx) and receiver (Rx) locations for survey #2.

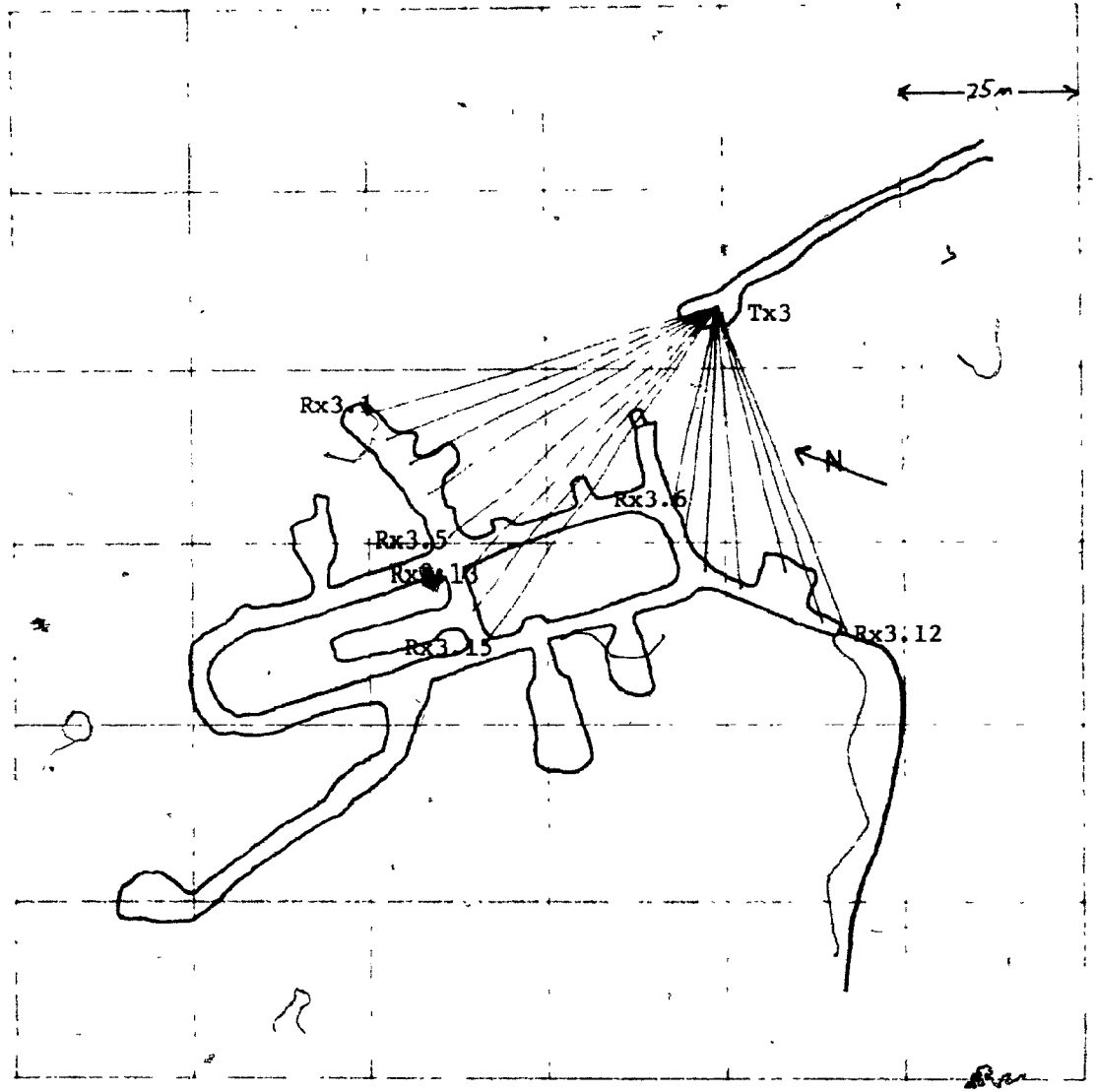

Figure 4.4.4 Transmitter (Tx) and receiver (Rx) locations for survey #3.

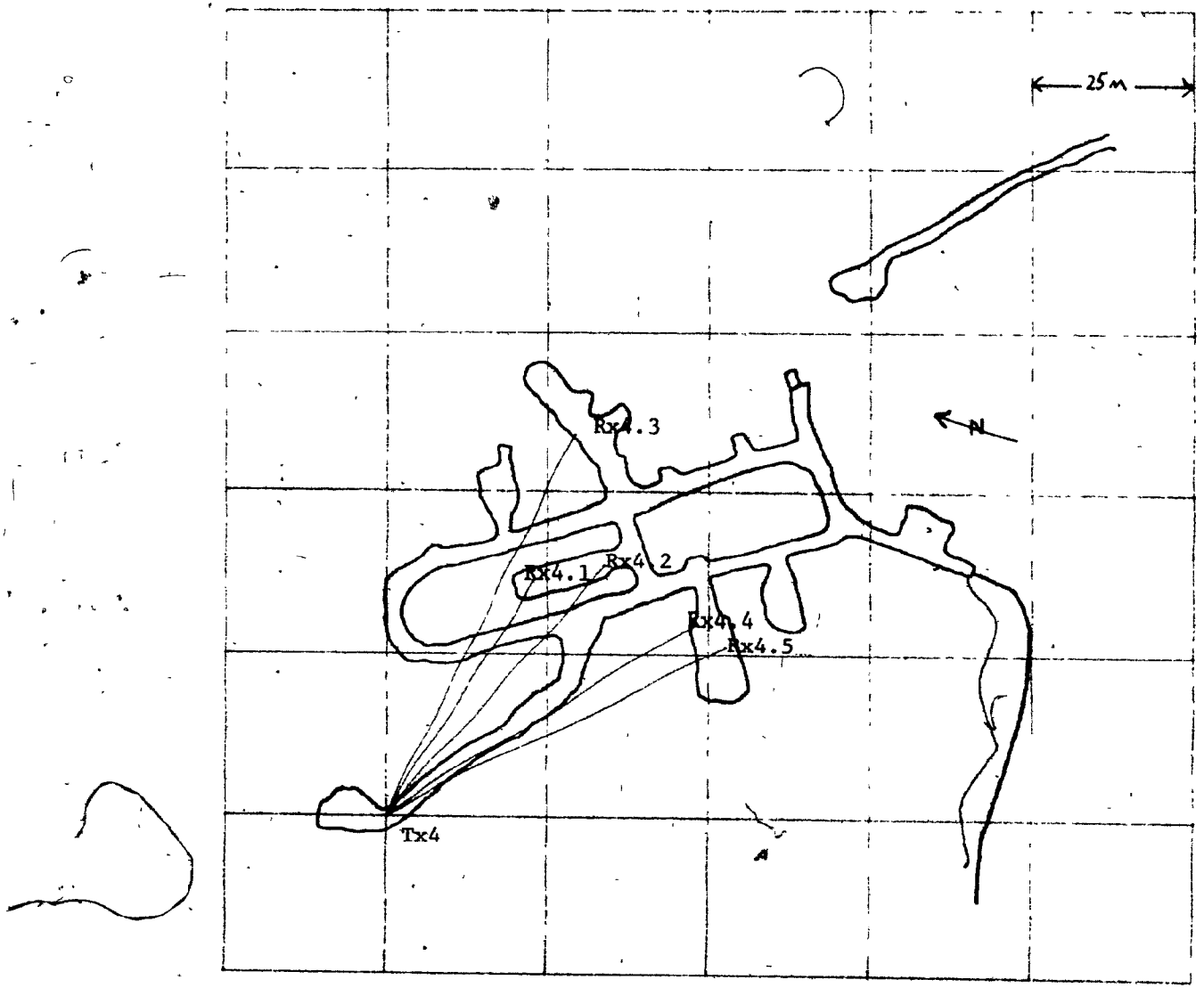

Figure 4.4.5 Transmitter (Tx) and receiver (Rx) locations for survey #4.

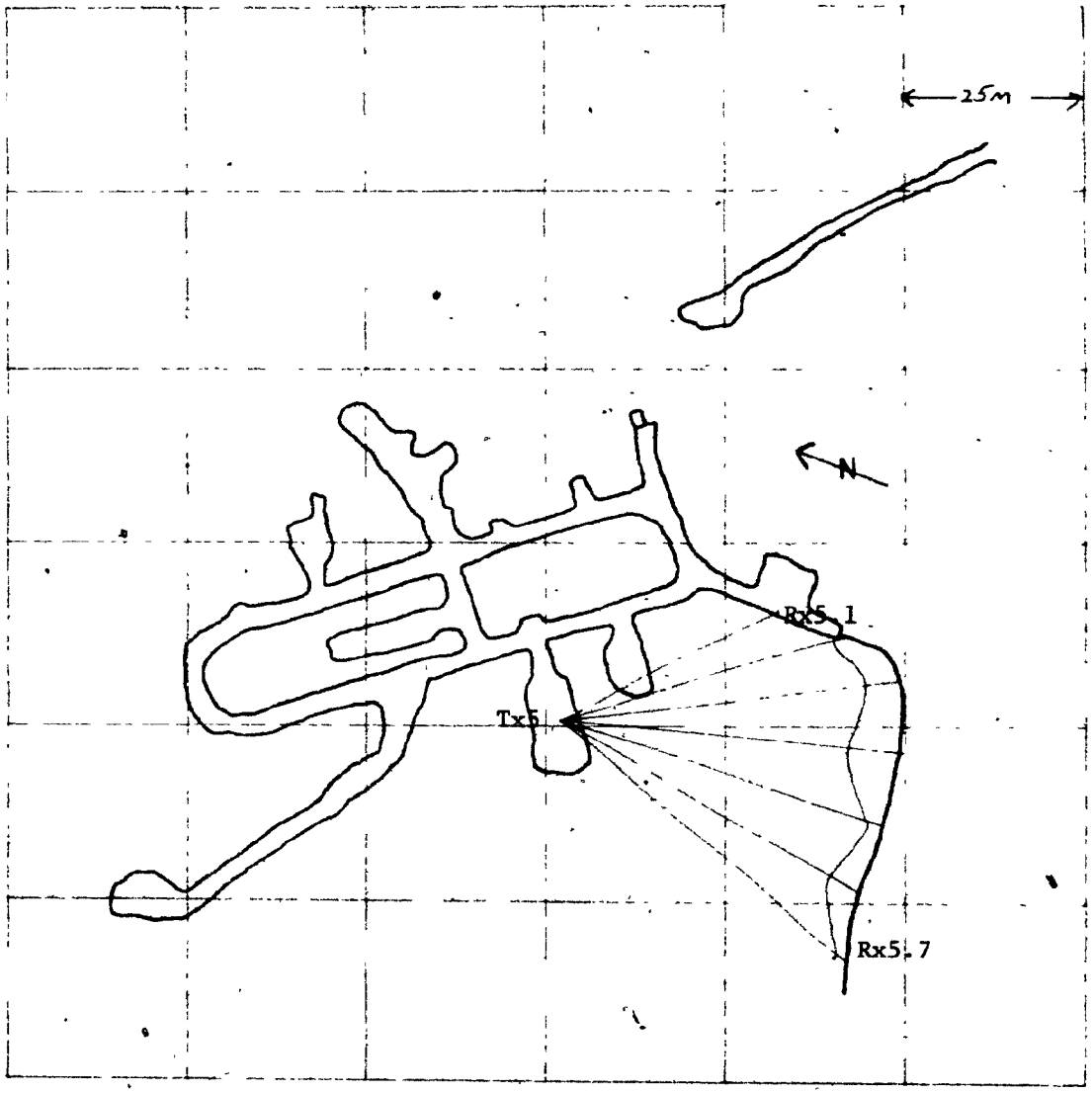

Figure 4.4.6 Transmitter (Tx) and receiver (Rx) locations for survey #5.

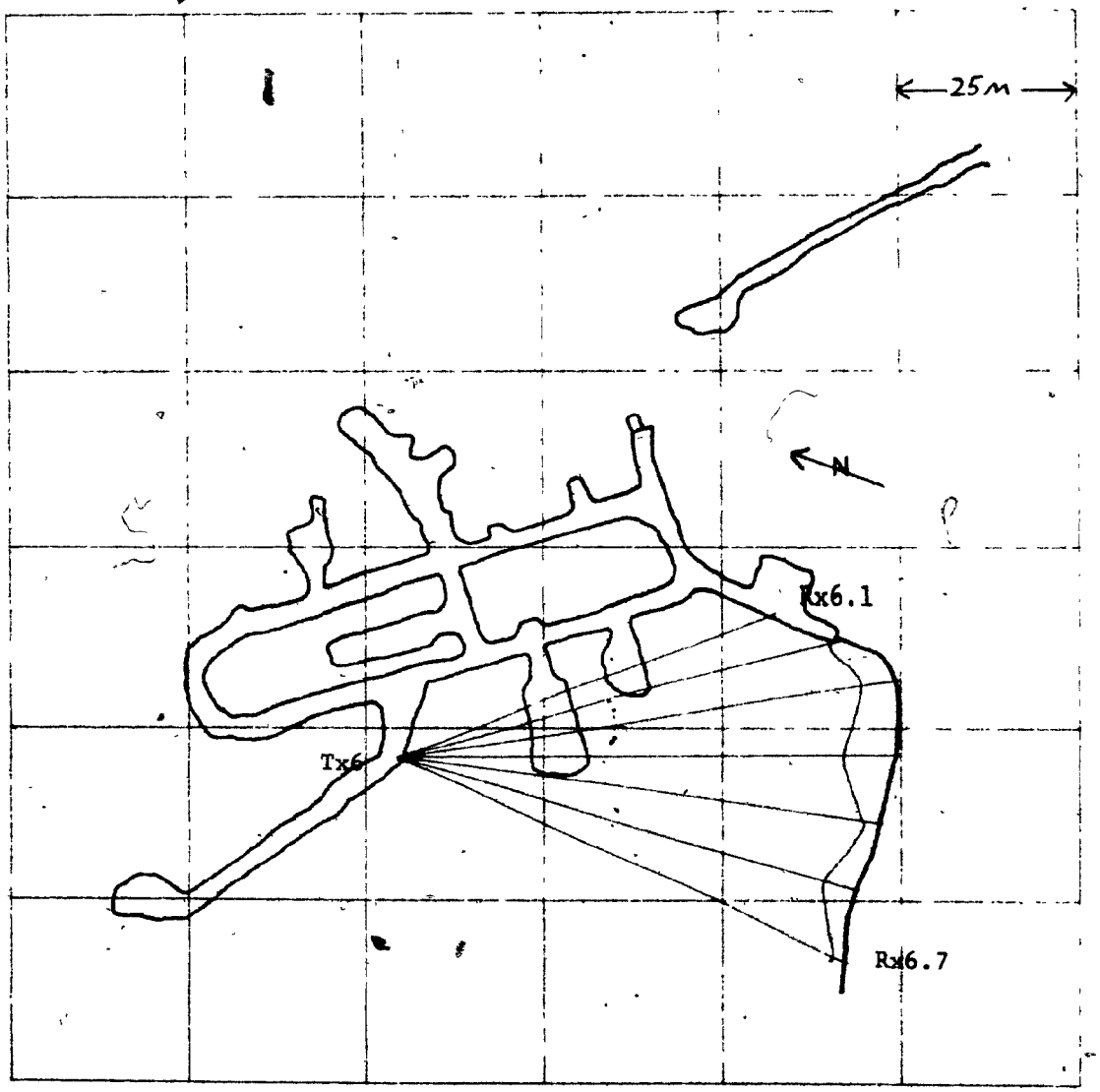

Figure 4.4.7 Transmitter (Tx) and receiver (Rx) locations for survey #6.

Receiver Stn.	distance (m) total	rock	Received Signal (dBv)
Rx1.1	7.0	4.0	-3.4
Rx1.2	8.5	4.5	-21.1
Rx1.3	14.0	8.0	-27.3
Rx1.4	21.0	15.0	-24.1
Rx1.5	21.5	18.0	-51.1
Rx1.6	22.0	17.5	-31.9
Rx1.7	20.5	13.5	-25.5
Rx1.8	16.5	8.5	-45.4
Rx1.9	8.0	3.5	-28.3

Table 4.4.1 Reduced attenuation results for survey #1.

Receiver Stn.	distance (m) total	rock	Reduced Attenuation (dB)	Absorption Rate (dB/m)
Rx2.1	45.0	40.0	58.9	1.47
Rx2.2	31.0	30.0	36.6	1.22
Rx2.3	54.5	48.5	44.1	0.91
Rx2.4	72.0	63.0	70.0	1.11

Table 4.4.2 Reduced absorption rate results for survey #2.

4.4.1 Survey #1

Survey #1 (Figure 4.4.2 and Table 4.4.1) consisted of a transmitter location in the central stope and nine receiver locations around the U-shaped tunnel connecting the east and west drifts at the northwest end of the mine. The received signal was found to be saturated at Tx1-Rx1.1. Given the short transmitter-receiver separation at this location the result was expected. The Weinschel 10 dB power attenuator was inserted in the transmitter line for all measurements. In order that all the receiver stations obtain valid non-saturated measurements the transmitter antenna had to be replaced by the resistive dummy load. The position of the dummy load was rotated with receiver position such that its long axis was always oriented toward the receiver. As the radiation pattern or gain of the dummy load is not known, this was the only way to ensure that the transmitter-receiver antenna coupling remain identical for all receiver stations. The absorption rates are not directly calculable here as the power transmitted is unknown. A tunnel-propagated wave was detected as a second or in some cases a third lobe in the received field pattern. At Rx1.8 one secondary maximum, ie. a received signal lobe detected in a receiver antenna position other than the free space maximum-coupled position, was detected with the antenna pointing directly south down the west drift. This secondary maximum, in fact, exceeded the direct raypath (maximum coupled) maximum in amplitude. At Rx1.9 the same secondary maximum

position resulted in receiver saturation.

4.4.2 Survey #2

Survey #2 (Figure 4.4.3 and Table 4.4.2) consisted of a transmitter located at the end of the Sewer Drift and four receiver stations located within the mine. The following procedure for taking a measurement was used for survey site #2 and all subsequent survey locations.

The transmitter and receiver antennas were oriented for maximum coupling at each receiver station. The receiver locations were predetermined before starting the survey and transmitter antenna directions were marked on the wall at the end of the sewer drift. The transmitter operator would change the direction of his antenna at predetermined times so that its horizontal axis was aligned with the direct-line raypath between the transmitter and receiver locations. The receiver operator would then point his antenna in the direction of the transmitter as determined from the map of the mine area. A final receiver antenna orientation would then be determined by scanning about this estimated direction for the maximum received signal. At each receiver station the receiver antenna was also quickly scanned through 360° in the horizontal plane to check for a second maximum position which could indicate a tunnel guided or diffracted wave arriving from another direction. The antenna was also rotated about its horizontal axis to check for a rotation of the plane of propagation of the wave.

Receiver Stn.	distance (m) total	rock	Reduced Attenuation (dB)	Absorption Rate (dB/m)
Rx3.1	51.5	50.5	62.9	1.25
Rx3.2	50.0	49.0	60.9	1.24
Rx3.3	48.5	47.5	60.5	1.27
Rx3.4	48.0	47.0	50.7	1.08
Rx3.5	50.0	49.0	52.7	1.08
Rx3.6	29.5	27.5	40.8	1.48
Rx3.7	32.0	31.0	30.6	0.99
Rx3.8	37.0	36.0	41.7	1.16
Rx3.9	39.0	38.0	63.9	1.68
Rx3.10	38.0	36.0	40.6	1.13
Rx3.11	46.5	43.5	61.3	1.41
Rx3.12	49.0	46.0	54.9	1.19
Rx3.13	52.0	43.0	67.4	1.57
Rx3.14	55.0	49.0	77.9	1.59
Rx3.15	57.5	51.5	72.0	1.40

Table 4.4.3 Reduced absorption rate results for survey #3.

Receiver Stn.	distance (m) total	rock	Reduced Attenuation (dB)	Absorption Rate (dB/m)
Rx4.1	42.0	38.0	56.7	1.49
Rx4.2	51.0	42.0	46.0	1.10
Rx4.3	66.0	59.0	78.8	1.34
Rx4.4	58.5	42.5	48.8	1.15
Rx4.5	54.0	38.0	56.5	1.49

Table 4.4.4 Reduced absorption rate results for survey #4.

Five receiver sites, in addition to those listed in Table 4.4.2, were occupied. These are labelled as Rx2.5 to Rx2.9 in Figure 4.4.3. Valid readings were taken at Rx2.5 and Rx2.6 but the antennas were unfortunately not oriented for maximum coupling. These positions were subsequently repeated with maximum antenna coupling as stations Rx3.10 and Rx3.11. Extremely low or non existant received signal levels were obtained at stations Rx2.7 and Rx2.8. The receiver was saturated at site Rx2.9.

4.4.3 Survey #3

Survey #3 (Figure 4.4.4 and Table 4.4.3) consisted of a transmitter located at the end of the sewer drift and fifteen receiver stations located within the mine. The transmitter and receiver antennas were oriented for maximum coupling at each receiver location as discussed in section 4.4.2, above.

A weak secondary maximum, approximately 20 dB below the direct wave, was obtained at station Rx3.16. The reading was found to be unreliable at this location due to the high level of signal attenuation needed, 60 dB, to obtain a measurement.

4.4.4 Survey #4

Survey #4 (Figure 4.4.5 and Table 4.4.4) consisted of a transmitter located at the end of the Big Nickel drift and five receiver locations located throughout the mine.

Receiver Stn.	distance (m) total	rock	Reduced Attenuation (dB)	Absorption Rate (dB/m)
Rx5.1	33.5	29.5	40.7	1.38
Rx5.2	41.0	37.5	64.9	1.73
Rx5.3	48.0	41.0	49.6	1.21
Rx5.4	47.5	38.0	59.6	1.57
Rx5.5	47.5	42.5	60.7	1.43
Rx5.6	48.0	40.5	55.1	1.36
Rx5.7	52.0	45.5	61.9	1.36

Table 4.4.5 Reduced absorption rate results for survey #5.

Receiver Stn.	distance (m) total	rock	Reduced Attenuation (dB)	Absorption Rate (dB/m)
Rx6.1	56.5	44.5	44.1	0.99
Rx6.2	65.0	56.0	68.9	1.23
Rx6.3	71.5	64.5	73.1	1.13
Rx6.4	70.5	62.5	71.7	1.15
Rx6.5	69.0	66.0	93.4	1.42
Rx6.6	67.5	62.0	78.6	1.27
Rx6.7	69.5	67.0	83.4	1.24

Table 4.4.6 Reduced absorption rate results for survey #6.

4.4.5 Survey #5

Survey #5 (Figure 4,4.6 and Table 4.4.5) consisted of a transmitter located in the south stope and several receiver locations located just to the north of the rail line that exits the South Adit.

4.4.6 Survey site #6

Survey site #6 (Figure 4.4.7 and Table 4.4.6) consisted of a transmitter located within the Big Nickel drift and the equivalent receiver positions to survey # 5, above.

4.5 Analysis of the results of test survey #2

Received signal levels for the thirty-eight receiver stations from which valid measurements were obtained are plotted versus transmitter-receiver separation in Figures 4.5.1 and 4.5.2. As there was a considerable spread in transmitter-receiver separations available in the data an attempt was made to compare the slope of a least-squares fitted line to the directly calculated absorption rates. This would provide a confirmation of the directly calculated absorption rates. As previously discussed in sections 2.7 and 3.8, above, the calculated absorption rates can be in error due to the reflection of a finite amount of transmitted power from the rock wall surface. A portion of this reflected power will be recaptured by the transmitter antenna and is measurable in terms of a reverse power in the transmission line. The indices of refraction of the wall rock material provide a measure of the amount of transmitted

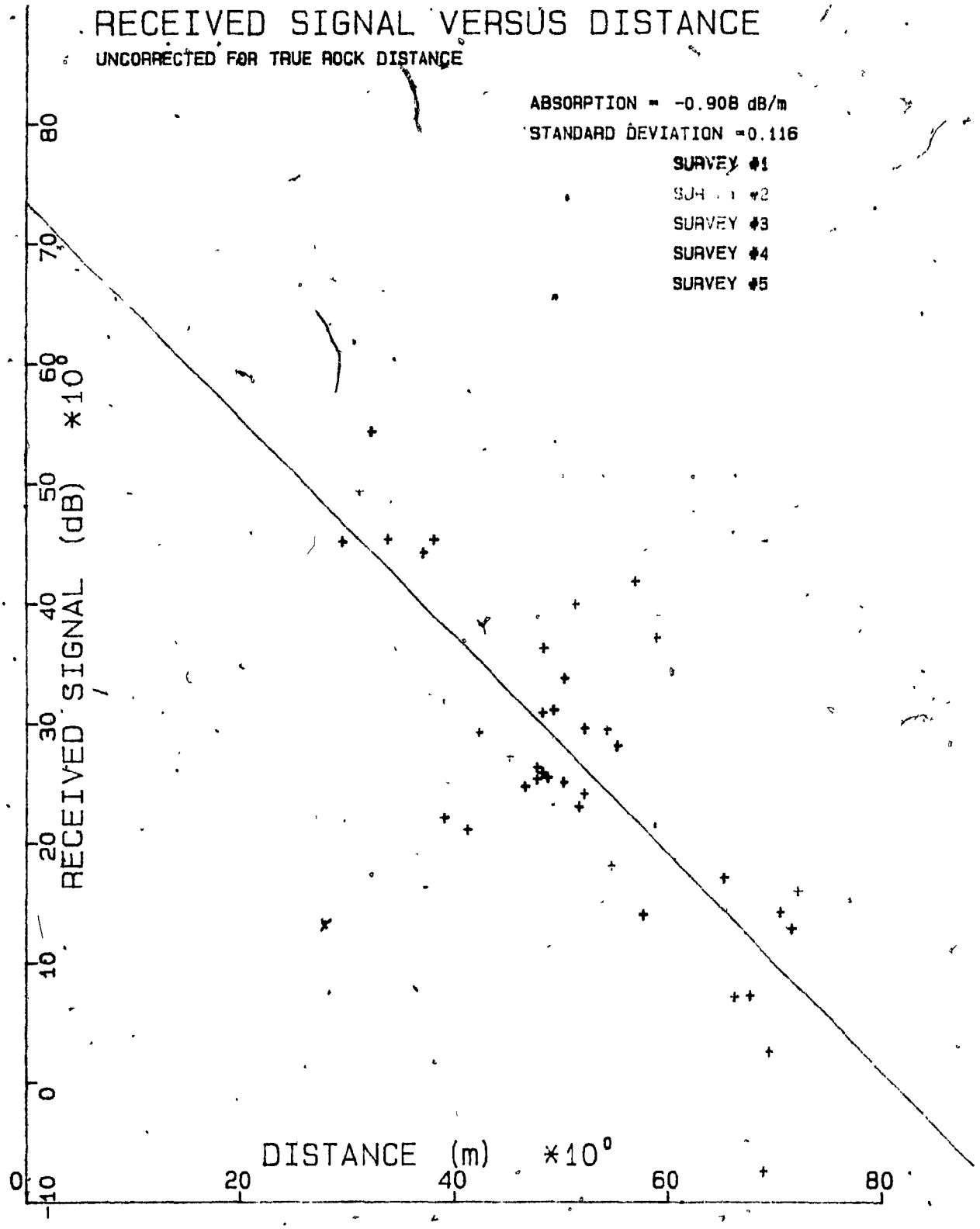

Figure 4.5.1 Received signal versus distance plot for the results of test survey #2. The distances used are the true physical separation between the transmitter and receiver.

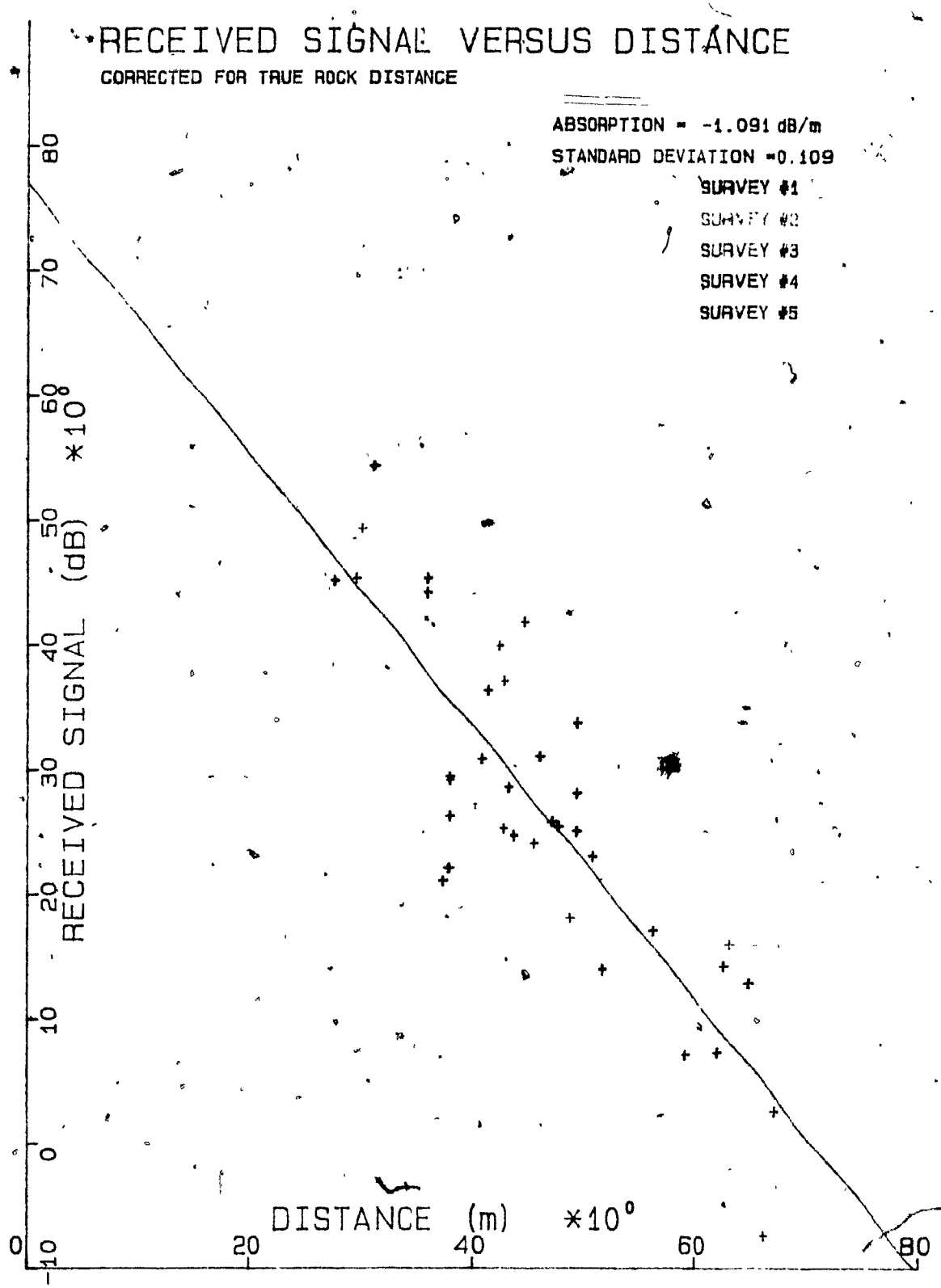

Figure 4.5.2 Received signal versus distance plot for the results of test survey #2. The distances have been corrected to account for the true distance through rock between the transmitter and receiver.

power which is being reflected back off the air-rock interface. These are presented in Table 4.3.1 for station Tx5-Rx5, test survey #1. The coefficients of reflection and transmission, for a wave at normal incidence, for these indices of refraction can be read off Figure 2.7.2. The indices of refraction, and thus the coefficients of reflection are observed to increase with increasingrelative permittivity for a constant value of the attenuation factor. Given that the measured reverse power in the transmission line is only 0.4% of the transmitted power, and even allowing for the fact that the transmitter antenna will not recollect all of the wave energy reflected off the wall rock, it must be assumed that the measurement is not indicative of the true wall rock permittivity as the calculated value is unrealistically low. The reverse power in the transmission line remains quite constant for all the transmitter stations. In the worst case, aiming the transmitter antenna directly at a moist rock face from a short distance away, the reverse power was only 0.5 W.

The least-squares fit of a straight line to the data in Figure 4.5.1, which considers the transmitter-receiver separation as being equivalent to the true rock distance, yields an absorption rate of 0.908 dB/m with a standard deviation of 0.116. Figure 4.5.2 illustrates the improvement in fit which occurs when the transmitter-receiver separation is replaced by the true distance of rock between the the transmitter and receiver. This allows for

the known intervening air passageways, but neglects the effects of reflection at their interfaces. The absorption rate is 1.09 dB/m and the standard deviation is reduced to 0.109. This indicates that the void spaces due to open-air passageways along the straight-line raypath between transmitter and receiver are detectable. The latter figure compares well with the average value for the absorption rate of 1.30, as determined from the direct calculation method.

Figures 4.5.3 and 4.5.4 show the absorption rate as a function of distance for the two mine areas designated in Figure 4.4.1. A sufficient spread of distances, for a least squares fit, is only available in the case of mine area #2. The absorption rate determined is 1.01 (+0.171) dB/m. Table 4.5.1 lists the absorption rates for mine areas #1 and #2. Mine area #2 has been subdivided into area #2a and #2b. The average absorption rate for the survey stations which cover both area #2a and #2b are lower than those which encompass only area #2a, indicating a lower absorption rate over area #2b. The average absorption rate for area #1 is also slightly lower than that determined in area #2a. Calculated electrical parameters based upon the average absorption rates for the three mine areas are listed in Table 4.5.2. The index of refraction for such low conductivities is wholely dependent upon the relative permittivity. This arises because the loss tangent is very much less than unity in equation 2.2.21. The index of refraction can therefore be considered independent of absorption loss over the range

Mine area	Station	Absorption rate (dB/m)
1	Rx3.1	1.25
	Rx3.2	1.24
	Rx3.3	1.27
	Rx3.4	1.08
	Rx3.5	1.08
	Rx2.1	1.47
Average		1.23
2a	Rx5.1	1.38
	Rx5.2	1.73
	Rx5.3	1.21
	Rx5.4	1.57
	Rx5.5	1.43
	Rx5.6	1.36
	Rx5.7	1.36
Average		1.43
2a+2b	Rx6.1	0.99
	Rx6.2	1.23
	Rx6.3	1.13
	Rx6.4	1.15
	Rx6.5	1.42
	Rx6.6	1.27
	Rx6.7	1.24
Average		1.20

Table 4.5.1 Absorption rates for the three different areas of the mine indicated in Figure 4.4.1.

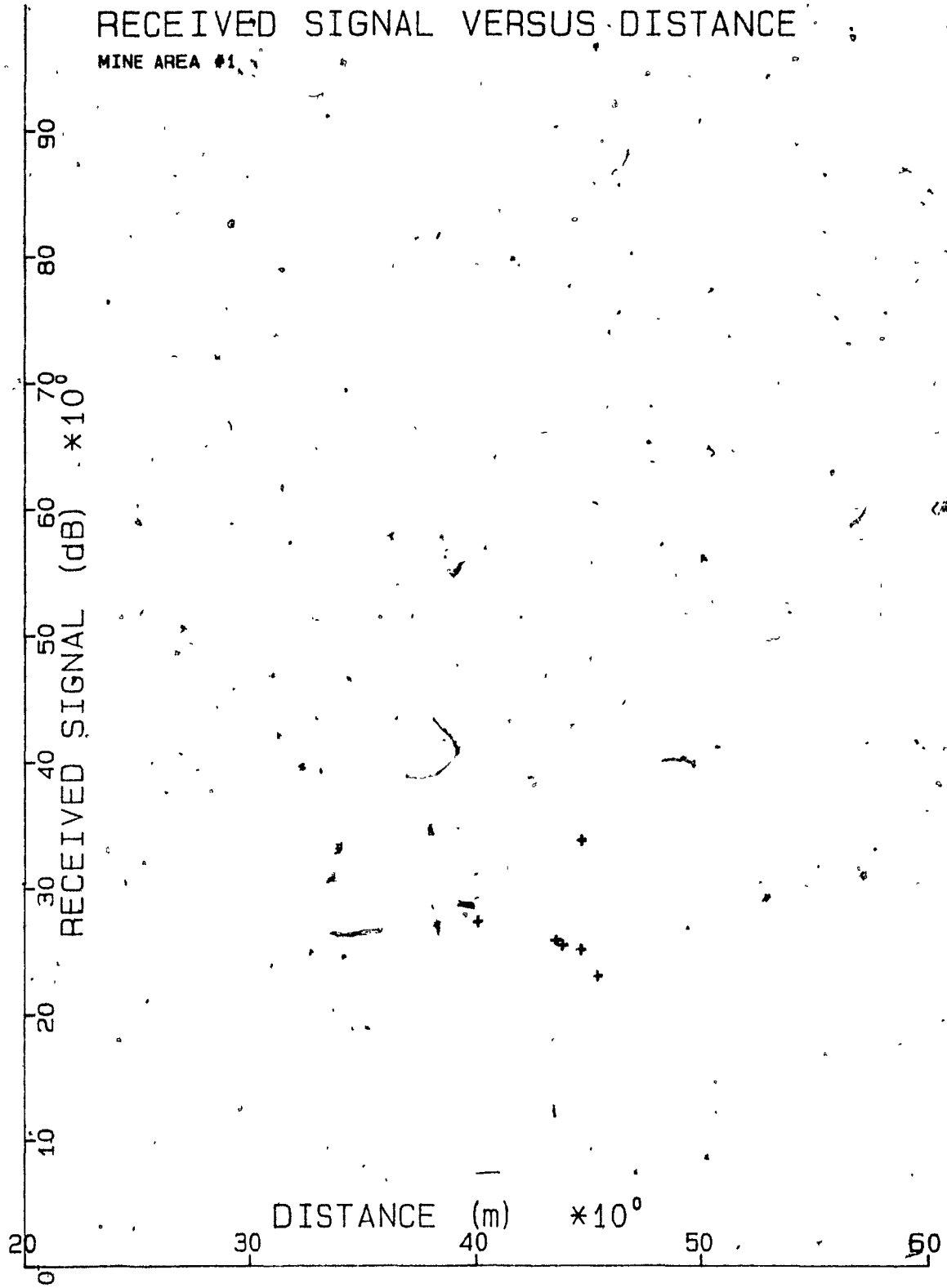

Figure 4.5.3 Received signal versus distance plot for the results from mine area #1, Figure 4.4.1.

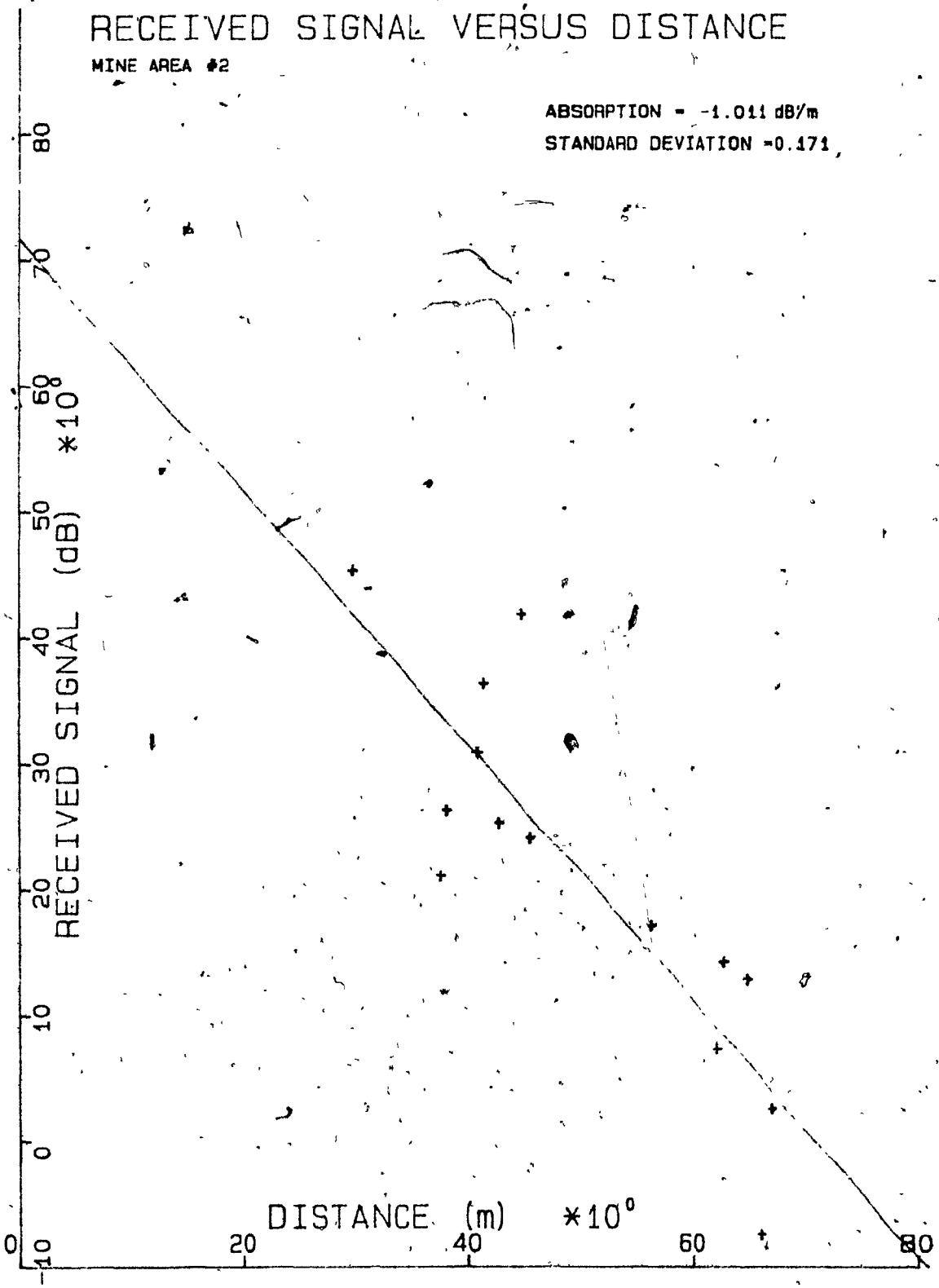

Figure 4.5.4 Received signal versus distance plot for the results from mine area #2, Figure 4.4.1.

of absorption losses encountered in the test surveys. The permittivity can be indirectly estimated from the index of refraction. If the reverse power in the transmission line is considered to represent fully the amount of power reflected off the air-rock interface, the index of refraction of the rock would approximate 1.0, corresponding to a permittivity of approximately unity. This value is significantly lower than those typically reported in the literature. Relative permittivities, as measured by other researchers, commonly vary between 5 and 10 for similiar materials at VHF/UHF frequencies. The measurement, therefore, is not useful in estimating the relative permittivity. The relative permittivities for the dry samples listed in Table 2.3.1 are 10.0 or less. Making the above assumptions, it can be estimated that the average, in situ resistivity of the rock in the mine area is approximately 500-1500 ohm-m at 445 MHz.

Unfortunately the majority of the raypaths were parallel to bedding making it difficult to determine whether or not the variation in grain size across the bedding plane affected the absorption rate. No striking difference in absorption rate is observed between the raypaths that cross bedding and those that are roughly parallel to it. This is expected since the thin section examination shows the rock to be extremely impermeable to fluid in all directions and the that the pyrite grain distribution is roughly isotropic. The only factor that would affect the absorption rates is

Relative Permittivity	1.	5.	10.	30.	81.
Mine area #1 Conductivity (S)	.752E-03	.168E-02	.238E-02	.412E-02	.676E-02
Resistivity (ohm-m)	1330.37	595.01	420.74	242.92	147.84
Index of Refraction	1.00	2.24	3.16	5.48	9.01
Mine area #2a Conductivity (S)	.874E-03	.195E-02	.276E-02	.479E-02	.786E-02
Resistivity (ohm-m)	1144.26	511.79	361.90	208.94	127.16
Index of Refraction	1.00	2.24	3.16	5.48	9.01
Mine area #2b Conductivity (S)	.733E-03	.164E-02	.232E-02	.402E-02	.660E-02
Resistivity (ohm-m)	1363.64	609.89	431.26	248.99	151.53
Index of Refraction	1.00	2.24	3.16	5.48	9.01

Table 4.5.2 : Calculated electrical properties for mine areas #1, #2a and #2b. The relative permeability is assumed to be equal to unity.

the presence of fluid filled cracks or metallic stringers within the rock mass. The presence of these could greatly alter the absorption rate, an effect which is not apparent in the data. The slightly higher absorption rates measured in mine area #2a can be accounted for if one allows for some error in estimating the shape of the irregular wall rock surface on the exterior of the mine.

Chapter 5

Core Resistivity Measurements

5.1 General

It is desirable to confirm the resistivity values obtained from the in-situ UHF measurements using another, more conventional, technique. Several approaches are available. Most directly, a DC or low frequency AC (1-100Hz) galvanic survey could be used to obtain measures of apparent earth resistivity. A common survey configuration is shown in Figure 5.1.1. The apparent resistivity of the subsurface is defined as,

$$\rho_a = G \cdot V/I \qquad (\Omega\text{-m}) \qquad (5.1.1)$$

where: V= measured potential difference between the two potential probes (volts)

I= transmitted current through the current electrodes (amperes)

G= geometrical factor dependant upon the geometrical relationship between the potential and current electrodes and a resistive halfspace.

The geometrical constant for the Wenner array shown in Figure 5.1.1 is

$$G = 2 \cdot \pi \cdot a \qquad (5.1.2)$$

Commonly in geophysical resistivity surveys the electrode separation is chosen according to the volume of interest in

the investigation. The survey penetration depth is scaled in proportion to the geometrical factor. The model assumed for the subsurface is essentially that of a uniformily resistive halfspace and consequently the presence of nearby tunnels, fencing, railroad tracks, mine vehicles, etc. can greatly prejudice a galvanic apparent resistivity measurement of the rock. The VHF/UHF electromagnetic technique has the advantage of greater directionality, thereby allowing one to avoid effects arising from such conditions in the measurement.

Apart from the in-situ methods mentioned above, laboratory measurements can be made on hand samples or cores. Although this technique offers a high degree of control through the selection of the sample measured, the fact that the sample is not measured in place is a disadvantage. The sample can only be representative of a small volume of rock in the region from which it was taken. The fluid content of a lithologic unit can vary significantly from place to place. Natural fluids within the interstitial spaces of the sample can escape during transport and storage. A variation in the fluid content of a rock can result in very large changes in the rock's electrical properties (see Table 2.3.5). Despite this drawback, a laboratory measurement does allow one to measure the variation in resistivity over the survey area by selecting samples from different sites.

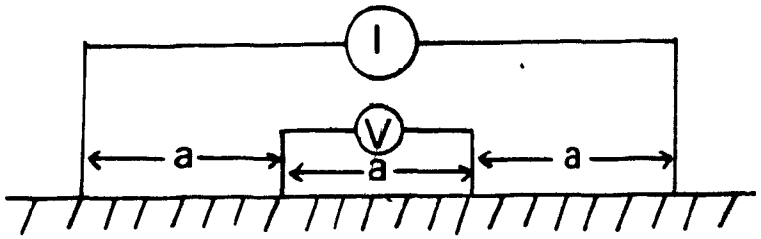

Figure 5.1.1 The Wenner resistivity spread. A current, I, isinjected into the ground through current electrodes C_1 and C_2 . The resulting potential difference, V, is measured between P_1 and P_2.

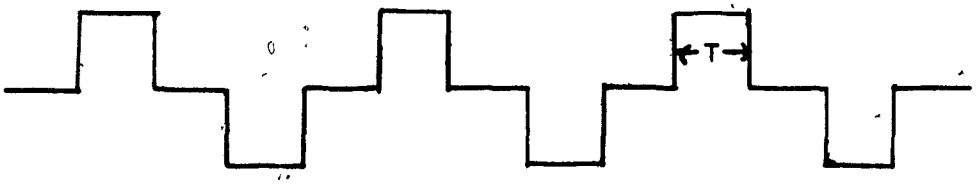

Figure 5.2.1 The commutated DC current output of the CTU-2 induced polarization transmitter.

5.2 DC resistivity measuring apparatus and procedure

Scintrex Ltd. of Concord, Ontario provided laboratory facilities and the use of their CTU-2 Physical Property Testing System. The CTU-2 is a portable system designed to measure the magnetic susceptibility, AC electrical conductivity, DC electrical conductivity and induced polarization (IP) chargeability of rock samples or drill core. The susceptibility and AC conductivity are measured inductively while the DC resistivity and chargeability are measured in a manner analogous to the standard galvanic resistivity survey technique described above. The author performed only the DC resistivity measurements. The CTU-2 is not designed to make AC inductive measurements on samples whose conductivities are below 50 S. The samples collected show no evidence of interconnected metallic mineralisation under thin section examination and are relatively impermeable to fluids. As the rock samples obtained from the Big Nickel Mine are clearly less conductive than 50 S, this instrument is incapable of making valid AC conductivity measurements.

The DC resistivity of a core sample is measured by means of the induced polarization module which can be incorporated as an option in the CTU-2. A commutated DC current (Figure 5.2.1) is injected into the sample by a low power transmitter. The resulting on-time potential difference is measured between two potential electrodes. The recommended electrode configuration is the symetrical

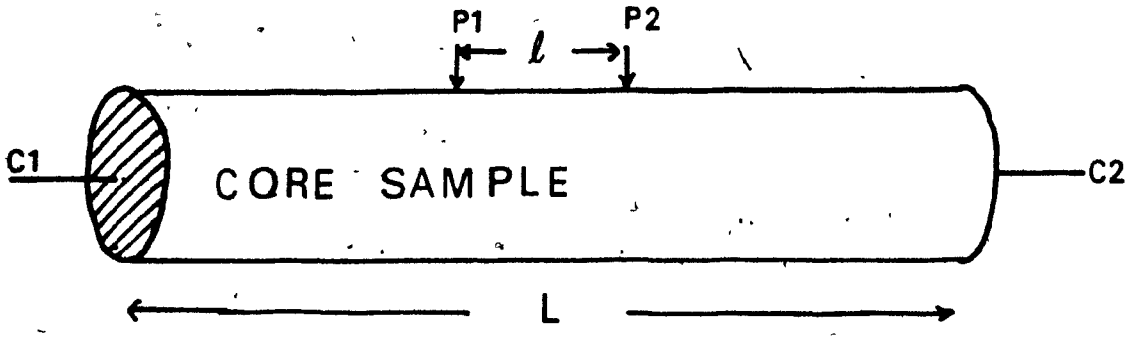

Figure 5.2.2 The symetrical Schlumberger array used in the core resistivity measurements.

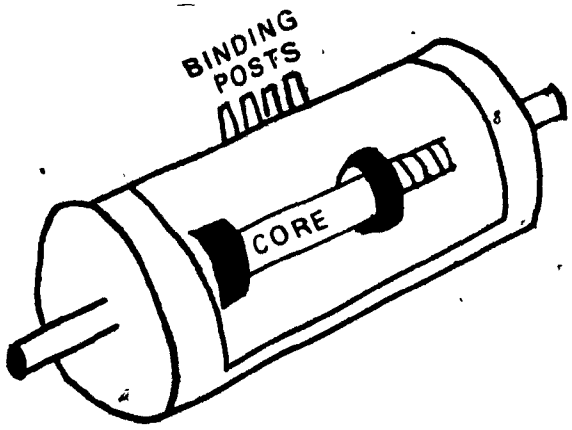

Figure 5.2.3 The CTU-2 measurement jig.

Schlumberger array shown in Figure 5.2.2. A standard Scintrex IPR-11 time-domain induced polarization (IP) receiver was used to record the on-time potential difference.

Ideally, for use in the CTU-2 system, samples should be cylindrical cores approximately 15 cm. long and less than 5 cm. in diameter. The cores can be whole or split (longitudinally) in two. The equivalent geometrical factors of equation 5.1.1 are then,

for cylindrical cores: $G = \pi (d/2)^2/l$ (5.2.1)

and for split cores: $G = \pi (d/2)^2/2l$ (5.2.2)

where d is the diameter of the core and l is the potential electrode separation in metres. The apparent resistivity of a cylindrical core sample is then,

$$\rho_a = \pi \frac{(d/2)^2}{l} \frac{V}{I} \quad . \qquad (5.2.3)$$

The cores are placed in a plastic measuring jig (Figure 5.2.3) and are held firmly in place, at each end, by spring-loaded clamps. Cloth pads saturated with a copper-sulfate solution are firmly pressed against the ends of the core by the flat clamping disks. These provide the electrical contact between the sample and a current electrode located in the center of the clamping disk directly behind the pad. The pads must be kept saturated and lie flat against the ends of the core to achieve good electrical contact and a uniform current density. This is especially critical when

measuring a non-porous, poorly-conductive rock. The two central potential electrodes are attached to the sample by cloth-covered copper wires which are wrapped around the center of the core and separated by approximately 2.5 cm. The cloth covering the copper wire is kept saturated with a copper-sulfate solution. If the sample is poorly conducting several tightly packed turns of the wire might be necessary to provide for a sufficiently low contact resistance between the electrodes and the sample.

A variation in the water content of the samples can greatly affect the conductivity measured. For this reason it is important to avoid any drying out of the sample between the time it is collected and measured. As a standard precaution samples are resaturated with water before they are measured. The samples are placed in a partial vacuum for 12 hours to remove the air in the pores and subsequently soaked in water for at least another 12 hours to allow full saturation. Generally it is best to leave the samples soaking until the time of measurement.

5.3 Results of the DC core measurements

Ten cylindrical cores and one rock sample taken from the mine wall were measured. The core samples were taken from sites in and around the mine with a small gasoline-powered drill which was provided by the Geological Survey of Canada. Figure 5.3.1 indicates the area from which each sample was taken. The cores produced vary in length from 10

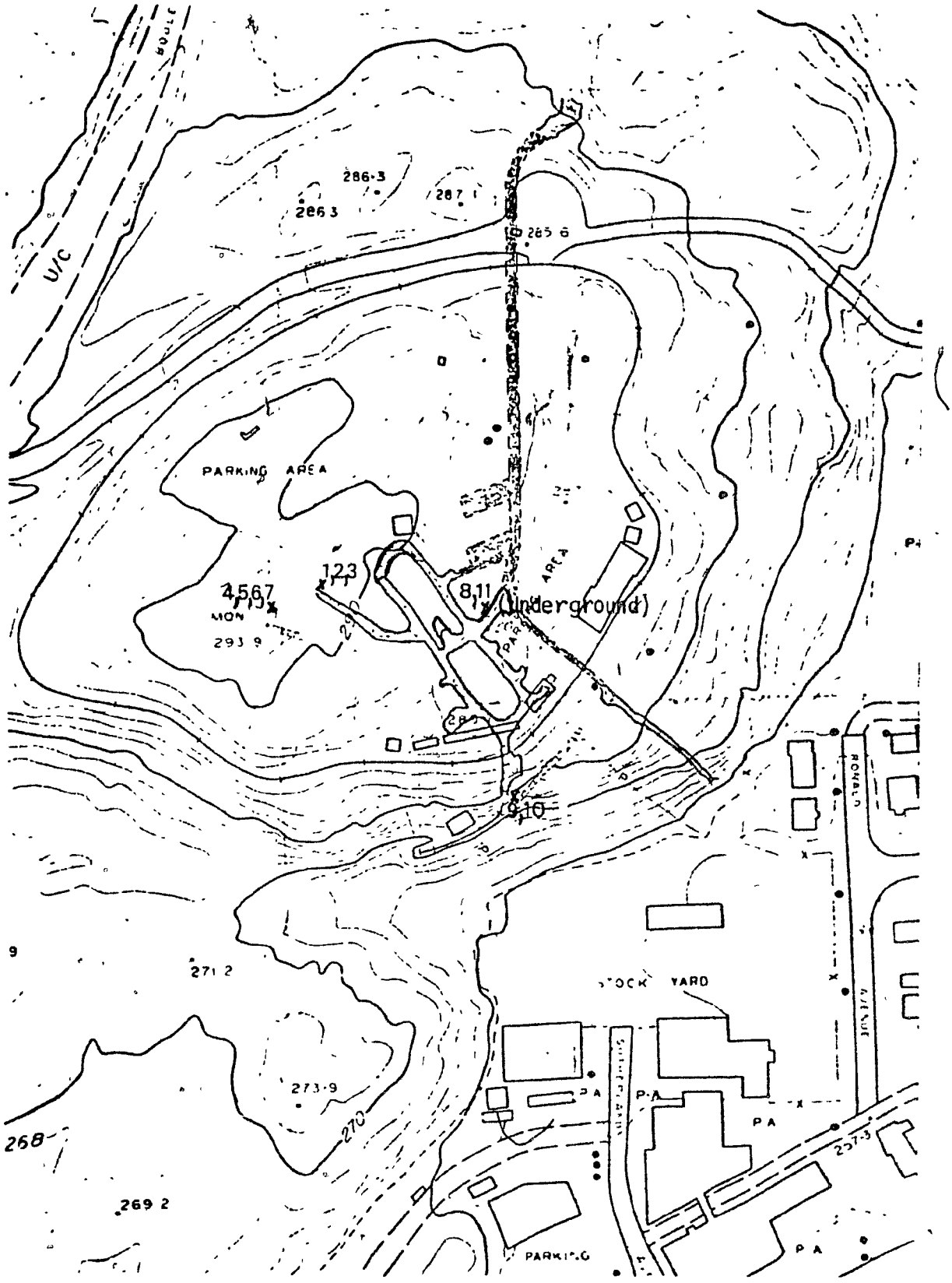

Figure 5.3.1 Locations of the core samples taken from the Big Nickel Mine site.

to 15 cm. and are 2.5 cm. in diameter. The one rock sample measured was cut into a 2.5 cm. square by 15 cm. long prism. The samples were collected and immediately transported to Scintrex's laboratory for measurement. The vacuum resaturation procedure described in Section 5.2, above, was carried out.

The measured resistivities for the 10 core samples (#1-#10) and the rock sample (#11) are listed in Table 5.3.1. The lowest potential electrode resistances achieved were in most cases only slightly below that required by the receiver according to specifications (50 k Ω). Good potential electrode contact was difficult to achieve and in most cases several attempts had to be made using numerous windings of the cloth-covered copper wire around the cores to increase the contact surface area of the potential electrodes. If the potential electrode resistance approaches an appreciable fraction of the receiver input impedance (4 M Ω), the measured apparent resistivity will be reduced. The error in the apparent resistivity should not, in principle, be more than 2% for a potential electrode resistance of 50 k Ω . High potential electrode resistance could, however, result in the receiver picking up extraneous noise due to nearby operating instrumentation or power lines. Furthermore an uncertainty in the potential electrode separation arises due to the broad areas of contact required to obtain low potential electrode resistance. Extreme care had to be taken that excess copper-sulfate solution did not short out the

Sample	Current (A)	Voltage (mV)	Resistivity (m)
1	52	2619	1000
2	46	2377	1000
3	30	3036	2000
4	40	4108	2100
	80	1679	400
5	32	3405	2100
	41	2790	1400
	72	2900	800
6	30	1974	1300
	24	943	800
7	44	3147	1400
	46	4278	1900
8	20	1027	1000
	26	1066	800
9	50	3497	1400
10	38	2896	1500
11	30	2230	1500

Average resistivity = 1300 Ω-m

Table 5.3.1 Apparent resistivities calculated from the DC measurements of rock cores from the Big Nickel Mine site.

potential electrodes. For the reasons outlined above the DC resistivity measurements on the cores must be considered somewhat suspect. Repeat measurements were performed on several samples. In no case did remeasurement exactly reproduce the initial result. Repeated readings varied as much as 80%. The limitations of the instrumentation are such that the measurement of resistivities, for cylindrical cores, of over 5,000 Ω-m is not practical.

The average DC resistivity of 1300 Ω-m compares well with the average resistivity of 500 - 1500 Ω-m obtained using the 445 MHz transillumination equipment as calculated from the absorption rate data in Chapter 4. The effective resistivity of a rock sample would normally be expected to decrease with frequency between DC and 1 GHz. The effect is especially apparent if fluid is present in the pore spaces of the rock (see Table 2.3.5). The extremely low porosity of the sample could account for the small decrease in resistivity observed over the DC to 445 MHz frequency range. Telford (1976) lists DC resistivity values for two greywacke samples of 4700 Ω-m and 58000 Ω-m. The effective resistivity as a function of frequency between 100 Hz and 1 MHz for the basalt and granite samples (Figures 2.3.1 and 2.3.2) measured by Saint Amant and Strangway (1970) can be determined using equation 2.2.32. In this case the resistivity is found to decrease from 7.1×10^{7} Ω-m to 3.3×10^{4} Ω-m and from $3. \times 10^{8}$ Ω-m to 1×10^{5} Ω-m over the above frequency range for the basalt and granite samples

respectively. The above measurements were made on dry samples. As a consequence of the inconclusive results of the DC resistivity measurements, the author initiated a series of AC resistivity measurements on the cores.

5.4 AC resistivity measuring apparatus and procedure

The circuit schematic used in taking AC resistivity measurements on the core samples is illustrated in Figure 5.4.1. The measurement jig and electrode configuration is identical to that described in section 5.2, above, for the DC resistivity measurements. The AC signal source is a Wavetek model 114 signal generator which has been set for a sine wave output. The potential difference across the potential electrodes is measured with a Princeton Applied Research model 186A differential input lock-in amplifier. The transmitter current is obtained by measuring the voltage drop across a 1.2 M Ω resistor, placed in series with the signal generator and rock-core, with an identical lock-in amplifier. The signal generator provides a reference output for both lock-in amplifiers so that extremely low-level signals (100 nV) can be measured. The frequency range of the lock-in amplifiers used is from 0.5 Hz to 100 kHz.

5.5 Results of the AC core measurements

Measurements of the amplitude and phase of the potential difference between the potential electrodes with respect to the amplitude and phase of the transmitted signal

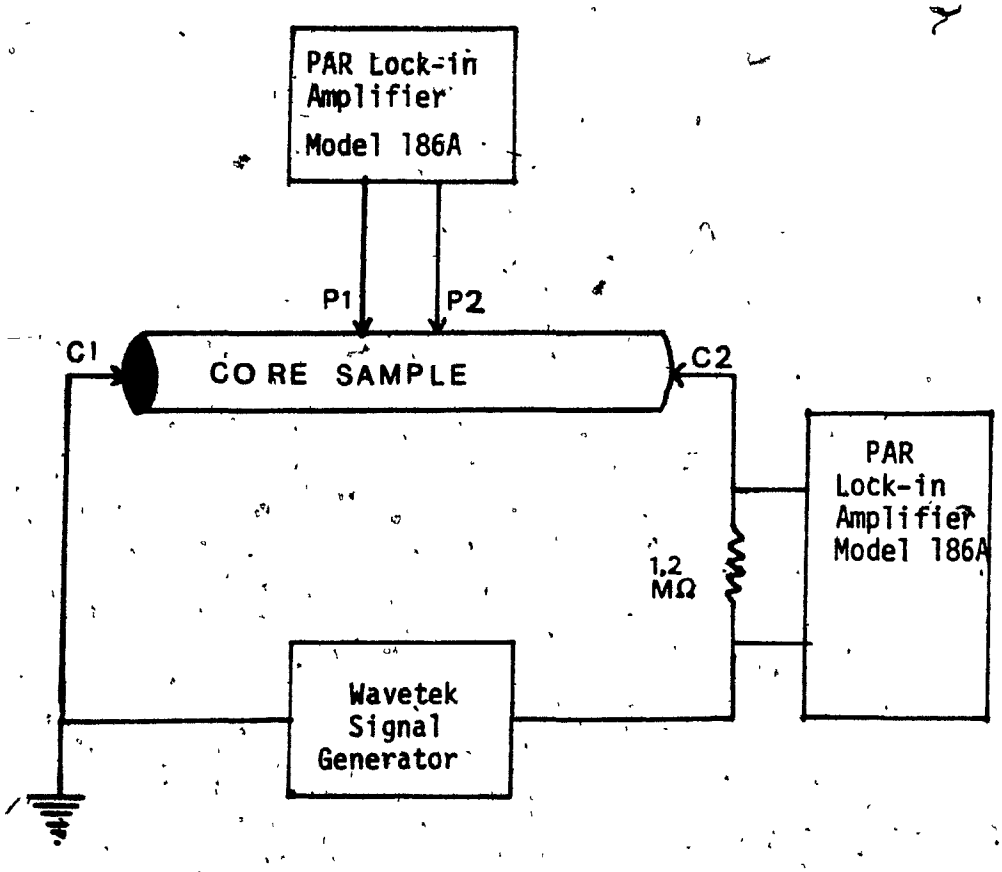

Figure 5.4.1 The AC resistivity measurement equipment.

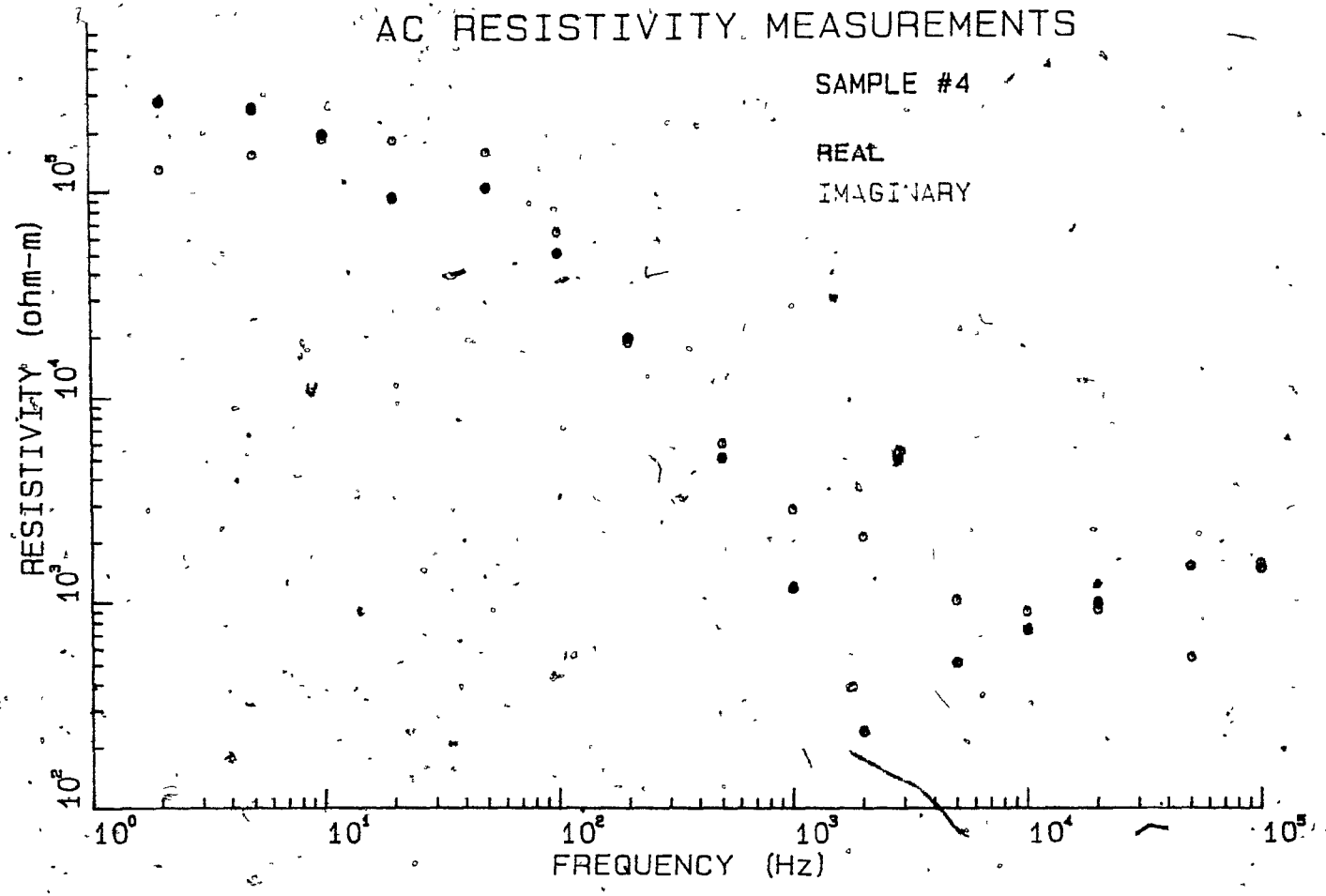

Figure 5.5.1 Real and imaginary components of the apparent resistivity of core sample #4 as a function of frequency.

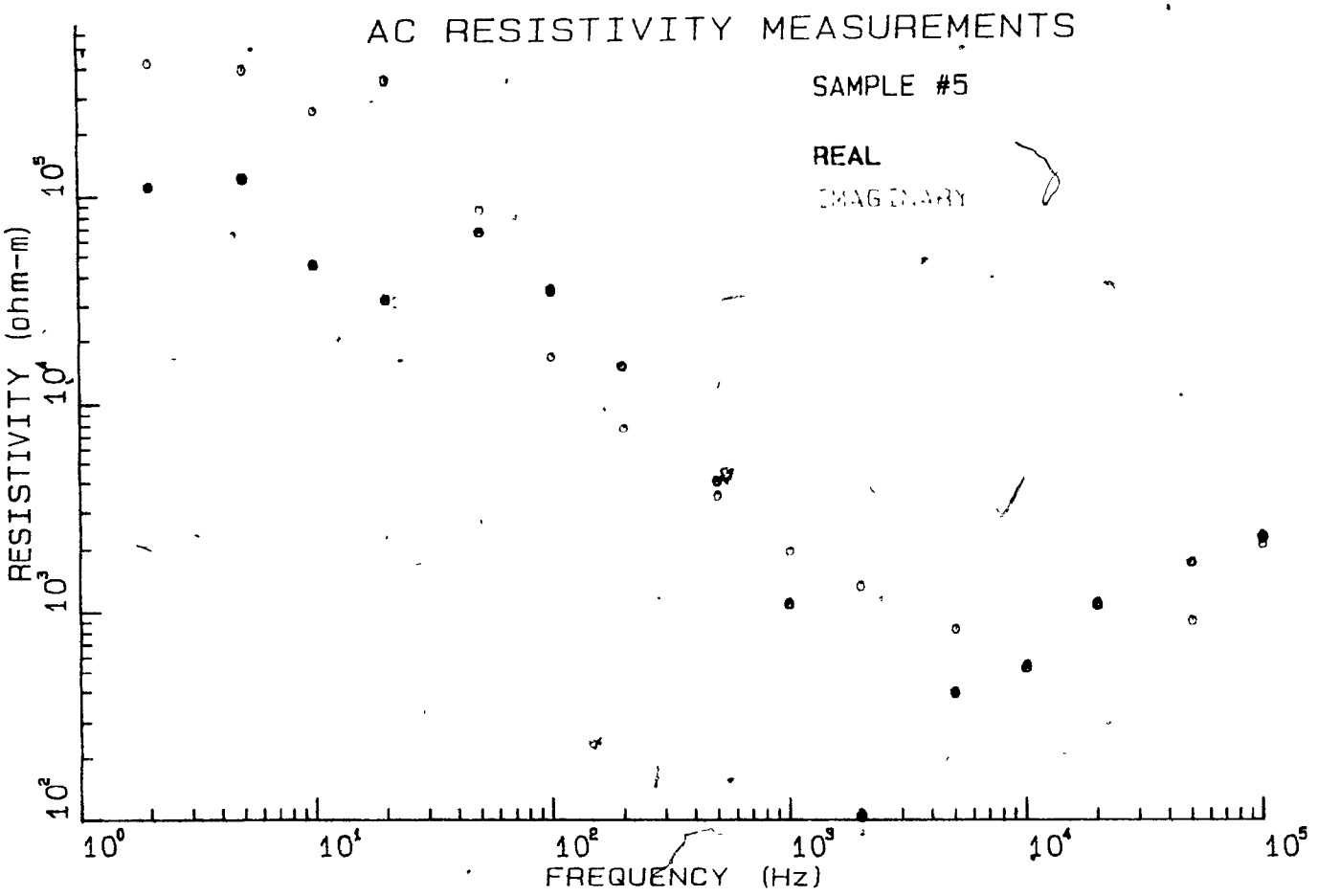

Figure 5.5.2 Real and imaginary components of the apparent resistivity of core sample #5 as a function of frequency.

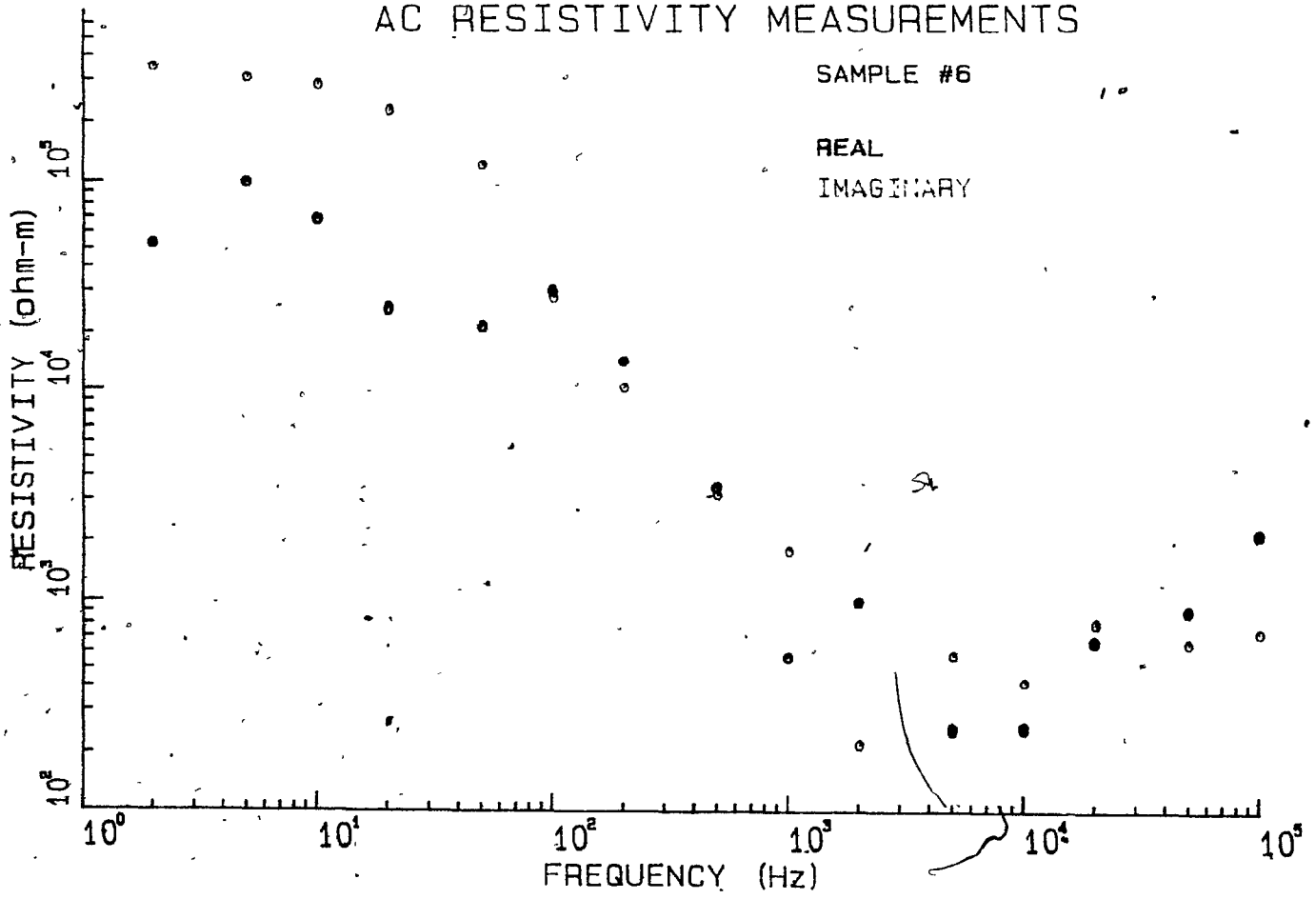

Figure 5.5.3 Real and imaginary components of the apparent resistivity of core sample #6 as a function of frequency.

were taken for three core samples. These measurements were subsequently converted into inphase (real) and quadrature (imaginary) components which correspond to the effective complex-valued resistivity (equation 2.2.27) and permittivity (equation 2.2.26) respectively. The results are presented as log-log plots in Figures 5.5.1 to 5.5.3. In all three case the effective resistivity and effective permittivity exhibit the classical relaxation phenomenon. Zablocki (1964) measured the effective permittivities and conductivities of several serpentinite samples as a function of temperature and frequency (Figure 5.5.4a and 5.5.4b). Keller (see Carmichael,1982; Wait, 1959) made measurements of the relative effective permittivity versus frequency for several sandstone cores from the Morrison formation (Figure 5.5.5). The results presented in Figures 5.5.4a and 5.5.5 illustrate a dielectric relaxation phenomenon not unlike that observed in the three cores from the Big Nickel Mine. Several physical and empirical models have been proposed to describe these relaxation phenomena, the most popular of which is the empirical Cole-Cole permittivity model (Cole-Cole, 1941). Baranyi (1984) has solved for the real and imaginary components of the permittivity and conductivity by a joint Cole-Cole inversion of the effective conductivity and permittivity data for the above serpentinite at 200^{0} C.

The AC resistivity results obtained, here, are entirely consistent with the results obtained by previous researchers. Likewise the resistivity measured at the

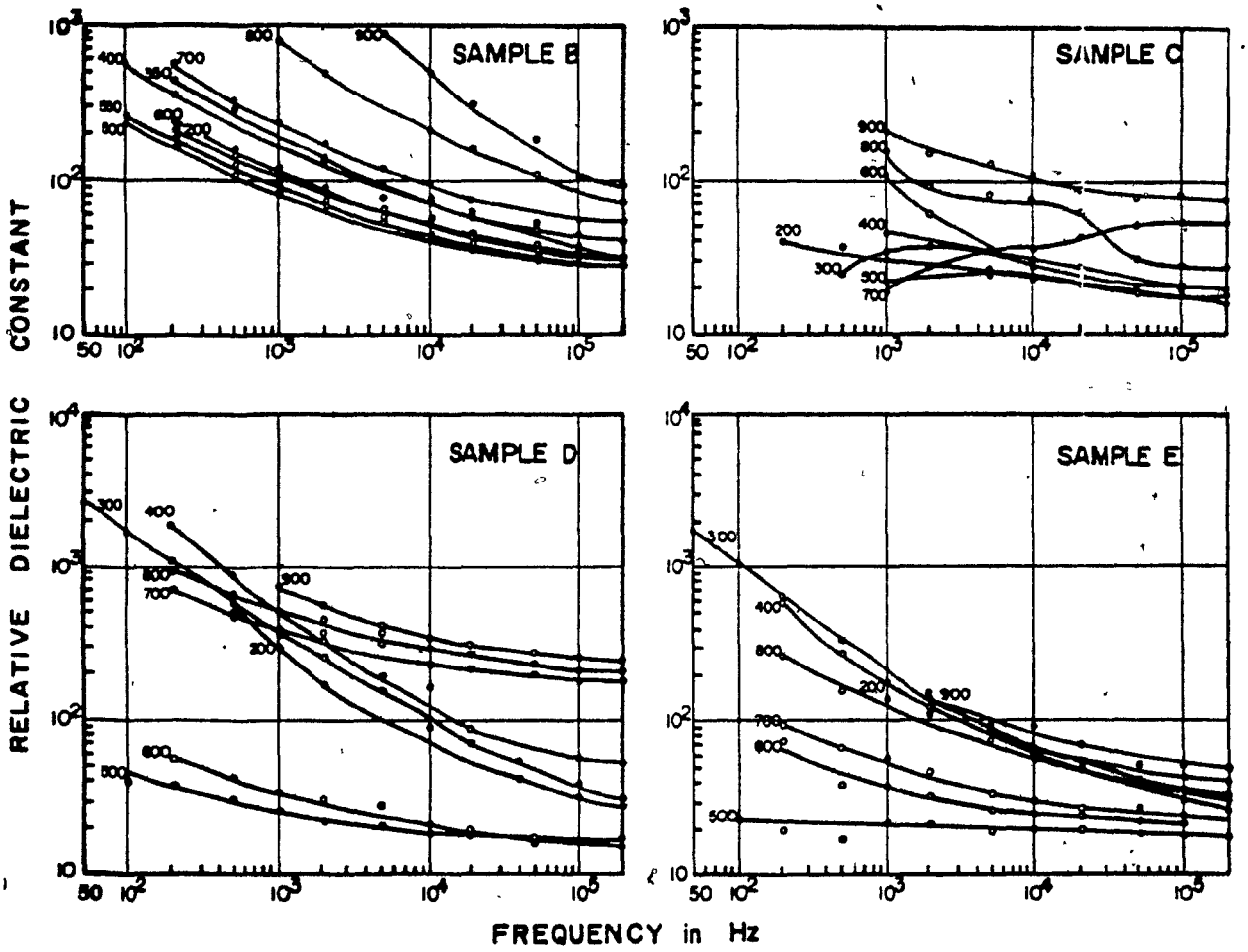

Figure 5.5.4a Laboratory measured effective permittivity as a function of frequency (after Zablocki, 1964).

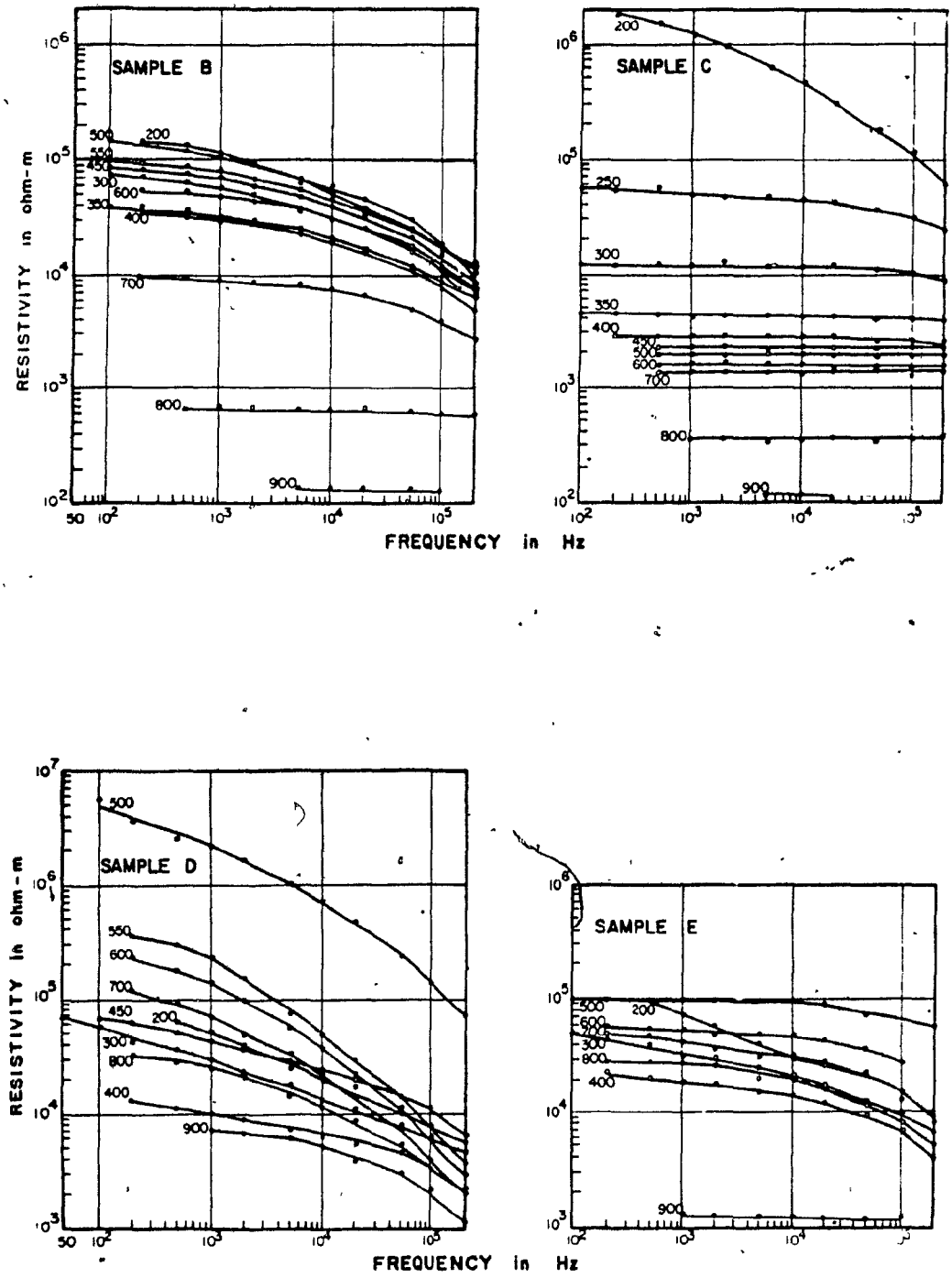

Figure 5.5.4b Laboratory measured effective resistivity as a function of frequency (after Zablocki, 1964).

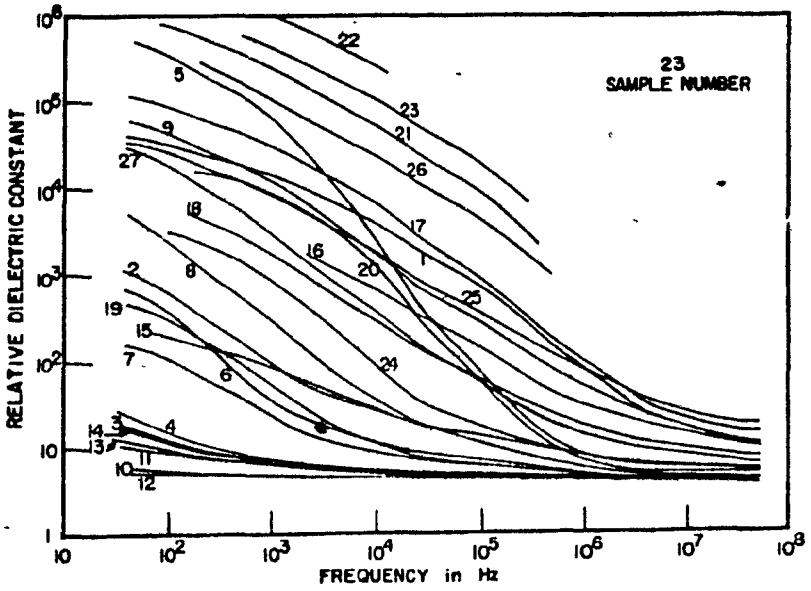

Figure 5.5.5 Effective permittivity as a function of frequency for natural state Morrison cores (after Wait, 1959).

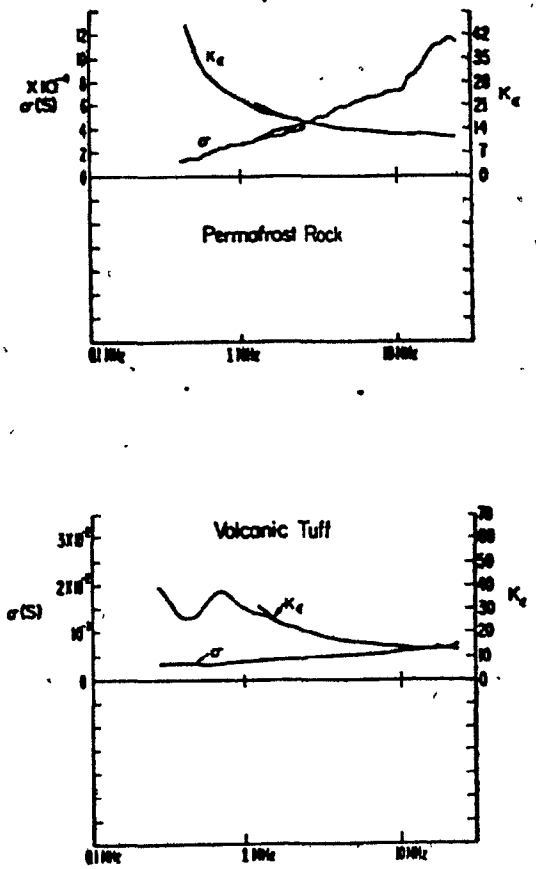

Figure 5.5.6 The effective conductivity and permittivity as a function of frequency measured in situ (after Grubb et al., 1976).

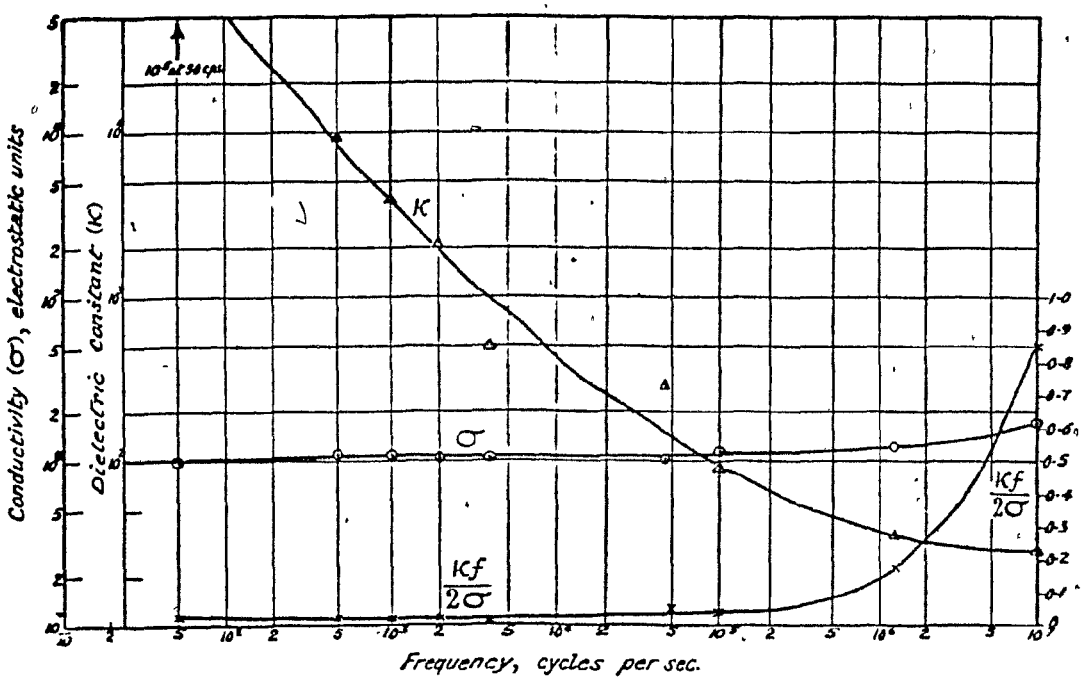

Figure 5.5.7 Laboratory measured effective conductivity and permittivity as function of frequency for a loamy soil sample (after Smith-Rose, 1934).

highest measuring frequency (100 kHz) is similiar to that obtained at 445 MHz from the transillumination results. It is not unreasonable, then, to expect the effective resistivity to be relatively constant or decrease only slightly with increasing frequency between 100 kHz and 445 MHz. The conductivity of water (Table 2.3.5) changes very little between 100 kHz and 10 MHz. Grubb et al. (1976) obtained in-situ measurements between boreholes of the effective conductivity and permittivity between 300 kHz and 25 MHz. Figure 5.5.6 shows that the conductivity is relatively constant over the range of frequencies measured. Smith-Rose (1934) conducted laboratory measurements of the electrical properties of various soils as a function of frequency. Figure 5.5.7 shows the results for the effective permittivity and the effective conductivity of a loamy soil measured over the frequency range 50 Hz to 10 MHz. The conductivity is again observed to be fairly independent of frequency in this range. These early measurements are consistent with those obtained by many other researchers who have studied other materials (Keller, 1963; Carmichael, 1982; Collett and Katsube, 1973; Cook, 1970).

Chapter 6

Conclusions and Recommendations

6.1 Summary of the work

The original intention of this research work was to conduct a feasibility study into the use of continuous UHF electromagnetic fields and waves in geophysical surveys. The author has approached this goal by demonstrating that UHF-EM waves can indeed sufficiently penetrate a rock mass and that useful measurements that are indicative of the geophysical properties of the rock mass can be made. Changes in these properties within a rock mass can be interpreted in terms of anomalous zones. In the transillumination survey configuration more than 60 metres of rock mass was penetrated at the 445 MHz operating frequency. The absorption rates, calculated directly from the performance specifications of the prototype equipment used in the field surveys, agreed well with the bulk absorption rates calculated from the analysis of the received signal strength as a function of transmitter-receiver separation. The effective resistivities at 445 MHz, calculated from this absorption rate data, varied from 500 to 1500 Ω -m, depending upon the estimated value for the effective permittivity. These results are consistent with the conductivities measured by other researchers at UHF

frequencies using several different techniques. AC and DC measurements of effective conductivity and permittivity taken on core samples collected at the Big Nickel Mine site exhibited the classical relaxation phenomenon and corroborated the UHF-EM transillumination survey results.

6.2 Conclusions and recommendations for further work

This project was initiated to investigate the feasibility of making geophysical electromagnetic measurements at UHF frequencies. The prototype equipment designed and subsequently used in the field surveys is not meant to represent an ideal survey instrument. Furthermore the survey configuration employed was not necessarily meant to represent the best configuration under all conditions likely to be encountered in the field. The research was meant to provide insight into the potential limitations on the use of UHF-EM continuous-wave techniques in geophysics and the type of equipment required for taking high quality, informative and cost effective measurements. It is clear that no effort has been made to fully exploit the potential of the transillumination technique; for logistical reasons it was only possible to take a few measurements of rock-mass absorption rates at the single frequency with several scattered transmitter and receiver locations. In a more elaborate survey, the construction of a series of fan-like arrays, as described in section 2.9, would allow one to treat the absorption rate data using the well-developed

tomographic inversion processing techniques. This would provide a two dimensional "absorption image" of the rock mass between the transmitter and receiver. Unfortunately, as discussed in section 2.9, the data collected during this research by the author was inadequate for a complete tomographic reconstruction. Using this prototype system, one measurement could easily take more than twenty minutes. The time which could have been required to collected enough data for a true tomographic survey would have been impossibly long: free access to the Big Nickel Mine site was limited to about one week each summer at a time when the normal preparation of the site and the major tourist traffic was minimal. The more efficient packaging of the electronics in a second-generation field survey system and the use of antenna mounts allowing for rotation about both horizontal and vertical axes could result in a considerably improved survey productivity.

The transillumination type survey is expected to be best suited for inter-borehole work where strict geometric control and automated transmitter/receiver movement and data collection is possible. Under such ideal conditions the tomographic imaging technique should find direct use in analysing the data obtained in underground rock-mass surveys. On the other hand the development of an inter-borehole system will bring new and difficult problems. The antennas that can be used underground in mine stopes and

drifts possess advantages over any conceivable borehole antenna design. Strictly speaking, the standard tomographic inversions as commonly performed in medical x-ray diagnostic procedures require antenna beamwidths which can be assumed to be negligible. In these UHF-EM transillumination studies, one must be content to work with finite beamwidths. The larger antennas or arrays allowed in the underground work, reported above, have advantage in this regard over any antenna which must be placed down a small diameter borehole. Similiarly as the antenna is located in air in an underground survey, a higher degree of control of the energy radiated into the wall rock is achievable. In the borehole mode, the presence of borehole fluid creates an additional interface at which the radiated energy can be reflected and refracted. Annan (1985) indicates that he has tried tuning underground pulse radar antennas to match the wall-rock impedance and found it to be impractable to perform this tuning on a continuous basis.

It was found during the Big Nickel surveys that interconnection of the underground drifts in which the transmitter and receiver were located often created serious problems in determining the signal path. Secondary propagation paths can exist and signals received by these routes could result in there being a major difficulty in isolating the through-rock path component. This problem can be reduced to some extent through the use of highly directional antennas although most UHF-EM antennas of a

manageable physical dimension typically possess finite back and side lobes.

The wide variation of electrical properties that can be encountered in crustal rocks requires that serious consideration must be given to providing for a sufficiently large dynamic range of measurement. The most practical manner of achieving this is to incorporate adjustable gain settings on the receiver while allowing for a variable transmitter output. The signal saturation condition rather than the insufficiency of the received signal level caused the initial problems encountered during the first Big Nickel Mine survey. A variable transmitter output power would reduce the need for the elaborate receiver shielding precautions which were found necessary in the prototype instrument.

UHF continuous-wave EM techniques should be useful in a restricted geologic condition. The rock mass must be relatively nonabsorbing so that sufficient penetration distances are achievable. Furthermore, the effective permittivity of the wall rock must be low enough that large reflections and refractions at the air-wall rock interface do not arise. The rock mass must, in general, be relatively homogeneous along the direction of measurement such that any inhomgeneities of interest within this homogeneous mass can be detected.

A measurement of the phase shift between the

transmitted and received signal would be desirable. This would allow for the separation of effective conductivities and permittivities. A phase and amplitude reference link could be established through the use of an optical-fiber cable connecting the transmitter and receiver. A phase measurement would also allow for a holographic reconstruction of the imaged area (Lorrain, 1985). Such a reconstruction could provide an immense advantage in testing the subsurface for structural integrity in advance of radioactive waste disposal or mine drifting in that only one borehole would be necessary.

It would be desirable to measure the electrical properties of a rock mass over a broad range of frequencies within the VHF/UHF bands. Given the character of the electrical properties of most earth materials as a function of frequency, discrimination of the material of an anomalous volume , could, inprinciple, be achieved under favorable conditions. Perhaps, unfortunately, if more than a few watts of output power is required, federal licencing of operating frequencies will be necessary and the choice of available frequencies will be severely limited. The effort required to obtain a licence is not insignificant. International agreements governing frequency allotment and licencing require that detailed performance and requirement specifications be submitted with all applications for an operating frequency. Since a UHF-EM system can be expected to be used all across Canada a very flexible permit is

required. International approval can be necessary if more than 10 Watts of power is requested. In this case it can take between six months and one year to obtain the required internationally valid licence.

6.3 Claims for originality

The research work upon which this thesis is based accomplished three principal original contributions to geophysical research:

a) The underground UHF-EM transillumination technique has been shown to be a geophysically feasible and useful survey method.

b) In-situ measurements of absorption rate and estimated conductivities have been calculated in a typical Canadian geological setting. A paucity of in-situ measurements have been previously made at VHF/UHF frequencies and almost exclusively in very different geological and glaciological environments.

c) A path has been laid for the further development of the transillumination technique, which through incorporation of several of the suggestions made above, could yield significant benefits to underground mining and exploration, to the search for rock masses of sufficient integrity to contain radioactive waste for geological times, to the delineation of structural features within a rock mass, to the search for thin mineralized zones and to the detection

and monitoring of zones of weakness within a rock mass.

References

Annan, A.P., 1985, Personal Communication.

Annan, A.P., and Davis, J.L., 1977, Radar range analysis for geologic materials, Geological Survey of Canada Paper 77-1B (1977).

Annan, A.P., and Davis, J.L., 1976, Impulse radar sounding in permafrost, Radio Science, Vol.11, no.4, pp.383-394.

Annan, A.P., 1970, Radio interferometry depth sounding: Part I-Theoretical discussion, Geophysics, Vol.38, pp.557-580.

Baranyi, E., 1984, Geophysical electromagnetics at Very-High and Ultra-High frequencies, unpublished M.Sc. thesis, McGill University, Montreal.

Bird, 1982, Instruction book for the thruline directional wattmeter.

Buselli, G., 1980, Electrical geophysics in the USSR, Geophysics, Vol.45, no.10, pp.1551-1562.

Campbell, M.J., and Ulrichs, J., 1969, Electrical properties of rocks and their significance for lunar radar observations, Journal of Geophysical Research, Vol.74, no.24, pp.5867-5881.

Carmichael, R.S., 1982, Handbook of Physical Properties of Rocks, CRC Press Inc., Florida.

Cole, K.S.,and Cole, R.H.,1941, Dispersion and absorption in dielectrics I, Alternating current characteristics, Journal of Chemical Physics, Vol.9, 1941, pp.341-353.

Collett, L.S., and Jensen, O.G., 1981, Geophysical applications of surface wave impedance measurements, Geological Survey of Canada Paper 81-15.

Collett, L.S., and Katsube, T.J., 1973, Electrical parameters of rocks in developing geophysical techniques, Geophysics, Vol.38, no.1, pp.76.

Cook, J.C., 1975, Radar transparancies of mine and tunnel rocks, Geophysics, Vol.40, no.5, pp.865-885.

Cook, J.C., 1978, RF electrical properties of bituminous coal samples, Geophysics, Vol.35, no.6, pp.1079-1085.

Coon, J.B., Fowler, J.C., and Schafers, C.J., 1981, Experimental uses of short pulse radar in coal seams, Geophysics, Vol.46, no.8, pp.1163-1168.

Davis, J.L., Annan, A.P., and Vaughan, C., 1984a, Placer exploration using radar and seismic methods, Abstracts of the fifty-fourth annual S.E.G. convention, 1984.

Davis, J.L., Killey, R.W.D., Annan, A.P., and Vaughan, C., 1984b, Surface and borehole ground penetration radar surveys for mapping geological structure, presented at the NWWA/U.S. EPA conference on surface and borehole geophysical methods.

deBettencourt, J.T., and Frazier, J.W., 1963, Rock electrical characteristics deduced from depth attenuation rates (in drill holes), IEEE Transactions on Antennas and Propagation, Vol.AP-11, no.5, pp.358-363.

Dines, K.A., and Lytle, R.J., 1979, Computerized geophysical tomography, Proceedings of the IEEE, Vol.67, no.7, pp.1065-1073.

Dolphin, L.T.,Beaty, W.B., and Tanzi, J.D., 1978, Radar probing of Vitorio Paek, New Mexico, Geophysics, Vol.43, no.7, pp.1441.

Dolphin Jr., L.T., Bollen, R.L., and Oetzel, G.N., 1974, An underground electromagnetic sounder experiment, Geophysics, Vol.39, no.1, pp.49-55.

Eve, A.S., Keys, D.A. and Lee, F.W., 1929, The penetration

of rock by electromagnetic waves at audio frequencies, Proceedings of the I.R.E., Vol.17, pp.2072.

Eve, D.A., and Steel, W.A., 1929, Reception experiments in Mount Royal tunnel, Proceeding of the Institute of Radio Engineers.

Fluke, 1983, Fluke general catalog.

Fowler, J.C., and Hale, S.D., 1980, Coal seam hazard detection using synthetic pulse radar, Abstracts of the fiftieth annual S.E.G. convention, 1980.

Fowler, J.C., 1981, Subsurface reflection profiling using ground probing radar, Mining engineering, Vol.33, no.7, pp.1266-1270.

Grubb, R.N.,Orswell, P.L., and Taylor, J.H., 1976, Borehole measurements of conductivity and dielectric constant in the 300 kHz to 25 MHz frequency range, Radio Science, Vol.11, no.4, pp.275-283.

Grubb, R.N., and Wait, J.R., 1971, In situ measurements of the complex propagation constant in rocks for frequencies from 1 MHz to 10 MHz, Electronics Letters, Vol.7, no.17, pp.506-507.

GSSI, 1982, Information brochure for Geophysical Survey Systems Inc..

Harrison, C.H., 1970, Reconstruction of subglacial releif from radar sounding echoes, Geophysics, Vol.35, no.6, pp.1099-1115.

Hewlett-Packard, 1981, General catalog.

Hoekstra, P., and Delaney, A., 1974, Dielectric properties of soils at UHF and microwave frequencies, Journal of Geophysical Research, Vol.79, no.11, pp.1699-1707.

Jackson, J.D., 1975, Classical Electrodynamics, John Wiley and Sons, Inc., Toronto, Canada.

and Sons, Inc., Toronto, Canada.

Jezek, K.C., 1985, Radar measurements of borehole geometry on the Greenland and Antarctic ice sheets, Geophysics, Vol.50, no.2, pp.242-251.

Judge, A., 1985, personal communication.

Kaspar, M., and Pecen, J., 1975, Detection of caves in a karst formation by means of electromagnetic waves. Geophysical Prospecting, Vol.23, pp.611-621.

Keller, G.V., and Frischknecht, F.,C., 1966, Electrical Methods in Geophysical Prospecting, Pergamon Press, Toronto, Canada.

Keller, G.V., 1963, Electrical properties in the deep crust, IEEE Transactions on Antennas and Propagation, Vol.11, no.3, pp.334.

Knight, C.,J., 1965, A petrographic study of the Spragge Group and discussion of its correlation with the Sudbury Series, M.Sc. thesis, University of Toronto.

Kyle, A.J., Deluca, F.R., Duke, I.N., Ludwig, A., and Waugh, D.C., 1983, Location a big advantage on Clover Hill potash project, Canadian Mining Journal, November, 1983.

Lager, D.L., and Lytle, R.J., 1977, Determining a subsurface electromagnetic profile from high-frequency measurements by applying reconstruction-technique algorithms, Radio Science, Vol.12, no.2, pp.249-260.

Lorrain, P., 1985, Personal communication.

Lorrain, P., and Corson, D.R., 1970, Electromagnetic fields and waves, W.H. Freeman and Company, San Francisco, California.

Lytle, R.J., and Lager, D.L., 1976, The Yosemite experiments: HF propagation through rock, Radio Science, Vol.11, no.4, pp.245-252.

Lytle, R.J., Laine, E.F., Lager, D.L., and Okada, J.T., 1976, Determination of the in situ high frequency electrical properties of permafrost rock, Radio Science, Vol.11, no.4, pp.285-293.

Moffatt, D.L., and Puskar, R.J., 1976, A subsurface electromagnetic pulse radar, Geophysics, Vol.41, no.3, pp.506-518.

Morey, R.M., 1974, Continuous subsurface profiling by impulse radar, Proceedings of Engineering Foundation Conference on Subsurface Exploration for Underground Excavation and Heavy Construction, American Society of Civil Engineers, pp.213-232.

Narod, B. and Clarke, G.K.C., 1980, Airborne UHF radio echo-soundings of three Yukon glaciers, Journal of Glaciology, Vol.25, no.1, pp.23-31.

Nickel, N., Sender, F., Thierbach, R. and Weichart, H., 1980, High frequency electromagnetic tools for the prospection of saltdome structures from boreholes, Abstracts of the fiftieth annual S.E.G. convention, 1980.

Ontario Geological Survey, 1984, The geology and ore deposits of the Sudbury structure, Special volume 1.

Owen, T.E., and Suhler, S.A., 1981, Borehole directional radar detection of subsurface cavities, Abstracts of the fifty-first annual S.E.G. convention, 1981.

Owen, T.E., and Suhler, S.A., 1980, Subsurface void detection using surface resistivity and borehole electromagnetic techniques, Abstracts of the fiftieth annual S.E.G. convention, 1980.

Oyo, 1984, Specification sheet for the Georadar YL-R2 Electromagnetic reflection profiling system.

Prichett, W.C., 1952, Attenuation of radio frequency waves through the earth, Geophysics, Vol.17, no.2, pp.193-207.

Radcliff, R.D. and Balanis, C.A., 1981, Electromagnetic geophysical imaging incorporating refraction and reflection, IEEE Transactions on Antennas and Propagation, Vol. AP-29, no.2, March, 1981.

Rao, V.M., and Ramaprasada Rao, I.B., 1983, Geophysics, Vol.48, no.3, pp.391-395.

Rossiter, J.R., Strangway, D.W., Annan, A.P., Watts, R.D., and Redmond, J.D., 1975, Detection of thin layers by radio interferometry, Geophysics, Vol.40, no.2, pp.299-308.

Saint-Amant, M., and Strangway, D.W., 1970, Dielectric properties of dry, geologic materials, Geophysics, Vol.35, no.4, pp.624-645.

Skolnick, M.L., 1980, Introduction to Radar Systems, McGraw-Hill Co., New York.

Sinclair Radio Laboratories, 1981, General catalog.

Silverman, D., and Sheffet, D., 1942, Note on the transmission of radio waves through the earth, Geophysivs, Vol.7, no.4, pp.400-413.

Smith-Rose, R.L., 1934, Electrical measurements on soil with alternating current, Journal of the institution of electrical engineers, vol. 75, pp.221-239.

Somerstein, S.F., Berg, M., Chang, D., Chung, H., Johnson, H., Richardson, B., Pizzicara, J., Salisbury, W.W., 1984, Radio-frequency geotomography for remotely probing the interiors of operating mini- and commercial- sized oil-shale retorts, Geophysics, Vol.49, no.8, pp.1288-1300.

Stewart, R.D., and Unterberger, R.R., 1976, Geophysics, Vol.41, no. 1, pp.123-132.

Stutzman, W.L., and Thiele, G.A., 1981, Antenna Theory and Design, John Wiley and Sons, New York, New York.

Tarantolo Jr., P.J., and Unterberger, R.R., 1978, Geophysical Prospecting, Vol.26, no.2, pp.359-382.

Tsao, C.K.H., and deBettencourt, J.T., 1968, Subsurface radio propagation experiments, Radio Science, Vol.3, no.11, pp.1039-49.

Telford, W.M., Geldart, L.P., Sheriff, R.E., and Keys, D.A., 1976, Applied Geophysics, Cambridge University Press, New York.

Unterberger, R.R., 1978, Radar propagation in rock salt, Geophysical Prospecting, Vol.26, no.2, pp.312-328.

Von Hippel, A.R., Editor, 1954, Dielectric materials and applications, The M.I.T. Press, Cambridge, Massachusetts.

Wait, J.R., Ed., 1959, Overvoltage research and geophysical applications, Pergamon Press, New York.

Waite, A.H., jr., 1966, International experiments in glacier sounding, 1963 and 1964, Canadian Journal of Earth Sciences, Vol.3, no.6, pp.887-92.

Watts, R.D., and England, A.W., 1976, Radio soundings of temperate glaciers: ice properties and sounder design criteria, Journal of Glaciology, Vol.17, no.75, pp.39-48.

Wavetek, 1982., Specification sheet for the Wavetek 5000/7000 series attenuators.

Weber, J.R., and Andrieux, P., 1970, Radar soundings on the Penny Ice Cap, Baffin Island, Journal of Glaciology, Vol.9, no.55, pp.49-53.

Weinschel, 1982, Specification sheet for the Weinschel medium power fixed attenuators.

Westman (editor), H.P., 1968, Reference data for radio engineers, Fifth edition, Howard W. Sams & Co., Inc., Indianapolis, Ohio.

Wright, D.L., Watts, R.D., and Bramsoe, E., 1984, Single-hole short-pulse borehole radar experiments and a cross-hole transponder, Preprint.

Xadar, 1981, Information bulletin, Xadar Exploration Services.

Bibliography

Ames, L.A., Frazier, J.W., and Orange, A.S., 1963, Geological and geophysical considerations in radio propagation through the Earth's crust, IEEE Transactions on Antennas and Propagation, Vol.AP-11, no.5, pp.369-371.

Card, K.D., 1968, Geology of the Denison-Waters area, Ontario Department of Mines Geological Report 60.

Card, K.D., 1978, Geology of the Sudbury-Manitoulin area, Districts of Sudbury and Manitoulin, Ontario Geological Survey Report 166.

Chan, L.C., Moffatt, D.L., Peters Jr., L., 1979, A characterization of subsurface radar targets, Proceedings of the IEEE, Vol.67, no.7, pp.991-1000.

Clough, J.W., 1976, EM lateral waves in earth-sounding radar, Geophysics, Vol.41, no.6a, pp.1126.

Eve, A.S., and Keys, D.A., 1956, Applied Geophysics, Cambridge University Press, New York.

Herman, G.T., and Lent, A., 1976, Iterative reconstruction algorithms, Computers in Biology and Medicine, Vol.6, pp.273-294.

Holser, W.T., Brown, R.J.S., Roberts, F.A., Fredriksson,

O.A., and Unterberger, R.R., 1972, Geophysics, Vol.37, no.5, pp.889-906.

Leckenby, R.J., 1982, Electromagnetic ground radar methods, United States Department of the Interior, Bureau of Mines Information Cicular, no.8891, pp.36-45.

Parkhomenko, E.I., 1967, Electrical properties of rocks, Plenum Press, New York.

Rubin, L.A., and Fowler, J.C., 1978, Ground probing radar for delineation of rock features, Engineering Geology, Vol.12, pp.163-170.

Von Hippel, A.R., 1966, Dielectrics and waves, The M.I.T. Press, Cambridge, Massachusetts.

Wait (editor), J.R., 1971, Electromagnetic probing in geophysics, The Golem Press, Boulder, Colorado.

Appendix A

International Frequency Allocations

and

Standard Broadcast Frequencies

Kilohertz	Service
Below 10 00	(not allocated)*
10.00–14.00	RADIO NAVIGATION*
	Radio location*
14 00–19.95	FIXED*
	MARITIME MOBILE*
19 95–20.05	STANDARD FREQUENCY*
20 05–70 00	FIXED*
	MARITIME MOBILE*
70 00–90 00	FIXED
	MARITIME MOBILE
	MARITIME RADIO NAVIGATION
	Radio location
90 00–110 0	RADIO NAVIGATION
	FIXED
	Maritime mobile
110 0–130 0	FIXED
	MARITIME MOBILE
	MARITIME RADIO NAVIGATION
	Radio location
130.0–160 0	FIXED
	MARITIME MOBILE
160 0–200.0	FIXED
200 0–285.0	AERONAUTICAL RADIO NAVIGATION
	Aeronautical mobile
285 0–325 0	MARITIME RADIO NAVIGATION
	(radio beacons)
	Aeronautical radio navigation

Kilohertz	Service
325.0–405.0	AERONAUTICAL RADIO NAVIGATION*
	Aeronautical mobile*
405.0–415.0	MARITIME RADIO NAVIGATION
	(radio direction-finding)
	Aeronautical radio navigation
	Aeronautical mobile
415.0–490.0	MARITIME MOBILE*
	(radiotelegraphy only)
490.0–510.0	MOBILE*
	(distress and calling)
510.0–525.0	MOBILE
	Aeronautical radio navigation
525.0–535 0	MOBILE
	Broadcasting
	Aeronautical radio navigation
535 0–1605	BROADCASTING*
1605–1800	FIXED
	MOBILE
	AERONAUTICAL RADIO NAVIGATION
	Radio location
1800–2000	AMATEUR
	FIXED
	MOBILE EXCEPT AERONAUTICAL
	RADIO NAVIGATION
2000–2065	FIXED
	MOBILE
2065–2107	MARITIME MOBILE
	(radiotelegraphy only)
2107–2170	FIXED
	MOBILE
2170–2194	MOBILE*
	(distress and calling)
2194–2300	FIXED
	MOBILE
2300–2495	FIXED
	MOBILE
	BROADCASTING
2495–2505	STANDARD FREQUENCY
2505–2850	FIXED
	MOBILE
2850–3025	AERONAUTICAL MOBILE (*R*)*

Megahertz	Service
3 025–3.155	AERONAUTICAL MOBILE (*OR*)*
3 155–3.200	FIXED*
	MOBILE EXCEPT AERONAUTICAL (*R*)*
3 200–3.400	FIXED*
	MOBILE EXCEPT AERONAUTICAL*
	BROADCASTING*
3.400–3.500	AERONAUTICAL MOBILE (*R*)*
3.500–4 000	AMATEUR
	FIXED
	MOBILE EXCEPT AERONAUTICAL (*R*)
4 000–4.063	FIXED*
4.063–4.438	MARITIME MOBILE*
4.438–4.650	FIXED
	MOBILE EXCEPT AERONAUTICAL (*R*)
4 650–4.700	AERONAUTICAL MOBILE (*R*)*

Megahertz	Service
4 700–4 750	AERONAUTICAL MOBILE (*OR*)*
4 750–4.850	FIXED
	BROADCASTING
4 850–4.995	FIXED*
	LAND MOBILE*
	BROADCASTING*
4.995–5.005	STANDARD FREQUENCY*
5 005–5 060	FIXED*
	BROADCASTING*
5 060–5 250	FIXED*
5.250–5 450	FIXED
	LAND MOBILE
5 450–5 680	AERONAUTICAL MOBILE (*R*)
5 680–5 730	AERONAUTICAL MOBILE (*OR*)*
5 730–5.950	FIXED*
5 950–6 200	BROADCASTING*
6 200–6.525	MARITIME MOBILE*

Table A.1a The International Telecommunications Union frequency allocations, 10 kHz to 6.525 MHz, for region 2, the Western hemisphere (after Westman, 1968).

Megahertz	Service
6 525-6 685	AERONAUTICAL MOBILE (*R*)*
6 685-6 765	AERONAUTICAL MOBILE (*OR*)*
6 765-7 000	FIXED*
7 000-7 300	AMATEUR
7 300-8 195	FIXED*
8 195-8 815	MARITIME MOBILE*
8 815-8 965	AERONAUTICAL MOBILE (*R*)*
8 965-9 040	AERONAUTICAL MOBILE (*OR*)*
9 040-9 500	FIXED*
9 500-9 775	BROADCASTING*
9 775-9 995	FIXED*
9 995-10 005	STANDARD FREQUENCY*
10 005-10 10	AERONAUTICAL MOBILE (*R*)*
10 10-11 175	FIXED*
11 175-11 275	AERONAUTICAL MOBILE (*OR*)*
11 275-11 40	AERONAUTICAL MOBILE (*R*)*
11 40-11 70	FIXED*
11 70-11 975	BROADCASTING*
11 975-12.33	FIXED*
12 33-13 20	MARITIME MOBILE*
13 20-13 26	AERONAUTICAL MOBILE (*OR*)*
13 26-13 36	AERONAUTICAL MOBILE (*R*)*
13 36-14 00	FIXED*
14 00-14 35	AMATEUR*
14 35-14 99	FIXED*
14 99-15 01	STANDARD FREQUENCY*
15 01-15 10	AERONAUTICAL MOBILE (*OR*)*
15 10-15 45	BROADCASTING*
15 45-15 762	FIXED*
15 762-15 768	FIXED* Space research*
15 768-16 46	FIXED*
16 46-17 36	MARITIME MOBILE*
17 36-17 70	FIXED*
17 70-17 90	BROADCASTING*
17 90-17 97	AERONAUTICAL MOBILE (*R*)*
17 97-18 03	AERONAUTICAL MOBILE (*OR*)*
18 03-18 036	FIXED* Space research*
18 036-19 99	FIXED*
19 99-20 01	STANDARD FREQUENCY*
20 01-21 00	FIXED*
21 00-21 45	AMATEUR*
21 45-21 75	BROADCASTING*
21.75-21.85	FIXED*
21.85-22 00	AERONAUTICAL FIXED* AERONAUTICAL MOBILE (*R*)*
22.00-22.72	MARITIME MOBILE*
22.72-23 20	FIXED*
23 20-23 35	AERONAUTICAL FIXED* AERONAUTICAL MOBILE (*OR*)*
23.35-24.99	FIXED* LAND MOBILE*
24.99-25.01	STANDARD FREQUENCY*
25 01-25 07	FIXED* MOBILE EXCEPT AERONAUTICAL*
25 07-25 11	MARITIME MOBILE*
25 11-25 60	FIXED* MOBILE EXCEPT AERONAUTICAL*
25 60-26 10	BROADCASTING*
26 10-27 50	FIXED* MOBILE EXCEPT AERONAUTICAL*
27 50-28 00	METEOROLOGICAL AIDS FIXED* MOBILE
28 00-29 70	AMATEUR*
29 70-30 005	FIXED* MOBILE*
30 005-30 01	FIXED* MOBILE* SPACE RESEARCH* SPACE* (satellite identification)
30 01-37 75	FIXED* MOBILE*
37 75-38 25	FIXED* MOBILE* Radio astronomy*
38 25-50 00	FIXED MOBILE
50 00-54 00	AMATEUR
54 00-73 00	FIXED MOBILE BROADCASTING
73 00-74 60	RADIO ASTRONOMY
74 60-75 40	AERONAUTICAL RADIO NAVIGATION
75 40-88 00	FIXED MOBILE BROADCASTING
88 00-108 0	BROADCASTING
108 0-117 975	AERONAUTICAL RADIO NAVIGATION*
117 975-132 0	AERONAUTICAL MOBILE (*R*)*
132 0-136 0	FIXED MOBILE
136 0-137 0	SPACE RESEARCH (telemetering and tracking)
137 0-138 0	METEOROLOGICAL—SATELLITE* SPACE RESEARCH* (telemetering and tracking) SPACE* (telemetering and tracking)
138 0-143 6	FIXED MOBILE *Radio location*
143 6-143 65	FIXED MOBILE SPACE RESEARCH (telemetering and tracking) *Radio location*
143 65-144 0	FIXED MOBILE *Radio location*

Table A.1b The International Telecommunications Union frequency allocations, 6.525 MHz to 144.Ø MHz, for region 2, the Western hemisphere (after Westman, 1968).

Megahertz	Service
144.0–148 0	AMATEUR
148 0–149 9	FIXED
	MOBILE
149 9–150 05	RADIO NAVIGATION—SATELLITE*
150 05–174 0	FIXED
	MOBILE
174.0–216 0	FIXED
	MOBILE
	BROADCASTING
216.0–220 0	FIXED
	MOBILE
	RADIO LOCATION
220 0–225 0	AMATEUR
	RADIO LOCATION
225.0–267 0	FIXED
	MOBILE
267.0–272 0	FIXED*
	MOBILE*
	SPACE*
	(telemetering)
272 0–273 0	FIXED*
	MOBILE*
	SPACE*
	(telemetering)
273 0–328 6	FIXED*
	MOBILE*
328 6–335 4	AERONAUTICAL RADIO NAVIGATION*
	(glide-path systems)
335 4–399 9	FIXED*
	MOBILE*
399 9–400 05	RADIO NAVIGATION—SATELLITE*
400.05–401 0	METEOROLOGICAL AIDS*
	METEOROLOGICAL—SATELLITE*
	(maintenance telemetering)
	SPACE RESEARCH*
	(telemetering and tracking)
401 0–402 0	METEOROLOGICAL AIDS*
	SPACE*
	(telemetering)
	Fixed*
	Mobile except aeronautical*
402 0–406 0	METEOROLOGICAL AIDS*
	Fixed*
	Mobile except aeronautical*
406.0–420 0	FIXED*
	MOBILE EXCEPT AERONAUTICAL*
420.0–450 0	RADIO LOCATION
	Amateur
450 0–460 0	FIXED*
	MOBILE*
460.0–470 0	FIXED*
	MOBILE*
	Meteorological—satellite*
470 0–890.0	BROADCASTING
890.0–942.0	FIXED
	RADIO LOCATION
942.0–960	FIXED
960.0–1215	AERONAUTICAL RADIO NAVIGATION*
1215–1300	RADIO LOCATION*
	Amateur*
1300–1350	AERONAUTICAL RADIO NAVIGATION*
	Radio location*
1350–1400	RADIO LOCATION
1400–1427	RADIO ASTRONOMY*
1427–1429	FIXED*
	MOBILE EXCEPT AERONAUTICAL*
	SPACE*
	(telecommand)
1429–1435	FIXED
	MOBILE
1435–1525	MOBILE
	Fixed
1525–1535	SPACE
	(telemetering)
	Fixed
	Mobile
1535–1540	SPACE*
	(telemetering)
1540–1660	AERONAUTICAL RADIO NAVIGATION*
1660–1664 4	METEOROLOGICAL AIDS*
	METEOROLOGICAL—SATELLITE*
1664.4–1668.4	METEOROLOGICAL AIDS*
	METEOROLOGICAL—SATELLITE*
	Radio astronomy*
1668.4–1670	METEOROLOGICAL AIDS*
	METEOROLOGICAL—SATELLITE*
1670–1690	METEOROLOGICAL AIDS*
	FIXED*
	MOBILE EXCEPT AERONAUTICAL*
1690–1700	METEOROLOGICAL AIDS
	METEOROLOGICAL—SATELLITE
1700–1710	SPACE RESEARCH
	(telemetering and tracking)
1710–1770	FIXED
	MOBILE
1770–1790	FIXED
	MOBILE
	Meteorological—satellite

Table A.1c The International Telecommunications Union frequency allocations, 144.0 MHz to 1.790 GHz, for region 2, the Western hemisphere (after Westman, 1968).

Gigahertz	Service
1790–2290	FIXED MOBILE
2290–2300	SPACE RESEARCH (telemetering and tracking in deep space)
2300–2450	RADIO LOCATION Amateur Fixed Mobile
2450–2550	FIXED MOBILE RADIO LOCATION
2550–2690	FIXED* MOBILE*
2690–2700	RADIO ASTRONOMY*
2700–2900	AERONAUTICAL RADIO NAVIGATION* Radio location*
2900–3100	RADIO NAVIGATION* (ground-based radars) Radio location*
3 100–3 300	RADIO LOCATION*
3 300–3 400	RADIO LOCATION Amateur
3 400–3.500	RADIO LOCATION COMMUNICATION—SATELLITE (satellite to earth) Amateur
3 500–3 700	FIXED MOBILE RADIO LOCATION COMMUNICATION—SATELLITE (satellite to earth)
3 700–4 200	FIXED MOBILE COMMUNICATION—SATELLITE (satellite to earth)
4 200–4.400	AERONAUTICAL RADIO NAVIGATION*
4 400–4 700	FIXED* MOBILE* COMMUNICATION—SATELLITE* (earth to satellite)
4 700–4.990	FIXED* MOBILE*
4 990–5 000	RADIO ASTRONOMY
5 000–5 250	AERONAUTICAL RADIO NAVIGATION*
5 250–5.255	RADIO LOCATION* Space research*
5 255–5 350	RADIO LOCATION*
5 350–5 460	AERONAUTICAL RADIO NAVIGATION* Radio location*
5 460–5 470	RADIO NAVIGATION* Radio location*
5 470–5 650	MARITIME RADIO NAVIGATION* Radio location*
5 650–5.670	RADIO LOCATION* Amateur*
5 670–5 725	RADIO LOCATION* Amateur* Space research* (deep space)
5 725–5 925	RADIO LOCATION Amateur
5 925–6 425	FIXED* MOBILE* COMMUNICATION—SATELLITE* (earth to satellite)
6 425–7 250	FIXED* MOBILE*
7 250–7 300	COMMUNICATION—SATELLITE* (satellite to earth)
7 300–7.750	FIXED* MOBILE* COMMUNICATION—SATELLITE* (satellite to earth)
7 750–7 900	FIXED* MOBILE*
7 900–7.975	FIXED* MOBILE* COMMUNICATION—SATELLITE* (earth to satellite)
7 975–8.025	COMMUNICATION—SATELLITE* (earth to satellite)
8 025–8 400	FIXED* MOBILE* COMMUNICATION—SATELLITE* (earth to satellite)
8 400–8 500	SPACE RESEARCH
8.500–8 750	RADIO LOCATION*
8 750–8 850	RADIO LOCATION* AERONAUTICAL RADIO NAVIGATION* (airborne doppler aids)
8 850–9 000	RADIO LOCATION*
9.000–9 200	AERONAUTICAL RADIO NAVIGATION* (ground-based radars) Radio location*
9 200–9.300	RADIO LOCATION*
9 300–9 500	RADIO NAVIGATION* Radio location*
9 500–9 800	RADIO LOCATION*
9 800–10 00	RADIO LOCATION* Fixed*
10 00–10 50	RADIO LOCATION* Amateur*

Table A.1d The International Telecommunications Union frequency allocations, 1.790 GHz to 10.50 GHz, for region 2, the Western hemisphere (after Westman, 1968).

10 50–10 55	RADIO LOCATION
	(continuous-wave systems only)
10 55–10.68	FIXED*
	MOBILE*
	Radio location*
10 68–10 70	RADIO ASTRONOMY*
10.70–11 70	FIXED*
	MOBILE*
11 70–12 70	FIXED*
	MOBILE EXCEPT AERONAUTICAL*
	BROADCASTING*
12.70–13 25	FIXED*
	MOBILE*
13.25–13 40	AERONAUTICAL RADIO NAVIGATION*
13 40–14 00	RADIO LOCATION*
14.00–14 30	RADIO NAVIGATION*
14 30–14.40	RADIO NAVIGATION—SATELLITE*
14.40–15.25	FIXED*
	MOBILE*
15.25–15.35	SPACE RESEARCH*
15 35–15.40	RADIO ASTRONOMY*
15.40–15.70	AERONAUTICAL RADIO NAVIGATION*
15.70–17.70	RADIO LOCATION*
17 70–19 30	FIXED*
	MOBILE*
19.30–19.40	RADIO ASTRONOMY*
19.40–21 00	FIXED*
	MOBILE*
21.00–22.00	AMATEUR*
22.00–23.00	FIXED*
	MOBILE*
23.00–24.25	RADIO LOCATION*
24.25–25.25	RADIO NAVIGATION*
25.25–31.00	FIXED*
	MOBILE*
31 00–31.30	FIXED*
	MOBILE*
	Space research*
31 30–31.50	RADIO ASTRONOMY*
31 50–31 80	SPACE RESEARCH
31.80–32.30	RADIO NAVIGATION*
	Space research*
32 30–33.40	RADIO NAVIGATION
33.40–34.20	RADIO LOCATION*
34.20–35.20	RADIO LOCATION*
	Space research*
35 20–36.00	RADIO LOCATION*
36.00–40.00	FIXED*
	MOBILE*
Above 40.00	(not allocated)*

Table A.1e The International Telecommunications Union frequency allocations, 10.50 GHz to 40.0 GHz, for region2, the Western hemisphere (after Westman, 1968).

TELEVISION CHANNEL FREQUENCIES

VHF

Channel no.	Frequency range (MHz)	Channel no	Frequency range (MHz)
2	54–60	8	180–186
3	60–66	9	186–192
4	66–72	10	192–198
5	76–82	11	198–204
6	82–88	12	204–210
7	174–180	13	210–216

UHF

Channel no	Frequency range (MHz)	Channel no	Frequency range (MHz)	Channel no	Frequency range (MHz)
14	470–476	30	566–572	46	662–668
15	476–482	31	572–578	47	668–674
16	482–488	32	578–584	48	674–680
17	488–494	33	584–590	49	680–686
18	494–500	34	590–596	50	686–692
19	500–506	35	596–602	51	692–698
20	506–512	36	602–608	52	698–704
21	512–518	37	608–614	53	704–710
22	518–524	38	614–620	54	710–716
23	524–530	39	620–626	55	716–722
24	530–536	40	626–632	56	722–728
25	536–542	41	632–638	57	728–734
26	542–548	42	638–644	58	734–740
27	548–554	43	644–650	59	740–746
28	554–560	44	650–656		
29	560–566	45	656–662	83	884–890

Note The carrier frequency for the video portion is the lower frequency plus 1 25 MHz The audio carrier frequency is the upper frequency minus 0 25 MHz. All channels have a 6-MHz bandwidth For example, Channel 2 video carrier is at 55 25 MHz and the audio carrier is at 59 75 MHz.

Table A.2 The standard television frequencies (after Stutzman and Thiele, 1981).